



DISSERTATION

Titel der Dissertation

Expression of G protein-coupled receptor 19 in human lung cancer cells is triggered by entry into S phase and supports G2/M cell cycle progression

Verfasser

Stefan Kastner

angestrebter akademischer Grad

Doktor der Naturwissenschaften (Dr.rer.nat.)

Wien, 2012

Studienkennzahl lt. Studienblatt: A 091 490

Dissertationsgebiet lt. Studienblatt: Dr.-Studium der Naturwissenschaften Molekulare Biologie

Betreuerin / Betreuer: Univ.-Doz. Dr. Wolfgang Sommergruber

Acknowledgement

I would like to thank Boehringer Ingelheim RCV – particularly my supervisor Dr. habil. Wolfgang Sommergruber – for the kind offer to conduct the research for my doctoral thesis in their laboratories. Wolfgang, your door was always open for great discussions about all the things a PhD student needs to ask during the course of a thesis and beyond!

Prof. Michael Freissmuth from the Institute of Pharmacology at the Medical University of Vienna deserves my deepest gratitude for his willingness to support my doctoral thesis. Mischa, your help and advice – ranging from the design of experiments over your offer to partly conduct them in your laboratories to assistance with manuscript preparation – were of greatest value. Despite being a 'hamster in a running wheel' you always offered me a time slot for discussions on my project. Thank you so much for your help!

I would further like to thank Dr. Christina Glöckel and Simon Keuerleber for their help with the adenylyl cyclase assay and the 'exchange' of expression constructs.

Special thanks go to Prof. Walter Berger and Dr. habil. Renate Voit for their willingness to be the appraisers of my doctoral thesis.

I'm also very thankful for excellent technical assistance by Teresa Gottschamel, Nathalie Harrer, Herwig Machat, and Diane Thompson, who assisted me in performing various molecular and cellular biology techniques – it was a pleasure to learn from your experience! Besides, thank you very much, Teresa, for taking care of my cells during my days off.

Dr. Anja Ebert from the Institute of Molecular Pathology in Vienna kindly offered her well-established chromatin immunoprecipitation protocol.

Dr. Tilman Voss helped me a lot with explanations regarding the high-throughput screening and the vast possibilities this technique has to offer – especially with regards to data analysis.

Dr. Andreas Wernitznig was always happy and patient to discuss bioinformatic issues regarding our inhouse TANGO database.

And last but not least: Special thanks to all the people from the F&E at Boehringer that helped my right from the beginning of my doctoral thesis. It has been a great time getting to know you and working together with you!

Table of contents

Abbreviations	9
I. Abstract.....	13
II. Zusammenfassung	14
III. Introduction	15
1. Cancer – a highly diverse disease	15
1.1. Fundamental characteristics of cancer	16
2. Lung cancer	19
2.1. Small cell lung cancer (SCLC)	20
2.2. Non-small cell lung cancer (NSCLC)	21
2.3. The neuroendocrine phenotype of lung cancer	21
2.4. Molecular characterization of lung cancer	22
3. Cell cycle	23
3.1. Cyclins and cyclin-dependent kinases (CDKs)	24
3.2. Cell cycle checkpoints	25
4. G protein-coupled receptors (GPCRs)	27
4.1. Classification of GPCRs.....	28
4.2. Classical GPCR signaling and GPCR-interacting proteins (GIPs)	29
4.3. GPCR oligomerization	30
4.4. Endocytosis of GPCRs from the plasma membrane.....	32
4.5. GPCRs are involved in cell cycle regulation and cancer	33
5. G protein-coupled receptor 19 (GPR19)	34
5.1. Gene and protein information	34
5.2. Expression of <i>Gpr19</i>	36
5.3. Signal transduction of GPR19	36
5.4. Functional implications for GPR19	37
6. Project definition.....	37
IV. Materials.....	39
1. Devices and accessory	39
2. Software	41
3. Chemicals.....	41
4. Kits, enzymes, and reagents	41
5. Buffers and solutions.....	44
6. Plasmid constructs.....	46
7. DNA oligodeoxynucleotides.....	49
8. Short interfering ribonucleic acids (siRNAs)	50
9. TaqMan® assays.....	50
10. Primary antibodies.....	51
11. Cell lines	52
12. Animals.....	52

V. Methods	53
1. Molecular biology and biochemistry (<i>in vitro</i> analyses)	53
1.1. Nucleic acid reconstitution	53
1.2. Nucleic acid concentration measurement – NanoDrop™	53
1.3. Isolation of total RNA from cultured cells	53
1.4. Complementary-deoxyribonucleic acid (cDNA) synthesis	54
1.5. Reverse transcription quantitative real-time polymerase chain reaction (RT-qPCR) gene expression and data analysis	54
1.6. Preparation of bacterial culture plates (selective medium)	55
1.7. Bacterial transformation	55
1.8. Bacteria culture	56
1.9. Bacteria glycerol stock	56
1.10. Plasmid preparation (Maxi Prep)	56
1.11. Plasmid sequencing	57
1.12. Phenol/chloroform/isoamylalcohol (PCI)/chloroform DNA extraction	57
1.13. Isopropanol/sodium acetate/glycogen DNA precipitation	57
1.14. Chromatin immunoprecipitation (ChIP)	58
1.15. Chromatin fragmentation control	59
1.16. ChIP PCR	59
1.17. Agarose gel electrophoresis of nucleic acids	59
1.18. Microarray sample preparation	60
1.19. Cell lysis for protein extraction	60
1.20. Protein concentration determination	62
1.21. Sodium dodecyl sulfate (SDS)-polyacrylamide gel electrophoresis (PAGE)	62
1.22. Immunoblotting (Western Blot)	62
1.23. Luciferase reporter assay	63
1.24. Antiserum purification on affinity peptide columns	63
2. Cellular biology (<i>in vivo</i> analyses)	64
2.1. Antiserum generation against human GPR19	64
2.2. Cell culture	64
2.3. Freezing of cells	64
2.4. siRNA transfection (96 well culture plate)	65
2.5. Forward plasmid transfection (6 well culture plate)	65
2.6. Reverse plasmid transfection (8 well chamber slide)	65
2.7. Electroporation	66
2.8. Cell cycle arrest (synchronization)	66
2.9. Flow cytometry – cell cycle analysis	66
2.10. Flow cytometry – transfection optimization	67
2.11. Proliferation – alamarBlue®	67
2.12. Proliferation – confluence	67
2.13. Immunofluorescence labeling	67
2.14. High content screening (HCS)	68
2.15. Confocal microscopy	70
2.16. Phase contrast microscopy	71
2.17. Adenylyl cyclase/cyclic adenosine monophosphate (cAMP) assay	71
3. <i>In silico</i> analyses	72
3.1. Phylogenetic analysis	72
3.2. Microarray gene expression analysis and hierarchical clustering (heat map)	73
3.3. Gene expression profiling (databases)	73
3.4. Copy number analysis	74
3.5. Statistical data analysis	74
VI. Results	75
1. Phylogenetic analyses of G protein-coupled receptor 19 (GPR19)	75
1.1. Orthologs	75

1.2. Paralogs	77
2. Method development	80
2.1. Reference gene selection	80
2.2. Selection of <i>Gpr19</i> -targeting siRNAs.....	83
2.3. GPR19 antiserum validation.....	88
3. <i>Gpr19</i> gene expression.....	93
3.1. <i>Gpr19</i> mRNA levels are high in SCLC patient samples.....	93
3.2. <i>Gpr19</i> is overexpressed in SCLC and pancreas islet cell carcinoma.....	95
3.3. <i>Gpr19</i> mRNA expression is high in SCLC cell lines.....	99
4. GPR19 localizes to the cytoplasmic membrane	103
5. Proliferation.....	105
5.1. RNA interference-mediated knockdown of <i>Gpr19</i> reduces cell proliferation	105
5.2. Poly (adenosine diphosphate (ADP)-ribose) polymerase 1 (PARP1) cleavage reveals apoptosis induction upon <i>Gpr19</i> knockdown	113
5.3. Transient GPR19 overexpression does not influence cell proliferation.....	114
6. G protein coupling of GPR19.....	118
6.1. GPR19 does not couple to a pertussis toxin-sensitive G protein	118
7. Cell cycle effects of GPR19	121
7.1. The relative number of cells in gap 2 (G2)/mitosis (M) phase increases upon <i>Gpr19</i> knockdown (flow cytometry)	121
7.2. The relative number of cells in G2/M phase increases upon <i>Gpr19</i> knockdown (high content screening).....	123
7.3. Cells show increased levels of cyclin B1 and phosphorylated histone H3 upon <i>Gpr19</i> knockdown.....	125
7.4. Cells show impairments in cell division upon <i>Gpr19</i> knockdown	128
7.5. High content screening data support inhibited proliferation upon <i>Gpr19</i> knockdown.....	128
7.6. The distribution of cells in different phases of the cell cycle is unaltered upon transient GPR19 overexpression	130
8. Cell cycle-dependent expression of <i>Gpr19</i> mRNA.....	133
8.1. <i>Gpr19</i> mRNA expression peaks during S phase.....	133
8.2. Relative <i>Gpr19</i> mRNA levels correlate with the amount of cells in S phase	140
9. <i>Gpr19</i> gene regulation	141
9.1. <i>In silico</i> analysis of the <i>Gpr19</i> promoter reveals E2 promoter binding factor (E2F) binding	141
9.2. Chromatin immunoprecipitation (ChIP) determines the recruitment of transcription factors E2F-1, E2F-2, E2F-3, and E2F-4 to the <i>Gpr19</i> promoter	142
9.3. Both E2F binding sites at positions -15 and -185 of the <i>Gpr19</i> promoter are crucial for luciferase reporter gene expression	144
9.4. The expression levels of <i>E2f-1</i> , <i>E2f-2</i> , and <i>E2f-3</i> are increased in SCLC patient samples relative to normal lung controls.....	145
VII. Discussion	148
1. G protein-coupled receptor 19 (GPR19) – an exceptional GPCR difficult to pigeonhole	148
2. High <i>Gpr19</i> mRNA expression is associated with malignant diseases	150
3. GPR19 is involved in proliferation and cell cycle regulation	152
3.1. GPR19 contributes to cell proliferation in human lung cancer-derived cell lines....	152
3.2. GPR19 plays a role during cell cycle progression in gap 2 (G2)/mitosis (M) phase and is the first GPCR to show differential mRNA expression over the course of the cell cycle.....	153

3.3. Overexpression of GPR19 influences neither proliferation nor cell cycle progression.....	157
4. E2 promoter binding factor (E2F) family members might regulate <i>Gpr19</i> gene expression in human lung cancer-derived cell lines.....	159
5. GPR19 might exhibit different functional characteristics in the central nervous system than in lung cancer.....	163
6. GPR19 ligand engagement and G protein coupling remain elusive.....	164
7. GPR19 – a receptor applicable for targeted cancer therapy	165
8. Summary	166
VIII. Appendix.....	167
1. <i>Gpr19</i> genomic sequence	167
2. <i>Gpr19</i> messenger ribonucleic acid (mRNA) sequence	168
3. <i>Gpr19</i> codon-optimized coding sequence (mRNA)	169
4. GPR19 protein sequence	170
5. <i>Gpr19</i> promoter sequence	171
IX. References	172
Curriculum Vitae	189

Abbreviations

2/3D	2/3-dimensional	CCPA	2-chloro-N ⁶ -cyclopentyl-adenosine
5-HT2A	serotonin 2A receptor	CCR2	CC chemokine receptor 2
7TM	seven transmembrane	CD95	cluster of differentiation 95
Barr	β-arrestin(s)	CDC6/20/25	cell division cycle 6/20/25
A1R	A1-adenosine receptor	CDK(1/2/4/6)	cyclin-dependent kinase (1/2/4/6)
ABL1	Abelson murine leukemia viral oncogene homolog 1	CDKN1B/2A	cyclin-dependent kinase inhibitor 1B/2A
AC	adenylyl cyclase	cDNA	complementary-deoxyribonucleic acid
ACh	acetylcholine	CDS	coding sequence
ACTB	β-actin	CELSR3	cadherin, epidermal growth factor laminin A G-type seven-pass receptor 3
ADA	adenosine deaminase	cfu	colony forming unit(s)
ADP	adenosine diphosphate	cGMP	cyclic guanosine monophosphate
AJCC	American Joint Committee on Cancer	ChIP	chromatin immunoprecipitation
ALL	acute lymphoblastic leukemia	CHK(1/2)	checkpoint kinase (1/2)
AMP	adenosine monophosphate	CHRM3	muscarinic cholinergic receptor 3
ANOVA	analysis of variance	CKI	cyclin-dependent kinase inhibitor
AP2	adaptor protein complex 2	CM	conditioned medium/-a
APC/C	anaphase-promoting complex/cyclosome	CML	chronic myeloid leukemia
ASK1	apoptosis signaling kinase 1	CMV	cytomegalovirus
AT1R	angiotensin type 1 receptor	CNS	central nervous system
ATCC	American Type Culture Collection	COS	CV-1 origin, SV40-immortalized
ATM	Ataxia telangiectasia mutated	CPM	count(s) per minute
ATP	adenosine triphosphate	Cq	quantification cycle(s)
ATR	Ataxia telangiectasia and RAD3-related	CRE(B/M)	cAMP-responsive element (binding protein/modulator)
B-Raf	rapidly accelerated fibrosarcoma isoform B	CRH(R1)	corticotrophin-releasing hormone (receptor 1)
B2M	β-2-microglobulin	CXCL12	CXC chemokine ligand 12
Bcl-2	B-cell lymphoma-leukemia gene 2	CXCR2/3/4/7	CXC chemokine receptor 2/3/4/7
BCR	breakpoint cluster region	CYPA	cyclophilin A
BEGM	bronchial epithelial cell growth medium	DAPI	4',6-diamidino-2-phenylindole
BLAST	basic local alignment search tool	DDM	doublet discrimination mechanism
bp	base pair(s)	DEPC	diethyl pyrocarbonate
BRCA1/2	breast cancer 1/2	DLP	discs large protein (<i>Drosophila</i>)
BSA	bovine serum albumin	DMEM	Dulbecco's modified eagle's medium
C-terminus	carboxy-terminus	DMSO	dimethyl sulphoxide
CAF	cancer-associated fibroblast	DNA	deoxyribonucleic acid
CAK	cyclin-dependent kinase activating kinase	dNTP	deoxyribonucleoside triphosphate
cAMP	cyclic adenosine monophosphate	Dox	doxorubicin
CBP	CREB-binding protein	DP(1/2/3/4)	dimerization partner (1/2/3/4)
CCL2	CC chemokine ligand 2		
CCNB1	cyclin B1		
CCNE1	cyclin E1		

Abbreviations

DPBS	Dulbecco's phosphate-buffered saline	GPCR	G protein-coupled receptor
DRD2	dopamine receptor D2	GPR6/19/30/87/110/158/173	G protein-coupled receptor 6/19/30/87/110/158/173
dTdT	double deoxythymidine triphosphate	GPS	G protein-coupled receptor proteolytic site
DTT	dithiothreitol	GRAFS	glutamate – rhodopsin – adhesion – frizzled/taste2 – secretin
dUMP	deoxyuridine monophosphate	GRK(5)	G protein-coupled receptor kinase (5)
dUTP	deoxyuridine triphosphate	GRM2/8	metabotropic glutamate receptor 2/8
E -cadherin	epithelial cadherin	GRPR	gastrin-releasing peptide receptor
e.g.	<i>exempli gratia</i> (for instance)	GTP	guanosine triphosphate
E2F	E2 promoter binding factor	GTPase	guanosine triphosphatase
ECACC	European Collection of Cell Cultures	HBSS	Hank's balanced salt solution
EDTA	ethylenediaminetetraacetic acid	HCS	high content screen(ing)
EGF(R)	epidermal growth factor (receptor)	HDAC(4/5)	histone deacetylase (4/5)
eGFP	enhanced green fluorescent protein	HEK	human embryonic kidney
EL	extracellular loop	HeLa	Henrietta Lacks (name of deceased patient)
EMEM	Eagle's minimum essential cell growth medium	HEPES	N-2-hydroxyethylpiperazine-N'-2-ethanesulfonic acid
ERK	extracellular signal-regulated kinase	HER2	human epidermal growth factor receptor 2
ERM	ezrin/radixin/moesin	hESC	human embryonic stem cell(s)
<i>et al.</i> , <i>et cetera</i> (and so forth)	<i>et alii</i> (and others) <i>et cetera</i> (and so forth)	HMVEC	human microvascular endothelial cell
EU	European Union	HPLC	high performance liquid chromatography
eYFP	enhanced yellow fluorescent protein	HPRT1	hypoxanthine-guanine phosphoribosyltransferase 1
FAM TM	6-carboxyfluorescein	HRP	horseradish peroxidase
FBS	fetal bovine serum	<i>i.e.</i>	<i>id est</i> (that ist)
FGF	fibroblast growth factor	ID	identification number
FL1/2(-A/H/W)	fluorescence channel 1/2 (-area/height/width)	Ig(G(1/2b))	immunoglobulin (G(1/2b))
fow	forward (primer)	IGF-I(R)	insulin-like growth factor-I (receptor)
G0 /1/2 (phase)	gap 0/1/2 (phase)	IL	intracellular loop
GABA-B-R1/2	gamma-aminobutyric acid type B receptor 1/2	INK4(A/B/C/D)	inhibitor(s) of CDK4(A/B/C/D)
GAP	GTPase-activating protein	IP-10	interferon- γ -inducible protein of 10 kDa
GAPDH	glyceraldehyde-3-phosphate dehydrogenase	IP3	inositol-1,4,5-trisphosphate
GDI	guanine nucleotide dissociation inhibitor	JAK	janus kinase
GDP	guanosine diphosphate	JNK3	Jun amino-terminal kinase 3
GEF	guanine nucleotide exchange factor	kb	kilobase(s)
GIP	G protein-coupled receptor-interacting protein	kDa	kilodalton(s)
GIRK	G protein-coupled inward rectifier potassium	KS	Kolmogorov-Smirnov
GLAD	gain and loss analysis of DNA	KSHV	Kaposi's sarcoma-associated herpesvirus
Glyc	glycosylation		
GO	Gene Ontology		

Abbreviations

LB	Luria Bertani	PARP1	poly (ADP-ribose)
LCNEC	large cell neuroendocrine carcinoma	PBD	polo-box domain
LPA(R1)	lysophosphatidic acid (receptor 1)	PCA	principal component analysis
LSM	laser scanning microscope	PCI	phenol/chloroform/ isoamylalcohol
M (phase)	mitosis (phase)	PCR	polymerase chain reaction
MA	minus-average	PDE	phosphodiesterase
MAP(K)	mitogen-activated protein (kinase)	PDZ	PSD-95/DLG/ZO-1
MDS	multidimensional scaling	pH3	phosphorylated histone H3
MEK	MAP/ERK kinase	PI3K	phosphatidylinositol 3-kinase
MGB	minor groove binder	PIP2	phosphatidylinositol-4,5- bisphosphate
mGluR2	metabotropic glutamate receptor 2	PK(A/B/C)	protein kinase (A/B/C)
MHC	major histocompatibility complex	PLCβ	phospholipase C β
MIG	monokine induced by interferon- γ	PLK(1/2/3/4)	polo-like kinase (1/2/3/4)
MIQE	minimum information for publication of quantitative real-time PCR experiments	POU	Pit1/Oct2/unc-86
MPF	maturation-promoting factor	PPIA	peptidylprolyl isomerase A
mRNA	messenger ribonucleic acid	PSD-95	postsynaptic density protein 95
mTOR	mammalian target of rapamycin	PSGR	prostate-specific G protein-coupled receptor
MVB	multivesicular body	PTX	pertussis toxin
Myc	myelocytomatosis oncogene	PVDF	polyvinylidene fluoride
MYT1	membrane-associated Tyr/Thr kinase 1	qPCR	quantitative polymerase chain reaction
N-cadherin	neural cadherin	R-PIA	(-)-N ⁶ -(2-phenylisopropyl)-adenosine
N-terminus	amino-terminus	Raf	rapidly accelerated fibrosarcoma
na	not assessed	RAMP1/2/3	receptor activity-modifying protein 1/2/3
NAD	nicotinamide adenine dinucleotide	Ras	rat sarcoma
NCAM	neural cell adhesion molecule	RB(1)	retinoblastoma(-associated protein 1)
NCBI	National Center for Biotechnology Information	rev	reverse (primer)
NCI	National Cancer Institute	RGS	regulator(s) of G protein signaling
NFQ	non-fluorescent quencher	Rho(A)	Ras-homology (A)
NGF	nerve growth factor	RIPA	radio immunoprecipitation assay
NMB-R	neuromedin B receptor	RISC	RNA-induced silencing complex
NSCLC	non-small cell lung cancer	RMA	robust multichip average
OD	optical density	RNA	ribonucleic acid
oligo-dT	oligo-deoxythymidine triphosphate	RNase (A/H/H+/P)	ribonuclease (A/H/H+/P)
ORF	open reading frame	ROCK	Rho-associated coiled-coil-containing protein kinase
p107	retinoblastoma-like protein 1	RPL32	ribosomal protein L32
p130	retinoblastoma-like protein 2	RPLP0	large ribosomal protein P0
p70S6K	ribosomal protein S6 kinase	rpm	rounds per minute
p75^{NTR}	p75 neurotrophin receptor	RPMI 1640	Roswell Park Memorial Institute 1640 medium
PAGE	polyacrylamide gel electrophoresis		
PAR	protease-activated receptor		

Abbreviations

RT-qPCR	reverse transcription quantitative real-time polymerase chain reaction	TFR	transferrin receptor
		TG	tris/glycine
		TGF- β	transforming growth factor β
		tGFP	turbo green fluorescent protein
S (phase)	(DNA) synthesis (phase)	TK	thymidine kinase
S1PR1	sphingosine-1-phosphate receptor 1	TM	transmembrane
SCLC	small cell lung cancer	TNM	tumor, lymph node, metastasis
SDS	sodium dodecyl sulfate	TP53	tumor protein 53
SIFT	Sorting Intolerant From Tolerant	TrkA	tropomyosin-related kinase A
siRNA	small interfering ribonucleic acid	tRNA	transfer ribonucleic acid
		TSH	thyroid-stimulating hormone
SMART	Simple Modular Architecture Research Tool	UCSC	University of California, Santa Cruz
SNP	single nucleotide polymorphism	UNG	uracil-N-glycosylase
		Untr	untreated
SOC	super optimal broth with catabolic repressor	VEGF	vascular endothelial growth factor
Src	Rous sarcoma virus oncogene	VICTM	(trademark)
STAT	signal transducer and activator of transcription	WEE1	Wee1-like kinase
SV40	Simian Virus 40	WGA	wheat germ agglutinin
TAMRA	tetramethylrhodamine	WHO	World Health Organization
TAS2R31	taste receptor type 2 member 31	Wnt	wingless – int-1
TBS	tris-buffered saline	ZO-1	zonula occludens protein 1

Amino acids:

Alanine (Ala; **A**)
 Arginine (Arg; **R**)
 Asparagine (Asn; **N**)
 Aspartic acid (Asp; **D**)
 Cysteine (Cys; **C**)
 Glutamic acid (Glu; **E**)
 Glutamine (Gln; **Q**)
 Glycine (Gly; **G**)
 Histidine (His; **H**)
 Isoleucine (Ile; **I**)
 Leucine (Leu; **L**)
 Lysine (Lys; **K**)
 Methionine (Met; **M**)
 Phenylalanine (Phe; **F**)
 Proline (Pro; **P**)
 Serine (Ser; **S**)
 Threonine (Thr; **T**)
 Tryptophan (Trp; **W**)
 Tyrosine (Tyr; **Y**)
 Valine (Val; **V**)

Bases:

Adenine (**A**)
 Cytosine (**C**)
 Guanine (**G**)
 Thymine (**T**)
 Uracil (**U**)

Note: According to the HUGO Gene Nomenclature Committee (HGNC), genes are written in italics (<http://www.genenames.org/hgnc-guidelines>). For visualization reasons, only the first letter in abbreviated genes is an upper-case letter (e.g., *Gpr19*). In contrast, the gene product is not written in italics (e.g., GPR19). Labels in figures do not follow this rule.

Abbreviations are introduced in each chapter.

I. Abstract

G protein-coupled receptors (GPCRs) represent the largest family of cell surface receptors. However, only a fraction of the more than 800 receptors have been characterized to an extent that their physiological role is reasonably well understood. In fact, current pharmacotherapy only addresses some 60 receptors with a large collection of compounds that represent about 30% of the available drugs.

It has long been known that GPCRs are subject to illegitimate expression in cancer cells. Presumably, hijacking the normal physiological functions of GPCRs contributes to all biological capabilities acquired during the multistep development of human cancers. With the goal of linking G protein-coupled receptors to malignant diseases, GPCRs were searched for that revealed high expression levels in small cell lung cancer (SCLC): The mRNA encoding orphan G protein-coupled receptor 19 (GPR19) was found to be frequently overexpressed in tissue samples obtained from patients with SCLC in contrast to samples derived from non-SCLC or normal lung.

Several observations indicate that overexpression of *Gpr19* confers a specific advantage to human lung cancer-derived cells regarding the transition through the cell cycle. Knockdown of *Gpr19* mRNA by RNA interference reduced cell growth of human lung cancer cell lines and led to cell death. Cell cycle progression through G2/M phase was impaired and this was associated with increased protein levels of cyclin B1 and phosphorylated histone H3.

Gpr19 exhibited a cell cycle-dependent expression pattern in lung cancer cell lines. When cell cycle distribution profiles of cells released from cell cycle arrest were related to *Gpr19* mRNA levels, a peak *Gpr19* expression was detected during S phase.

The control of *Gpr19* expression by E2F transcription factors, which drive gene expression of many genes important for cell cycle progression, was verified by chromatin immunoprecipitation: Antibodies directed against E2F-1 to E2F-4 allowed for the recovery of the *Gpr19* promoter in lung cancer-derived cell lines. E2F binding site deletion in the *Gpr19* promoter resulted in diminished luciferase reporter gene expression.

This is the first example of a G protein-coupled receptor showing cell cycle phase-specific mRNA expression. Further results point to a functional link between the cell cycle-dependent expression of *Gpr19*, a correct cell cycle passage, and cellular proliferation in human lung cancer-derived cells that exhibit higher than normal basal levels of *Gpr19* mRNA. Hence, the data also validate GPR19 as a candidate target when overexpressed in lung cancer.

II. Zusammenfassung

G Protein-gekoppelte Rezeptoren (GPCRs) stellen die größte Familie zellulärer Oberflächenrezeptoren dar. Jedoch sind nur ein Teil der mehr als 800 Rezeptoren in solchem Ausmaß charakterisiert, dass deren physiologische Rolle gut verstanden wird. Tatsächlich werden in der heutigen Pharmakotherapie lediglich etwa 60 Vertreter dieser Rezeptoren mit einer Vielzahl von Substanzen angegriffen, welche etwa 30% aller verfügbaren Medikamente ausmachen.

Es ist schon lange bekannt, dass GPCRs eine ungewöhnliche Expression in Krebszellen aufweisen können. An vielen Stellen der Karzinogenese tragen sonst normale, physiologische Funktionen von GPCRs mutmaßlich zur Krebsprogression bei, wenn diese unkontrolliert und missbräuchlich in einer Zelle verwendet werden.

Das Hauptziel dieser Arbeit besteht darin, GPCRs vermehrt in Bezug zu malignen Erkrankungen zu stellen. Konkret wurde nach GPCRs gesucht, die eine hohe Expression im kleinzelligen Lungenkarzinom aufweisen. Hierbei zeigte sich, dass die den G Protein-gekoppelten Rezeptor 19 (GPR19) kodierende mRNA in Proben von Patienten mit kleinzelligem Lungenkarzinom verglichen mit Proben anderer Lungenkarzinome und von untransformiertem Lungengewebe überexprimiert war.

Desweiteren deuten einige Beobachtungen darauf hin, dass eine *Gpr19* Überexpression in von humanen Lungenkarzinomen abgeleiteten Zelllinien diesen einen spezifischen Vorteil im Durchschreiten des Zellzykluses bietet. Die Abschwächung der *Gpr19* Genexpression mittels RNA Interferenz hemmte Lungenkarzinomzelllinien in ihrer Proliferation und führte letztlich zu deren Zelltod. Das Fortschreiten des Zellzykluses über die G2/M Phase hinweg war gestört, was mit einer erhöhten Präsenz an für diese Phasen charakteristischen Proteinmarkern (Zyclin B1, phosphoryliertes Histon H3) einherging.

In den untersuchten Lungenkarzinomzelllinien war die Expression der *Gpr19* mRNA abhängig vom Zellzyklus. Nachdem die Zellen in verschiedenen Phasen des Zellzykluses zunächst angehalten und danach aus dem Arrest entlassen wurden, konnte ein Höchststand der *Gpr19* Expression während der S Phase konstatiert werden.

Zudem zeigte sich mit Hilfe von Chromatin-Immunpräzipitation, dass die *Gpr19* mRNA Expression in diesen Zelllinien anscheinend unter der Kontrolle von Transkriptionsfaktoren der E2F Familie steht. Mitglieder dieser Familie sind bekannt dafür, dass sie die Genexpression vieler am Zellzyklus beteiligter Gene kontrollieren. So konnte die *Gpr19* Promotorregion bei der Anwendung von gegen E2F-1 bis 4 gerichteten Antikörpern nachgewiesen werden. Und die Zerstörung mutmaßlicher E2F Bindestellen in der *Gpr19* Promotorregion schwächte die Expression eines Luciferase Reporterkonstrukts ab.

Diese Arbeit offenbart zum ersten Mal die vom Zellzyklus abhängige mRNA Expression eines Vertreters der GPCR Familie, GPR19. Desweiteren stellt sie eine funktionelle Verbindung zwischen dieser differentiellen Expression, einem ungehinderten Durchschreiten des Zellzykluses und der Proliferation von humanen Lungenkarzinomzelllinien her, wenn diese eine erhöhte *Gpr19* Grundexpression aufweisen. Folglich validieren diese Daten GPR19 als mögliches Angriffsmolekül bei einer Überexpression im Lungenkarzinom.

III. Introduction

1. Cancer – a highly diverse disease

Cancer is a general term used for diseases in which abnormal cells of the human body divide in an uncontrolled manner and are able to infiltrate healthy tissues – which can eventually lead to death. According to the World Health Organization (WHO), cancer is one of the major causes of deaths worldwide and its incidence rises with age¹. Dozens of different cancer types exist and they are classified according to their tissue/organ or cell type of origin. Most cancers are grouped as **carcinoma** (derived from epithelia; accounting for 80 to 90% of all cancers), **sarcoma** (derived from cells of mesodermal origin like supportive or connective tissues such as bone, cartilage, fat, muscle, or blood vessels), **leukemia** (originating in blood-forming tissue such as the bone marrow), **lymphoma** (derived from lymphatic tissue), **myeloma** (derived from plasma cells of the bone marrow), or **central nervous system (CNS) cancers** (derived from neuronal cells). Except for leukemias, cancer is usually characterized by the formation of solid tumors. They are grouped into **benign tumors** (non-cancerous; non-invasive) and **malignant tumors** (cancerous; potential to invade nearby tissues and metastasize to distant organs)^{2,3}.

Predictions expect 1,283,101 deaths from cancer in the European Union (EU) in 2012 split up into 717,398 men and 565,703 women. This corresponds to standardized rates of 1,387/1 x 10⁶ (men) and 847/1 x 10⁶ (women). Yet, cancer rates in general decline due to improved diagnostic and treatment options (Malvezzi M *et al.*, 2012). The predominant **treatment options** for cancer include surgery, radiation therapy, chemotherapy, (anti-)hormone therapy, and biological therapy (e.g., targeted therapy with antibodies; American Cancer Society, 2012, p.1).

Cancer is predominantly a genetic disease. The multi-stage model of carcinogenesis describes the initial genetic mutation (e.g., in growth-regulatory genes) causing the pre-malignant transformation of a cell (**initiation**) followed by the proliferation of initiated cells (**promotion**) finally leading to tumor formation and autonomous growth (**progression**; Tsao AS *et al.*, 2004; Puntoni M and Decensi A, 2009). Genetic mutations can occur spontaneously, for instance through deoxyribonucleic acid (DNA) replication errors or impairments in DNA damage recognition and/or repair. However, the major causes for a normal cell to become malignantly transformed are **environment-related**. This includes effects of **chemical carcinogens** (e.g., aromatic hydrocarbons, nitrosamines, or aromatic amines) often related to tobacco smoking and daily diet, ultraviolet or ionizing radiation (**physical carcinogenesis**), and tumor viruses (e.g., Epstein-Barr virus, Hepatitis B virus, Human Papillomavirus; **biological carcinogenesis**; Hoppe-Seyler F and Hoppe-Seyler K, 2011). On the other hand, there are also **genetically inherited causes of cancer** proven by hereditary cancer syndromes such as Retinoblastoma, Ataxia telangiectasia (increased risk for leukemia

¹ www.who.int/mediacentre/factsheets/fs297/en/

² www.cancer.gov/cancertopics/cancerlibrary/what-is-cancer

³ training.seer.cancer.gov/disease/categories/classification.html

or breast cancer) or Familial Adenomatous Polyposis (colon adenomas; Ganjavi H and Malkin D, 2002). Furthermore, endogenous hormones often act as promoters by providing a growth stimulus to transformed cells, *i.e.*, to cells that have accumulated mutations caused by initiating agents (Clayton PE *et al.*, 2011).

1.1. Fundamental characteristics of cancer

The development of human cancers is usually a multistep process from the acquisition of genetic defects (e.g., mutations, translocations, amplifications) or epigenetic aberrations (e.g., chromatin remodeling) in a normal cell until the establishment of a malignant phenotype (Croce CM, 2008). During the course of this process, cancer cells need to acquire some critical capabilities in order to successfully proliferate and survive (figure 1). These capabilities are described as the hallmarks of cancer by Hanahan and Weinberg and very often result from the loss of function of tumor suppressor genes and the gain of function of oncogenes (Hanahan D and Weinberg RA, 2011). Additionally, the deregulation of micro-ribonucleic acid (RNA) genes, which do not encode proteins but whose RNA products regulate gene expression by RNA interference, can also contribute to cancer formation (Croce CM, 2008).

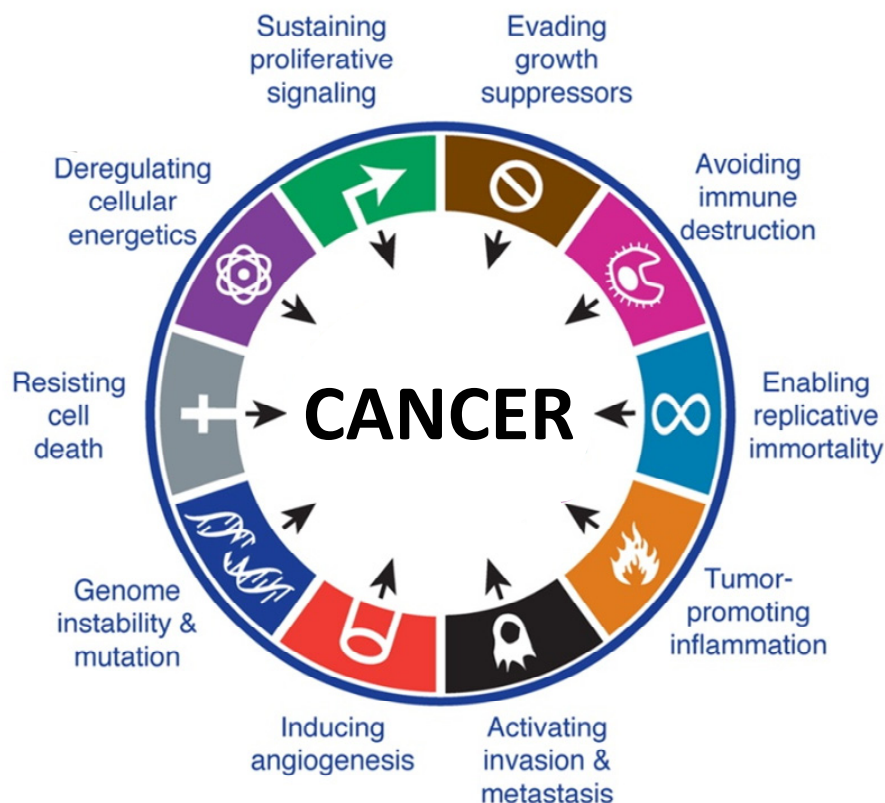


Figure 1: Ten capabilities are of key importance for cancers to successfully proliferate and survive. Among them are eight hallmarks of cancer (resisting cell death; deregulating cellular energetics; sustaining proliferative signaling; evading growth suppressors; avoiding immune destruction; enabling replicative immortality; activating invasion and metastasis; inducing angiogenesis) and two enabling characteristics providing the underlying rationale for these hallmarks (genome instability and mutation; tumor-promoting inflammation). The figure is adapted from Hanahan D and Weinberg RA, 2011.

Cancer cells must continuously enter into and progress through the cell cycle (**sustaining proliferative signaling**) which is often achieved by the activation of growth factor-induced signaling pathways (Lemmon MA and Schlessinger J, 2010; Witsch E *et al.*, 2010). Either growth factors and their cognate receptors or downstream effectors (e.g., oncogenes which, for example, encode the small guanosine triphosphatase (GTPase) Ras (*rat sarcoma*) or the transcription factor Myc (*myelocytomatosis oncogene*)) in respective signaling pathways are altered (Davies MA and Samuels Y, 2010; Larsson LG and Henriksson MA, 2010; Pylayeva-Gupta Y *et al.*, 2011). Further, cancer cells need to become insensitive to growth-preventing mechanisms (**evading growth suppressors**). The inactivation of cell cycle regulators such as the tumor suppressors retinoblastoma-associated protein 1 (RB1) and/or tumor protein 53 (TP53) is therefore pursued by many different cancers (Chen HZ *et al.*, 2009; Suzuki K and Matsubara H, 2011). Besides, cellular growth inhibition mediated by cell-cell contacts in normal tissues is also often abrogated in cancer cells (Liu Y and Dean DC, 2010).

Another important characteristic of cancer cells is their potential to avoid apoptosis (**resisting cell death**). Damaged cells are normally removed from the pool of cells in a tissue by programmed cell death. However, cancer cells counteract apoptosis-inducing mechanisms frequently by inactivation of TP53 or by shifting the balance between pro- (e.g., Bax and Bak) and anti-apoptotic factors (e.g., B-cell lymphoma-leukemia gene 2 (Bcl-2)) in favor of survival (Hanahan D and Weinberg RA, 2011). The insensitivity to death-receptor-mediated signaling (e.g., via cluster of differentiation 95 (CD95)/Fas) is also employed to resist apoptosis (Carey GB *et al.*, 2000).

In order to proliferate and produce a vast number of malignantly transformed cells, cancer cells must show unlimited replicative potential (**enabling replicative immortality**). Normal cells eventually enter a state of viable senescence as their number of cell divisions is finite. This is largely due to the shrinkage of telomeric sequences at the chromosome ends upon chromosomal duplication. Hence, cancer cells counteract the shrinkage of telomeres and therefore the induction of senescence mostly by the upregulation of telomerase expression (Chen CH and Chen RJ, 2011).

Tumors ensure their supply with nutrients and oxygen by the formation of a tumor-associated neovasculature (**inducing angiogenesis**) once this supply can no longer be maintained simply by diffusion. They cause existing capillaries to sprout new blood vessels in direction of the tumor. The most important pro-angiogenic regulators – often secreted by cancer cells – include vascular endothelial growth factor (VEGF), fibroblast growth factor (FGF), and nitric oxide (Ziche M and Morbidelli L, 2009).

Cancer cells frequently show the ability to disseminate from their original site of growth and to colonize different tissues/organ sites (**activating invasion and metastasis**). This multistep process starts with evasion from the primary tumor and invasion of surrounding tissue, intravasation into blood or lymphatic vessels, survival in the circulation, and eventually extravasation, homing to the new tissue/organ site, and the formation of metastases (Nguyen DX *et al.*, 2009). The characteristic changes happening to transformed epithelial cells in order to disseminate and invade tissues can be part of a process referred to as epithelial-to-mesenchymal transition which includes the switch from the expression of the epithelial cell adhesion

molecule E-cadherin towards the mesenchymal counterpart neural (N)-cadherin (Yilmaz M and Christofori G, 2009). Upon formation of micrometastases, this process can be reversed (mesenchymal-to-epithelial transition; Thiery JP and Sleeman JP, 2006). Additionally, extracellular matrix-remodeling enzymes such as matrix-metalloproteinases expressed by cancer cells facilitate their penetration of the basal membrane and adjacent tissues (Hua H *et al.*, 2011).

The energy metabolism of cancer cells can be adjusted in a way that it actively supports uncontrolled growth and proliferation (**deregulating cellular energetics**). It has been shown that cancer cells are able to limit their energy production to glycolysis neglecting further adenosine triphosphate (ATP) generation from pyruvate oxidation in the mitochondria. Hence, they use glycolysis intermediate products for the production of nucleosides and amino acids therefore benefiting energetically when generating macromolecular structures or duplicating their organelles and proteins as a prerequisite for cell division. Besides, their fueling with glucose is often enhanced upon upregulation of glucose transporters (DeBerardinis RJ *et al.*, 2008). Most cancer cells predominantly produce energy by a high rate of glycolysis followed by lactic acid fermentation in the cytosol. In normal cells, however, a rather low rate of glycolysis is followed by oxidation of pyruvate in mitochondria. The molecular process in tumor cells is referred to as the '**Warburg Effect**' also known as aerobic glycolysis. It is an aerobic process (using oxygen), regardless of the oxygen level in the tumor (Koppenol WH *et al.*, 2011).

As cells and tissues are under constant immune surveillance, cancer cells must circumvent their destruction by cells of the immune system (**avoiding immune destruction**). They can achieve this by the secretion of immunosuppressive factors (e.g., transforming growth factor β (TGF- β)) and the attraction of immuno-regulatory cells such as regulatory T cells (Mougiakakos D *et al.*, 2010; Yang L *et al.*, 2010).

The basis for acquiring these hallmarks described above is set by **genome instability and mutation** typically observed in cancer cells. This so-called enabling hallmark successively leads to genomic alterations in neoplastic cells finally conferring a selective advantage over cells with genetic integrity, which results in cell growth and formation of a tumor. Among the many mechanisms that increase the activity of oncogenes and cause the inactivation of tumor suppressor genes are for instance chromosomal aberrations, genomic mutations, and epigenetic events such as DNA or histone modifications (Hanahan D and Weinberg RA, 2011).

Another enabling hallmark is the **tumor-promoting inflammation** by cells of the immune system. Tumor inflammation results in a stroma enriched in signaling molecules that can be exploited by tumor cells to sustain their proliferative response. Inflammatory cells infiltrate the tumor and can release factors that support the growth, proliferation, and invasiveness of cancer cells as well as angiogenesis (Grivennikov SI *et al.*, 2010; Qian BZ and Pollard JW, 2010). Besides, the local concentration of reactive oxygen species can be increased through immune cells therefore favoring mutagenesis in adjacent cancer cells (Grivennikov SI *et al.*, 2010).

The heterogeneity of tumors is further supported by the idea of **cancer stem cells** observed in some tumor types. These cancer cells exhibit a phenotype of self-renewal and give rise to more differentiated daughter cells (Cho RW and Clarke MF, 2008). They may further express markers typical of normal tissue stem cells, be more

resistant to anti-tumor therapy, and account for tumor dormancy leading to the reestablishment of the malignancy after the end of treatment (Hanahan D and Weinberg RA, 2011).

Apart from malignant cells, cells from the tumor stroma contribute significantly to the whole tumor mass. Among them are **cancer-associated fibroblasts (CAFs)** which not only provide a structural framework to the tumor but are further involved in tumor-stroma crosstalk. They can support proliferation, angiogenesis, and tumor invasiveness therefore contributing to features characteristic of cancer (Micke P and Ostman A, 2005; Franco OE *et al.*, 2010).

Some cancers depend on the sustained activity of one or a few genes in order to maintain their malignant phenotype (**oncogene addiction**). Targeting an oncogene might lead to tumor regression and cell death – as observed in human epidermal growth factor receptor 2 (HER2)-amplified breast cancer patients treated with receptor-targeting antibodies like trastuzumab (Herceptin®; Brough R *et al.*, 2011). This phenomenon – interference with the action of a single deregulated oncogene can cause inhibitory effects on proliferation and survival – is exploited by targeted therapy (Weinstein IB and Joe A, 2008). Besides, it is closely related to the concept of **synthetic lethality** which explains the observation that mutations in two genes can lead to cell death whereas mutations in either of the genes alone are compatible with survival. This model can be applied both to activating mutations in oncogenes and inhibitory mutations in tumor suppressors (Nijman SM, 2011). For instance, a synthetically lethal phenotype has been demonstrated for the inhibition of two tumor suppressors involved in DNA repair: breast cancer 1 (BRCA1) or BRCA2 and poly (adenosine diphosphate (ADP)-ribose) polymerase 1 (PARP1; Brough R *et al.*, 2011).

2. Lung cancer

Lung cancer is among the leading causes of cancer-related deaths worldwide and strongly associated with smoking (figure 2). In the EU, lung cancer is predicted to account for 183,592 deaths in men and 78,658 deaths in women in the year 2012 (Malvezzi M *et al.*, 2012). These numbers correspond to a standardized rate of 372/1 x 10⁶ men (26% of total male cancer deaths; lowered by 10% compared to the year 2007) and 134/1 x 10⁶ women (14% of total female cancer deaths; increased by 7% compared to the year 2007). The relative figures for deaths arising from lung cancer are even higher in the United States – here, rates of 29% of total male cancer deaths (87,750 cases) and 26% of total female cancer deaths (72,590 cases) are predicted in 2012 (Siegel R *et al.*, 2012). The most common **symptoms** of lung cancer include chest pain, bloody sputum, cough, dyspnoea, and shortness of breath typically resulting from local compression or invasion of thoracic areas adjacent to the tumor. Primary lung cancers are of epithelial origin (carcinoma; except for malignant mesothelioma arising from the lung pleura) and they are classified into two major groups based on pathological features: **small cell lung cancer (SCLC)** and **non-small cell lung cancer (NSCLC)**.

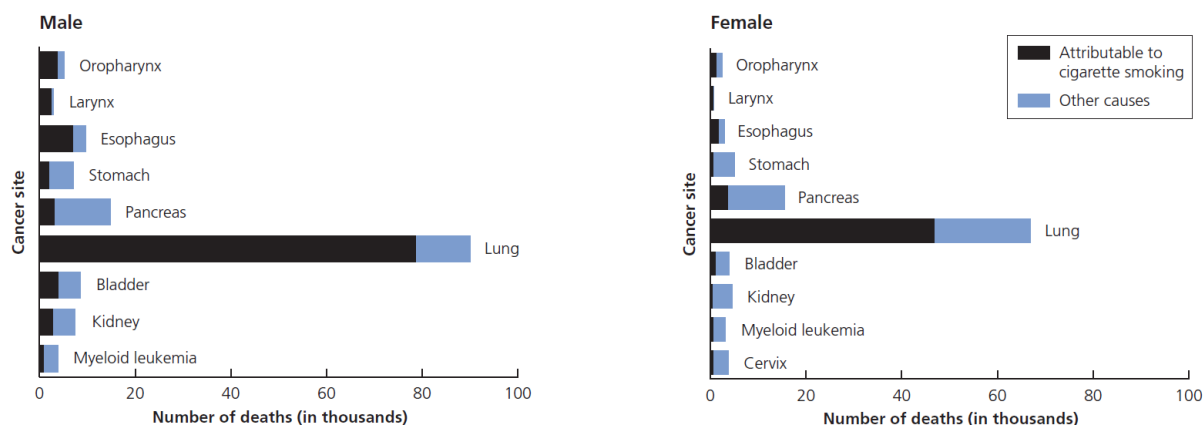


Figure 2: Cigarette smoking is associated with the majority of lung cancer deaths in the United States. Annual numbers (2000 till 2004) of cancer deaths are shown by sex and cancer site/organ (American Cancer Society, 2012, p. 37).

2.1. Small cell lung cancer (SCLC)⁴

SCLC accounts for 20% of all lung cancer cases and the WHO further defines **small cell carcinoma** (70%) and **combined small cell carcinoma** (30%; at least 10% of the tumor is characterized by a NSCLC component; Beasley MB *et al.*, 2005; Rekhtman N, 2010). It is almost exclusively found in smokers and characterized by a very low doubling time and a very aggressive phenotype (Nicholson SA *et al.*, 2002). **Morphological features** include scant cytoplasm, finely granular chromatin, indistinct cell borders, absence of nucleoli, high mitotic rate, large areas of necrosis, and predominantly small cells (smaller than the size of three lymphocytes; Brambilla E *et al.*, 2001; Rekhtman N, 2010).

In **limited-stage** SCLC, the tumor has not spread beyond supraclavicular lymph nodes and the median survival time is 18 to 20 months (five year survival rate of 15 to 25%; Dowell JE, 2010). However, in **extensive-stage** SCLC, the tumor has already spread beyond supraclavicular areas and the median survival time is only 7 to 12 months (five year survival rate of 2%; Jackman DM and Johnson BE, 2005). As SCLC is associated with early dissemination, it has usually established distant metastasis at the time of diagnosis (Jackman DM and Johnson BE, 2005). Preferred sites of metastasis include the brain (50 to 80% of patients), liver, adrenal, bone, and bone marrow (Rekhtman N, 2010). Without treatment, the median survival of SCLC patients is two to four months from the time of diagnosis. It is generally considered as a non-surgical disease but **responsive to chemotherapy** (cisplatinum (adduct formation with DNA) and etoposide (DNA intercalation and topoisomerase II inhibition)) and **radiation therapy** (Rekhtman N, 2010). Despite good initial response rates to first line chemotherapy and radiation therapy, relapse rates or disease progression within one year after treatment are very high (> 80% (estimated); Puglisi M *et al.*, 2010).

⁴ www.cancer.gov/cancertopics/pdq/treatment/small-cell-lung/healthprofessional

2.2. Non-small cell lung cancer (NSCLC)⁵

The most frequent subclasses of NSCLC are **squamous cell carcinoma** (30 to 40%), **adenocarcinoma** (30 to 40%), and **large cell carcinoma** (less than 10%; Beasley MB *et al.*, 2005; Kitamura H *et al.*, 2008). Further WHO-defined subclasses are adenosquamous carcinoma, carcinoma with pleomorphic, sarcomatoid or scromatous elements, carcinoid tumor, carcinoma of salivary gland type, and unclassified carcinoma. The most prominent **morphological characteristics** of NSCLC cells are a large cell size with abundant cytoplasm, prominent nucleoli and cell borders, and a vesicular clumpy chromatin (Rekhtman N, 2010).

A more distinct **staging** system than for SCLC is applied for NSCLC as NSCLC tumors grow more slowly and are less likely to spread to distant body sites: 0 – tumor has not spread beyond the inner lining of the lung; I – tumor has not spread to lymph nodes; II – tumor has spread to nearby lymph nodes; III – tumor has spread to nearby tissue or far away lymph nodes; IV – tumor has spread to other organs such as the brain or liver⁶. The five year survival rate very much depends on the disease stage ranging from 49% (locally confined stage) to 2% (distant spread stage). **Surgery** is usually the treatment option of choice and shows the best curative potential for localized NSCLC.

The correct **classification of lung cancers into SCLC or NSCLC** is crucial for patient treatment and prognosis. However, classification by pathologists is not always unequivocal. In a panel of SCLC-diagnosed specimen, Nicholson and coworkers found 28% of these samples to be misdiagnosed and to also display NSCLC characteristics (Nicholson SA *et al.*, 2002). In further studies, half the patients first diagnosed with SCLC revealed a mixture of NSCLC and SCLC or an exclusive NSCLC phenotype when re-diagnosed after the completion of initial treatment (Abeloff MD *et al.*, 1979; Elliott JA *et al.*, 1987). One possible explanation was the existence of a NSCLC component which had not been diagnosed but was selected due to its inadequate responsiveness towards first line chemotherapy that had been administered to treat the SCLC component.

2.3. The neuroendocrine phenotype of lung cancer

Primary lung neoplasms are often characterized by a neuroendocrine phenotype (25% of all lung cancers). They show histopathological features of neuroendocrine differentiation and stain positive for **neuroendocrine markers**. This neuroendocrine phenotype is characteristic for the vast majority of SCLC but is also observed in a subset of NSCLC (Beasley MB *et al.*, 2005) – large cell neuroendocrine carcinoma (LCNEC; 3% of all lung cancers) are high grade neuroendocrine tumors whereas typical carcinoid (2% of all lung cancers) and atypical carcinoid (0.2% of all lung cancers) are classified as low and intermediate grade neuroendocrine tumors,

⁵ www.cancer.gov/cancertopics/pdq/treatment/non-small-cell-lung/healthprofessional

⁶ www.nlm.nih.gov/medlineplus/ency/article/007194.htm

respectively. In addition, the presence of neuroendocrine markers is revealed in 10 to 20% of all NSCLC cases and they are therefore called NSCLC with neuroendocrine features (Rekhtman N, 2010). Of these markers, either chromogranin A⁷, neuron-specific enolase⁸, synaptophysin⁹, or neural cell adhesion molecule (NCAM) is detected in 75 to 90% of SCLC (Guinee DG Jr *et al.*, 1994; Dowell JE, 2010; Rekhtman N, 2010). Minor neuroendocrine markers found in lung cancers include dopa decarboxylase, calcitonin, gastrin-releasing peptide, neuromedin B, or bombesin receptor subtype 3 (Jackman DM and Johnson BE, 2005; Rekhtman N, 2010).

2.4. Molecular characterization of lung cancer

Apart from the expression of neuroendocrine markers, both SCLC and NSCLC are characterized by several molecular abnormalities and deregulated signal transduction pathways. Genetic alterations are very likely to result from the multitude of carcinogens found as tobacco smoke constituents or their metabolites (Kitamura H *et al.*, 2008). They can cause the **loss of function of tumor suppressor genes or the gain of function of putative oncogenes**.

The vast majority of lung cancers show depletions in the short arm of chromosome three, an area believed harbor multiple tumor suppressor genes such as RASSF1A, a protein supposed to be involved in cell cycle progression from gap 1 (G1) to DNA synthesis (S) phase (Zabarovsky ER *et al.*, 2002). TP53 inactivation is found in 50% of NSCLC and 70 to 100% of SCLC cases and leads to the evasion of cells from cell cycle arrest or apoptosis (Jackman DM and Johnson BE, 2005; Kitamura H *et al.*, 2008; Pleasance ED *et al.*, 2010).

About 30% of all SCLC tumors show an amplification of the regulator of gene transcription **Myc**, which is – however – only rarely observed in NSCLC (Jackman DM and Johnson BE, 2005; Kitamura H *et al.*, 2008). Besides, the protein family of receptor tyrosine kinases has been described to contribute to both SCLC and NSCLC tumorigenesis (Coulson JM *et al.*, 2003). SCLC often shows high expression levels of **c-kit** (Jackman DM and Johnson BE, 2005) and **insulin-like growth factor-I receptor** (IGF-IR). Additionally, an autocrine loop was described by the co-expression of its ligand, insulin-like growth factor-I (IGF-I), which finally initiates the phosphatidylinositol 3-kinase (PI3K) – protein kinase B (PKB) pathway (Fischer B *et al.*, 2007). **Epidermal growth factor receptor** (EGFR) gain-of-function mutations are prevalent in NSCLC (adenocarcinoma) but virtually absent in SCLC. Activation of the EGFR further involves the Ras – Raf (rapidly accelerated fibrosarcoma) – MEK (mitogen-activated protein (MAP)/ERK kinase) – ERK (extracellular signal-regulated kinase) and PI3K-PKB pathways resulting in the stimulation of cell cycle progression and cell motility and in the inhibition of apoptosis (Kitamura H *et al.*, 2008). Ras mutations – however – are

⁷ Chromogranin A is a precursor protein released from secretory granules that – after cleavage – gives rise to bioactive proteins such as pancreastatin, catestatin, and vasostatin I and II (Modlin IM *et al.*, 2010).

⁸ The neuron-specific enolase (γ enolase) converts 2-phospho-D-glycerate into phosphoenolpyruvate and water (www.uniprot.org/uniprot/P09104).

⁹ Synaptophysin is a calcium-binding glycoprotein of presynaptic vesicles (Wiedenmann B *et al.*, 1986).

only rarely found in SCLC (Fischer B *et al.*, 2007). For SCLC, there is evidence for the expression of mitogenic neuropeptides such as gastrin, neurotensin, cholecystokinin, or arginine-vasopressin together with G protein-coupled receptors (GPCRs) to which these peptides bind. These autocrine signaling loops are thought to promote tumor proliferation and progression (Coulson JM *et al.*, 2003).

The RB1 regulatory pathway is among the most frequently deregulated signal transduction pathways in lung cancer. RB1 is the main negative regulator of the E2F promoter binding factor (E2F) family of transcription factors at the G1-S transition of the cell cycle. Hyperphosphorylation of RB1 causes its dissociation from E2Fs leading in turn to the transcription of genes crucial for cell cycle progression. These phosphorylation reactions can be performed by upstream regulators of RB1 such as the cyclin-dependent kinase (CDK)4/cyclin D or CDK6/cyclin D complexes. On the other hand, the cyclin-dependent kinase inhibitor 2A (CDKN2A) can interact with CDK4 and CDK6 therefore preventing their D-type cyclin-mediated activation and the phosphorylation of RB1 (mainly attributed to CDKN2A isoform 1; Wikenheiser-Brokamp KA, 2006; Kitamura H *et al.*, 2008).

SCLC and NSCLC differ in their mode of RB1 pathway deregulation. In many SCLC tumors, RB1 protein function is lost due to *Rb1* gene deletion or inactivating mutations (Jackman DM and Johnson BE, 2005; Kitamura H *et al.*, 2008; Pleasance ED *et al.*, 2010). *Rb1* mutations occur at a frequency comparable to that seen in retinoblastoma which is also characterized by a neuroendocrine phenotype (Wikenheiser-Brokamp KA, 2006). In contrast, mutations in the gene encoding RB1 are only seen in 15 to 30% of NSCLC (Wikenheiser-Brokamp KA, 2006). Besides, a high number of LCNEC (68%) show mutations in *Rb1* therefore reflecting the shared pathological phenotype with SCLC (Beasley MB *et al.*, 2003). Additionally, E2F-1 overexpression occurs in nearly all SCLC tumors and is less prevalent in NSCLC (Wikenheiser-Brokamp KA, 2006; Kitamura H *et al.*, 2008). The same histology-specific expression pattern was observed for E2F-3 (Cooper CS *et al.*, 2006). On the other hand, NSCLC preferentially renders RB1 inactive by hyperphosphorylation as a result of *p16* (CDK4 inhibitor family) gene inactivation (30 to 70% of NSCLC cases) and/or cyclin D1 overexpression (30 to 60% of NSCLC cases) – two events very rarely observed in SCLC (Wikenheiser-Brokamp KA, 2006; Kitamura H *et al.*, 2008).

3. Cell cycle

The mammalian cell cycle is a succession of strictly ordered cellular events that finally lead to the separation of genetically identical daughter cells. It is generally divided into DNA synthesis/chromosomal replication (**S phase**) and separation of sister chromatids (mitosis; **M phase**). Gap phases prior to S (gap 1 phase (**G1**)) and M (gap 2 phase (**G2**)) phases prepare the cell for growth (doubling of cell volume, organelle and protein content), DNA replication and mitosis. Mitosis can be further subdivided into **pro-** (nuclear envelope breakdown; chromosome condensation), **prometa-** (attachment of mitotic spindle to chromosome kinetochore), **meta-** (chromosome alignment in metaphase plate), **ana-** (sister chromatid separation), and **telophase** (chromosome decondensation and mitotic ring ingression) followed by **cytokinesis**

(figure 3; Pines J, 2011). Non-proliferating cells, however, are in a so-called paused state (gap 0 (**G0**) phase) from which they can reenter the active cell cycle.

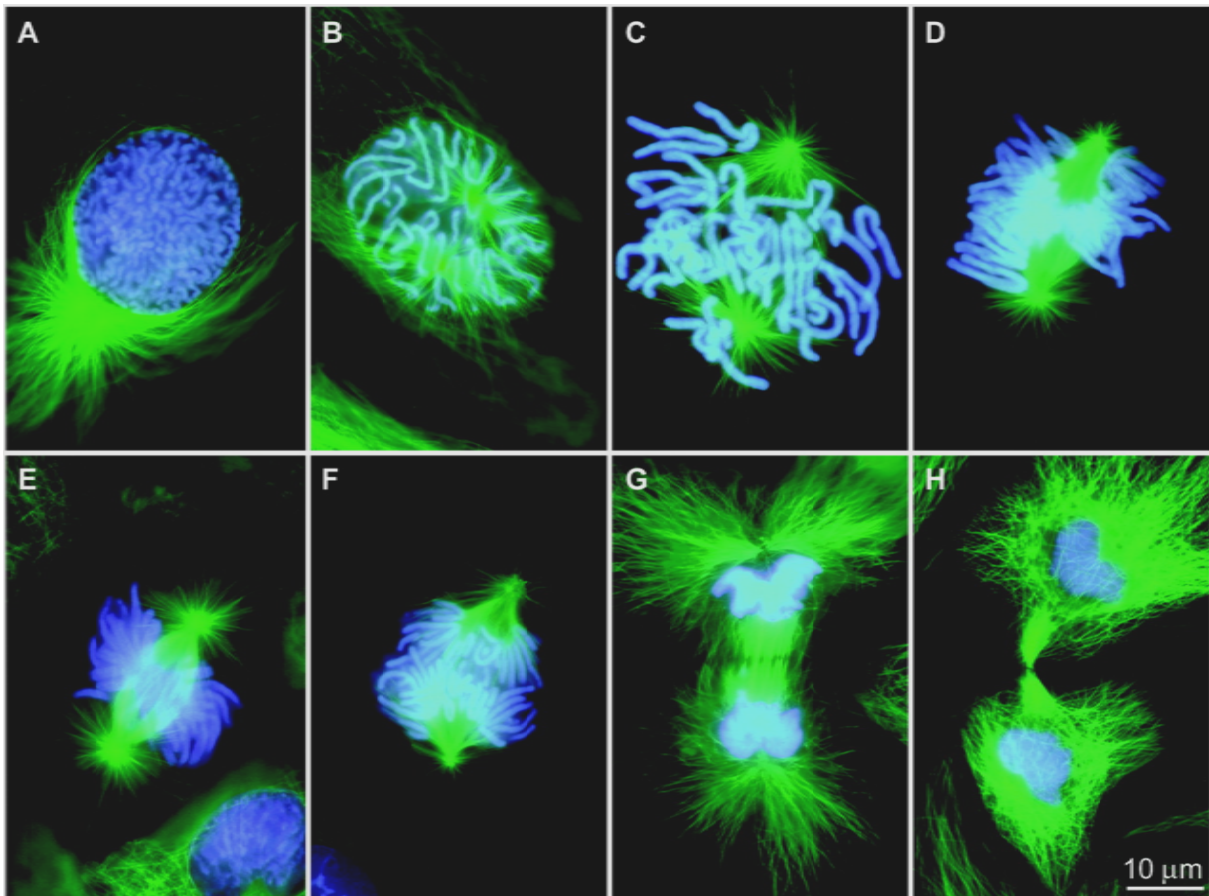


Figure 3: The different phases of mitosis. Shown are immunofluorescence pictures of newt lung cells during early (**A**), mid (**B**), and late (**C**) prophase, prometaphase (**D**), metaphase (**E**), anaphase (**F**), telophase (**G**), and cytokinesis (**H**). Chromosomes (**blue**) condense in prophase and centrosomes with microtubule fibers (**green**) assemble at the poles of the cell. The mitotic spindle attaches to the condensed chromosomes aligned at the metaphase plate during (pro)metaphase. Sister chromatids are segregated from each other in anaphase. Chromosomes decondense in telophase and the separation of the cytoplasm into two cells is performed during cytokinesis. The figure is adapted from Rieder CL and Khodjakov A, 2003.

3.1. Cyclins and cyclin-dependent kinases (CDKs)

Among many cellular players, CDKs are the main gatekeepers of cell cycle progression. They are positively regulated upon binding to cyclins and these interactions are cell cycle phase-specific for particular CDK/cyclin pairs. Cyclins are responsible for the correct timing of respective CDK activation. Besides, they can also determine subcellular localization, target specificity, or interaction with regulators of CDK signaling (Pines J, 2011).

During the course of the cell cycle, protein levels of cyclins are subjected to constant fluctuation and are in turn regulated by oscillating messenger ribonucleic acid (mRNA) levels, whereas CDK concentrations are in general rather unaltered

(Hochegger H *et al.*, 2008). CDK activation not only depends on cyclin binding but also on the action of CDK activating kinase (CAK) which catalyzes Thr phosphorylation in the CDK activating loop. CDK/cyclin complexes are rendered inactive upon inhibitory phosphorylations performed by membrane-associated Tyr/Thr kinase 1 (MYT1) and Wee1-like kinase (WEE1) on the CDK subunit. These phosphate residues are in turn removed by cell division cycle (CDC)25 phosphatases (Castedo M *et al.*, 2002). Besides, the activity of the CDK/cyclin complexes is negatively controlled by CDK inhibitors (CKIs) such as inhibitors of CDK4 (INK4)/CDKN2A proteins (p16^{INK4A}, p15^{INK4B}, p18^{INK4C}, p19^{INK4D}) and p21, p27, or p57 (Chen HZ *et al.*, 2009; Malumbres M and Barbacid M, 2009).

Different types of cyclins with varying preference for CDKs exist. During early G1 phase, **D-type cyclins** (D1, D2, D3) associate with CDK4 and CDK6 which activate growth-stimulating proteins and prepare the cell for DNA replication (Malumbres M and Barbacid M, 2009). **E-type cyclins** (E1, E2) complex with CDK2 in late G1 phase and drive the cell into S phase. Complex formation between CDK2 and **cyclin A2** (A1 in germ cells) is observed during S phase, while cyclin A2 preferentially binds to CDK1 during S-G2 transition to ensure the completion of S phase and transition to mitosis (Malumbres M and Barbacid M, 2009). The major type of CDK/cyclin complex for G2-M progression and regulation of mitosis is formed by **B-type cyclins** (B1, B2) and CDK1 which is then called the maturation-promoting factor (MPF). CDK1/cyclin B catalyzes the phosphorylation of various proteins that are, for instance, involved in chromatin condensation, breakdown of the nuclear envelope, mitotic spindle formation, or actin reorganization (Castedo M *et al.*, 2002). CDC25 and WEE1 are targets of CDK1/cyclin B resulting in phosphatase activation and kinase inhibition and therefore generating a feedback loop for rapid CDK1/cyclin B activity at the onset of mitosis (Hochegger H *et al.*, 2008). Attachment of the mitotic spindles to kinetochores of condensed chromosomes aligned at the metaphase plate triggers the activation of the E3 ubiquitin ligase anaphase-promoting complex/cyclosome (APC/C) which induces the rapid ubiquitination and proteasomal degradation of cyclin B, a prerequisite for M phase progression (Hochegger H *et al.*, 2008).

3.2. Cell cycle checkpoints

The progression of the cell cycle can be stalled at different checkpoints due to unfavorable cellular conditions like the loss of genomic integrity leading to cell cycle arrest. Hence, checkpoints guarantee the fidelity of cell division and cells are given the opportunity to correct arrest-causing events (Clarke PR and Allan LA, 2009). Major checkpoints exist at entry into S phase (G1-S transition) and mitosis (G2-M transition) as well as during S phase (intra-S checkpoint) and in M phase (metaphase-to-anaphase transition; spindle assembly checkpoint). Upon activation, they stop the action of CDK/cyclin complexes at respective stages of the cell cycle (Poehlmann A and Roessner A, 2010).

The G1/S checkpoint controls the entrance of cells into the phase of DNA replication (S phase). Members of the retinoblastoma protein family (RB1, retinoblastoma-like protein 1 (p107), and retinoblastoma-like protein 2 (p130)) are the key regulators of

checkpoint control during G1 progression. RB1, for example, binds to activator E2F transcription factors and inhibits their transcription-activating performance on genes important for G1-S progression (Polager S and Ginsberg D, 2008; Poznic M, 2009; Brown KC *et al.*, 2010). Hyperphosphorylation of RB1 by CDK4 or CDK6 in complex with D-type cyclins (D1, D2, or D3) or CDK2/cyclin E prevents it from binding to E2Fs (Wikenheiser-Brokamp KA, 2006; Kitamura H *et al.*, 2008; Chen HZ *et al.*, 2009). Both the inactivation of CDC25 and the transcription of CKIs favor the inhibition of E2Fs by RB1 and therefore prohibit cells from entering S phase (Poehlmann A and Roessner A, 2010).

DNA damage like double-strand breaks or single-stranded regions of DNA is sensed by Ataxia telangiectasia mutated (ATM) and Ataxia telangiectasia and RAD3-related (ATR) leading to the activation of checkpoint kinase 1 (CHK1) and CHK2 and effector protein phosphorylation mainly at the **G1/S, intra-S, and G2/M checkpoints**. CDC25 phosphatases are among the CHK effectors and targeted for ubiquitination and proteasomal degradation upon phosphorylation therefore preventing the removal of inhibitory phosphates on CDKs. Besides, TP53 stabilization and activation result from direct or indirect ATM activation leading in turn to the transcription of CKIs (*e.g.*, *p21*) – a crucial factors in the G1/S and G2/M checkpoints (Poehlmann A and Roessner A, 2010). Additionally, the mitogen-activated kinase (MAPK) p38 can induce CDC25 inactivation, TP53 stabilization, and CKI gene expression in both G1/S and G2/M checkpoints (Poehlmann A and Roessner A, 2010). Apart from damaged DNA, the G2/M checkpoint is also triggered by incomplete DNA replication (Castedo M *et al.*, 2002).

Correct chromosomal segregation is monitored by the spindle assembly checkpoint. Unaligned chromosomes lead to the inhibition of separase-mediated separation of cohesin-trapped sister chromatids. Bipolar chromosome attachment to the mitotic spindle activates the APC/C cofactor CDC20 and causes APC/C-mediated destruction of B-type cyclins as well as activation of separase. Sister chromatid cohesion is terminated by cleavage of cohesin therefore assisting metaphase-to-anaphase transition (Waizenegger IC *et al.*, 2000; Clarke PR and Allan LA, 2009; Malumbres M and Barbacid M, 2009; Pines J, 2011). At the end of mitosis, APC/C further targets members of the mitotic kinase family (*e.g.*, Aurora kinases, polo-like kinase 1 (PLK1)) for destruction (Pines J, 2011).

The induction of cell cycle arrest upon DNA damage or distraction of mitosis may not necessarily lead to the elimination of arrest-causing factors and cell cycle progression. In case of severe genomic or cellular damage with low chances of proper repair, cells are subject to programmed cell death. However, this balance is often shifted in favor of detrimental survival in several malignancies (Clarke PR and Allan LA, 2009).

In fact, **the vast majority of cells in multicellular organisms do not continuously cycle**. These quiescent cells enter a paused stage (G0 phase) but can be reactivated upon mitogenic stimulation (Clarke PR and Allan LA, 2009). In addition, many differentiated cells are no longer capable of dividing at all. Hence, enhanced proliferation is caused by recruiting cells from G0 into G1 phase due to elevated levels of growth factors or due to activating mutations. Alternatively or concomitantly, gatekeepers are progressively eliminated. This process relieves checkpoint controls, further

enhances the propensity of cells to proliferate and increases the genomic instability of the cancer cells. Accordingly, cancer cells can accumulate further activating mutations.

4. G protein-coupled receptors (GPCRs)

The human complement of GPCRs consists of more than 800 members and the defining features of this protein family are the hydrophobic core of **seven transmembrane (7TM)-spanning α -helices** and their eponymous action, *i.e.*, the activation of their cognate **heterotrimeric G protein(s)** (Fredriksson R *et al.*, 2003; Krishnan A *et al.*, 2012). Genes encoding GPCRs account for more than 2% of the total human genes (Fredriksson R *et al.*, 2003). Exact numbers vary from about 800 to 850 due to uncertainties arising mostly from pseudogenes of pheromone and odorant receptors, and there are still about 150 orphan receptors lacking an endogenous ligand (Gruber CW *et al.*, 2010).

All GPCRs share a common structure. They harbor an extracellular amino-terminus, seven transmembrane helices, which are connected by alternating intracellular and extracellular flexible loops, and an intracellular carboxy-terminus. Apart from the amino- and carboxy-terminus, most structural variability is observed in the extracellular loops of these receptors, which are involved in ligand binding and receptor activation. Their flexibility contributes notably to the conformational diversity of a GPCR (Peeters MC *et al.*, 2011).

The plasma membrane is home to most GPCRs. They are exported to the plasma membrane via the classical secretory pathway (synthesis at the endoplasmic reticulum, processing in the Golgi apparatus, export to the plasma membrane from the trans-Golgi network) where they are capable of initiating signal transduction upon activation (Achour L *et al.*, 2008). However, there are also GPCRs which mostly reside in intracellular vesicles from where they can initiate downstream signaling cascades (*e.g.*, G protein-coupled receptor 6 (GPR6); Padmanabhan S *et al.*, 2009; Prasad BM *et al.*, 2010). Typical posttranslational modifications of GPCRs include phosphorylation, glycosylation, and the attachment of a lipid membrane anchor¹⁰.

GPCRs are involved in diverse physiological functions such as neurotransmission, smooth muscle and cardiac contraction, blood pressure regulation, hormone secretion, or immune responses (Dorsam RT and Gutkind JS, 2007; Rozengurt E, 2007). As diverse as their physiological roles is the nature of their ligands ranging from photons, ions, and biogenic amines over nucleotides and peptides to odorants, hormones, and bioactive lipids (Ji TH *et al.*, 1998). In addition, extracellular proteases can cleave the amino-terminus of protease-activated receptors (PARs) therefore generating a new amino-terminus capable of acting as the receptor's own ligand (Arora P *et al.*, 2007).

¹⁰ S-palmitoylation of GPCRs can occur at Cys residues of the intracellular carboxy-terminus. A C16 fatty acid chain is covalently attached (thioester linkage) and anchors the carboxy-terminus to the inner layer of the plasma membrane therefore generating a 'fourth intracellular loop' (Marchese A *et al.*, 2008).

GPCRs have gained much interest as well-druggable targets. They could be associated with multiple disease areas, e.g., malignant, neurodegenerative, infectious, cardiovascular, psychiatric, and immunological diseases, and about half of today's drug targets are in fact GPCRs (Lundstrom K, 2009). However, only about 60 members of this large receptor family are currently targeted by drugs approved for clinical use (Gruber CW *et al.*, 2010).

4.1. Classification of GPCRs

Based on their primary sequence and similarities in structure, vertebrate GPCRs are divided into five families: glutamate, rhodopsin, adhesion, frizzled/taste2, and secretin receptors form the so-called **GRAFS classification system** (Fredriksson R *et al.*, 2003; Krishnan A *et al.*, 2012). The **rhodopsin** family contains by far the most GPCRs (683 members in humans) and it was therefore subdivided into four subfamilies (α , β , γ , and δ). Most family members are characterized by short amino-termini and the presence of two motives which are important for their functional integrity (Krishnan A *et al.*, 2012): E/DRY at the boundary of transmembrane (TM) region 3 and intracellular loop region 2 (Rovati GE *et al.*, 2007) and NPxxY¹¹ at the boundary of TM region 7 and the intracellular carboxy-terminus (Bockaert J *et al.*, 2004). Odorant receptors (part of the δ subgroup) constitute the largest subgroup among human rhodopsin GPCRs and they comprise more than 350 members (Spehr M and Munger SD, 2009). The **adhesion** family of GPCRs (33 members in humans) is characterized by large extracellular amino-terminal regions which are composed of multiple structural protein domains (e.g., epidermal growth factor (EGF)-like, leucine-rich repeats, immunoglobulin (Ig)). Members of this family are heavily glycosylated. Upon receptor synthesis at the endoplasmic reticulum, most amino-terminal tails of adhesion GPCRs are autocatalytically cleaved at a conserved G protein-coupled receptor proteolytic site (GPS) but reassemble with their remaining 7TM receptor in a non-covalent manner at the cell surface (Yona S *et al.*, 2008). GPCRs of the **glutamate** family (22 members in humans) also have a very long amino-terminus involved in the binding of endogenous ligands. Besides, the majority of human glutamate receptors have a conserved Cys-rich domain in the amino-terminus (Krishnan A *et al.*, 2012). A closely related GPCR family, the **secretin** receptors (15 members in humans), share with adhesion GPCRs the long amino-terminus important for peptide hormone ligand interaction, thus they lack the GPS domain. Most family members contain conserved Cys residues that stabilize an amino-terminal structure by the formation of three Cys-bridges (Lagerström MC and Schiöth HB, 2008; Krishnan A *et al.*, 2012). Members of the **frizzled/taste2** family (10 members in humans) act as receptors for wingless – int-1 (Wnt) proteins and are also characterized by a long amino-terminus (Krishnan A *et al.*, 2012). Besides, the smoothed receptor (involved in patched/sonic hedgehog signaling) is included in the frizzled/taste2 GPCR family though not being a frizzled receptor (Lagerström MC and Schiöth HB, 2008). In addition, pheromone and cyclic adenosine monophosphate (cAMP) receptors extend the classification system to GPCRs found only in non-mammalian species (Gruber CW *et al.*, 2010).

¹¹ The amino acid positions indicated with 'x' in the NPxxY motif allow the presence of any amino acid.

4.2. Classical GPCR signaling and GPCR-interacting proteins (GIPs)

Upon ligand-induced receptor activation, GPCRs expose intracellular moieties that can interact with membrane-anchored heterotrimeric G-proteins and facilitate the **exchange of guanosine diphosphate (GDP) to guanosine triphosphate (GTP) in the α -subunit**. This leads to a conformational change and causes the dissociation and activation of α - and $\beta\gamma$ -subunits followed by stimulation of multiple downstream signaling cascades (Dorsam RT and Gutkind JS, 2007). The exchange of GTP for GDP is favored by guanine nucleotide exchange factors (GEFs) and hindered by guanine nucleotide dissociation inhibitors (GDIs; Gruber CW *et al.*, 2010). Signal termination results from GTP hydrolysis performed by the intrinsic GTPase activity of the α -subunit leading to a reassociation of α - and $\beta\gamma$ -subunits (reformation of the heterotrimeric G protein). This reaction is assisted by GTPase-activating proteins (GAPs).

Various isoforms of G_α (20), G_β (5), and G_γ (12) have been described in mammals which can be assembled in multiple combinations giving rise to a diverse set of heterotrimeric G proteins (Gruber CW *et al.*, 2010). Thus, the canonical signaling features of heterotrimeric G proteins are attributed to four different G_α subgroups whose members are defined on the basis of amino acid sequence homology. Activation of **$G_{\alpha s}$ /olfactory** leads to the stimulation of adenylyl cyclase and the formation of cAMP which in turn activates protein kinase A (PKA). Activation of **$G_{\alpha i/o}$ /transducin/gustducin** inhibits adenylyl cyclase¹². **$G_{\alpha q/11/14/15/16}$** activation engages phospholipase C β (PLC β) which breaks down phosphatidylinositol-4,5-bisphosphate (PIP₂) at the inner layer of the plasma membrane into the second messengers inositol-1,4,5-trisphosphate (IP₃) and diacylglycerol leading to the activation of protein kinase C (PKC) and Ca²⁺ release from intracellular stores. PKC in turn phosphorylates regulators of calcium signaling such as calmodulin. **$G_{\alpha 12/13}$** engagement activates small GTP-binding proteins of the Ras-homology (Rho) family which activate Rho-associated coiled-coil-containing protein kinase (ROCK) therefore affecting the actin cytoskeleton (Cotton M and Claing A, 2009; Gruber CW *et al.*, 2010). The **$G_{\beta\gamma}$** subunits can also transmit signals to activate effectors like PLC β , PI3K, or the G protein-coupled inward rectifier potassium (GIRK) channel (Woehler A and Ponimaskin EG, 2009).

GPCRs are not only capable of interacting with G proteins, their key mediators of downstream signal transduction, **but also with many accessory proteins named GPCR-interacting proteins (GIPs)**. GIPs are involved in the correct folding of GPCRs, fine tuning of GPCR-mediated signaling responses (including the type of G protein recruited), receptor trafficking (to specific cellular compartments or the plasma membrane), receptor complex formation, oligomerization, or desensitization (Bockaert J *et al.*, 2004; Ritter SL and Hall RA, 2009). **GPCR kinases (GRKs)** can phosphorylate the receptor which results in the recruitment of **β -arrestins**. They in turn can serve as scaffolding proteins and lead to the formation of a signaling complex which can, for instance, involve the human Rous sarcoma virus oncogene homolog Src, ERK, apoptosis signaling kinase 1 (ASK1), or Jun amino-terminal kinase 3 (JNK3;

¹² Transducin and gustducin activate phosphodiesterases (PDEs) leading to the hydrolysis of cyclic guanosine monophosphate (cGMP) and cyclic adenosine monophosphate (cAMP), respectively (Catty P *et al.*, 1992; Margolske RF, 2002).

Bockaert J *et al.*, 2004; Luttrell DK and Luttrell LM, 2004). Receptor activity-modifying proteins (RAMP1, 2, and 3) regulate ligand binding to GPCRs and GPCR trafficking to the cell surface (Cooray SN *et al.*, 2009; Ritter SL and Hall RA, 2009). The carboxy-terminus of GPCRs can serve as a **PDZ¹³ ligand** that interacts with PDZ domains of diverse proteins involved in signal transduction. PDZ-binding proteins were shown to play a role in receptor clustering, signal transduction, desensitization, or recycling to the plasma membrane (Bockaert J *et al.*, 2004).

In addition, GPCRs have demonstrated their ability to **transactivate growth factor receptors** like the EGFR leading to the activation of MAPK, janus kinase (JAK)/signal transducer and activator of transcription (STAT), and PI3K signaling pathways (Rozengurt E, 2007; Cotton M and Claing A, 2009). A link between G proteins and **gene transcription** was established by the observation that $G_{\beta 5}$ could shuttle between the plasma membrane and the nucleus and $G_{\beta \gamma}$ was described to directly interact with histone deacetylase (HDAC)4 and 5 (Spiegelberg BD and Hamm HE, 2007). Surprisingly, G protein-coupled receptor 30 (GPR30) was found to act as a **transcription factor in the nucleus** (Madeo A and Maggiolini M, 2010).

GPCRs are believed to harbor very flexible conformations. Ligands that bind with different affinities stabilize a particular receptor conformation therefore favoring the interaction with specific effectors of signal transduction (Schröder R *et al.*, 2010). This model explains the possible **coupling of a GPCR to different G proteins or G protein independent effectors** (Rosenbaum DM *et al.*, 2009). Nevertheless, considerable crosstalk and bifurcations between the signals transduced by different G_{α} isoforms as well as $G_{\beta \gamma}$ subunits and GPCRs themselves exist (figure 4; Woehler A and Ponimaskin EG, 2009).

4.3. GPCR oligomerization

GPCRs can associate with other GPCRs forming either homo- or heteromers – often observed in a tissue-specific manner. Examples for GPCR heteromerization include the gamma-aminobutyric acid type B receptor 1 (GABA-B-R1) and GABA-B-R2, $\beta 1$ - $\beta 2$ adrenergic receptors, D1-D2 dopamine receptors, 2A-3 somatostatin receptors, angiotensin type 1 receptor (AT1R) and the $\beta 2$ -adrenergic receptor, serotonin 2A receptor (5-HT2A) and metabotropic glutamate receptor 2 (mGluR2), or the chemokine¹⁴ receptors CC chemokine receptor 2 (CCR2) and CXC chemokine

¹³ PDZ stands for the three proteins in which this domain was identified first: P_{SD}-95 (postsynaptic density protein 95), D_LP (*Drosophila* discs large protein), and the tight junction protein Z_O-1 (zonula occludens protein 1; Bockaert J *et al.*, 2004). The Simple Modular Architecture Research Tool (SMART) database reports PDZ domains in 364 human proteins (smart.embl-heidelberg.de).

¹⁴ Chemokines are defined as small secreted, chemoattractant proteins with low molecular weight (8 to 14 kilodaltons (kDa)). The biological activity of chemokines is exerted upon binding to their respective GPCR(s). They regulate migration/chemotaxis and activation status of responsive cells and are involved in a number of different processes including leukocyte migration/homing, lymphoid organ development, inflammation, allergy, angiogenesis, wound healing, cancer development, and cancer metastasis. Chemokines are subdivided into four groups depending on a conserved amino-terminal Cys motif. The 'C only chemokine' lymphotactin is characterized by only one cysteine, the CC chemokines bear two adjacent cysteines whereas cysteines in CXC and CX3C chemokines are separated by one or three amino acid(s), respectively (Yoshie O *et al.*, 2001; Stievano L *et al.*, 2004).

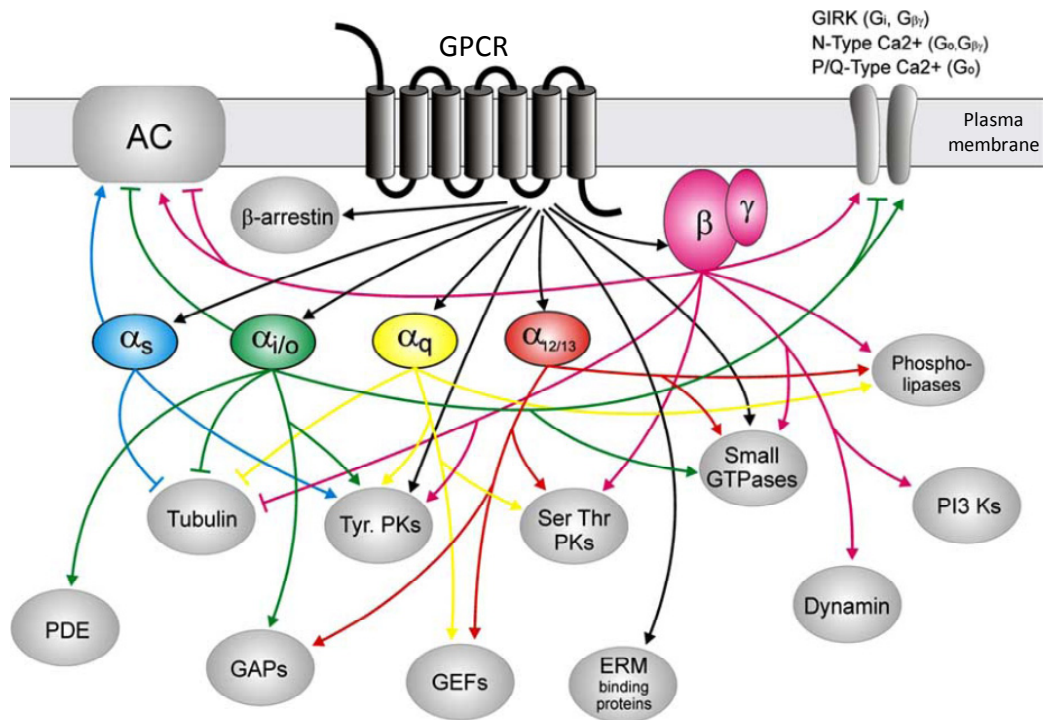


Figure 4: Most downstream players of GPCR signaling are interconnected. Activation of a GPCR leads to the initiation of downstream signaling cascades involving both G_{α} (isoforms s , i/o , q , $12/13$) and $G_{\beta\gamma}$ subunits of heterotrimeric G proteins. They mediate the activation (\rightarrow) or inhibition (\top) of a number of effectors including membrane-associated ion channels (G protein-coupled inward rectifier potassium (GIRK) channel, N- and P/Q-type Ca²⁺ channels) and adenylyl cyclase (AC) as well as phosphodiesterases (PDEs), GTPase-activating proteins (GAPs), Tyr- and Ser/Thr-protein kinases (Tyr and Ser Thr PKs), guanine nucleotide exchange factors (GEFs), small GTPases, dynamin, phospholipases, phosphatidylinositol 3-kinases (PI3Ks), and proteins involved in cytoskeleton organization (ezrin/radixin/moesin (ERM) binding proteins, tubulin). Many bifurcations to different types of effectors exist among functional heterotrimeric G protein subunits and the preferred modes of action are often cell-type specific. However, these effectors can also be activated directly upon recruitment to the activated GPCR in a G protein independent manner (or via β -arrestin). The figure is adapted from Woehler A and Ponimaskin EG, 2009.

receptor 4 (CXCR4), to name but a few (Marshall FH *et al.*, 1999; Percherancier Y *et al.*, 2005; Franco R *et al.*, 2007; Rozenfeld R and Devi LA, 2010). These complexes mainly differ from their monomeric partners in terms of ligand binding and specificity, preference of G protein activation and signal transduction as conformational changes are induced in interacting receptors upon oligomerization (Rozenfeld R and Devi LA, 2011). In fact, it is thought that **the majority of GPCRs can form homo- or heterodimers**, which seems to occur at an early stage of receptor trafficking to the plasma membrane (Franco R *et al.*, 2007; Achour L *et al.*, 2008). This is particularly true for the glutamate GPCR family, whose members exist as constitutive dimers often interconnected by a disulfide bridge (Pin JP *et al.*, 2005).

4.4. Endocytosis of GPCRs from the plasma membrane

GPCRs residing on the plasma membrane are rapidly desensitized following ligand-induced activation (figure 5). Most receptors are internalized by **clathrin-coated pit formation**. Upon phosphorylation of their carboxy-terminus and the intracellular loop 3 by GRKs, β -arrestins are recruited and bind to phosphorylated residues. This in turn leads to the binding of clathrin and the adaptor protein complex 2 (AP2) and the receptor is internalized into clathrin-coated pits through the action of the large G protein dynamin (Hanyaloglu AC and von Zastrow M, 2008). Internalization can also occur as the result of receptor **ubiquitination** (Marchese A *et al.*, 2008).

Internalized GPCRs present in endosomes may on the one hand be destined to **proteasomal degradation** in lysosomes. On the other hand, GPCRs can be **recycled back to the plasma membrane** following dephosphorylation and resensitization and promote rapid recovery of cellular response mechanisms (Hanyaloglu AC and von Zastrow M, 2008). Besides, internalized GPCRs such as sphingosine-1-phosphate receptor 1 (S1PR1; G_i -coupled) or thyroid-stimulating hormone (TSH) receptors (G_s -coupled) have been shown to keep on modifying the production of the second messenger cAMP from intracellular compartments. GPCRs are further capable of signaling via the MAPK or PI3K pathway once internalized. The concept that activated receptors on the plasma membrane continue signaling after sequestration into endosomes was also described for receptor tyrosine kinases (e.g., EGFR) and might in general lead to the generation of '**signaling endosomes**' (Jalink K and Moolenaar WH, 2010).

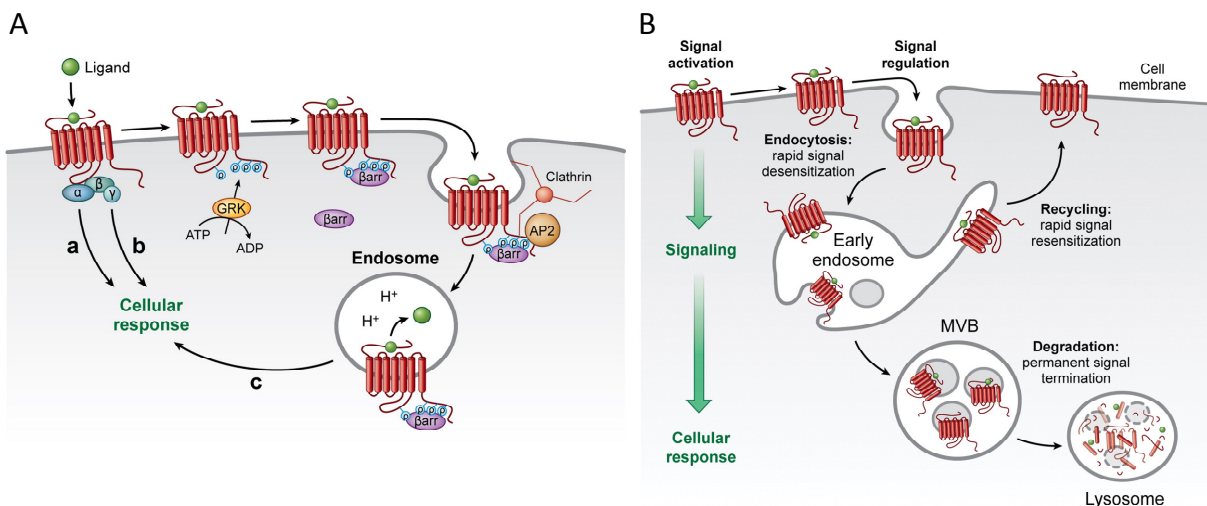


Figure 5: GPCRs are sequestered from the plasma membrane upon ligand-induced receptor activation. (A) Ligand binding leads to the activation of G_α (a) and $G_{\beta\gamma}$ (b) subunits which can mediate signal transduction causing cellular responses. G protein-coupled receptor kinases (GRKs) phosphorylate the carboxy-terminus and the intracellular loop 3 of the activated GPCR which prevents further activation of heterotrimeric G proteins and enables binding of β -arrestins (β arr). Subsequently, clathrin and adaptor protein complex 2 (AP2) proteins are recruited for clathrin-coated pit formation and receptor internalization into endosomes. However, GPCRs can continue signaling from endosomal compartments (c). (B) Internalized GPCRs can be sorted for destruction from early endosomes over multivesicular bodies (MVBs) into lysosomes. In contrast, GPCRs can be recycled back to the plasma membrane leading to the quick resensitization of a cell to the respective extracellular ligand. Figures are adapted from Hanyaloglu AC and von Zastrow M, 2008; ADP – adenosine diphosphate; ATP – adenosine triphosphate.

4.5. GPCRs are involved in cell cycle regulation and cancer

It has long been known that illegitimate expression of GPCRs occurs in tumor cells (Schorr I and Ney RL, 1971). Several arguments support the assumption that GPCRs may also be specifically targeted to limit the growth of cancer cells. **Signaling pathways controlled by GPCRs promote proliferation, survival, cell migration and metastasis, angiogenesis, inflammation, and subversion of the immune system** (Dorsam RT and Gutkind JS, 2007; Spiegelberg BD and Hamm HE, 2007; Borensztajn KS and Spek CA, 2008; Hurst JH and Hooks SB, 2009; Wu X *et al.*, 2009; Lappano R and Maggiolini M, 2011). Their unrestrained exploitation – mostly seen by overexpression of GPCRs – can in turn contribute to the malignant transformation of cells (Li S *et al.*, 2005; Rozengurt E, 2007; Spiegelberg BD and Hamm HE, 2007). Besides, the uncontrolled action of GPCR-associated G proteins or regulators of G protein signaling (RGS) that accelerate the intrinsic GTPase activity of G_{α} subunits (GAPs) was described to contribute to tumorigenesis (Hurst JH and Hooks SB, 2009). And the crosstalk of activated GPCRs and receptor tyrosine kinases like the EGFR leading to their transactivation is a proven concept in the progression of many cancers (Lappano R and Maggiolini M, 2011). Downstream signaling mediators whose pathway activation can be initiated by activated GPCRs and that contribute to cancer cell proliferation, survival, or migration and angiogenesis include PKA, Ras-Raf-MEK-ERK, PKB-mammalian target of rapamycin (mTOR)-ribosomal protein S6 kinase (p70S6K), Rho-ROCK, JAK/STAT, or PI3K (Lappano R and Maggiolini M, 2011).

The involvement in cell cycle control was shown for several GPCRs and GPCR-associated proteins. For instance, the H4 histamine receptor was found to mediate a reversible cell cycle arrest in growth factor-induced hematopoietic progenitor cells (Petit-Bertron AF *et al.*, 2009). An essential role in the regulation of prostate tumor growth by affecting cell cycle control was assigned to GRK5 (Kim JI *et al.*, 2012). The transactivation of the EGFR by GPCRs established a link to cell cycle progression and various endogenous GPCR agonists were reported to induce the expression of cyclins and modulate RB1 phosphorylation (Rozengurt E, 2007).

Furthermore, **viruses have hijacked GPCRs from the host genome and adapted them to drive cells into S phase and/or to promote immune evasion** (Cannon M, 2007; Beisser PS *et al.*, 2008; Martin D and Gutkind JS, 2008). Cancer-causing viruses like Kaposi's sarcoma-associated herpesvirus (KSHV) were described to encode for constantly active GPCRs (Hurst JH and Hooks SB, 2009). The human cytomegalovirus (CMV) encodes a chemokine GPCR (US28) capable of stimulating proliferation pathways and is associated with glioblastoma, colon and breast cancer (Lappano R and Maggiolini M, 2011).

In general, non-viral GPCRs were also attributed to play a role in the development of various human cancers such as lung, breast, or prostate cancer. Overexpression of prostate-specific G protein-coupled receptor (PSGR) was detected in prostate tumors and prostate intraepithelial neoplasms (Weng J *et al.*, 2005). PSGR was therefore discussed as a biomarker for urine-based prostate cancer detection (Rigau M *et al.*, 2010). CCR2 and its ligand CC chemokine ligand 2 (CCL2) were proposed to contribute to prostate cancer carcinogenesis. CCR2 expression could be correlated with prostate cancer progression (Lu Y *et al.*, 2007). Inactivation of the

CCL2/CCR2 auto- or paracrine axis could counteract prostate cancer metastasis to the bone and prevent prostate cancer cell growth (Lu Y *et al.*, 2006; Lu Y *et al.*, 2009). In lung squamous cell carcinoma, G protein-coupled receptor 87 (GPR87) was identified to be overexpressed (Gugger M *et al.*, 2008) and to contribute to the viability of tumor cells (Glatt S *et al.*, 2008). A poorly-described member of the adhesion family of GPCRs, orphan G protein-coupled receptor 110 (GPR110), was found to be overexpressed in lung and prostate adenocarcinomas and characterized as a proto-oncogene (Lum AM *et al.*, 2010). Likewise, the chemokine receptor CXCR4 was proposed to contribute to lung cancer metastasis (Burger JA *et al.*, 2011). However, CXCR4 has been most prominently described in breast cancer. High CXCR4 expression in breast cancer could be correlated with poor prognosis and prevalence for bone metastasis as bone marrow stromal cells highly express the CXCR4 ligand CXCL12 (CXC chemokine ligand 12; Burger JA and Kipps TJ, 2006; Luker KE and Luker GD, 2006; Rose AA and Siegel PM, 2010). It is conceivable that CXCR4 might exert its effects in conjunction with CXC chemokine receptor 7 (CXCR7; heterodimerization), which binds CXCL12 with ten times higher affinity than CXCR4 and was also linked to breast and lung cancer cell proliferation and metastatic tendency (Maksym RB *et al.*, 2009). In SCLC cells, it was suggested that an autocrine loop sustained RhoA activation via the engagement of a GPCR (Touge H *et al.*, 2007). Wnt proteins and their cognate GPCRs have been implicated in the transduction of signals in multiple cancers such as colon or lung carcinoma (Lappano R and Maggiolini M, 2011). In addition, the G protein-coupled receptors GRPR (gastrin-releasing peptide receptor), NMB-R (neuromedin B receptor), prostaglandin-E2 receptors, and the CXC chemokine receptor 2 (CXCR2) were reported to contribute to lung cancer tumorigenesis (Dorsam RT and Gutkind JS, 2007; Lappano R and Maggiolini M, 2011).

5. G protein-coupled receptor 19 (GPR19)

5.1. Gene and protein information

As a member of the large G protein-coupled receptor family, the gene encoding human *Gpr19* (National Center for Biotechnology Information (NCBI) gene identification number (ID) 2842 ¹⁵, Ensembl gene ID ENSG00000183150 ¹⁶, NCBI mRNA accession number NM_006143 ¹⁷, UniProt protein ID Q15760 ¹⁸, NCBI protein reference sequence ID NP_006134.1 ¹⁹) is located on the reverse strand of **chromosome 12** (short arm; 12p12.3) at position 12,849,121 to 12,813,995. It is composed of **four exons** (spliced transcript length of 1743 bases) **with the last one harboring the intronless**

¹⁵ <http://www.ncbi.nlm.nih.gov/gene/2842>

¹⁶ http://www.ensembl.org/Homo_sapiens/Gene/Summary?db=core;g=ENSG00000183150;r=12:12813825-12849141

¹⁷ http://www.ncbi.nlm.nih.gov/nuccore/NM_006143.2

¹⁸ <http://www.uniprot.org/uniprot/Q15760>

¹⁹ www.ncbi.nlm.nih.gov/protein/NP_006134

coding sequence (CDS) that gives rise to a **415 amino acid protein** predicted to have topological characteristics of 7TM receptors (figure 6; extracellular amino-terminus, seven transmembrane regions with alternating cytoplasmic/intracellular and extracellular loops, cytoplasmic carboxy-terminus). Additional expected features include sites of glycosylation and a disulfide bond bridging extracellular loops 1 and 2. The carboxy-terminus further contains multiple Ser and Thr residues which could be phosphorylated by GPCR kinases for reasons of receptor activity regulation. It also harbors the consensus sequence of a type I PDZ-binding motif (amino acids TFV) at the very carboxy-terminal end (Liu M and Horowitz A, 2006). The possibility of palmitoylation on carboxy-terminal Cys residues (lipid membrane anchor) and for PKC-mediated phosphorylation of the intracellular loops is also based on the primary sequence of GPR19 (O'Dowd BF *et al.*, 1996). GPR19 further contains a strict **cholesterol consensus motif**²⁰ (Phe103, Lys182, Ile184, Trp188) and

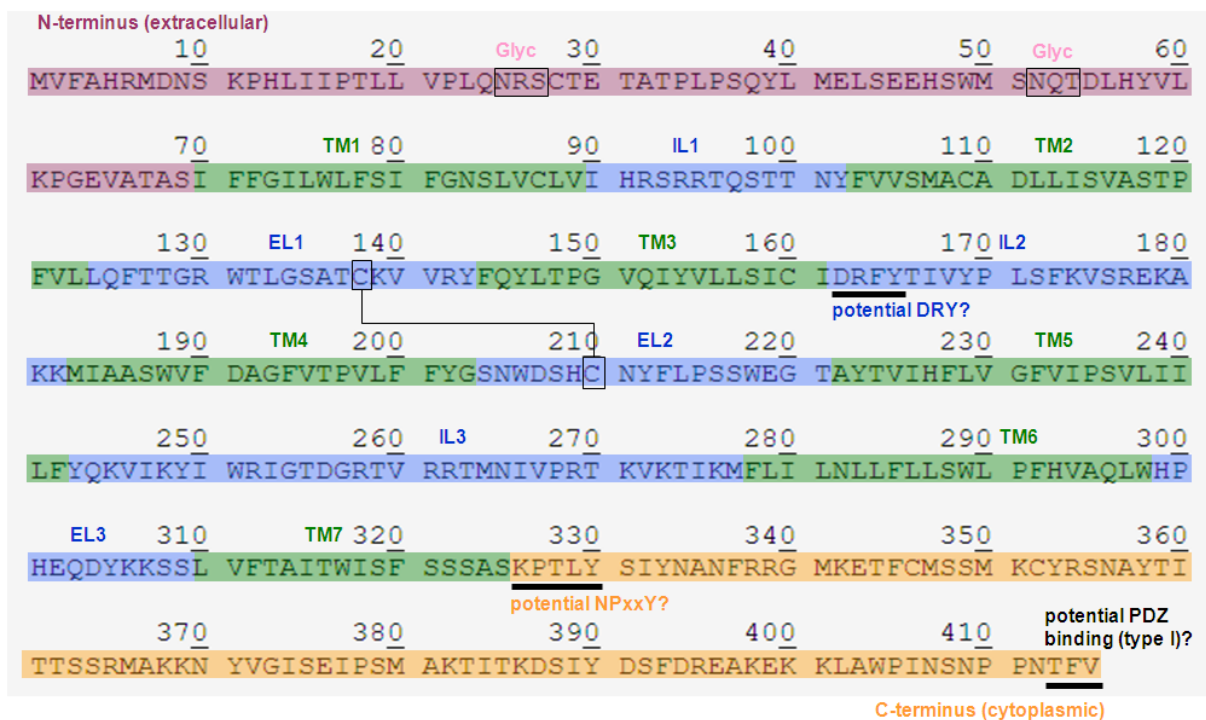


Figure 6: Primary sequence and predicted topological features of GPR19. The amino acid sequence is based on UniProt protein ID Q15760. All highlighted features (external amino (N)-terminus, transmembrane (TM), intracellular loop (IL) or extracellular loop (EL) regions, cytoplasmic carboxy (C)-terminus; sites of glycosylation (Glyc); disulfide bridge between two Cys residues; positions of potential DRY, NPxxY, or PDZ binding motives) are hypothetical and have not been experimentally verified. N-linked glycosylation sites were predicted using the NetNGlyc 1.0 algorithm²¹.

²⁰ Cholesterol is an essential part of the cellular plasma membrane. Apart from its necessity for the membrane's physicochemical properties, it also ensures correct functioning or stabilization of membrane-spanning receptors by direct interaction. This is the case for the β 2-adrenergic and the serotonin 1A receptor, both members of the GPCR family (Hanson MA *et al.*, 2008; Paila YD *et al.*, 2009). A cholesterol consensus motif consisting of four consensus sites was defined to be crucial for GPCR-cholesterol interaction. The amino acid numbering system of Ballesteros and Weinstein was used to specify these positions (Ballesteros JA and Weinstein H, 1995). Site 1 covers positions 4.39 to 4.43 in/near TM region 4 and requests Arg or Lys at least once. Sites 2 and 3 are also in TM region 4 and must be either occupied by Trp or Tyr (4.50) and Ile, Leu, or Val (4.46). TM region 2 harbors site 4 (2.41) which requests Phe or Tyr (Hanson MA *et al.*, 2008; Paila YD *et al.*, 2009).

²¹ www.cbs.dtu.dk/services/NetNGlyc/

was therefore suggested to have cholesterol binding properties (Hanson MA *et al.*, 2008). Parts of the genomic sequence (table 15), the mRNA and the protein sequence of GPR19 are listed in the Appendix section.

Twenty-four single nucleotide polymorphisms (SNPs) lying within the CDS of *Gpr19* are listed according to Ensembl²², with half of them affecting the protein sequence (amino acid substitution). An overview of these non-synonymous SNPs including frequency of occurrence and predicted effects of amino acid substitution on the protein's function is given in the Appendix section (table 16).

5.2. Expression of *Gpr19*

In normal tissues, *Gpr19* was found most prominently expressed in the **central nervous system, the ovaries, and the testis** (Vassilatis DK *et al.*, 2003; Hoffmeister-Ullerich SA *et al.*, 2004). Abundant mRNA levels were detected in the brain of human, mouse, and rat. The human brain regions with the strongest signals detected included the caudate nucleus, putamen, and thalamus (O'Dowd BF *et al.*, 1996). The regions of the mature mouse brain with highest *Gpr19* expression were functionally distinct including specific parts of the olfactory bulb, cerebral cortex (mostly layers 2 and 6), hippocampus, hypothalamus, and cerebellum. During mouse embryogenesis, highest *Gpr19* mRNA expression levels could be seen prominently in the developing CNS (neuroepithelium, neural plate) starting from embryonic day 8.5. As embryonic development continued, the areas with highest *Gpr19* signals were the ones containing dividing cells (lining of the neural canal; ventricles) and cells undergoing differentiation (ventral horns of the spinal cord). Besides, overall *Gpr19* signals in the adult mouse brain declined after embryogenesis (Hoffmeister-Ullerich SA *et al.*, 2004). In addition, *Gpr19* mRNA expression levels were high in murine **cells involved in the sperm maturation process**: Hoffmeister-Ullerich and coworkers assigned high *Gpr19* expression to spermatogonia stem cells (Hoffmeister-Ullerich SA *et al.*, 2004). In contrast, Rossi and coworkers identified murine spermatocytes as the primary source of *Gpr19* mRNA (Rossi P *et al.*, 2004). Furthermore, a meta-analysis found *Gpr19* to be upregulated in human **embryonic stem cells** (hESC) but on the other hand failed to detect it in non-hESC tissues including the CNS (Assou S *et al.*, 2007).

5.3. Signal transduction of GPR19

To date, **GPR19 remains an orphan GPCR**, its endogenous ligand has not been identified, yet. Most approaches to answer this question were based on primary sequence comparisons with other GPCRs whose ligands are known. Human GPR19 shows sequence similarity to dopamine D2 and neuropeptide Y GPCRs. Catecholaminergic receptors mediate ligand binding with the help of an aspartic acid residue located within TM region 3. As GPR19 lacks this aspartic acid residue, its

²² useast.ensembl.org/Homo_sapiens/Gene/Variation_Gene/Table?g=ENSG00000183150;r=12:12813825-12849141#NON_SYNONYMOUS_CODING_tablePanel

endogenous ligand is unlikely to be aminergic (O'Dowd BF *et al.*, 1996). Comparing TM regions of known GPCRs, GPR19 was assigned to be a member of the rhodopsin family of GPCRs (Vassilatis DK *et al.*, 2003) though it does neither harbor a strict NPxxY nor E/DRY motif. However, based on the whole protein sequence, GPR19 could not be assigned to any of the GPCR GRAFS families (Fredriksson R *et al.*, 2003). Due to its phylogenetic proximity to receptors activated by peptides, GPR19 was proposed to have a peptide ligand and might as well be an endo-GPCR (activated by an endogenous ligand; Vassilatis DK *et al.*, 2003)

GPR19 was proposed to signal via G_i therefore inhibiting adenylyl cyclase but neither via G_s nor G_q as determined by a transcription-based reporter assay and receptor activation using transient receptor overexpression (Bresnick JN *et al.*, 2003). Besides, *Gpr19* mRNA expression in the murine striatum and hippocampus was found to be attenuated when cAMP-responsive element modulator (CREM) and cAMP-responsive element binding protein (CREB) had been inactivated in these animals (Lemberger T *et al.*, 2008).

5.4. Functional implications for GPR19

Based on its chromosomal location, *Gpr19* was postulated to play a role in cancer development as it resides in a region that is frequently rearranged in **childhood leukemia** and to a lesser extent in other neoplasms. In acute lymphoblastic leukemia (ALL), a hemizygous deletion of the short arm of chromosome 12 was observed in 15 to 47% of the children examined (Montpetit A and Sinnett D, 1999). The deleted 12p12.3 region just excluded *Gpr19* but contained the gene *cyclin-dependent kinase inhibitor 1B* (*Cdkn1B*) with both genes being separated by about 40 kilobases. Additionally, high levels of mRNA encoding GPR19 were found in **metastatic melanoma** (Li S *et al.*, 2005) showing a sixfold increased expression of *Gpr19* in comparison to melanomas-*in-situ*/thin melanomas and a fivefold increased expression when basal and squamous cell carcinoma had also been included (Riker AI *et al.*, 2008). In a genome-wide short interfering ribonucleic acid (siRNA) screen, human *Gpr19* was identified as a **potential cell division gene** (Neumann B *et al.*, 2010).

6. Project definition

Despite the fact that the human genome encodes more than 800 G protein-coupled receptors, the conceptual integration of GPCRs into the multistep process of tumorigenesis – compared to, for instance, receptor tyrosine kinases or downstream effector kinases and phosphatases – remains sparse. Hence, the basic rationale of this thesis project was the search for GPCRs that are associated with malignant diseases in general and lung cancer in particular. Pioneer expression profiling studies allowed the identification of several GPCRs that revealed high mRNA expression levels in SCLC patient samples relative to NSCLC or normal lung controls. One of these receptors that had so far been only poorly characterized became the

focus of this work: orphan receptor GPR19. Apart from gene expression data, the functional characterization of GPR19 was elusive and neither an endogenous ligand nor details about downstream signaling had been unraveled. Thus, the goal was to investigate underlying biological functions of GPR19 focusing on its potential contribution to tumorigenesis.

The first inquiries included *in silico* analyses regarding the tissue and cell line expression of *Gpr19* as well as phylogenetic analyses (orthologs and paralogs). Human lung cancer-derived cell lines were selected and proliferation studies were performed with a loss-of-function (RNA interference) and gain-of-function (expression plasmid transfection) phenotype for GPR19. Due to the lack of mechanistic data, a potential autocrine receptor stimulation combined with G protein coupling ($G_{i/o}$) was explored here. Similarly, the GPR19 loss- and gain-of-function phenotypes were investigated for their influence on the cell cycle in lung cancer-derived cell lines. Further examinations comprised the expression of *Gpr19* during the course of the cell cycle as well as its transcriptional regulation.

IV. Materials

1. Devices and accessory

Standard plastic lab ware for molecular biology and cell culture were from Becton Dickinson, Corning, Eppendorf, Greiner Bio-One, and Thermo Fisher Scientific, if not specified differently.

Table 1: Overview of used materials, devices, and accessory including manufacturing company and product code (if applicable; arranged in alphabetical order).

Name	Manufacturer	Product code
Adhesive optical seal film BZO	Biozym	712350
Agarose gel casting kit	Hofer	HE 47-10
Agarose gel electrophoresis unit Maxi-Plus standard submarine, horizontal	Hofer	SUB25
Agarose gel electrophoresis unit Mini submarine, horizontal	Hofer	HE 33
Amersham™ Hyperfilm™ MP	GE Healthcare	28906844
Autoradiography cassette Amersham™ Hypercassette™ (18 x 24 cm; 24 x 30 cm)	GE Healthcare	RPN 1263 RPN 11643
Backing tape, black	PerkinElmer	6005189
Cell culture flask, 75 cm ² , collagen IV-coated	Becton Dickinson	354523
Cell culture plate (6 well, poly-D-lysine-coated; BioCoat®)	Becton Dickinson	356413
Cell culture plate (96 well, poly-D-lysine-coated; BioCoat®)	Becton Dickinson	354632
Cell strainer (40 µm; nylon)	Becton Dickinson Falcon™	352340
Cell viability analyzer Vi-Cell™ XR	Beckman Coulter	
Centrifuge 5415R	Eppendorf	
Centrifuge 5801R	Eppendorf	
Centrifuge Heraeus Megafuge 40R	Thermo Fisher Scientific	
CloneSelect™ Imager	Molecular Devices	
Criterion™ XT precast gel, 10% Bis-Tris, 18 well, 30 µl of sample per slot	Bio-Rad	345-0112
Criterion™ XT precast gel, 10% Bis-Tris, 26 well, 15 µl of sample per slot	Bio-Rad	345-0113
Criterion™ XT precast gel, 4-12% Bis-Tris, 18 well, 30 µl of sample per slot	Bio-Rad	345-0124
Criterion™ XT precast gel, 4-12% Bis-Tris, 26 well, 15 µl of sample per slot	Bio-Rad	345-0125
CryoTube™ vial (1.8 ml)	Nunc	109804
Dry incubator	IPS	
Electroporation cuvette	Lonza	VKA-1001
Electroporation device Amaxa™ Nucleofector™ 2b, single cuvette-based	Lonza	AAB-1001
Filtration plate MultiScreen	Millipore	MAHVN4510
Flow cytometry accessory FACSCalibur	Becton Dickinson	
Freezing container Nalgene® Mr Frosty	Sigma Aldrich	C-1562
GeneChip® Fluidics Station 450	Affymetrix	
GeneChip® Human Exon 1.0 ST Array	Affymetrix	900649
GeneChip® Hybridization Oven 640	Affymetrix	

IV. Materials

Name	Manufacturer	Product code
GeneChip® Scanner 3000	Affymetrix	
Genetic Analyzer 3130xl	Life Technologies	
High content screening reader ArrayScan® VTI	Thermo Fisher Scientific	
Image analyzer G:Box Chemi	Syngene	
Imager Gel iX	INTAS Science Imaging Instruments	
Incubator shaker Multitron	Infors HT	
Laser scanning microscope (LSM) 510	Carl Zeiss MicroImaging	
Microplate OptiPlate™-96 (96 well, white, opaque)	PerkinElmer	6005290
Mounting medium VECTASHIELD, hardset, with 4',6-diamidino-2-phenylindole (DAPI)	Vector Laboratories	H-1500
Multilabel Reader EnVision™, 2101	PerkinElmer	
Multilabel Reader VICTOR™ X5, 2030	PerkinElmer	
Nucleic Acid PrepStation ABI Prism® 6100	Life Technologies	
Optical reaction plate (96 well) MicroAmp®	Life Technologies	N801-0560
Optical reaction plate (96 well) with barcode	Life Technologies	4306737
Orbital shaker IKA® MTS 2/4 digital	IKA-Werke	
Orbital shaker Multi PSU-20	Biosan	
PCR system GeneAmp® 9700	Life Technologies	
Phase contrast microscope Leica DMIL	Leica Microsystems	
pH-meter S20 SevenEasy™	Mettler Toledo	
Pipettor CyBi®-Well, 96 channel	CyBio	
Polyvinylidene fluoride (PVDF) membrane sandwich Immuno-Blot®	Bio-Rad	162-0238
Power supply PowerPac HC	Bio-Rad	164-5052
Protein A Sepharose™ CL-4B beads	GE Healthcare	17-0780-01
Protein gel chamber Criterion™ Cell	Bio-Rad	165-6001
Quantitative PCR machine Mx2005P	Stratagene	
Reaction folders	Thermo Fisher Scientific	10483064
Roller mixer Stuart® SRT6D	Bibby Scientific	
Rotor for test tubes (10 rounds per minute)	NeoLab	2-1175
Scintillation counter Packard Tri-Carb 1900CA	PerkinElmer	
Scintillation vial	Sarstedt	73.662.500
Sonicator Misonix Ultrasonic Liquid Processor S-4000 (microplate horn; indirect sonication)	Qsonica	
Spectrophotometer NanoDrop™ 8000	Thermo Fisher Scientific	
Spectrophotometer SpectraMax® Plus 384	Molecular Devices	
Splash guard	Life Technologies	4311758
SulfoLink immobilization kit for peptides	Thermo Fisher Scientific	44999
Syringe needle Sterican®, 26 G	B. Braun Melsungen	4657683
Thermal shaker Thermomixer comfort	Eppendorf	5355000.011
Total RNA Purification Tray	Life Technologies	4305673
Wave platform shaker Polymax 2040	Heidolph Instruments	
Wet blot chamber Criterion™ Blotter	Bio-Rad	170-4070
X-ray film processor OPTIMAX®	Protec	1170-1-0000

2. Software

Table 2: Overview of used software including manufacturing company (arranged in alphabetical order).

Name	Manufacturer
2030 Manager, version 4.0	PerkinElmer
ArrayScan® VTI (500 series), version 5.6.2.1	Thermo Fisher Scientific
CellQuest™ Pro, version 4.0.2	Becton Dickinson
CloneSelect™ Imager, version 1.3	Molecular Devices
Genesis, version 1.5.0	University of Graz, Austria
GeneSnap, version 7.08	Syngene
GeneTools, version 4.01	Syngene
GeNorm applet for Microsoft® Excel®, version 3.5	University of Ghent, Belgium
GraphPad Prism®, version 5.04	GraphPad Software
FlowJo, version 7.5	Tree Star
Foundation Data Collection, version 3.0 (sequencing analysis)	Life Technologies
INTAS GDS	INTAS Science Imaging Instruments
iView™, version 1.0.182.1	Thermo Fisher Scientific
Lasergene, Protean application, version 9.1.0	DNASTAR
Lasergene, SeqMan II application, version 9.1.0	DNASTAR
Leica Application Suite, version 2.8.1	Leica Microsystems
LSM Image Examiner, version 4.2.0	Carl Zeiss MicroImaging
MxPro, version 4.1	Stratagene
NanoDrop™ 8000, version 2.0.0	Thermo Fisher Scientific
Sequencing Analysis, version 5.3.1	Life Technologies
SoftMax® Pro, version 5.2	Molecular Devices
Spotfire® DecisionSite®, version 9.1.2	TIBCO
Vi-Cell™ XR, version 2.03	Beckman Coulter
Wallac EnVision™ Manager, version 1.1.2	PerkinElmer
ZEN 2008, version 5.0	Carl Zeiss MicroImaging

3. Chemicals

All chemicals and solvents were purchased from Carl Roth, Merck, Riedel-de-Haën, and Sigma Aldrich, if not declared differently.

4. Kits, enzymes, and reagents

Table 3: Overview of used kits, enzymes, and reagents including manufacturing company and product code (arranged in alphabetical order).

Name	Manufacturer	Product code
(-)-N ⁶ -(2-phenylisopropyl)adenosine (R-PIA; 5 mM in dimethyl sulphoxide (DMSO))	Sigma Aldrich	P4532
2-chloro-N ⁶ -cyclopentyladenosine (CCPA; 5 mM in DMSO)	Sigma Aldrich	C7938
[2,8- ³ H]Adenine	PerkinElmer	NET063005MC
Absolute RNA Wash Solution	Life Technologies	430554

IV. Materials

Name	Manufacturer	Product code
Accumax™	Sigma Aldrich	A7089
Adenosine 3',5'-cyclic monophosphate sodium salt monohydrate (cyclic adenosine monophosphate (cAMP); 100 mM in deionized water)	Sigma Aldrich	A6885
Adenosine deaminase (ADA; 5 mg/ml; 200 units/mg)	Roche Applied Science	10102105001
Agarose powder for gel electrophoresis	Serva Electrophoresis	11404
AlamarBlue® solution	Life Technologies	DAL1100
Albumin bovine fraction V	Serva Electrophoresis	11945.04
Aluminum oxide	Sigma Aldrich	199974
Ampicillin (100 mg/ml in deionized water)	Sigma Aldrich	A9518
Aphidicolin from <i>Nigrospora sphaerica</i> (1mM in DMSO)	Sigma Aldrich	A0781
Bionic buffer (10x)	Sigma Aldrich	B6185
Bovine serum albumin (BSA; 50 mg/ml)	Life Technologies	15561-020
Bronchial epithelial cell growth medium (BEGM)	Lonza	CC3170
Cation exchange resin Dowex AG 50W-X4, 100-200 µm dry mesh size, 4% crosslinkage, hydrogen form	Bio-Rad	142-1341
Cell lysis buffer (10x)	Cell Signaling Technology	9803
Competent bacteria JM109, > E8 colony forming units (cfu)/µg	Promega	L2001
Complementary-deoxyribonucleic acid (cDNA) synthesis kit iScript™	Bio-Rad	170-8891
Corticotropin-releasing hormone (CRH; 100 µM in deionized water)	PolyPeptide Laboratories	SC060
CryoStor® CS10	BioLife Solutions	210102
Cycle Sequencing kit BigDye® Terminator v3.1	Life Technologies	4336919
Deoxyribonucleic acid (DNA) ladder plus O'GeneRuler, 100 base pairs (bp)	Thermo Fisher Scientific	SM1153
Doxorubicin	Sigma Aldrich	D1515
Dulbecco's modified eagle's medium (DMEM; with 4.5 g/L glucose, with L-glutamine)	Lonza	BE12-604F
Dulbecco's phosphate-buffered saline (DPBS; 1x); [-] MgCl ₂ , [-] CaCl ₂	Life Technologies	14190
DY-647-phalloidin (200 units/ml in methanol)	Dyomics	647-33
Eagle's minimum essential cell growth medium (EMEM)	Lonza	BE12-662F
Electroporation suspension Amaxa™ Cell Line Nucleofector™ Kit V	Lonza	VCA-1003
<i>Escherichia coli</i> FastMedia™ AMP X-GAL (ampicillin resistance)	InvivoGen	fas-am-x
<i>Escherichia coli</i> FastMedia™ KAN Agar (kanamycin resistance)	InvivoGen	fas-kn-s
Ethidium bromide solution (10 mg/ml)	Sigma Aldrich	E1510
FACSClean	Becton Dickinson	340345
FACSFlow	Becton Dickinson	342003
FACSRinse	Becton Dickinson	340346
Fetal bovine serum (FBS)	Life Technologies	26140
Formaldehyde (36.5-38%)	Sigma Aldrich	F8775
Formamide	Sigma Aldrich	F9037
Forskolin from <i>Coleus forskohlii</i> (10 mM in DMSO)	Sigma Aldrich	F6886
G protein-coupled receptor 6 (GPR6)-derived peptide TAAGGPDGTGEWGPPAAX	Peptide Specialty Laboratory	Synthesis on demand

Name	Manufacturer	Product code
GeneChip® Hybridization Wash and Stain Kit	Affymetrix	900720
Glycerol (99%)	Sigma Aldrich	G5516
Glycogen (20 mg/ml)	Roche Applied Science	10901393001
Goat serum	Dako	X0907
Hank's balanced salt solution (HBSS)	Life Technologies	14170
Hoechst 33342 (10 mg/ml in deionized water)	Life Technologies	H3570
Hydroxyurea (1 M in deionized water)	Sigma Aldrich	H8627
Imidazol	Carl Roth	X998.4
Kanamycin (50 mg/ml in deionized water)	Sigma Aldrich	K1876
Loading Dye solution Orange (6x)	Thermo Fisher Scientific	R0631
Luciferase substrate Beetle-Juice	PJK	102511
Luria Bertani (LB) broth liquid medium	Life Technologies	10855
Nocodazole (10 mM in DMSO)	Sigma Aldrich	M1404
Nucleic Acid Purification Elution Solution	Life Technologies	4305893
Nucleic Acid Purification Lysis Solution (2x)	Life Technologies	4305895
Paraformaldehyde (16%)	Electron Microscopy Sciences	15700
PCR mix JumpStart™ REDTaq® ReadyMix™ Reaction Mix	Sigma Aldrich	P0982
Perchloric acid, 60% in water	Sigma Aldrich	77234
Pertussis toxin from <i>Bordetella pertussis</i> (0.2 mg/ml)	Sigma Aldrich	P2980
Phenol/chloroform/isoamylalcohol (PCI; pH 8 after addition of equilibration buffer)	Sigma Aldrich	P2069
Phosphodiesterase IV inhibitor Ro-20-1724 (100 mM in DMSO)	Calbiochem	557502
Plasmid Maxi kit, EndoFree®	Qiagen	12362
Ponceau S solution	Sigma Aldrich	P7170
Propidium iodide (1 mg/ml)	Sigma Aldrich	P4864
Protease inhibitor Complete, tablets, ethylenediaminetetraacetic acid (EDTA)-free	Roche Applied Science	04693132001
Protein concentration assay (5x)	Bio-Rad	500-0006
Protein ladder PageRuler™, prestained	Thermo Fisher Scientific	SM0671
Protein ladder PageRuler™ plus, prestained	Thermo Fisher Scientific	SM1811
Protein loading buffer pack	Thermo Fisher Scientific	R0891
Proteinase K	Life Technologies	25530-015
Reduced serum medium opti-MEM® I	Life Technologies	31985
Ribonuclease (RNase) A, Concert (20 mg/ml)	Life Technologies	12091-039
RNA Purification Wash Solution 1	Life Technologies	4305891
RNA Purification Wash Solution 2	Life Technologies	4305890
RNaseZap® solution	Ambion	AM9780
Roswell Park Memorial Institute (RPMI) 1640 with GlutaMAX™ cell culture medium	Life Technologies	61870
Running buffer XT MES (20x)	Bio-Rad	161-0789
Running buffer XT MOPS (20x)	Bio-Rad	161-0788
Scintillation solution Rotiszint® eco plus	Carl Roth	0016.3
Secondary immunoglobulins donkey anti rabbit, Alexa555	Life Technologies	A31572
Secondary immunoglobulins goat anti mouse Alexa488	Life Technologies	A11017
Secondary immunoglobulins polyclonal goat anti-mouse (horseradish peroxidase (HRP)-conjugated)	Dako	P0447

Name	Manufacturer	Product code
Secondary immunoglobulins polyclonal goat anti-rabbit (HRP-conjugated)	Dako	P0448
Secondary immunoglobulins polyclonal rabbit anti-goat (HRP-conjugated)	Dako	P0449
Sephadex-G50	Sigma Aldrich	G5050
siRNA buffer (5x)	Thermo Fisher Scientific	B-002000-UB-100
siRNA transfection reagent Lipofectamine® RNAiMAX	Life Technologies	13778-075
Skim milk powder	Sigma Aldrich	70166
Super optimal broth with catabolic repressor (SOC) medium	Life Technologies	15544-034
TaqMan® Gene Expression Master Mix	Life Technologies	4369016
Transfection reagent Lipofectamine™ 2000	Life Technologies	11668-019
Transfection reagent TurboFect™ (<i>in vitro</i>)	Thermo Fisher Scientific	R0531
Tris-buffered saline (TBS; 10x)	Bio-Rad	170-6435
Tris/glycine (TG) buffer (10x)	Bio-Rad	161-0771
Triton X-100 (10%)	Fluka	93443
Trypsin-EDTA	Life Technologies	043-90317FU
Tween 20 solution (10%)	Bio-Rad	161-0781
Water, diethyl pyrocarbonate (DEPC)-treated, nuclease-free	Ambion	AM9916
Western Blotting Detection Reagents Amersham™ ECL™	GE Healthcare	RPN 2106
Western Blotting Detection System Amersham™ ECL™ Plus	GE Healthcare	RPN 2132
Wheat germ agglutinin (WGA), Alexa Fluor® 647 conjugate (1 mg/ml in DPBS)	Life Technologies	W32466

5. Buffers and solutions

All buffers were prepared using deionized water, if not specified differently.

Table 4: Overview of used thematically-sorted buffers and solutions showing commonly-used name, concentrations, and ingredients (arranged in alphabetical order).

Name	Composition
Adenylyl cyclase/cyclic adenosine monophosphate (cAMP) assay	
Imidazol buffer	20 mM imidazol, 200 mM NaCl, pH 7.4
Bacteria glycerol stock	
Glycerol solution	1:1 mixture of glycerol (50%; diluted from 99% with deionized water) and LB liquid medium containing selective antibiotic
Chromatin immunoprecipitation (ChIP)	
Dilution buffer	16.7 mM Tris, 167 mM NaCl, 1.2 mM EDTA, 1.1% Triton X-100, 0.01% sodium dodecyl sulfate (SDS), pH 8.0; 1 protease inhibitor tablet per 50 ml
Elution buffer	100 mM NaHCO ₃ , 1% SDS
HI salt buffer	500 mM NaCl, 50 mM Tris, 0.1% SDS, 1% NP40, pH 8.0
LiCl buffer	250 mM LiCl, 50 mM Tris, 0.5% NaDeoxycholate, 1% NP40, pH 8.0

Name	Composition
Lysis buffer	1% SDS, 10 mM EDTA, 50 mM Tris, pH 8.0; 1 protease inhibitor tablet per 50 ml
Protein A beads buffer	TE buffer containing 1 mg/ml BSA, 0.1 %NaN ₃
Proteinase K buffer	10 mM Tris HCl, 20 mM CaCl ₂ , 50% glycerol, pH 7.5
Radio immunoprecipitation assay (RIPA) buffer	150 mM NaCl, 50 mM Tris, 0.1% SDS, 1% NP40, 0.5% NaDeoxycholate, pH 8.0
TE buffer	10 mM Tris, 1 mM EDTA, pH 8.0
Confocal microscopy	
WGA staining solution	WGA solution (1 mg/ml), diluted to 5 µg/ml with HBSS
Deoxyribonucleic acid (DNA) sequencing	
Sequencing mix	1:1 mixture of dye-containing buffer and dilution buffer (Life Technologies; 4336919)
High content screening	
Antibody-containing staining solution (primary or secondary)	5% BSA in DPBS
Blocking buffer	1% goat serum, 2% BSA in DPBS
Fixation buffer	7.4% formaldehyde, 0.2% Triton® X-100 in DPBS
Luciferase Assay	
Luciferase cell lysis buffer	Cell lysis buffer (10x; Cell Signaling Technology; 9803), diluted to 1x with deionized water, 1 protease inhibitor tablet per 50 ml, stored at -20°C
Reconstituted Beetle-Juice	Beetle-Juice containing supplied D-luciferin and adenosine triphosphate (ATP), stored at -80°C
Oligonucleotide reconstitution	
Short interfering ribonucleic acid (siRNA) buffer (1x)	siRNA buffer (5x), diluted to 1x with DEPC-treated nuclease-free water
Ribonucleic acid (RNA) preparation	
RNA lysis buffer (1x)	Nucleic Acid Purification Lysis Solution, diluted to 1x with DPBS
Western Blot	
Blocking buffer	TBS-T containing 5% skim milk
ECL™ plus Western Blotting Detection solution	39:1 mixture of reagents RPN2132V1 and RPN2132V2 (GE Healthcare)
HEPEX Complete lysis buffer	20 mM HEPES ²³ , 100 mM NaCl, 5 mM EDTA, 1 mM Na ₃ VO ₄ , 30 mM NaF, 5% glycerol, 0.1% SDS, 1% Triton X-100, 1 mM glycerophosphate, 1 mM dithiothreitol (DTT), pH 7.4; 1 protease inhibitor tablet per 50 ml, stored at -20°C
Normal ECL™ Western Blotting Detection solution	1:1 mixture of both detection reagents (GE Healthcare; RPN 2106)
Primary antibody solution	TBS-T containing 5% skim milk with primary antibody at respective dilution indicated in table 9.
Reducing protein loading buffer (4x)	5x protein loading buffer, 20x reducing agent (2 M DTT); both reagents combined to 4x
Secondary antibody solution	TBS-T containing 5% skim milk with respective secondary antibodies (1:2,000 dilution).
TBS-T buffer	TBS (1x), 0.1% Tween 20
Towbin buffer	TG buffer (1x), 10% methanol

²³ N-2-hydroxyethylpiperazine-N'-2-ethanesulfonic acid

6. Plasmid constructs

G protein-coupled receptor 19 (GPR19) expression constructs were purchased from OriGene Technologies. The GPR19 complementary-deoxyribonucleic acid (cDNA) had been cloned into the pCMV6-XL5 expression vector downstream of a cytomegalovirus (CMV) promoter (GPR19 true clone). A construct encoding a turbo green fluorescent protein (tGFP)²⁴-tagged version of GPR19 and the G protein-coupled receptor 6 (GPR6; carboxy-terminal tag) had been constructed by cloning the GPR19/GPR6 coding sequence (CDS) into the pCMV6-AC-GFP expression vector (GPR19-tGFP; GPR6-tGFP).

The codon-optimized GPR19 expression construct was purchased from GeneArt (Life Technologies) and had been cloned into the pcDNA3.1 (+) expression vector downstream of a CMV promoter (pCMV-pcDNA3.1 (+); GPR19 (codon-optimized)). The codon-optimized messenger ribonucleic acid (mRNA) sequence encoding GPR19 is shown in the Appendix section.

Sequence-verified expression constructs for murine corticotropin-releasing hormone receptor 1 (CRHR1)-enhanced yellow fluorescent protein (eYFP²⁵; pEYFP-N1-CRHR1) and A1-adenosine receptor (A1R)-eYFP (pEYFP-N1-A1R) were a kind gift from Prof. Michael Freissmuth of the Medical University of Vienna. The modified firefly luciferase expression plasmid pGL3-Basic was from Promega and cloning of *Gpr19* promoter fragments (300 or 1,000 base pairs (bp) upstream of the *Gpr19* open reading frame (ORF)) or the CMV promoter into the multiple cloning region ahead of the luciferase CDS was performed by GeneArt (Life Technologies). In addition, a minimal promoter fragment of the herpes simplex virus thymidine kinase (TK) promoter (mini-TK) was introduced into all luciferase reporter constructs for basal luciferase expression. Besides, potential E2 promoter binding factor (E2F) transcription factor binding sites at positions -15 and/or -185 upstream of the *Gpr19* ORF were deleted in pGL3-Basic-300GPR19-miniTK constructs. Expression vectors are listed in table 5 and all empty vectors are schematically shown in figure 7 to figure 11.

Table 5: Overview of used expression vectors (arranged in alphabetical order).

Expressed gene	Vector	<i>Escherichia Coli</i> selection
A1R-eYFP	pEYFP-N1	Kanamycin
CRHR1-eYFP	pEYFP-N1	Kanamycin
	pCMV6-XL5	Ampicillin
GPR19 (codon-optimized)	pCMV-pcDNA3.1 (+)	Ampicillin
GPR19 (true clone)	pCMV6-XL5	Ampicillin
GPR19-tGFP	pCMV6-AC-GFP	Ampicillin
GPR6-tGFP	pCMV6-AC-GFP	Ampicillin
Luciferase	pGL3-Basic-miniTK	Ampicillin
Luciferase	pGL3-Basic-300GPR19-miniTK	Ampicillin

²⁴ Turbo green fluorescent protein (tGFP) has a molecular weight of 26 kDa, its excitation maximum is at 482 nm and its emission maximum is at 502 nm. The protein has no known cellular toxicity and is brighter than enhanced green fluorescent protein (eGFP; www.evrogen.com/products/TurboGFP/TurboGFP_Detailed_description.shtml).

²⁵ The enhanced yellow fluorescent protein (eYFP) has an excitation maximum at 513 nm and an emission maximum at 527 nm (www.liv.ac.uk/physiology/ncs/catalogue/Cloning/pEYFP-N1-Map.htm).

Expressed gene	Vector	<i>Escherichia Coli</i> selection
Luciferase	pGL3-Basic-1000GPR19-miniTK	Ampicillin
Luciferase	pGL3-Basic-CMV-miniTK	Ampicillin
Luciferase	pGL3-Basic-300GPR19-miniTK (mut 15)	Ampicillin
Luciferase	pGL3-Basic-300GPR19-miniTK (mut 185)	Ampicillin
Luciferase	pGL3-Basic-300GPR19-miniTK (mut 15+185)	Ampicillin
tGFP	pCMV6-AC-GFP	Ampicillin

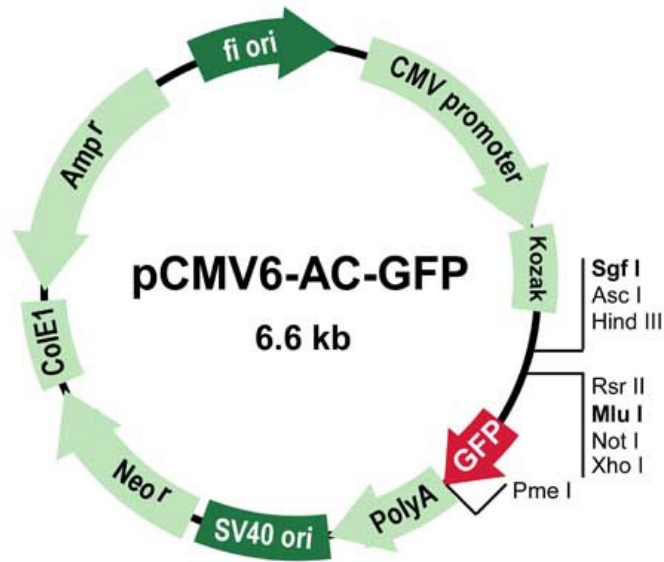


Figure 7: Schematic representation of the OriGene Technologies pCMV6-AC-GFP expression vector (PS100010; RG207204 for pCMV6-AC-GPR6-GFP, accession number NM_005284.2 and RG220379 for pCMV6-AC-GPR19-GFP, accession number NM_006143.1).

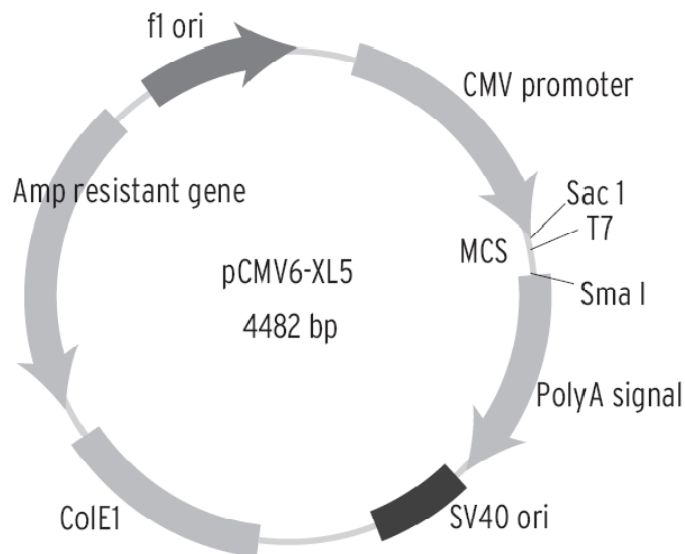


Figure 8: Schematic representation of the OriGene Technologies pCMV6-XL5 expression vector (PCM6XL5; SC126612-20 for pCMV6-XL5-GPR19 (true clone), accession number NM_006143.1).

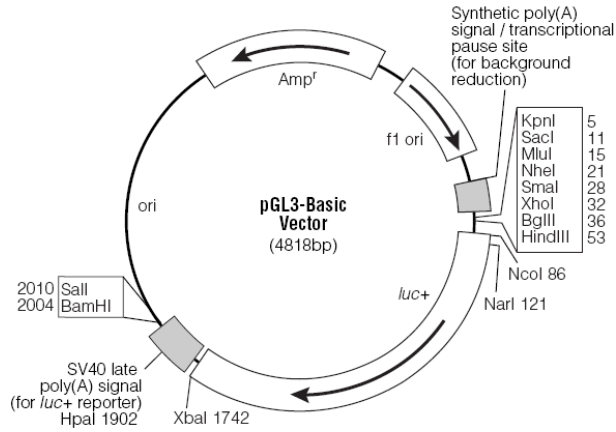


Figure 9: Schematic representation of the Promega pGL3-Basic luciferase expression vector (E1751).

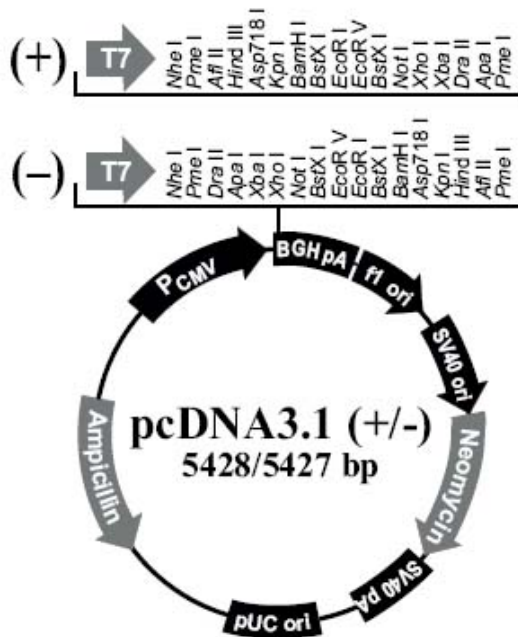


Figure 10: Schematic representation of the Life Technologies pcDNA3.1 (+/-) expression vector (V790-20).

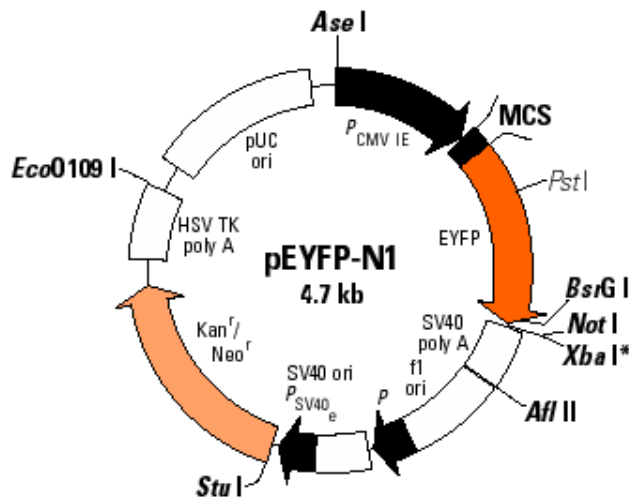


Figure 11: Schematic representation of the Clontech Laboratories pEYFP-N1 expression vector (6006-1).

7. DNA oligodeoxynucleotides

DNA oligodeoxynucleotides were purchased from Metabion and Sigma Aldrich.

Table 6: Overview of used thematically-sorted oligodeoxynucleotide/primer sequences showing name, sequence, and genomic or plasmid target (arranged in alphabetical order. fow – forward primer; rev – reverse primer).

Name	Sequence (5'-3')	Target
Chromatin immunoprecipitation polymerase chain reaction (PCR; 10 µM)		
15fow1	CTCAACGCCACGGAAAACC	Promoter <i>Gpr19</i> (-15)
15rev1	CTACAACCTCATTAAATCGGCT	Promoter <i>Gpr19</i> (-15)
185fow1	CCAAGGTGATAAACTGGCTG	Promoter <i>Gpr19</i> (-185)
185rev1	GAGCCAGACGCATGCGCAA	Promoter <i>Gpr19</i> (-185)
3184fow1	CTTGGGCTCAAGGGATATTC	Promoter <i>Gpr19</i> (-3184)
3184rev3	GAAAACATACATATTAGGGCCA	Promoter <i>Gpr19</i> (-3184)
3769fow1	GTGCAGTGGCTCATACTG	Promoter <i>Gpr19</i> (-3769)
3769rev3	CCATCTACTGGCATGTTTGC	Promoter <i>Gpr19</i> (-3769)
ALBfow2	GTAATGTCCCCAATATCTCTCC	Promoter <i>albumin</i>
ALBrev1	CCCAAACCCAGTACTAATTCCC	Promoter <i>albumin</i>
CDC6fow1	CCCGGATGTAGATTCCCTC	Promoter <i>Cdc6</i>
CDC6rev1	CCTCGAGCAATCCTCTTCTT	Promoter <i>Cdc6</i>
CDSfow1	CATCGTGGGTCTTTGATGCA	CDS <i>Gpr19</i>
CDSrev1	GGATATCCATGTGATAGCTGT	CDS <i>Gpr19</i>
Plasmid sequencing (GPR6/GPR19 expression plasmids; 10 µM)		
GPR6-1	GACGTGCTCCTGTGCGT	<i>Gpr6</i>
GPR6-2	GCTGGAAGTGCCTGGCA	<i>Gpr6</i>
GPR6-3	CCTACAAGTCCATGATCAAT	<i>Gpr6</i>
GPR19-1	CAACTACTTTGTGGTCTCCA	<i>Gpr19</i>
GPR19-2	CACTTCTTGGTGGGCTTTG	<i>Gpr19</i>
GPR19-3	CCTCTATGAAATGTTACCGAA	<i>Gpr19</i>
GPR19-4	GGCCACAGCCAGCATCTT	<i>Gpr19</i>
GPR19-5	CAGTCATTGTAAGTATTTCTT	<i>Gpr19</i>
GPR19opti-1	CCAAGTACTTCGTGGTGTGTC	<i>Gpr19</i> (codon-optimized)
GPR19opti-2	GCGTGCTGATCATCCTGTT	<i>Gpr19</i> (codon-optimized)
GPR19opti-3	GCTTACACCATCACCACCA	<i>Gpr19</i> (codon-optimized)
tGFP	CTTCAGCCCCTACCTGCT	<i>Gfp</i>
Vfow1	GCTACAACAAGGCAAGGCT	pCMV-pcDNA-3.1 (+)
Vfow2	CCATGGTGATGCGGTTTTG	pCMV-pcDNA-3.1 (+)
Vfow3	CGACTCACTATAGGGAGAC	pCMV-pcDNA-3.1 (+)
Vrev1	GCTATTGTCTTCCCAATCCT	pCMV-pcDNA-3.1 (+)
VT1.5	GGACTTTCCAAAATGTGCG	pCMV6-AC-GFP/XL5 backbone
XL39	ATTAGGACAAGGCTGGTGGG	pCMV6-AC-GFP/XL5 backbone
Plasmid sequencing (luciferase assay; 10 µM)		
CMVfow1	GTAAACTGCCCACTTGGC	Promoter CMV
GPR19-300-fow1	CTCAACGCCACGGAAAACC	Promoter fragment <i>Gpr19</i>
GPR19-1000-fow1	CATTACGAATTACACGTCAAG	Promoter fragment <i>Gpr19</i>
GPR19-1000-fow2	CCTGGACTGGTAAACAAAC	Promoter fragment <i>Gpr19</i>
pGL3fow1	GTGTGAATCGATAGTACTAAC	pGL3 Basic backbone
pGL3fow2	CTAACATACGCTCTCCATC	pGL3 Basic backbone
pGL3rev1	GCCCATATCGTTTCATAGC	pGL3 Basic backbone
pGL3rev2	GAAATGCCCATACTGTTGAG	pGL3 Basic backbone

8. Short interfering ribonucleic acids (siRNAs)

Table 7: Overview of used siRNA oligonucleotides in mRNA knockdown experiments (arranged in alphabetical order). Oligonucleotides (19mers) contained a 3'-dTdT (double deoxythymidine triphosphate) overhang. GPR19 – G protein-coupled receptor 19; PLK1 – polo-like kinase 1.

Name	Target	Target sequence (5'-3')	Accession number	Manufacturer	Product code
CTL #1	none			Thermo Fisher Scientific	D-001810-10
GPR19 Dh3	<i>Gpr19</i>	AAACUACGUUGGCAUUUCA	NM_006143	Thermo Fisher Scientific	ON-TARGETplus J-005553-08
GPR19 Sig2 (CTL #2)	<i>Gpr19</i>	CAGCAUCUUCUUUGGGAUU	NM_006143	Sigma Aldrich	SASI_Hs02_00340980, SASI_Hs02_00340980_AS
GPR19 Sig3	<i>Gpr19</i>	CCACUUCUUGGUGGGCUUU	NM_006143	Sigma Aldrich	SASI_Hs01_00133100, SASI_Hs01_00133100_A
GPR19 Sig4 (GPR19 #1)	<i>Gpr19</i>	CUGACCUUCUCAUCAGCGU	NM_006143	Sigma Aldrich	SASI_Hs01_00133104, SASI_Hs01_00133104_AS
GPR19 Sig5 (GPR19 #2)	<i>Gpr19</i>	CUCAGUCUACCACCACTUA	NM_006143	Sigma Aldrich	SASI_Hs01_00133101, SASI_Hs01_00133101_AS
PLK1	<i>Plk1</i>	GUCUCAAGGCCUCCUAAUA	NM_005030	Sigma Aldrich	SASI_Hs01_00194343, SASI_Hs01_00194343_AS

9. TaqMan® assays

Table 8: Information about TaqMan® assays used in reverse transcription quantitative real-time PCR (RT-qPCR; arranged in alphabetical order). Assays were purchased from Life Technologies. FAM™ – 6-carboxyfluorescein; MGB – minor groove binder; NFQ – non-fluorescent quencher; TAMRA – tetramethylrhodamine; VIC™ (trademark).

Gene symbol	Gene name	NCBI gene reference (different transcript variants)	Chromosome	Assay ID	Part number	Reporter dye	Reporter quencher	Amplicon length [bp]	Assay location [bp]	Assay design
<i>Actb</i>	β-actin	NM_001101.2	7		4326315E	VIC	NFQ-MGB	171	53	Amplicon spans exons and probe does not span exons.
<i>B2m</i>	β-2-microglobulin	NM_004048.2	15		4326319E	VIC	NFQ-MGB	75	409	Probe spans exons.
<i>Ccnb1</i>	Cyclin B1	NM_031966.2	5	Hs00259126_m1	4331182	FAM	NFQ	104	723	Probe spans exons.
<i>Ccne1</i>	Cyclin E1	NM_001238.1	19	Hs00233356_m1	4331182	FAM	NFQ	101	368	Probe spans exons.
<i>Chrm3</i>	Muscarinic cholinergic receptor 3	NM_000740.2	1	Hs00265216_s1	4331182	FAM	NFQ	72	1891	Both primers and probe map within a single exon.
<i>Cypa</i>	Cyclophilin A	NM_021130.3	7		4326316E	VIC	NFQ-MGB	98	433	Amplicon spans exons and probe does not span exons.
<i>Gapdh</i>	Glyceraldehyde-3-phosphate dehydrogenase	NM_002046.3	12		4326317E	VIC	NFQ-MGB	122	157	Amplicon spans exons and probe does not span exons.
<i>Gpr19</i>	G protein-coupled receptor 19	NM_006143.2	12	Hs00272049_s1	4331182	FAM	NFQ	98	691	Both primers and probe map within a single exon.
<i>Hprt1</i>	Hypoxanthine-guanine phosphoribosyl transferase 1	NM_000194.1	X		4326321E	VIC	NFQ-MGB	100	649	Probe spans exons.
<i>Lpar1</i>	Lysophosphatidic acid receptor 1	NM_057159.2 (NM_001401.3)	9	Hs00173500_m1	4331182	FAM	NFQ	73	472 (394)	Probe spans exons.
<i>Plk1</i>	Polo-like kinase 1	NM_005030.3	16	Hs00153444_m1	4331182	FAM	NFQ	91	872	Probe spans exons.
<i>Rnase P (H1)</i>	RNase P (H1)	NR_002312.1	14		4316844	VIC	TAMRA	87	41	Both primers and probe map within a single exon.
<i>Rpl32</i>	Ribosomal protein L32	NM_001007073.1 (NM_001007074.1; NM_000994.3)	3	Hs00851655_g1	4331182	FAM	NFQ	146	597 (617; 498)	Both primers and probe map within a single exon.
<i>Rplp0</i>	Large ribosomal protein P0	NM_001002.3	12		4326314E	VIC	NFQ-MGB	105	268	Amplicon spans exons and probe does not span exons.
<i>Tfr</i>	Transferrin receptor	NM_003234.1	3		4326323E	VIC	NFQ-MGB	105	1784	Amplicon spans exons and probe does not span exons.

10. Primary antibodies

Table 9: Overview of used thematically-sorted antibodies (arranged in alphabetical order). E2F – E2 promoter binding factor; GAPDH – glyceraldehyde-3-phosphate dehydrogenase; GPR19 – G protein-coupled receptor 19; IgG – immunoglobulin G; PARP1 – poly (adenosine diphosphate (ADP) ribose) polymerase 1; pH3 – phosphorylated histone H3; tGFP – turbo green fluorescent protein.

Antigen	Species	Isotype	Concentration [mg/ml]	Dilution	Manufacturer	Product code
Chromatin immunoprecipitation						
E2F-1 (C-20)	rabbit	polyclonal IgG	2		Santa Cruz Biotechnology	sc-193 X
E2F-2 (C-20)	rabbit	polyclonal IgG	2		Santa Cruz Biotechnology	sc-633 X
E2F-3 (C-18)	rabbit	polyclonal IgG	2		Santa Cruz Biotechnology	sc-878 X
E2F-4 (C-20)	rabbit	polyclonal IgG	2		Santa Cruz Biotechnology	sc-866 X
E2F-5 (E-19)	rabbit	polyclonal IgG	2		Santa Cruz Biotechnology	sc-999 X
E2F-6 (H-50)	rabbit	polyclonal IgG	2		Santa Cruz Biotechnology	sc-22823 X
E2F-7 (H-300)	rabbit	polyclonal IgG	2		Santa Cruz Biotechnology	sc-66870 X
Isotype control	rabbit	Polyclonal IgG	1		Cell Signaling Technology	2729
High content screening						
Cyclin B1	mouse	IgG1	0.5	1:250	Becton Dickinson Biosciences	554176
pH3 (Ser10)	rabbit	polyclonal	1	1:500	Millipore	06-570
α -tubulin	mouse	IgG1	1	1:1,000	Sigma Aldrich	T-6199
Western Blot						
GAPDH	mouse	IgG1	2	1:10,000	Abcam	ab8245
GPR19	rabbit	polyclonal	1	1:1,000	Abcam	ab75558
GPR19	rabbit	polyclonal	1	1:1,000	Genway Biotech	18-461-10271
GPR19	rabbit	polyclonal	1	1:1,000	Imgenex	IMG-71507
GPR19	rabbit	polyclonal	1	1:1,000	Imgenex	IMG-71508
GPR19	rabbit	polyclonal	1	1:1,000	LifeSpan Biosciences	LS-A97
GPR19	rabbit	polyclonal	1	1:1,000	Novus Biologicals	NLS97
GPR19	rabbit	polyclonal	1	1:1,000	Novus Biologicals	NLS98
GPR19	goat	polyclonal	0.2	1:500	Santa Cruz Biotechnology	sc-74634
GPR19	goat	polyclonal	0.2	1:500	Santa Cruz Biotechnology	sc-74635
GPR19	rabbit	polyclonal	0.04	1:500	Sigma Aldrich	HPA013955
GPR19	rabbit	polyclonal	1	1:1,000	Sigma Aldrich	SAB4501254
GPR19	rabbit	polyclonal	1	1:1,000	Thermo Fisher Scientific	PA1-20406
PARP1	rabbit	polyclonal	0.05	1:2,000	Cell Signaling Technology	9542
tGFP	mouse	IgG2b	1.47	1:2,000	OriGene Technologies	TA150041

11. Cell lines

Human lung-derived cell lines were obtained from American Type Culture Collection (ATCC) or European Collection of Cell Cultures (ECACC).

Table 10: Overview of used human cell lines (small cell lung cancer (SCLC), non-small cell lung cancer (NSCLC), normal lung, human embryonic kidney (HEK)-293; arranged by histology and in alphabetical order). BEGM – bronchial epithelial cell growth medium; DMEM – Dulbecco's modified eagle's medium; EMEM – Eagle's minimum essential cell growth medium; FBS – fetal bovine serum; NCI – National Cancer Institute; RPMI – Roswell Park Memorial Institute.

Cell line	Source	Number	Biosafety	Morphology	Organ	Disease (histology)	Derived from metastatic site	Gender	Age [y]	Ethnicity	Growth properties	Growth medium
COR-L88	ECACC	92031917	1		Lung	SCLC; carcinoma	Pleural effusion	Male	55	Caucasian	Semi-adherent aggregates	RPMI 1640 GlutaMAX + 10% FBS
DMS 114	ATCC	CRL-2066	1		Lung	SCLC; carcinoma		Male	68	Caucasian	Adherent	RPMI 1640 GlutaMAX + 10% FBS
DMS 53	ATCC	CRL-2062	1	Epithelial	Lung	SCLC; carcinoma		Male	54	Caucasian	Adherent	RPMI 1640 GlutaMAX + 10% FBS
NCI-H209	ATCC	HTB-172	1	Epithelial	Lung	SCLC; carcinoma	Bone marrow	Male		Caucasian	Aggregates in suspension	RPMI 1640 GlutaMAX + 10% FBS
NCI-H345	ATCC	HTB-180	1	Epithelial	Lung	SCLC; carcinoma	Bone marrow	Male	64	Caucasian	Aggregates in suspension	RPMI 1640 GlutaMAX + 10% FBS
NCI-H446	ATCC	HTB-171	1	Epithelial	Lung	SCLC; carcinoma	Pleural effusion	Male	61	Caucasian	Adherent aggregates	RPMI 1640 GlutaMAX + 10% FBS
SHP-77	ATCC	CRL-2195	1	Epithelial	Lung (apical portion of upper lobe of the left lung)	SCLC; carcinoma		Male	54	Caucasian	Suspension and loosely adherent aggregates	RPMI 1640 GlutaMAX + 10% FBS
NCI-H1703	ATCC	CRL-5889	1	Epithelial	Lung	NSCLC; adenocarcinoma; squamous cell		Male	54	Caucasian	Adherent	RPMI 1640 GlutaMAX + 10% FBS
NCI-H2122	ATCC	CRL-5985	1	Epithelial and rounded	Lung	NSCLC; adenocarcinoma; squamous cell	Pleural effusion	Female	46	Caucasian	Adherent	RPMI 1640 GlutaMAX + 10% FBS
NCI-H2170	ATCC	CRL-5928	1		Lung	NSCLC; squamous cell carcinoma		Male			Adherent	RPMI 1640 GlutaMAX + 10% FBS
BEAS-2B	ATCC	CRL-9609	2	Epithelial	Lung	Normal (bronchus)					Adherent	RPMI 1640 GlutaMAX + 10% FBS
CCD-8Lu	ATCC	CCL-201	1	Fibroblast	Lung	Normal (fibroblast)		Male	48	Caucasian	Adherent	EMEM + 10% FBS
IB3-1	ATCC	CRL-2777	2	Epithelial	Lung	Cystic fibrosis (bronchus)		Male	7	White	Adherent	BEGM (no gentamycin-amphotericin B supplement) + 10% FBS
NuLi-1	ATCC	CRL-4011	2	Epithelial	Lung	Normal (bronchus)					Adherent	BEGM (no gentamycin-amphotericin B supplement) + 10% FBS
WI-38	ATCC	CCL-75	1	Fibroblast	Lung (embryonic)	Normal (fibroblast)		Female	Fetus (3 months)	Caucasian	Adherent	EMEM + 10% FBS
HEK-293	ATCC	CRL-1573	2	Epithelial	Kidney (embryonic)	Normal			Fetus		Adherent	DMEM + 10% FBS

12. Animals

The immunization of rabbits with human GPR19 peptides was performed by Peptide Specialty Laboratories.

Table 11: Human GPR19 peptides were used for immunization of rabbits in order to generate GPR19-specific antisera. Aberrances from the human GPR19 primary sequence are indicated in red (Cys). Those Cys residues were introduced for reasons of peptide coupling to affinity column matrices.

Rabbits	GPR19 peptides used for immunization (amino- to carboxy-terminus)
#1, #2	AQLWHPHEQDYKKSSLV C (extracellular loop 3) KPTLYSIYNANFRRGMKET F C (carboxy-terminus)
#3, #4	YQKVIKIWRIGTDGRTV C (intracellular loop 3) RRTMNIVPRTKVKTIK M C (intracellular loop 3)
#5, #6	CTETATPLPSQYLMELSEEHSWMS (amino-terminus) CIDRFYTIIVYPLSFKVSREKAK M (intracellular loop 2)
#7, #8	MSSMKCYRSNAYTITSSRM A KKN (carboxy-terminus) YVGISEIP S MAKTI T KDSI Y D S C (carboxy-terminus) FDREA K E K L L A W P I N S N P P N T F V C (carboxy-terminus)

V. Methods

All experiments were carried out at room temperature, if not indicated differently. Centrifugation of 15 and 50 ml conical tubes was done in an Eppendorf 5801R centrifuge; 1.5 and 2 ml reaction tubes were centrifuged in an Eppendorf 5415R centrifuge. Cell culture plates and microplates were centrifuged in an Heraeus Megafuge 40R.

1. Molecular biology and biochemistry (*in vitro* analyses)

1.1. Nucleic acid reconstitution

Tubes containing nucleic acids were briefly centrifuged in order to collect the lyophilisate at the tube bottom. Respective stock solutions (10 μ M for deoxyribonucleic acid (DNA) oligodeoxynucleotides; 20 μ M for short interfering ribonucleic acids (siRNAs); 100 ng/ μ l for plasmid constructs) were generated using nuclease-free water or 1x siRNA buffer (placement of nucleic acid solution on an orbital shaker at 300 rounds per minute (rpm) for 30 min in order to ensure good resuspension of lyophilisates), aliquoted, and stored at -20°C.

1.2. Nucleic acid concentration measurement – NanoDrop™

Nucleic acid quantification was done using the NanoDrop™ 8000 spectrophotometer and corresponding software (nucleic acid method). Samples (1 μ l) were pipetted onto the water-initialized system optics and either DNA-50 or RNA-40 sample types were selected²⁶. The spectrophotometer had been blanked with 1 μ l of the respective solution buffer.

1.3. Isolation of total RNA from cultured cells

The ABI Prism® 6100 Nucleic Acid PrepStation was used to isolate total RNA from cultured cells (96 well format) according to the manufacturers' instructions. The growth medium was aspirated from cells grown in 96 well plates (suspension cells were first pelleted by centrifugation (250 x g, 5 min)) and the cells were subjected to lysis in 200 μ l of 1x RNA lysis buffer. Cell lysis was enforced by pipetting the lysate up and down multiple times and by freezing the lysate at -20°C.

²⁶ An optical density (OD) of 1 at 260 nm wavelength (OD₂₆₀) corresponds to either 50 μ g/ml of double-stranded DNA or 40 μ g/ml of single-stranded RNA based on absorbance measured in a spectrophotometer using a cuvette with a light path length of 1 cm). The purity of the nucleic acid solution was assessed by the OD₂₆₀/OD₂₈₀ ratio. High purity samples were considered to lie within the range of 1.8 to 2 with protein contaminations lowering this ratio (peak absorbance at 280 nm wavelength).

After thawing, the lysate was transferred onto a Total RNA Purification Tray pre-wetted with 40 μ l of RNA Purification Wash Solution 1. The 'waste' position of the station was covered by a splash guard and vacuum application (20%, 2 min) at that position was used to suck the lysate through the purification tray filter unit. Samples were washed with 500 μ l of RNA Purification Wash Solution 1 (20% vacuum, 2 min) and 650 μ l of RNA Purification Wash Solution 2 (80% vacuum, 3 min). For digestion of filter-bound DNA, 50 μ l of Absolute RNA Wash Solution (DNase treatment) were applied per slot (incubation for 15 min). Samples were further subjected to washing with RNA Purification Wash Solution 2 (400 μ l; incubation for 5 min followed by 20% vacuum, 2 min; twice 300 μ l, 20% vacuum, 2 min). The filter units were dried (90% vacuum, 5 min), any residual liquid was touched off at the 'waste' position, and the tray was transferred to the 'collection' position on top of an archive 96 well Optical Reaction Plate. RNA was eluted using 100 μ l of Nucleic Acid Purification Elution Solution (20% vacuum, 2 min) and any residual liquid was touched off into the archive plate at the 'collection' position. RNA solutions were stored at -20°C (short-term).

1.4. Complementary-deoxyribonucleic acid (cDNA) synthesis

For cDNA synthesis from isolated total RNA, the iScript™ cDNA synthesis kit from Bio-Rad was used. Per reaction, 15 μ l of RNA were mixed with 4 μ l of 5x iScript reaction mix (contains oligo-deoxythymidine triphosphate (oligo-dT)) and random hexamer primers) and 1 μ l of iScript™ reverse transcriptase (ribonuclease (RNase) H+). cDNA was synthesized in a GeneAmp® polymerase chain reaction (PCR) System 9700 (Life Technologies) under the following conditions: 5 min at 25°C, 30 min at 42°C, 5 min at 85°C, holding at 4°C. The resulting cDNA was diluted with nuclease-free water (1:5 to 1:8) for direct use in quantitative polymerase chain reaction (qPCR) applications.

1.5. Reverse transcription quantitative real-time polymerase chain reaction (RT-qPCR) gene expression and data analysis

The TaqMan® technology²⁷ from Life Technologies was used for performance of RT-qPCR with an Mx2005P qPCR machine. Per reaction, 10 μ l of TaqMan® Gene Expression Master Mix were mixed with 1 μ l of 6-carboxyfluorescein (FAM™)- (gene of interest) and VIC™-labeled (reference gene) TaqMan® assays each (duplexing)

²⁷ The TaqMan® technology allows polymerase chain reaction (PCR) product detection with the help of a probe which hybridizes specifically to complementary-DNA amplification products in between the binding sites of the forward and reverse primers. A reporter dye (5') and a non-fluorescent quencher (NFQ; 3') are attached at the respective probe ends. Besides, a minor groove binder (MGB) at the 3' end is included for melting temperature increase. In an intact probe, the NFQ is in close proximity to the reporter dye and suppresses its fluorescence signal. During each PCR amplification cycle, any DNA-bound probe is destroyed (exonuclease activity of the DNA polymerase). The NFQ can no longer quench the dye's signal, which results in the accumulation of fluorescence with each amplification cycle. This fluorescence signal is product-specific as only DNA-bound probes are erased therefore leaving any non-specific amplification undetected (www3.appliedbiosystems.com/cms/groups/mcb_support/documents/generaldocuments/cms_042996.pdf).

together with 8 μ l of diluted cDNA (reporter concentration: 5 μ M; primer forward and reverse concentration: 18 μ M). Gene-specific TaqMan® assays for expression analysis of human genes were purchased from Life Technologies and assay features are listed in table 8. The G protein-coupled receptor 19 (GPR19)-detecting assay was selected based on its property to lie entirely within the *Gpr19* coding sequence (CDS) of exon four. PCR initiation conditions were 2 min at 50°C (required for optimal AmpErase® uracil-N-glycosylase (UNG) activity²⁸) and 10 min at 95°C (AmpliTaq Gold® DNA polymerase activation) followed by 40 cycles of 15 sec at 95°C (duplex denaturation) and 1 min at 60°C (primer annealing and elongation; data collection). RT-qPCR data analysis was done using the software MxPro. Fluorescence signals were automatically baseline-corrected. Data collection thresholds were set in the log-linear dynamic signal range and resulting quantification cycle (Cq) values of the reference gene and the gene of interest were converted into relative expression ratios ($2^{-(Cq_{\text{gene of interest}} - Cq_{\text{reference gene}})} = 2^{-\Delta Cq}$; relative quantification). For qPCR assays with comparable efficiency, this method was equally precise as when relative messenger ribonucleic acid (mRNA) levels were determined on the basis of a standard curve. Pairwise duplexing was done for all genes of interest against all selected reference genes and they were normalized by geometric averaging. Relative expression ratios were normalized against a control sample (e.g., untreated cells) in the respective experimental setup ($2^{-\Delta\Delta Cq}$ method; Livak KJ and Schmittgen TD, 2001). Assay controls (either devoid of template or lacking reverse transcriptase) were included in all experiments and gave negative results (detection signals higher than Cq 38 which was above the detection range of any sample signal).

1.6. Preparation of bacterial culture plates (selective medium)

FastMedia™ agar powder (Luria Bertani (LB)-based; containing ampicillin or kanamycin as selective antibiotic) was dissolved in 200 ml of deionized water by microwave-heating until clearance of the medium was reached. 20 ml of resulting liquid medium was poured into petri dishes (10 cm diameter) and allowed to harden. Dishes were then incubated at 37°C (dry incubator) for several hours to remove superfluous liquid from the growth medium and stored at 4°C.

1.7. Bacterial transformation

50 μ l of competent bacteria and 20 ng of plasmids were mixed and incubated on ice for 30 min. Bacteria were heat-shocked at 42°C (water bath) for 45 sec and

²⁸ The enzyme uracil-N-glycosylase (UNG) is applied to prevent any carryover PCR product amplification whose synthesis was performed with deoxyuridine triphosphate (dUTP). UNG removes uracil from deoxyuridine monophosphate (dUMP)-containing DNA resulting in apyrimidinic sites. During the HotStartTaq DNA polymerase activation step, UNG gets inactivated and molecular cleavage at abasic sites destroys any contaminating molecules (www3.appliedbiosystems.com/cms/groups/mcb_support/documents/generalocuments/cms_042996.pdf; www.qiagen.com/literature/render.aspx?id=104373).

incubated on ice for 2 min. 950 μ l of super optimal broth with catabolic repressor (SOC) medium were added onto transformed bacteria followed by shaking at 250 rpm at 37°C (incubator shaker) for 1 h. Bacteria were pelleted by centrifugation at 3,300 x g for 2 min and 850 μ l of the supernatant were discarded. Pelleted bacteria were resuspended in remaining medium, 100 μ l were distributed onto prewarmed petri dishes containing LB growth medium with selective antibiotic, and incubated upside down at 37°C (dry incubator) for 12 to 16 h.

1.8. Bacteria culture

Colonies grown on agar plates were picked with a toothpick and cultured in 3 ml of LB broth liquid medium containing a selective antibiotic (ampicillin: 100 μ g/ml final concentration; kanamycin: 25 μ g/ml final concentration) in an incubator shaker (250 rpm, 8 h, 37°C). The starter culture was transferred into an Erlenmeyer flask containing 240 ml of LB broth liquid medium with the respective antibiotic and cultured in an incubator shaker (250 rpm, 16 h, 37°C).

1.9. Bacteria glycerol stock

Bacteria from 5 ml of the starter culture were pelleted by centrifugation (3,300 x g, 2 min) and the supernatant was discarded. Bacteria were resuspended in 1.7 ml of glycerol solution, transferred into a 1.8 ml CryoTube™ vial, and stored at -80°C.

1.10. Plasmid preparation (Maxi Prep)

The EndoFree® Plasmid Maxi kit was used for plasmid preparation. Bacteria were pelleted by centrifugation (4,500 x g, 10 min, 4°C), the supernatant was completely removed, and they were subjected to alkaline lysis: The bacteria pellet was resuspended in 10 ml of buffer (P1) containing RNase A (100 μ g/ml) and 10 ml of lysis buffer (P2) was added. The solution was mixed thoroughly by vigorously inverting the tube five times followed by incubation for 5 min. After addition of 10 ml of chilled neutralization buffer (P3), the solution was again mixed thoroughly by vigorously inverting the tube five times and poured into the barrel of a QIAfilter Cartridge (incubation for 10 min). The lysate was filtered through the cartridge, 2.5 ml of endotoxin removal buffer ER were added, and the solution was incubated on ice for 30 min.

The sample was applied onto a Qiagen-tip 500 column, which had been equilibrated with 10 ml of buffer QBT, and the column was allowed to empty by gravity flow. The column was washed twice with 30 ml of buffer QC and the DNA was eluted with 15 ml of buffer QN. DNA precipitation was done by adding 0.7 volumes of isopropanol to the eluate. The solution was mixed, incubated for 2 min, and centrifuged (16,000 x g, 30 min, 4°C). After removal of the supernatant, the plasmid DNA pellet was washed with 70% of ethanol (centrifugation: 16,000 x g, 10 min), air-dried, dissolved in 450 μ l of buffer TE, and stored at -20°C.

1.11. Plasmid sequencing

Linear amplification for plasmid sequencing was performed using 4 μ l of sequencing mix, 0.5 μ l of sequencing primer (10 μ M stock), and 0.3 to 0.7 μ g of DNA. The reaction mix was filled to 10 μ l with nuclease-free water. Start conditions were 1 min at 96°C followed by 28 cycles of 15 sec at 96°C (duplex denaturation), 10 sec at 53°C (primer annealing), 90 sec at 60°C (elongation), and completed by a final elongation step for 2 min at 72°C. Reaction products were diluted with an equal volume of deionized water and stored at -20°C till sample purification by Sephadex gel filtration was performed. For this purpose, a 10% slurry of Sephadex-G50 was prepared in deionized water and incubated for 2 h (soaking). 400 μ l per well were filled into a MultiScreen filtration plate which was pre-dried by vacuum filtration and excess water was removed by centrifugation at 900 x g for 4 min. A sample collection plate (MicroAmp® optical 96 well reaction plate) was filled with 30 μ l of formamide per well and placed underneath the filtration plate. Diluted linear amplification reaction products were transferred onto the wells of the filtration plate and filtered into the formamide-containing wells of the sample collection plate (centrifugation: 900 x g, 4 min). The plate was sealed with a silicone rubber gasket, locked with a snap-on lid, and loaded into the 3130xl Genetic Analyzer for sequencing. Sequences were analyzed using the SeqMan II application from the Lasergene software package.

1.12. Phenol/chloroform/isoamylalcohol (PCI)/chloroform DNA extraction

An equal volume of basic PCI (pH 8.0) was added to the DNA-containing aqueous solution and mixed by vigorous shaking. Due to a density greater than the one of water (> 1 kg/m³), organic and aqueous phases were separated by centrifugation (16,000 x g, 5 min) with the upper aqueous phase containing nucleic acids and proteins being collected at the organic/aqueous interface. The aqueous phase was transferred into a new 2 ml reaction tube and the sample was subjected to another round of PCI DNA extraction. In order to remove any residual phenol, the procedure was repeated using chloroform instead of PCI.

1.13. Isopropanol/sodium acetate/glycogen DNA precipitation

For DNA precipitation, 0.1 volumes of sodium acetate (pH 5.2; 3 M), 0.7 volumes of isopropanol, and 20 μ g of glycogen (20 mg/ml) were added per sample, mixed by vigorous shaking, and incubated for 2 min. Centrifugation (16,000 x g, 15 min) was used to pellet the DNA at the bottom of the reaction tube and the supernatant was discarded. The DNA pellet had been washed with 3 volumes of 100% ethanol (centrifugation: 16,000 x g, 5 min; removal of supernatant) and air-dried before it was resuspended in 10 mM Tris (pH 7.2) and stored at -20°C.

1.14. Chromatin immunoprecipitation (ChIP)

Cells (5×10^7) were resuspended in 20 ml of culture medium. Crosslinking of proteins on nucleic acids was performed using formaldehyde (1% final concentration). The formaldehyde-containing cell suspension was rotated on a roller mixer at 60 rpm for 10 min. Crosslinking was stopped by application of 1 ml of 2.5 M glycine solution (rotation for 5 min). Cells were pelleted (centrifugation: 250 x g, 5 min, 4°C) and the supernatant was discarded. They were washed twice with 20 ml of Dulbecco's phosphate-buffered saline (DPBS; 4°C; centrifugation: 250 x g, 5 min, 4°C; removal of supernatant), lysed in 1 ml of lysis buffer, transferred into a 2 ml reaction tube, and incubated at 4°C for 16 h.

The chromatin solution was subjected to multiple rounds of sonication to shear genomic DNA. The number, duration, and intensity of sonication pulses varied among different cell lines. In order to remove cellular debris, the lysate was centrifuged (16,000 x g, 5 min, 4°C) and the supernatant was transferred into a new 2 ml reaction tube.

350 µg of chromatin were applied per immunoprecipitation reaction and 3.5 µg were stored at 4°C as input control sample until the DNA was harvested. The respective lysate volume was diluted tenfold in dilution buffer and 5 µg of the respective antibody solution were added. Immunoprecipitation was performed on a test tube rotor (10 rpm) at 4°C for 16 h. Immune complexes were harvested with protein A sepharose CL-4B beads that target rabbit immunoglobulins. For preparation of beads, 0.02 g were dissolved in 100 µl of deionized water and washed three times with 1 ml of TE buffer (centrifugation: 500 x g, 3 min; removal of supernatant). Washed beads were resuspended in 100 µl of protein A beads buffer which resulted in a final volume of about 200 µl (dissolved beads).

The harvest of immune complexes was done by addition of protein A beads-containing solution (100 µl) and rotation on a test tube rotor (10 rpm) at 4°C for 2 h. Beads were collected by centrifugation (500 x g, 3 min; removal of supernatant) and washed with radio immunoprecipitation assay (RIPA) buffer (1 ml; rotation at 4°C for 10 min; centrifugation: 500 x g, 3 min; removal of supernatant), HI salt buffer (1 ml; rotation at 4°C for 10 min; centrifugation: 500 x g, 3 min; removal of supernatant), LiCl buffer (1 ml; rotation at 4°C for 10 min; centrifugation: 500 x g, 3 min; removal of supernatant), and twice with TE buffer (1 ml; rotation at 4°C for 10 min; centrifugation: 500 x g, 3 min; removal of supernatant). Immune complexes were eluted with 200 µl of freshly prepared elution buffer (twice; rotation at room temperature for 15 min; centrifugation: 500 x g, 3 min; collection of supernatant in new 2 ml reaction tube)²⁹. The input control sample was included from now on in subsequent steps and diluted with elution buffer (400 µl).

Samples were adjusted to 200 mM NaCl and RNase A was added to a final concentration of 300 µg/ml followed by incubation on a thermal shaker (300 rpm) at

²⁹ Washing of the antibody-bound beads was performed with buffers containing mild detergents (NaDeoxycholate, NP40, sodium dodecyl sulfate (SDS)) and different types of salts (NaCl, LiCl) in order to effectively disrupt weak non-specific interactions. Antigens are released from antibody binding upon induction of a pH-shift by the application of an acidic elution buffer (www.millipore.com/catalogue/item/17-611#; www.proteinguru.com/protocols/IP%20guide2.pdf).

37°C for 1 h in order to remove any contaminating RNA. Reversal of protein-DNA crosslinking was performed on a thermal shaker (300 rpm) at 65°C for 16 h. For protein digestion, proteinase K (20 mg/ml in proteinase K buffer; 500 µg/ml final concentration) was applied and the solution was adjusted to 9 mM ethylenediaminetetraacetic acid (EDTA) and 35 mM Tris (pH 6.5). Protein digestion was done by incubating the solution on a thermal shaker (300 rpm) at 45°C for 1 h. DNA was recovered by PCI/chloroform extraction, precipitated using isopropanol/sodium acetate/glycogen, and resuspend in 100 µl of 10 mM Tris (pH 7.2).

1.15. Chromatin fragmentation control

In order to examine the successful fragmentation of chromatin by sonication, the lysate was diluted (1:20) in deionized water and the RNA was digested by addition of RNase A (300 µg/ml final concentration) and incubation on a thermal shaker (300 rpm) at 37°C for 1 h. Protein digestion and reversal of protein-DNA crosslinking was done using proteinase K (500 µg/ml final concentration) and incubating the solution on a thermal shaker (300 rpm) at 65°C for 6 h. The DNA was recovered by PCI/chloroform extraction, precipitated using isopropanol/sodium acetate/glycogen, and resuspend in 40 µl of 10 mM Tris (pH 7.2).

20 µl of the DNA solution were mixed with 4 µl of 6x Orange Loading Dye solution and half the sample was loaded onto a slot of a 2% agarose gel for DNA separation by agarose gel electrophoresis. 5 µl of O`GeneRuler 100 base pairs (bp) DNA Ladder Plus were applied onto a slot as size marker.

1.16. ChIP PCR

ChIP PCR was performed using 2 µl of DNA solution, 0.5 µl of respective forward and reverse primer solution (10 µM stock), 12.5 µl of 2x JumpStart™ REDTaq® ReadyMix™ Reaction Mix, and 9.5 µl of nuclease-free water per reaction in a GeneAmp® PCR System 9700. PCR start conditions were 45 sec at 95°C followed by 32 to 36 cycles of 15 sec at 95°C (duplex denaturation), 15 sec at 59°C (primer annealing), and 40 sec at 72°C (elongation). In the end, a final elongation step was performed (3 min at 72°C) and the reaction was stopped by incubation at 4°C. Agarose gel electrophoresis (2% agarose gel) was performed using 10 µl of the PCR sample. 5 µl of O`GeneRuler 100 bp DNA Ladder Plus were applied onto a slot as size marker.

1.17. Agarose gel electrophoresis of nucleic acids

PCR products were size-separated by agarose gel electrophoresis. For small DNA residues (< 1 kilobase), a 2% agarose gel was used. Agarose powder and 1x Bionic buffer were mixed and boiled in a microwave on maximal intensity. The clear agarose solution was allowed to cool down for 5 min and ethidium bromide was

added to a final concentration of 0.5 µg/ml. The solution was poured into an agarose gel casting kit with slot-forming combs and allowed to become solid. This solidified gel was placed into a horizontal agarose gel unit and covered with 1x Bionic buffer. Samples and size standard were loaded into slots and a charge of 5 V per centimeter gel length was applied for 90 to 120 min. DNA-representing bands were visualized by ultraviolet light due to ethidium bromide intercalation and recorded and analyzed using a Gel iX imager.

1.18. Microarray sample preparation

RNA from human small cell lung cancer (SCLC), non-small cell lung cancer (NSCLC), and normal lung samples was purchased from OriGene Technologies. Detailed sample information is listed in table 12. Affymetrix microarray analysis was performed on the Human Exon 1.0 ST Array platform. SCLC and normal lung samples were prepared and hybridized on chips following the GeneChip® Whole Transcript Sense Target Labeling Assay manual from Affymetrix omitting the ribosomal RNA reduction step by the Boehringer Ingelheim RCV gene expression core facility. In brief, 300 ng of total RNA were applied for first cycle cDNA synthesis (first and second strand). After *in vitro* transcription, 10 µg of antisense copy RNA were subjected to second cycle cDNA synthesis followed by hydrolysis of copy RNA by RNase H. The sense strand cDNA (5.5 µg) was fragmented, biotin end-labeled, and hybridized on a microarray at 45°C in a GeneChip® Hybridization Oven for 16 h. Microarrays were washed and stained in a GeneChip® Fluidics Station using the GeneChip Hybridization Wash and Stain Kit and signals were recorded in a GeneChip® Scanner 3000. NSCLC sample preparation and hybridization was performed by Atlas Biolabs.

1.19. Cell lysis for protein extraction

After removal of the culture medium from adherent cells, 300 µl of HEPES lysis buffer were added per 1×10^6 cells and lysis was allowed to occur at 4°C for 15 min. Cells were scraped off the culture well bottom, transferred into a reagent test tube, and frozen at -20°C. The lysate was thawed, cellular debris was collected at the tube bottom by centrifugation (16,000 x g, 5 min, 4°C), and the supernatant was transferred into a new reaction tube and stored at -20°C.

Table 12: Detailed information for NSCLC, SCLC, and normal lung RNA samples from OriGene Technologies. TNM³⁰ – tumor, lymph node, metastasis (tumor staging system); AJCC³¹ – American Joint Committee on Cancer (tumor grading system); na – not assessed.

Abbreviation	Catalog number	Case ID	Sample pathology from pathology verification	Tissue of (origin/finding)	Appearance	% Tumor	% Normal	% Lesion	% Tumor hypercellular stroma	% Tumor hypo/acelluar stroma	% Necrosis	Sample pathology verification notes	Age [y]	Gender	Race	Tumor grade	TNM
Normal #1	CR561576	CJ000005278	Within normal limits	Lung / Lung	Normal	0	100	0	0	0	0	95% alveoli, 5% bronchioles	72	Female	na	Not applicable	Not applicable
Normal #2	CR562424	CD000018461	Within normal limits	Lung: right upper lobe / Lung: right upper lobe	Normal	0	100	0	0	0	0	90% alveoli, 5% bronchioles, 5% fibrovascular septa	66	Female	Caucasian	Not applicable	Not applicable
Normal #3	CR561107	CD000008641	Within normal limits	Lung / Lung	Normal	0	100	0	0	0	0	90% alveoli, 5% bronchioles, 5% fibrovascular septa	49	Female	Caucasian	Not applicable	Not applicable
Normal #4	CR560571	CD000013181	Within normal limits	Lung / Lung	Normal	0	100	0	0	0	0	85% alveoli, 5% bronchioles, 10% fibrovascular septa	66	Male	Caucasian	Not applicable	Not applicable
Normal #5	CR561589	CJ000005332	Within normal limits	Lung / Lung	Normal	0	100	0	0	0	0	85% alveoli, 5% bronchioles, 10% fibrovascular tissue	65	Male	na	Not applicable	Not applicable
Normal #6	CR560046	CD000000104	Within normal limits	Lung / Lung	Normal	0	100	0	0	0	0	91% alveoli, 1% bronchioles, 8% fibrovascular tissue	61	Female	Black	Not applicable	Not applicable
Normal #7	CR559282	CD000006947	Within normal limits	Lung / Lung	Normal	0	100	0	0	0	0	90% alveoli, 5% bronchioles, 5% fibrovascular septa	62	Female	Caucasian	Not applicable	Not applicable
Normal #8	CR560573	CD000013164	Within normal limits	Lung / Lung	Normal	0	100	0	0	0	0	90% alveoli, 5% bronchioles, 7% fibrovascular septa	64	Male	Caucasian	Not applicable	Not applicable
Normal #9	CR560259	CD000000029	Within normal limits	Lung / Lung	Normal	0	100	0	0	0	0	95% alveoli, 5% bronchioles, 5% fibrovascular tissue	38	Female	Caucasian	Not applicable	Not applicable
Normal #10	CR561643	CJ000005265	Within normal limits	Lung / Lung	Normal	0	100	0	0	0	0	90% alveoli, 5% bronchioles, 5% fibrovascular tissue	78	Male	na	Not applicable	Not applicable
Normal #11	CR561388	CJ0000005967	Within normal limits	Lung / Lung	Normal	0	100	0	0	0	0	90% alveoli, 10% fibrovascular septa	80	Male	na	Not applicable	Not applicable
Normal #12	CR560898	CD000007037	Within normal limits	Lung / Lung	Normal	0	100	0	0	0	0	95% alveoli, 5% fibrovascular septa	65	Female	Caucasian	Not applicable	Not applicable
Normal #13	CR559249	CD000005593	Within normal limits	Lung / Lung	Normal	0	100	0	0	0	0	85% alveoli, 5% bronchioles, 10% fibrovascular septa	76	Male	Caucasian	Not applicable	Not applicable
Normal #14	CR560495	CD000013452	Within normal limits	Lung / Lung	Normal	0	100	0	0	0	0	90% alveoli, 5% bronchioles, 5% fibrovascular septa	70	Female	Caucasian	Not applicable	Not applicable
NSCLC #1	CR560583	CD000013181	Adenocarcinoma of lung	Lung / Lung	Tumor	50	0	0	50	0	0	Tumor stroma (cellular): inflammatory cells	66	Male	Caucasian	AJCC G3: poorly differentiated	pT2pN0pMX
NSCLC #2	CR560096	CD000005937	Adenocarcinoma of lung	Lung / Lung	Tumor	90	0	0	0	10	0		48	Female	Black	AJCC G3: poorly differentiated	pT2pN0pMX
NSCLC #3	CR560574	CD000013164	Adenocarcinoma of lung	Lung / Lung	Tumor	60	0	15	20	0	5	Tumor stroma (cellular): desmoplastic reaction; inflammatory cells; lesion (15%); pneumonia, post-obstructive 100%; inflammation: moderate mixed inflammatory infiltrate	64	Male	Caucasian	AJCC G3: poorly differentiated	pT2pN0pMX
NSCLC #4	CR561441	CJ0000006152	Adenocarcinoma of lung	Lung / Lung	Tumor	90	0	0	5	0	5		72	Female	na	AJCC G3: poorly differentiated	pT1pN2pMX
NSCLC #5	CR561028	CD000008195	Carcinoma of lung, large cell	Lung / Lung	Tumor	85	0	0	5	0	10		56	Female	Black	AJCC G3: poorly differentiated	pT2pN2pMX
NSCLC #6	CR561109	CD000008641	Carcinoma of lung, neuroendocrine	Lung / Lung	Tumor	70	0	0	15	0	15	Tumor: large cell type	49	Female	Caucasian	Not reported	pT2pN0pMX
NSCLC #7	CR561590	CJ000005332	Carcinoma of lung, non-small cell	Lung / Lung	Tumor	90	0	0	10	0	0		65	Male	na	AJCC G3: poorly differentiated	pT2pN1pMX
NSCLC #8	CR560266	CD000000029	Carcinoma of lung, squamous cell	Lung / Lung	Tumor	80	0	0	20	0	0		38	Female	Caucasian	Not reported	pT2pN0pMX
NSCLC #9	CR561170	CD000007511	Carcinoma of lung, squamous cell	Lung / Lung	Tumor	90	0	0	7	0	3		59	Male	Caucasian	AJCC G2: moderately differentiated	pT2pN0pMX
NSCLC #10	CR562233	CJ0000000135	Carcinoma of lung, squamous cell	Lung / Lung	Tumor	90	0	0	5	0	5		80	Male	na	Not reported	pT2pN0pMX
NSCLC #11	CR561641	CJ000005265	Carcinoma of lung, squamous cell	Lung / Lung	Tumor	50	5	0	40	0	5		78	Male	na	AJCC G2: moderately differentiated	pT2pN1pMX
NSCLC #12	CR560051	CD000000104	Adenocarcinoma of lung	Lung / Lung	Tumor	70	0	0	15	15	0		61	Female	Black	AJCC G2: moderately differentiated	pT1pN0pMX
NSCLC #13	CR560699	CD000007037	Adenocarcinoma of lung	Lung / Lung	Tumor	50	0	0	45	0	5		65	Female	Caucasian	AJCC G2: moderately differentiated	pT1pN0pMX
NSCLC #14	CR560830	CD000005602	Adenocarcinoma of lung	Lung / Lung	Tumor	90	0	0	10	0	0		74	Male	Caucasian	AJCC G3: poorly differentiated	pT2pN0pMX
NSCLC #15	CR561632	CJ0000005115	Adenocarcinoma of lung	Lung / Lung	Tumor	90	0	0	5	5	0		59	Female	na	AJCC G3: poorly differentiated	pT2pN0pMX
NSCLC #16	CR561735	CJ000005381	Carcinoma of lung, large cell	Lung / Lung	Tumor	85	0	0	10	0	5		79	Female	na	Not reported	pT2pN1pMX
SCLC #1	CR562270	CF7000000173	Carcinoma of lung, small cell	Lung / Lung	Tumor	75	0	0	20	0	5	Tumor stroma (cellular): desmoplastic reaction	74	Male	Caucasian	Not reported	pT1pN0pMX
SCLC #2	CR560494	CD000013452	Carcinoma of lung, small cell	Lung / Lung	Tumor	95	0	0	2	0	3		70	Female	Caucasian	Not reported	pT2pN0pMX
SCLC #3	CR562708	CJ0000001180	Carcinoma of lung, small cell	Lung / Lung	Tumor	35	0	0	63	0	2	Tumor: morphologically consistent w th large cell neuroendocrine carcinoma of the lung (intermediate subtype of small cell carcinoma of lung); other features/comments: sample contains chronic inflammatory cells in stromal component	71	Male	na	Not reported	pT2pN0pMX
SCLC #4	CR562578	CD000021816	Carcinoma of lung, small cell	Lung / Lung	Tumor	50	5	0	0	5	40		68	Male	Caucasian	Not reported	pT1pN2pMX
SCLC #5	CR562629	CD000019503	Carcinoma of lung, small cell	Lung: left upper lobe / Lung: left upper lobe	Tumor	40	0	0	0	0	60	Tumor: only small cell carcinoma seen in this section	61	Male	Caucasian	AJCC G3: poorly differentiated	pT4pN0pMX
SCLC #6	CR560848	CD000005593	Carcinoma of lung, small cell	Lung / Lung	Tumor	75	0	0	20	0	5		76	Male	Caucasian	Not reported	pT4pN0pMX
SCLC #7	CR561968	CJ0000014767	Carcinoma of lung, small cell, metastatic	Lung: right middle lobe / Lymph node	Tumor	50	0	0	5	5	40		63	Male	na	AJCC G3: poorly differentiated	pT1pN1pMX
SCLC #8	CR560068	CD000005518	Carcinoma of lung, small cell	Lung / Lung	Tumor	85	0	0	5	0	10		54	Male	Caucasian	Not reported	pT2pN2pMX

³⁰ The TNM tumor staging system evaluates the size of the tumor (T1 to T4), the disease spread to regional lymph nodes (number and extent of affected lymph nodes; N1 to N3), and the involvement of distant metastasis (M0 – no metastasis; M1 – present metastasis; MX – no information about metastasis; <http://www.cancer.gov/cancertopics/factsheet/detection/staging>).

³¹ The AJCC tumor grading systems evaluates the differentiation status of cancer cells from G1 (well-differentiated; low grade) to G4 (poorly differentiated; high grade; <http://www.cancer.gov/cancertopics/factsheet/detection/tumor-grade>).

1.20. Protein concentration determination

Protein concentrations were determined using a Bradford-based protein assay³². 2 µl of the protein lysate were diluted with 200 µl of the protein concentration assay solution (1x) in a 96 well test plate and absorbance at 595 nm was measured with a spectrophotometer. Absorbance values were correlated to those of a bovine serum albumin (BSA) standard curve ranging from 500 µg/ml to 1.95 µg/ml in order to obtain protein concentrations of the samples.

1.21. Sodium dodecyl sulfate (SDS)-polyacrylamide gel electrophoresis (PAGE)

Equal amounts of protein were diluted in 4x reducing loading buffer (1x final) and boiled at 95°C for 5 min³³. Samples (and 5 to 10 µl of the respective PageRuler™ protein ladder) were loaded onto slots of Criterion™ XT precast protein separation gels assembled in a Criterion™ Cell protein gel chamber which had been filled with either XT MES (1x) or MOPS (1x) running buffer. Protein electrophoresis was performed by application of a constant charge (150 V).

1.22. Immunoblotting (Western Blot)

The gel containing separated proteins was assembled with an Immuno-Blot® polyvinylidene fluoride (PVDF) membrane which had been equilibrated with methanol for 10 sec. Both the membrane and the gel were transferred into Towbin buffer and fixed between absorbent filter paper and a foam pad on both sides in a gel holder cassette. Membrane transfer of proteins was done using a Criterion™ Blotter wet blot chamber filled with Towbin buffer at a constant current intensity of 900 mA for 30 to 50 min depending on the number of applied blotting cassettes.

The membrane was incubated on an orbital shaker (70 rpm) for 1 h in blocking buffer. Specific protein detection was done by incubating the membrane in primary antibody solution at 4°C for 16 h (wave platform shaker, 20 rpm) followed by washing in TBS-T buffer for 10 min (three times). Respective horseradish peroxidase (HRP)-conjugated secondary antibodies were applied to the membrane for 1 h (orbital shaker; 70 rpm). The membrane was washed in TBS-T buffer for 10 min (three times), rinsed with deionized water, and soaked either with normal ECL™ (1 min) or ECL™ plus (2 min) Western Blotting Detection solution. Excess detection reagent was drained off the membrane and after transfer into a reaction folder, chemiluminescence signals were detected using light sensitive films (Amersham™

³² The Coomassie blue dye preferentially binds to aromatic and basic amino acid residues. Upon protein binding, its absorbance maximum is shifted from 465 nm to 595 nm (labs.fhcr.org/fero/Protocols/BioRad_Bradford.pdf).

³³ Denaturation and negative charging of proteins is achieved by boiling of cell lysates in a sodium dodecyl sulfate (SDS)-containing loading buffer – a prerequisite for their subsequent size/weight separation by polyacrylamide gel electrophoresis (PAGE).

Hyperfilm™) in an autoradiography cassette³⁴. Exposure times varied considerably depending on the protein amount loaded or primary antibodies used. They had been optimized to prevent oversaturated signals. Films were developed using an OPTIMAX® X-ray film processor. Alternatively, chemiluminescence signals were detected using a G:Box Chemi image analyser and the software GeneSnap for image acquisition and GeneTools for image analysis.

Equal protein loading/transfer was examined by Ponceau S solution application to the membrane for 1 min and the membrane was rinsed with deionized water until a stained band pattern appeared (red protein bands)³⁵.

1.23. Luciferase reporter assay³⁶

Cells were washed with DPBS and lysed using 60 µl of 1x lysis buffer (shaking on an orbital shaker (500 rpm, 4°C)). 20 µl of the lysate were transferred into wells of a white 96 well microplate (OptiPlate™) and 100 µl of reconstituted Beetle-Juice® (ambient) were added per well. The light signal (glow) was measured in an EnVision™ 2101 Multilabel Reader (2 sec) after 10 min.

1.24. Antiserum purification on affinity peptide columns

Peptides immobilized on SulfoLink affinity column matrices via a Cys residue were provided by Peptide Specialty Laboratories. 1 mg of the respective peptide was coupled to 0.5 ml of the column matrix. The matrix was equilibrated with 10 ml of DPBS. The rabbit serum (5 ml) was diluted with an equal volume of DPBS and incubated with 0.5 ml of the peptide-bound matrix (resuspended in 4 ml of DPBS) on a roller mixer (30 rpm) at 4°C for 16 h. The suspension was transferred back to an affinity column and the flow-through was applied onto the column a second time. Washing of the column was performed first with 10 ml of DPBS (three times) followed by 10 ml of 10 mM Na₃PO₄ (pH 6.8; twice). Column-peptide-bound antibodies were eluted in ten fractions using 0.5 ml of 0.1 M glycine (pH 2.4) each and collected in reaction test tubes containing 35 µl of 2 M K₂HPO₄ for neutralization of the eluate. The protein concentration of each fraction was determined using a Bradford-based protein assay. Fractions with highest protein concentrations were pooled and split in 100 µl portions. An equal volume of glycerol and NaN₃ to a final concentration of

³⁴ The application of luminol-based ECL™ Western Blotting detection solutions results in enhanced chemiluminescence through the oxidation of luminol which is catalyzed by the peroxidase of horseradish peroxidase (HRP)-labeled secondary antibodies bound to primary antibodies allowing for the detection of respective antigens on the membrane (www.gelifesciences.com/aptrix/upp01077.nsf/Content/Products?OpenDocument&moduleid=46853).

³⁵ Due to its negative charges, Ponceau S binds to positively charged protein groups. It further binds to non-polar protein regions (www.sigmaaldrich.com/etc/medialib/docs/Sigma-Aldrich/Product_Information_Sheet/p7170pis.Par.0001.File.tmp/p7170pis.pdf).

³⁶ Firefly luciferase catalyzes the oxidation of luciferin to oxyluciferin with the help of adenosine triphosphate (ATP) and oxygen emitting light in the green to yellow spectrum (www.promega.com/resources/product-guides-and-selectors/protocols-and-applications-guide/bioluminescent-reporters/).

0.05% were added and aliquots were stored at -20°C . Columns were regenerated upon washing with 10 ml of 10 mM Na_3PO_4 (pH 6.8), 10 ml of 1 M DPBS-based NaCl (twice), and 10 ml of DPBS containing 0.05% NaN_3 (twice) and stored at 4°C .

2. Cellular biology (*in vivo* analyses)

2.1. Antiserum generation against human GPR19

Rabbits were immunized with human GPR19 peptides in order to generate specific antisera against GPR19. Peptide synthesis and immunizations were performed by Peptide Specialty Laboratories. GPR19 peptides with which respective animals had been immunized are listed in table 11. Immunizations (0.2 μmol total peptide coupled to maleimide-activated keyhole limpet hemocyanin as peptide carrier) were done on day 0 with complete Freund's adjuvant and on days 28, 42, and 56 with incomplete Freund's adjuvant. Animals were sacrificed on day 70 (final bleed).

2.2. Cell culture

Frozen cells were thawed at 37°C , cultured without antibiotics in normal growth medium (Roswell Park Memorial Institute (RPMI) 1640 with GlutaMAX™, 10% fetal bovine serum (FBS; heat-inactivated at 55°C for 1 h)) except for IB3-1 and NuLi-1 (bronchial epithelial cell growth medium (BEGM), 10% FBS), CCD-8Lu and WI-38 (Eagle's minimum essential cell growth medium (EMEM), 10% FBS), and HEK-293 (Dulbecco's modified eagle's medium (DMEM), 10% FBS), and maintained in the logarithmic growth phase. NuLi-1 cells were cultured in collagen IV-coated flasks. Trypsin-EDTA was used for detachment of adherent cells from the bottom of any culture device. Cells growing in aggregates in suspension were dissociated by incubation in an equal volume of Accumax™ at 37°C for 10 min and squeezed through a 26 G needle. Remaining cell clumps were removed by filtering the suspension through a cell strainer. Cell numbers and viability was assessed using the Vi-Cell™ XR cell viability analyzer. Cell lines were cultured in incubators at 37°C , 5% CO_2 , and 95% humidity and discarded when a high passage number (> 40) was reached. They were authenticated using short tandem repeat analysis and tested for mycoplasma contamination on a regular basis by the Boehringer Ingelheim Genomics Core Facility.

2.3. Freezing of cells

Cells (5×10^6) were pelleted by centrifugation (250 x g, 5 min), resuspended in 1 ml of CryoStor® solution, and transferred into a 1.8 ml CryoTube™ vial. Freezing was done at a cooling rate of $-1^{\circ}\text{C}/\text{min}$ in a freezing container filled with isopropanol at -80°C and cells were finally stored in liquid nitrogen.

2.4. siRNA transfection (96 well culture plate)

Reverse transfection of cells was done using Lipofectamine® RNAiMAX in a 96 well cell culture plate. 0.3 µl of transfection reagent were mixed with 20 µl of siRNA-containing opti-MEM® I reduced serum medium (2 to 60 nM final siRNA concentration) and transfection complexes were allowed to form for 20 min. 100 µl of the cell suspension containing 2,000 to 3,500 NCI-H1703 or 10,000 DMS 53 cells were added per well. In order to reduce toxicity caused by the transfection procedure, 80 µl of normal growth medium were added per well 8 h after transfection.

2.5. Forward plasmid transfection (6 well culture plate)

Transfection of HEK-293 cells with expression plasmids in 6 well culture plates was performed using TurboFect™ transfection reagent. Cells (2.5 to 3×10^5) were seeded in 1.8 ml of DMEM containing 10% FBS into wells of a poly-D-lysine-coated³⁷ 6 well cell culture plate 8 h prior to transfection. 2 µg of plasmid DNA (0.5 µg of the plasmid of choice (each); the empty vector control plasmid pCMV6-XL5 was used to account for the residual amount of plasmid DNA) were diluted in 200 µl of serum-free DMEM followed by addition of TurboFect™ transfection reagent (3 µl). The solution was mixed and transfection complexes were allowed to form for 20 min. The transfection solution was added onto cells and the medium was changed to DMEM containing 10% FBS 4 h after transfection.

2.6. Reverse plasmid transfection (8 well chamber slide)

HEK-293 cells were reverse-transfected with turbo green fluorescent protein (tGFP)- or enhanced yellow fluorescent protein (eYFP)-tagged receptor-encoding plasmids in chambers of a BioCoat™ poly-D-lysine-coated 8 well culture slide using TurboFect™ transfection reagent. 0.1 µg of plasmid DNA (0.05 µg of the plasmid of choice, 0.05 µg of the empty vector control plasmid (pCMV6-XL5)) were diluted in 20 µl of serum-free DMEM followed by addition of TurboFect™ transfection reagent (0.45 µl). The solution was mixed and transfection complexes were allowed to form for 20 min at the well bottom. Cells (10,000 in 200 µl of DMEM containing 10% FBS) were added per chamber.

Reverse transfection of DMS 53 and NCI-H2170 cells was performed with Lipofectamine™ 2000. Per chamber, 0.6 µl of transfection reagent were diluted in 25 µl of opti-MEM® I and incubated for 5 min. Diluted plasmid DNA (0.2 µg in 25 µl of opti-MEM® I) was added to the diluted transfection reagent, mixed, and incubated for 20 min to allow the formation of transfection complexes. Cells (10,000 in 100 µl of culture medium (RPMI 1640 with GlutaMAX™ containing 10% FBS)) were added per chamber and 200 µl of fresh culture medium were added 8 h later.

³⁷ Poly-D-lysine can be used to facilitate the attachment of cells to plastic surfaces.

2.7. Electroporation

Plasmid transfer into DMS 53, HEK-293, and NCI-H1703 cells was done using the single cuvette-based Nucleofector™ system. Cells (5 to 6×10^5) were resuspended in $100 \mu\text{l}$ of Amaxa™ Cell Line Nucleofector™ Kit V solution, mixed with 2.5 to $5 \mu\text{g}$ of DNA, and transferred into an electroporation cuvette. Electroporation was performed using program X-005 for DMS 53 and NCI-H1703 cells and program Q-001 for HEK-293 cells. Electroporated cells were flushed out of the cuvette with prewarmed normal growth medium. Cells were seeded in culture plates and the medium was changed the day after transfection. The medium change was not performed in luciferase reporter assays.

2.8. Cell cycle arrest (synchronization)

For arresting cells at different stages of the cell cycle 1×10^5 cells were seeded in wells of a 6 well culture plate followed by 24 h incubation with hydroxyurea (arrest at gap 1 (G1)-DNA synthesis (S) phase transition; final concentration: 1 mM), aphidicolin (arrest at G1-S transition; final concentration: $2.5 \mu\text{M}$), or nocodazole (arrest at mitosis (M) phase; final concentration: 300 nM). Cells were released from cell cycle arrest by washing off the arrest-causing agent and subsequent culturing using normal growth medium.

2.9. Flow cytometry – cell cycle analysis

For cell cycle analysis, siRNA-transfected cells seeded in wells of a 96 well culture plate or cell cycle-arrested cells seeded in wells of a 6 well culture plate were detached from the well bottom, pelleted, resuspended in 4 ml of 70% ethanol (fixation; -20°C), and stored at -20°C for at least 24 h. Cells from six wells were pooled when they had been grown in 96 well plates. Fixed cells were washed with DPBS and subjected to RNase A treatment (1 mg/ml final concentration) for 5 min followed by propidium iodide³⁸ DNA staining ($50 \mu\text{g/ml}$ final concentration). Data collection was done using a FACSCalibur flow cytometer and at least 10,000 cells were recorded, if possible. The flow rate was kept below 200 counts per second in order to assure proper separation of detected cells. Data were analyzed with FlowJo software. The Watson Pragmatic model (Watson JV *et al.*, 1987) was chosen as curve fitting algorithm for cell cycle analysis in order to classify cells into the different phases of the cell cycle. This model fits G1 and gap 2 (G2)/M phase populations with Gaussian

³⁸ Propidium iodide is frequently used to stain nucleic acids and to differentiate between alive and dead cells. This intercalating agent and fluorescent dye can only enter cells that have lost their plasma membrane integrity and become permeable. In addition, propidium iodide can be utilized to determine the DNA content of fixed (permeabilized) cells in flow cytometric cell cycle analyses. As it both binds to DNA and RNA, ribonuclease treatment is necessary in order to account for a specific signal resulting from its binding to DNA. Fluorescence is enhanced about 20 to 30 fold when propidium iodide has bound to nucleic acids. Its excitation maximum then lies at 535 nm wavelength with an emission maximum at 617 nm (www.biolegend.com/propidium-iodide-solution-2651.html; probes.invitrogen.com/media/pis/mp01304.pdf).

curves and the S phase exactly based on the propidium iodide area signal (fluorescence channel 2 (FL2)-area (A)) histogram. Cell doublets were removed prior to analysis (doublet discrimination mechanism (DDM) on the FL2 (propidium iodide) signal: gating on singlets on a propidium iodide area (FL2-A) versus width (FL2-W) signal graph).

2.10. Flow cytometry – transfection optimization

Turbo GFP-plasmid-transfected cells seeded in wells of a 6 well culture plate were removed from the culture dish, pelleted, and washed with DPBS. The cell pellet was resuspended in 400 μ l of propidium iodide solution (50 μ g/ml in DPBS) and subjected to flow cytometric analysis. Turbo GFP positive, propidium iodide negative cells were determined using a fluorescence channel 1 (FL1; tGFP)-height (H) versus fluorescence channel 2 (FL2; propidium iodide)-H dot plot with quadrant statistics.

2.11. Proliferation – alamarBlue®

The alamarBlue® assay solution was added to the culture medium (1:10 dilution) of cells grown in 96 well culture plates. Fluorescence signals arising from the indicator dye resazurin (dark blue; non-fluorescent) being reduced to resorufin (pink; fluorescent) by metabolically active cells were recorded using a 2030 Multilabel Reader VICTOR™ X5 (560 excitation/590 emission nm filter settings). The cells' metabolic activity corresponds to the number of living cells which is proportional to the amount of fluorescence measured.

2.12. Proliferation – confluence

Cellular proliferation was assessed by 96 well confluence determination using a CloneSelect™ Imager. Focus and brightness levels were kept constant during time series measurements and cell detection method 1 was applied.

2.13. Immunofluorescence labeling

siRNA-transfected cells cultured in black poly-D-lysine-coated 96 well culture plates were fixed for 10 min with an equal volume of fixation buffer, washed twice with DPBS (CyBi®-Well 96 channel pipettor), and incubated in 50 μ l of blocking buffer for 5 min followed by twice DPBS washing. Cells were stained for cyclin B1 and phosphorylated histone H3 (pH3) or for tubulin with 50 μ l of antibody-containing staining solution for 1 h and washed with 0.01% Tween in DPBS and DPBS only. They were incubated in 50 μ l of secondary antibody and Hoechst-containing staining solution (goat anti mouse Alexa488, 1:2,000 dilution; donkey anti rabbit, Alexa555,

1:4,000 dilution; Hoechst 33342³⁹, 1:1,500 dilution) for 1 h. For actin filament staining, DY-647-phalloidin (1:100 dilution) was included (Capani F *et al.*, 2001). Cells were washed with 0.01% Tween in DPBS and DPBS only and 180 µl of DPBS were added per well. The plate was sealed with black backing tape and stored at 4°C.

2.14. High content screening (HCS)

Fluorescence-based cell staining detection was done with an ArrayScan® VTI HCS reader. Six wells per reaction condition and 36 fields per well were recorded, each with multiparameter fluorescence, at 20x magnification. Multiple numerical feature values (e.g., object area and shape, signal intensity) for each signal within an optical field were generated using the software ArrayScan® VTI. The total number of detected cells per well was in the range of 300 to 1,000 depending on siRNA treatment and time after siRNA transfection. Measurements were performed with the following settings and features:

Settings:

- Acquisition camera mode: standard
- Autofocus interval: 2
- Background correction: 0
- Fields per well: 36 (maximal)
- Filter set: XF93
- Fixed exposure time (set to 25% the saturation of negative controls)
- Fixed threshold (adjusted to staining intensities)
- Nuclear smooth factor channel1: 0
- Objective: 20x magnification
- Segmentation channel1: 6

General features of detection channels 1, 2, 3, and 4:

- Hoechst 33342 staining⁴⁰:
 - cellsperfieldch1
 - objectareach1⁴¹
 - objecttotalintench1⁴²
 - objectvarintench1⁴³
 - nucfragch2⁴⁴

³⁹ The cell permeable dye Hoechst 33342 stains DNA by preferential binding to the DNA minor groove in adenine-thymine-rich regions. It is excited by ultraviolet light (excitation maximum at 350 nm when bound to DNA) and emits fluorescent light in the blue spectrum (emission maximum at 461 nm) being sensitive to chromatin state and DNA conformation (tools.invitrogen.com/content/sfs/manuals/mp21486.pdf; www.thermoscientific.com/ecomm/servlet/productsdetail_11152_L10704_92518_13575985_-1).

⁴⁰ Both channels 1 and 2 detected Hoechst 33342 DNA staining. However, channel 1 was used for nuclei detection and channel 2 detected nuclear subfragmentation of objects identified in channel 1.

⁴¹ Total nuclear area.

⁴² Total intensity: sum of intensities of a detected object.

⁴³ Variance: standard deviation of pixel intensities in a detected object.

- totalintench2
- Alexa488 (pH3/tubulin staining):
 - totalintench3
- Alexa555/Phalloidin647 (cyclin B1/actin staining):
 - totalintench4

The data were processed and visualized by Spotfire® DecisionSite® and iView™. For cell cycle analysis, the relative amount (percentage) of cells in sub G1 (ccy_psub2n), G1 (ccy_p2n), S (ccy_ps), G2/M (ccy_p4n), and above G2/M (ccy_pabove4n) phases was calculated on the basis of Hoechst 33342 DNA staining (nuclear area, fragmentation and shape, total and average signal intensity).

Changes in cellular population parameters, e.g., intensities of pH3, cyclin B1, actin, or tubulin staining were determined by a Kolmogorov-Smirnov (KS) goodness-of-fit analysis (KS statistic) as described (Giuliano KA *et al.*, 2004). In brief, population density distributions of replicate wells (immunofluorescence histograms) were transformed into cumulative distribution frequency plots. The KS statistic value for each experimental condition was calculated as the maximal height difference (d) between its cumulative distribution function and the one from all controls combined (Perlman ZE *et al.*, 2004).

Principal component analysis (PCA) and multidimensional scaling (MDS)⁴⁵ of recorded data were performed in order to select *Gpr19* siRNAs with minimal off-target effects. The following parameters obtained from Hoechst 33342 (channel 1 and channel 2; MDS only), actin (channel 3), and tubulin (channel 4; PCA only) stainings were used for PCA and MDS (KS statistic (d)):

PCA:

- d_entropych3 and d_entropych4 ⁴⁶
- d_spotfibercountch3 and d_spotfibercountch4 ⁴⁷
- d_spotfibertotalareach3 and d_spotfibertotalareach4 ⁴⁸
- d_totalintench3 and d_totalintench4
- d_varintench3 and d_varintench4

⁴⁴ Nuclear fragmentation.

⁴⁵ Principal component analysis (PCA) and multidimensional scaling (MDS) are methods of data reduction. Both methods aim at reducing the dimensionality of a data set (i.e., they convert a high-dimensional data set into one with fewer variables) without notable loss of information. Using linear combinations, correlated original variables are transformed into a final small set of uncorrelated variables (usually three dimensions) which are called principal components. Here, PCA neglects the variations when multiple variables are combined. However, MDS takes these variations into consideration and attempts to preserve distances between pairs of variables (astor.som.jhmi.edu/~cope/687/pdf/pca-mds.pdf; www.math.uwaterloo.ca/~aghodsib/courses/f10stat946/notes/lec10-11.pdf).

⁴⁶ Entropy: distribution of pixel intensities in a detected object.

⁴⁷ Spot fiber count: number of detected fibers.

⁴⁸ Spot fiber total area: area of detected fibers.

MDS:

- d_nucavgintench1 ⁴⁹
- d_nucentropych1 ⁵⁰
- d_nucperimch1 ⁵¹
- d_nuctotalareach1
- d_nucshapelwrch1 ⁵²
- d_nucshapep2ach1 ⁵³
- d_nucfragch2
- d_entropych3
- d_spotfibercountch3
- d_spotfibertotalareach3
- d_totalintench3
- d_varintench3
- ccy_psubG1
- ccy_p2N
- ccy_pS
- ccy_p4N
- ccy_pabove4N

The proliferation index refers to identified cellular objects per field. The following parameters were integrated into the apoptotic index⁵⁴:

- ccy_psubG1
- r_gr_nucavgintench1
- r_gr_nuctotalareach1
- r_gr_nucperimch1
- r_gr_nucshapep2ach1
- r_gr_sm_nucentropych1
- r_gr_nucfragch2

2.15. Confocal microscopy

Cells grown on chamber slides were fixed with paraformaldehyde (4% final concentration) for 10 min and washed three times with Hank's balanced salt solution (HBSS). Membrane staining was done for 10 min with wheat germ agglutinin (WGA)⁵⁵ staining solution. Cells were washed twice with HBSS and the chambers were removed from the glass slide. They were mounted with DAPI⁵⁶-containing mounting medium and a glass cover slip and incubated at 4°C for at least 10 h. Confocal microscopy analysis was performed on a Zeiss Laser Scanning Microscope (LSM) 510 (60x magnification) using the software ZEN 2008 and LSM Image Examiner.

⁴⁹ Nuclear average signal intensity.

⁵⁰ Nuclear entropy.

⁵¹ Nuclear perimeter.

⁵² Length versus width ratio of a nuclear object.

⁵³ Discrepancy between actual nuclear perimeter line and smoothed perimeter line (ellipse).

⁵⁴ Apart from the relative number of cells assigned to the sub G1 phase of the cell cycle, data were compared to control samples and the percentage lying above (gr = greater) or below (sm = smaller) was determined (r = responder).

⁵⁵ Wheat germ agglutinin (WGA) selectively detects N-acetyl glucosamine and N-acetyl neuraminic acid residues often present on proteins of the plasma membrane (Wright CS, 1984; Prasad BM *et al.*, 2010).

⁵⁶ DAPI (4',6-diamidino-2-phenylindole) preferentially stains double-stranded DNA by favoring binding to the DNA minor groove in adenine-thymine-rich regions. It is excited by ultraviolet light (excitation maximum at 358 nm when bound to DNA) and emits fluorescence light in the blue spectrum (emission maximum at 461 nm). DAPI is often used in multilabel fluorescence applications to stain cellular nuclei (probes.invitrogen.com/media/pis/mp01306.pdf).

2.16. Phase contrast microscopy

Pictures of cells were recorded (20x magnification) and processed using a Leica DMIL phase contrast microscope.

2.17. Adenylyl cyclase/cyclic adenosine monophosphate (cAMP) assay

Assays measuring the formation of cAMP from adenosine triphosphate (ATP) by adenylyl cyclase were performed with adherent cells grown in wells of a poly-D-lysine-coated 6 well culture plate (a schematic overview is given in figure 12). The growth medium was removed and cells were radioactively labeled by incubation with 1 ml of [3H]adenine labeling medium (1 μ Ci/ml; 27.78 nM in culture medium containing 10% FBS) at 37°C for 16 h. Removal of labeling medium was followed by starvation of cells with 1 ml of growth medium lacking FBS at 37°C for 90 min. Starvation medium further contained a phosphodiesterase IV inhibitor (Ro-20-1724⁵⁷; 100 μ M) and adenosine deaminase (ADA⁵⁸; 1 U/ml). After removal of the starvation medium, cells were incubated with 1 ml of stimulation medium containing Ro-20-1724 (100 μ M) and ADA (1 U/ml) at 37°C for 30 min. Cells were lysed using 1 ml of 2.5% perchloric acid containing surplus unlabeled cAMP⁵⁹ (100 μ M) and incubated at 4°C for 40 min. Leaving behind cellular debris, the lysate was removed from the tilted culture well and neutralized with 110 μ l of 4.2 M KOH solution which resulted in salt precipitation.

Separation of cAMP from ATP was performed by sequential chromatography using Dowex anion resin and alumina oxide columns⁶⁰. The Dowex slurry was prepared by saturating the resin (500 g) with 500 ml of deionized water. 500 ml of 1 M HCl were added and the supernatant was poured off after incubation for 10 min. The suspension was washed three times with 1 l of deionized water followed by incubation in 500 ml of 1 M NaOH for 10 min. After pouring off the supernatant, the slurry was resuspended in deionized water (1:1 suspension). 2 ml of the Dowex suspension were added per separation column (5 ml pipet tip into which glass wool had been filled) and the slurry was washed with 3 ml of 1 M HCl and three times with

⁵⁷ The selective inhibitor of cyclic adenosine monophosphate (cAMP)-specific phosphodiesterase IV, Ro-20-1724, prevents the hydrolysis of cAMP.

⁵⁸ Adenosine deaminase (ADA) was present here to destroy adenosine released from cells.

⁵⁹ In order to counteract the hydrolysis of 3H-labeled cyclic adenosine monophosphate (cAMP) by cyclic nucleotide phosphodiesterases, a vast excess of unlabeled cAMP was added to the lysis buffer in this experiment.

⁶⁰ The separation of the cyclic 3',5'-adenosine monophosphate (cAMP) from 2', 3', or 5' adenosine monophosphate (AMP), adenosine diphosphate (ADP), and adenosine triphosphate (ATP) can be achieved by sequential chromatography (Dowex cation exchange resin and neutral alumina columns) as described (Salomon Y *et al.*, 1974; Johnson RA and Salomon Y, 1991). ATP and ADP are eluted earlier and 5'-AMP is eluted later than cAMP from the Dowex column (Krishna G *et al.*, 1968). Utilizing this elution profile, one can capture the elution fraction containing most cAMP. Further sample cleanup is achieved by applying this fraction to hydrous aluminum oxide columns to which multivalent ions preferentially bind. At neutral pH, cAMP is a univalent anion whereas ATP, ADP, and AMP are all multivalent anions. This only allows cAMP but neither AMP nor ADP nor ATP to pass the alumina column (Ramachandran J, 1971; White AA and Zenser TV, 1971).

5 ml of deionized water. For preparation of alumina columns, 0.75 g of aluminum oxide were mixed with 3 ml of 100 mM imidazole and incubated for 12 to 16 h. The solution was poured into a separation column which was washed four times with 5 ml of imidazol buffer followed by two washing steps with 5 ml of deionized water. As Dowex and alumina columns were reused multiple times, respective washing steps had been performed each time before the sample was applied (column regeneration).

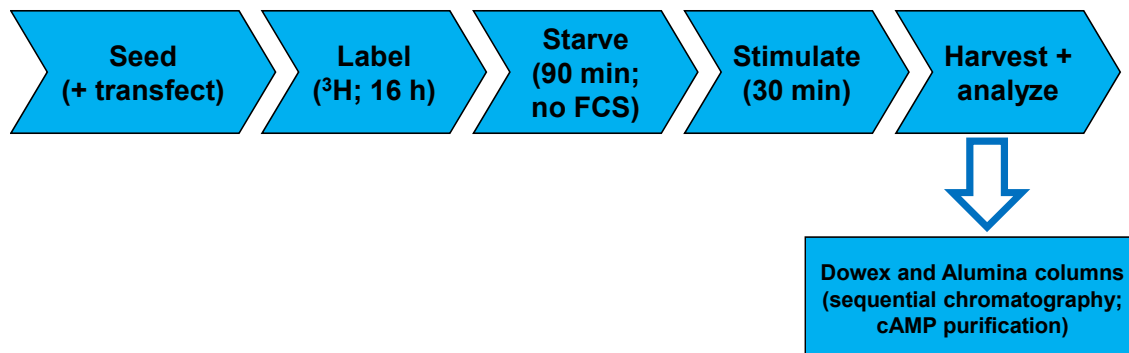


Figure 12: Schematic overview of the different cell treatments during an adenylyl cyclase assay.

Prior to sample loading onto Dowex columns, the salt precipitate was concentrated at the tube bottom by centrifugation (5,000 x g, 10 sec). 970 μ l of the clear supernatant were loaded onto a Dowex column and columns were washed twice with 1 ml of deionized water. They were placed on top of the Alumina columns and cAMP was eluted with 2 ml of deionized water (twice). Alumina columns were placed on top of scintillation vials and cAMP was eluted with 3 ml of imidazol buffer (twice). The eluate was mixed with 10 ml of liquid scintillation solution and radioactive decay was measured in a liquid scintillation counter for 3 min.

3. *In silico* analyses

3.1. Phylogenetic analysis

Proteins which are evolutionary related to GPR19 were searched for using the basic local alignment search tool (BLAST) algorithm (2.2.26+)⁶¹. Full-length sequences were aligned using ClustalW2⁶² for multiple sequence alignment and displayed as phylogenetic tree.

⁶¹ blast.ncbi.nlm.nih.gov/Blast.cgi

⁶² www.ebi.ac.uk/Tools/msa/clustalw2/

3.2. Microarray gene expression analysis and hierarchical clustering (heat map)

Raw (CEL) files were robust multichip average (RMA)-normalized using the affy package in R/Bioconductor (Irizarry RA *et al.*, 2003). Quality control was performed by visual inspection of box plots, minus-average (MA)⁶³-plots, and density plots of the normalized data.

Genes encoding proteins with G protein-coupled receptor (GPCR) activity (which included GPCRs and GPCR-associated proteins) were selected on the basis of Gene Ontology (GO)⁶⁴ number 0004930 and their microarray expression values in NSCLC, SCLC, and normal lung samples were extracted. Only one probe set was chosen per gene resulting in 773 genes. Geometric mean values across all normal lung samples were calculated and used for normalization of NSCLC and SCLC patient sample expression values. A cluster analysis of the log 2-transformed normalized expression data was performed using the hierarchical clustering method (average linkage clustering, Euclidean distance) from Genesis (Sturn A *et al.*, 2002).

3.3. Gene expression profiling (databases)

Gene expression levels of *Gpr19* (probe set 207183_at) in various human normal and cancerous tissues were investigated by utilization of the Gene Logic BioExpress® database⁶⁵ as described (Dolznig H *et al.*, 2005; Glatt S *et al.*, 2008). The database constitutes of expression data generated with Affymetrix GeneChip® technology (chip sets Human Genome U133A and Human Genome U133B, Human Genome U133 plus 2.0). Chip data analysis was performed with the statistical algorithm of Affymetrix Microarray Suite version 5.0 software. In order to allow for comparisons between chips, a global scaling factor was used for multiplication of the raw expression intensities. Both the lowest and highest 2% of the non-normalized expression values were removed and the mean of the remaining values was calculated (trimmed mean). The scaling factor is defined by Gene Logic as 100 divided by the trimmed mean. The comparison of the absolute signal intensities of corresponding perfect match and mismatch oligonucleotides allowed for the calculation of absent and present calls (oligonucleotide-specific background normalization).

For the investigation of *Gpr19* (probe set NM_006142_at) gene expression levels in various human lung-derived cell lines, a proprietary Boehringer Ingelheim gene expression database was utilized. The database constitutes of expression data generated with Affymetrix GeneChip® technology (Human Exon 1.0 ST Array). CEL files were RMA-normalized and data were inspected as described in 3.2.

⁶³ Minus-average (MA) plots are used for visualization of the average (A) logarithmic signal intensities versus the differences in these intensities (minus, M; Göhlmann H and Talloen W, 2009).

⁶⁴ www.geneontology.org

⁶⁵ www.genelogic.com/knowledge-suites/bioexpress-system

3.4. Copy number analysis

Deletions and amplifications of genomic regions in lung-cancer derived cell lines were detected using single nucleotide polymorphism (SNP) microarray analysis as part of a proprietary Boehringer Ingelheim cell line database. The data had been collected using the Affymetrix GeneChip® Human Mapping 250K Nsp array which covers the human genome with 2.62×10^5 SNPs. DNA copy numbers had been determined using the gain and loss analysis of DNA (GLAD) algorithm (Hupé P *et al.*, 2004).

3.5. Statistical data analysis

GraphPad Prism® was used for statistical data analysis. Comparisons between multiple test groups were either done using the non-parametric Kruskal Wallis test followed by Dunn's multiple comparison test or by one way analysis of variance (ANOVA) followed by Tukey's test. For the comparison of two test groups, a t test with Welch's correction was applied. The level of uncertainty in rejecting the null hypothesis is indicated by significance values * $p < 0.05$, ** $p < 0.01$, *** $p < 0.001$, and **** $p < 0.0001$, respectively.

VI. Results

1. Phylogenetic analyses of G protein-coupled receptor 19 (GPR19)

1.1. Orthologs

A protein basic local alignment search tool (BLAST) search was performed with the human GPR19 protein sequence to examine the similarity to predicted or putative GPR19 proteins from various species. The GPR19 receptors from different species were the best hits ranging from a total score of 859 to 140. However, there were also five proteins not explicitly called GPR19 in *Branchiostoma floridae* (hypothetical protein BRAFLDRAFT_69363), *Drosophila mojavensis* (GI24301), *Equus caballus* (predicted: similar to hCG2039474), *Nematostella vectensis* (unnamed predicted protein), and *Strongylocentrotus purpuratus* (predicted: similar to G protein-coupled receptor) included in these best scoring hits. The accession numbers for all these proteins are depicted in table 13 and full-length sequences were aligned using ClustalW2 for multiple sequence alignment (figure 13).

Table 13: (Predicted/probable/putative GPR19) proteins from various species were identified by BLAST using the human GPR19 protein sequence as reference. Shown are the species, National Center for Biotechnology Information (NCBI) protein reference sequence accession numbers, and protein annotation; results are arranged in alphabetical order.

Species	Accession number	Protein (BLAST annotation)
<i>Ailuropoda melanoleuca</i> (giant panda)	XP_002918034.1	Predicted: probable G protein-coupled receptor 19-like
<i>Anolis carolinensis</i> (green anole)	XP_003228174.1	Predicted: probable Gprotein-coupled receptor 19-like
<i>Bos taurus</i> (cow)	NP_001094684.1	Probable G protein-coupled receptor 19
<i>Branchiostoma floridae</i> (Florida lancelet)	XP_002591081.1	Hypothetical protein BRAFLDRAFT_69363
<i>Callithrix jacchus</i> (white-tufted-ear marmoset)	XP_002752176.1	Predicted: probable G protein-coupled receptor 19
<i>Canis lupus familiaris</i> (dog)	XP_003433621.1	Predicted: probable G protein-coupled receptor 19
<i>Cavia porcellus</i> (guinea pig)	XP_003470461.1	Predicted: probable G protein-coupled receptor 19-like
<i>Danio rerio</i> (zebrafish)	NP_957288.1	Probable G protein-coupled receptor 19
<i>Drosophila mojavensis</i> (fly)	XP_001999054.1	GI24301
<i>Equus caballus</i> (horse)	XP_001496867.1	Predicted: similar to hCG2039474
<i>Gallus gallus</i> (chicken)	XP_003643346.1	Predicted: probable G protein-coupled receptor 19-like
<i>Heterocephalus glaber</i> (naked mole-rat)	EHB14318	Putative G protein-coupled receptor 19
<i>Homo sapiens</i> (human)	NP_006134.1	Probable G protein-coupled receptor 19
<i>Loxodonta africana</i> (African elephant)	XP_003405704.1	Predicted: probable G protein-coupled receptor 19-like
<i>Macaca mulatta</i> (rhesus monkey)	XP_001085321.1	Predicted: probable G protein-coupled receptor 19
<i>Meleagris gallopavo</i> (turkey)	XP_003202592.1	Predicted: probable G protein-coupled receptor 19-like
<i>Mus musculus</i> (mouse)	NP_001161166.1	Probable G protein-coupled receptor 19 isoform a
<i>Mustela putorius furo</i> (domestic ferret)	AER99336.1	Putative G protein-coupled receptor 19
<i>Nematostella vectensis</i> (starlet sea anemone)	XP_001639290.1	Predicted protein
<i>Nomascus leucogenys</i> (northern white-cheeked gibbon)	XP_003265718.1	Predicted: probable G protein-coupled receptor 19-like
<i>Oreochromis niloticus</i> (nile tilapia)	XP_003448851.1	Predicted: probable G protein-coupled receptor 19-like
<i>Pan troglodytes</i> (chimpanzee)	XP_001153454.1	Predicted: G protein-coupled receptor 19
<i>Pongo abelii</i> (Sumatran orangutan)	XP_002822997.1	Predicted: probable G protein-coupled receptor 19-like

Species	Accession number	Protein (BLAST annotation)
<i>Rattus norvegicus</i> (rat)	NP_542146.1	Probable G protein-coupled receptor 19
<i>Saccoglossus kowalevskii</i> (acorn worm)	XP_002741289.1	Predicted: G protein-coupled receptor 19-like
<i>Strongylocentrotus purpuratus</i> (sea urchin)	XP_001200143.1	Predicted: similar to G protein-coupled receptor
<i>Taeniopygia guttata</i> (bird)	XP_002193564.1	Predicted: similar to G protein-coupled receptor 19
<i>Xenopus tropicalis</i> (frog)	NP_001016208.1	G protein-coupled receptor 19

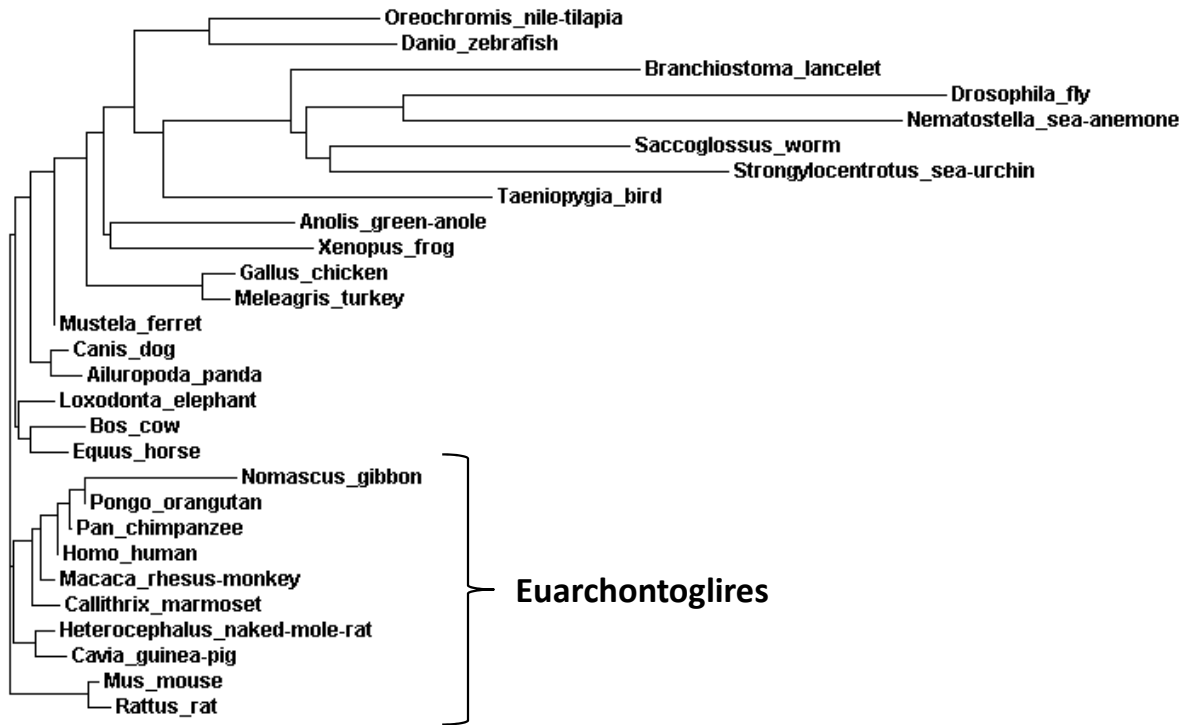


Figure 13: The GPR19 protein is conserved during evolution. The phylogenetic tree of GPR19 proteins from various species (ClustalW2) included orthologs that were identified by a BLAST search using human GPR19 as reference. Full-length amino acid sequences of the receptors were aligned. Relative branch lengths are indicative of evolutionary distances between GPR19 proteins from different species.

Based on the phylogenetic tree of GPR19 orthologs, this G protein-coupled receptor (GPCR) is present in a vast variety of animals (metazoa), the common kingdom of all species that gave a positive BLAST result. However, GPR19 is not only found in mammalia (e.g., *Homo sapiens*, *Mus musculus*), amphibia (*Xenopus tropicalis*), and other chordata/craniata/vertebrata (e.g., *Gallus gallus*) but also in the phyla of arthropoda (*Drosophila mojavensis*), hemichordata (*Saccoglossus kowalevskii*), echinodermata (*Strongylocentrotus purpuratus*), and cnidaria (*Nematostella vectensis*). The very diverse spectrum of species in which GPR19 was found points to a rather general but essential role of this receptor in cell biology. In addition, GPR19 seems to be highly conserved among euarchontoglires (supra-primates), as these species reside on a separate branch of the phylogenetic tree.

The ortholog classification of GPR19 identifies this GPCR as a highly conserved protein not only present in mammals but also in evolutionary distant species such as the sea anemone of the cnidaria phylum.

1.2. Paralogs

The BLAST search was repeated for GPR19 proteins from *Homo sapiens*, *Pan troglodytes*, *Macaca mulatta*, *Mus musculus*, and *Danio rerio* in order to search for GPR19-related GPCRs within the proteome of these species. The best scoring hits according to the maximum score are listed in table 14 and full-length protein sequences underlying the listed accession numbers were used for the generation of phylogenetic trees using ClustalW2 (paralogs; figure 14 and figure 15). Proteins residing on the same branches might have evolved from genome duplications of a common ancestor and acquired different cellular functions with time. A comparison of putative paralogs might therefore generate hypotheses on the physiological roles of uncharacterized GPCRs and on their candidate cognate ligands.

Table 14: GPCRs were identified by species-specific GPR19 similarity search (BLAST) in *Homo sapiens*, *Pan troglodytes*, *Macaca mulatta*, *Mus musculus*, and *Danio rerio*. The best scoring hits (maximum score) were selected and are listed in alphabetical order. Protein sequences used for phylogenetic tree analysis (NCBI reference sequence accession numbers) and exemplary ligands for all GPCRs are shown.

Abbreviation	Receptor	Ligand (example)	<i>Homo sapiens</i>	<i>Pan troglodytes</i>	<i>Macaca mulatta</i>	<i>Mus musculus</i>	<i>Danio rerio</i>
5HT2AR	5-hydroxytryptamine receptor 2A	Serotonin (biogenic amine)	NP_000612.1				
5HT4R	5-hydroxytryptamine receptor 4	Serotonin (biogenic amine)	NP_000861.1			NP_032339.2	
ADRA1B	Alpha-1B adrenergic receptor	Adrenaline (biogenic amine)	NP_000670.1				NP_001122161.1
ADRB2	Beta-2 adrenergic receptor	Adrenaline (biogenic amine)	NP_000015.1	NP_001182193.1	NP_001036239.1	NP_031446.2	NP_001082940.1
CCKAR	Gastrin/cholecystokinin type A receptor	Gastrin (peptide)	NP_000721.1	XP_526545.1	XP_001084186.1		XP_002663361.2
CCKBR	Gastrin/cholecystokinin type B receptor	Gastrin (peptide)	NP_795344.1				
DRD2	Dopamine receptor D2	Dopamine (biogenic amine)	NP_000786.1				
DRD3	Dopamine receptor D3	Dopamine (biogenic amine)	NP_387512.3				
GALR1	Galanin receptor type 1	Galanin (peptide)	NP_001471.2	XP_523975.2	XP_001086740.1	NP_032108.1	XP_696215.1
GALR2	Galanin receptor type 2	Galanin (peptide)	NP_003848.1	XP_523721.1	XP_001103768.1	NP_034384.3	XP_001339169.1
GALR3	Galanin receptor type 3	Galanin (peptide)	NP_003605.1				
GnlHR1	Gonadotropin-inhibitory hormone receptor 1	Gonadotropin-inhibitory hormone (peptide)					NP_001165167.1
GnlHR2	Gonadotropin-inhibitory hormone receptor 2	Gonadotropin-inhibitory hormone (peptide)					NP_001165168.1
GnRHR3	Gonadotropin-releasing hormone receptor 3	Gonadotropin-releasing hormone (peptide)					NP_001170921.1
GPR19	GPR19	Orphan	NP_006134.1	XP_001153454.1	XP_001085321.1	NP_001161166.1	NP_957288.1
GPR83	GPR83	Orphan	NP_057624.3	XP_522151.2	XP_001088588.1	NP_034417.1	XP_001342488.1
HCRTR1	Orexin receptor type 1	Orexin (peptide)	NP_001516.2	XP_524646.2	XP_001099090.1	NP_945197.2	
HCRTR2	Orexin receptor type 2	Orexin (peptide)	NP_001517.2	XP_518552.2	XP_001109616.1	NP_945200.1	
HRH2	Histamine H2 receptor	Histamine (biogenic amine)	NP_071640.1				
KISS1R	KISS-1 receptor	Kisspeptin (peptide)	NP_115940.2				
LOC	Hypothetical protein LOC243407 (7TM receptor)	Orphan				NP_780733.2	
NK2R (TACR2)	Substance-K receptor (tachykinin receptor 2)	Tachykinin (peptide)	NP_001048.2	XP_507831.2	XP_001110044.1	NP_033340.3	
NK3R	Neurokinin-K receptor	Neurokinin (peptide)	NP_001050.1				
NPFFR1	Neuropeptide FF receptor 1	Neuropeptide FF	NP_071429.1		XP_001107552.2	NP_001170982.1	NP_001082858.1
NPFFR2	Neuropeptide FF receptor 2	Neuropeptide FF	NP_004876.2	XP_001158813.1		NP_573455.2	XP_690069.4
NPFFR2.1	Neuropeptide FF receptor 2.1	Neuropeptide FF					NP_001098579.1
NPSR1	Neuropeptide S receptor 1	Neuropeptide S	NP_997055.1	XP_001168798.1	NP_001028114.1		
NPY2R	Neuropeptide Y receptor type 2	Neuropeptide Y	NP_000901.1	NP_001012655.1	NP_001028004.1	NP_032757.2	XP_001343301.2
NPY2Rlike	Neuropeptide Y receptor type 2-like, LOC795311	Neuropeptide Y					XP_001332759.1
OPRM1	Mu-type opioid receptor isoform MOR-1B5	Beta-endorphin (peptide)	NP_001138758.1		NP_001027996.1		
PGR15L	G protein-coupled receptor 15-like (neuropeptide Y receptor activity)	Orphan				NP_001028533.1	
QRFR	Orexigenic neuropeptide QRFP receptor	QRFP (peptide)	NP_937822.2	XP_001143462.1			XP_001920042.2
SSR1	Somatostatin receptor type 1	Somatostatin (peptide)	NP_001040.1	XP_522831.1	XP_001091429.1	NP_033242.1	
SSR2	Somatostatin receptor type 2	Somatostatin (peptide)	NP_001041.3	XP_001167728.1	XP_001085574.1	NP_033243.2	
SSR4	Somatostatin receptor type 4	Somatostatin (peptide)	NP_001043.2	XP_525282.1	XP_001095303.1	NP_033245.2	
SSR5	Somatostatin receptor type 5	Somatostatin (peptide)	NP_001044.1	XP_510725.2			XP_695365.1
TAAAR2	Trace amine-associated receptor 2	Tryptamine (biogenic amine)	NP_001028252.1		XP_001103648.2		
V1BR	Vasopressin V1b receptor	Vasopressin (peptide)	NP_000698.1				

Phylogenetic trees for *Homo sapiens*, *Pan troglodytes*, *Macaca mulatta*, *Mus musculus*, and *Danio rerio* (figure 14 and figure 15) include either 30 (*Homo sapiens*) or 16 (*other species*) best BLAST search hits and GPR19. Generally speaking, most

GPCRs retrieved from the BLAST search were called close relatives of GPR19 in more than one species and only few were uniquely present in a single species. Those GPCRs mainly existed in *Danio rerio* – the examined species which is evolutionary most distant from all the others. These findings further point to an evolutionary conserved history of GPR19 across species borders. Additionally, the GPCRs called as best hits by the BLAST search in all species are activated either by biogenic amines or by peptides (or are still orphan receptors).

In the *Homo sapiens* phylogenetic tree, GPR19 resides on an individual branch with its closest neighbors being GPCRs activated by biogenic amines (TAAR2, ADRA1B, ADRB2, HRH2, 5HT4R, DRD2, DRD3, and 5HT2AR) on the one hand and GPCRs activated by peptides (NPSR1, V1BR, CCKAR, CCKBR, GALR1, GALR2, GALR3, KISS1R, OPRM1, SSR1, SSR4, SSR2, SSR5, QRFPR, etc.; except for orphan receptor GPR83) on the other hand (figure 14). GPR19 exactly 'separates' these two GPCR subclasses according to the nature of their known ligands, its branch is not assigned to belong to any of them.

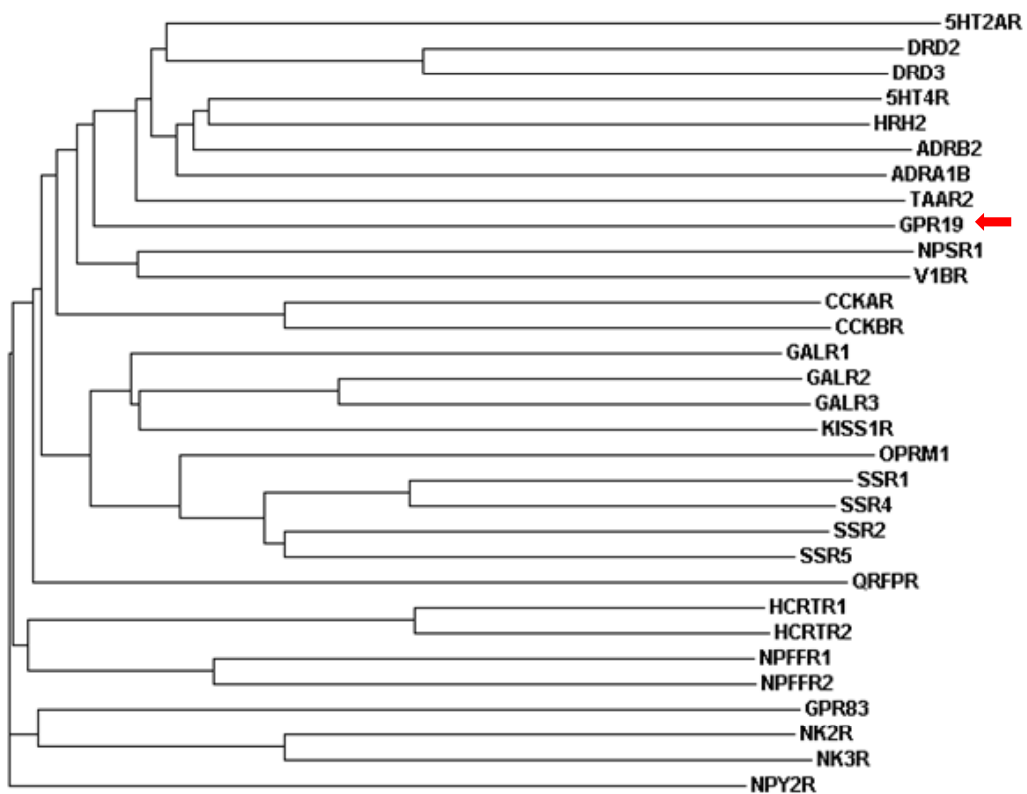


Figure 14: Human GPR19 resides on an individual branch between biogenic amine- and peptide-activated GPCRs. The phylogenetic tree shows 30 GPCRs and GPR19 (←; best hits based on maximum score from BLAST protein search for GPR19 similarity) from *Homo sapiens* (ClustalW2). Receptor abbreviations are specified in table 14.

Closest relatives to the *Pan troglodytes* and *Macaca mulatta* GPR19 protein are almost exclusively GPCRs which have been described to be activated by peptides – except for ADRB2 and TAAR2 (activated by biogenic amines; figure 15). In both species, GPR19 shares a very open branch with NPSR1. In the *Mus musculus* phylogenetic tree, GPR19 resides on a single branch between 5HT4R and ADRB2 receptors on the one hand and galanin and somatostatin receptors on the other hand. As observed in *Homo sapiens*, GPR19 again seems to 'separate' receptors

activated by biogenic amines from the ones activated by peptides in these species. This was not observed for the GPR19 protein of *Danio rerio*, whose closest relatives are – nevertheless – receptors activated by galanin and somatostatin.

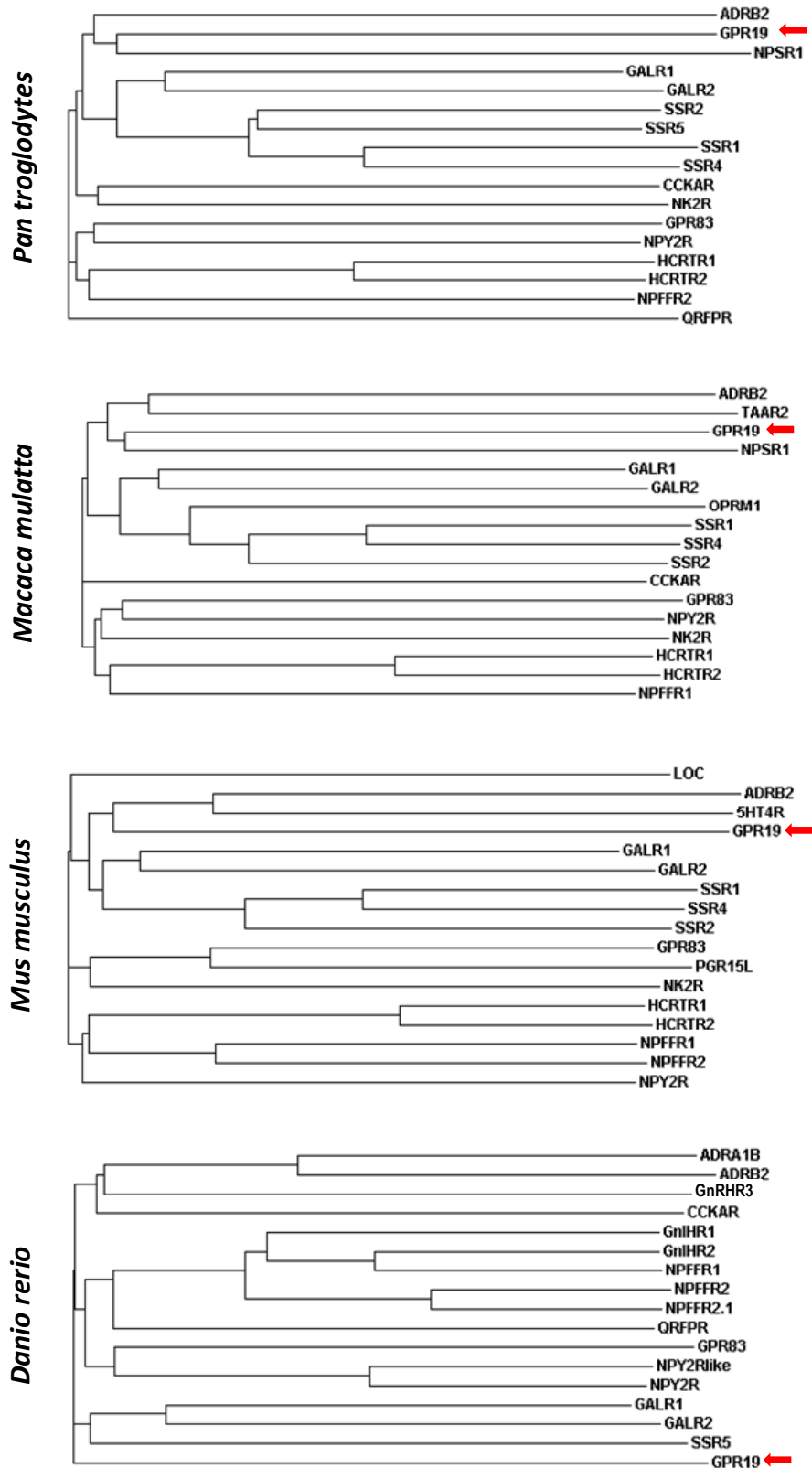


Figure 15: GPR19 has closest similarity to GPCRs activated by biogenic amines or peptides in different species. The phylogenetic trees show 16 GPCRs and GPR19 (←; best hits based on maximum score from BLAST protein search for GPR19 similarity) from *Pan troglodytes*, *Macaca mulatta*, *Mus musculus*, and *Danio rerio* (ClustalW2). Receptor abbreviations are specified in table 14.

Phylogenetic tree analyses of potential GPR19 paralogs in five different species revealed its similarity to GPCRs activated by biogenic amines and peptides. Except for *Danio rerio*, GPR19 could be considered as an evolutionary connector between GPCRs activated by biogenic amines on the one hand and those activated by peptides on the other hand as its phylogenetic distance to both these groups is rather balanced.

2. Method development

2.1. Reference gene selection

When utilizing reverse transcription quantitative real-time polymerase chain reaction (RT-qPCR) for examination of the relative expression level of a gene of interest, results can vary considerably depending on the selected reference gene. This is particularly true when expression levels of genes from cells at different stages of the cell cycle are analyzed. For example, increases in the message of *glyceraldehyde-3-phosphate dehydrogenase (Gapdh)* – a reference gene frequently used in RT-qPCR data normalization – were reported to be cell cycle-specific (Mansur NR *et al.*, 1993). According to the guidelines for ‘minimum information for publication of quantitative real-time PCR experiments’ (MIQE; Bustin SA *et al.*, 2009), a single reference gene for normalization has to be avoided. Instead, data should be normalized against multiple reference genes that had been tested for stable expression.

Different frequently used reference genes (*Actb*⁶⁶, *B2m*⁶⁷, *Cypa*⁶⁸, *Gapdh*⁶⁹, *Hprt1*⁷⁰, *Rplp0*⁷¹, *Rnase P*⁷², *Tfr*⁷³) were tested for stable expression in representative

⁶⁶ β -actin (ACTB; NCBI gene ID 60; UniProt protein ID P60709) belongs to the β group of the three main vertebral groups of actins (α , β , and γ) and plays an important role in the cellular contractile apparatus. Upon polymerization, actins are involved in a number of cellular physiological events including cellular structure, motility, and integrity (www.ncbi.nlm.nih.gov/gene/60; www.uniprot.org/uniprot/P60709).

⁶⁷ β -2-microglobulin (B2M; NCBI gene ID 567; UniProt protein ID P61769) is part of the class I major histocompatibility complex (MHC). In association with the MHC class I heavy chain, it forms the MHC class I dimer which is involved in presenting peptide antigens to cells of the immune system (www.ncbi.nlm.nih.gov/gene/567; www.uniprot.org/uniprot/P61769).

⁶⁸ Cyclophilin A (CYPA; also known as peptidylprolyl isomerase A (PPIA); NCBI gene ID 5478; UniProt protein ID P62937) is a member of the peptidyl-prolyl cis-trans isomerase family of enzymes. These enzymes are involved in catalyzing cis-trans isomerization of proline imidic peptide bonds. They therefore assist in the acceleration of protein folding (www.ncbi.nlm.nih.gov/gene/5478; www.uniprot.org/uniprot/P62937).

⁶⁹ Glyceraldehyde-3-phosphate dehydrogenase (GAPDH; NCBI gene ID 2597; UniProt protein ID P04406) is an enzyme involved in cellular carbohydrate metabolism. It is composed of four identical 36 kDa subunits and catalyzes the conversion of glyceraldehyde-3-phosphate into 3-phosphoglycerol phosphate in the presence of nicotinamide adenine dinucleotide (NAD; oxidative phosphorylation). In addition, the enzyme also possesses nitrosylase activity mediating cysteine-S-nitrosylation of nuclear target proteins and was therefore supposed to play a role in nuclear functions such as transcription, RNA transportation, or DNA replication. Two different isoforms of GAPDH exist arising from two different transcript variants (www.ncbi.nlm.nih.gov/gene/2597; www.uniprot.org/uniprot/P04406).

⁷⁰ The protein encoded by the hypoxanthine-guanine phosphoribosyltransferase 1 (HPRT1; NCBI gene ID 3251; UniProt protein ID P00492) gene forms a homotetrameric transferase. It catalyzes the transfer of the 5-phosphoribosyl group from 5-phosphoribosyl 1-pyrophosphate to either hypoxanthine or guanine giving rise to inosine or guanosine monophosphate. Its main cellular role is elucidated during the purine salvage pathway in which it is crucial for purine nucleotide generation (www.ncbi.nlm.nih.gov/gene/3251; www.uniprot.org/uniprot/P00492).

complementary-deoxyribonucleic acid (cDNA) sample panels as proposed by Vandesompele and coworkers (Vandesompele J *et al.*, 2002; GeNorm⁷⁴ applet for Microsoft® Excel®). For each possible reference gene, all samples were normalized to the sample in which this gene was detected first, *i.e.*, most highly expressed (relative expression ratio). This was done for all reference genes. Expression values of one reference gene were compared with those of all other reference genes (gene expression instability measure M or average pairwise variation: standard deviation of logarithmically transformed expression ratios)⁷⁵. Genes with high M values are less stably expressed than genes with low M values and should not be considered as reference genes in a respective sample set.

When testing for stable expression of reference genes, the outcome tremendously depends on the sample set used. The data shown in figure 16 included samples from small cell lung cancer (SCLC) and non-small cell lung cancer (NSCLC) cells subjected to different synchronization conditions, which were collected at various time points after release from cell cycle arrest. Results displayed in figure 17 are based on a representative set of cDNA samples which included different untreated or short interfering ribonucleic acid (siRNA)-transfected SCLC and NSCLC cell lines (up to 60 nM final siRNA concentration).

The most stably expressed reference genes in the example illustrated in figure 16 (synchronized cells harvested at various time points after release from cell cycle arrest) were *Rplp0* and *Cypa* followed by *Actb* and *Hprt1*. Reference genes *Gapdh*, *Rnase P* or *B2m* were unstably expressed. *Hprt1*, *Cypa*, and *Rplp0* were also called stable expression genes in the second sample set examined (figure 17; untreated or siRNA-transfected cells). Besides, *Tfr* was characterized by stable expression whereas *Rnase P*, *Actb*, or *B2m* were unstably expressed.

⁷¹ Protein synthesis takes place at ribosomes. Eucaryotic ribosomes are composed of a small 40 S and a large 60 S subunit. About 80 proteins and 4 RNA species make up for an entire ribosome and the large ribosomal protein P0 (RPLP0; NCBI gene ID 6175; UniProt protein ID P05388) is a phosphoprotein member of the 60 S subunit. In conjunction with the ribosomal phosphoproteins P1 and P2, RPLP0 is part of a preformed pentameric complex (dimers of P1 and P2, P0 monomer; www.ncbi.nlm.nih.gov/gene/6175; www.uniprot.org/uniprot/P05388).

⁷² The catalytic riboprotein ribonuclease P (RNase P) utilizes its endonuclease activity to mature the 5' end of precursor transfer ribonucleic acids (tRNAs). Nuclear forms of this enzyme have been assigned a role in tRNA gene transcription by RNA polymerase III. It consists of multiple protein subunits (Jarrous N and Reiner R, 2007) and one RNA species with catalytic activity. In the present RT-qPCR application, the RNA part of RNase P termed H1 is detected (NCBI gene ID 85495 (<http://www.ncbi.nlm.nih.gov/gene/85495>); products.appliedbiosystems.com/ab/en/US/adirect/ab?cmd=catNavigate2&catID=601337).

⁷³ The transferrin receptor (TFR); NCBI gene ID 7037; UniProt protein ID P02786) is involved in the cellular uptake of iron by receptor-mediated endocytosis. TFR is expressed at the cell surface of most cells in the human body as a homodimer with the monomer being a single-pass type II membrane glycoprotein. Once coupled to its ligand, one iron-loaded serum transferrin per subunit, the ligand-receptor complex is internalized and iron ions are released by acidification in endosomes. Receptor recycling to the cell surface and exposure to neutral pH results in the dissociation of transferrin from the receptor (Lambert LA and Mitchell SL, 2007; www.ncbi.nlm.nih.gov/gene/7037; www.uniprot.org/uniprot/P02786)

⁷⁴ medgen.ugent.be/~jvdesomp/genorm/

⁷⁵ Two perfect internal control genes would exhibit an identical gene expression ratio in all samples of a sample set independent from any experimental influence (with the assumption that both genes are not co-regulated). However, if the expression of one gene or of both these genes was influenced by experimental conditions, increased variations in their relative expression ratios would correspond to decreased expression stability (Vandesompele J *et al.*, 2002).

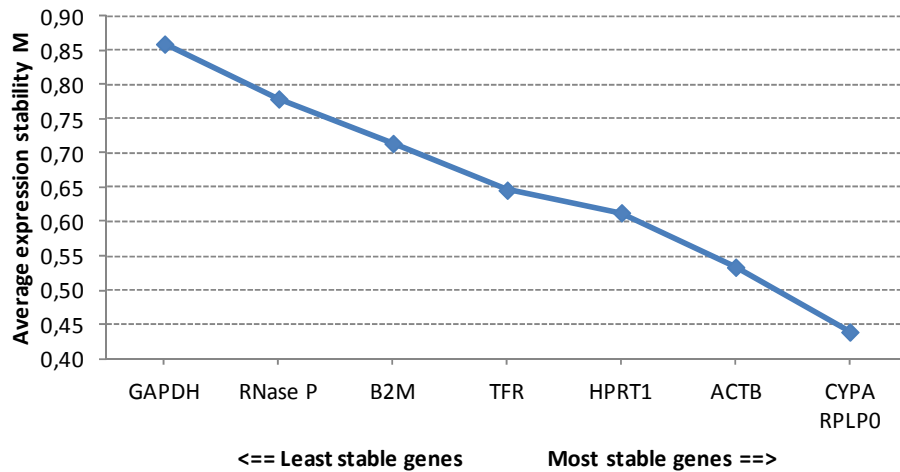


Figure 16: Reference genes *Cypa*, *Rplp0*, *Actb*, and *Hprt1* are stably expressed in synchronized cells. Average expression instability values M of possible reference genes (*Actb*, *B2m*, *Cypa*, *Gapdh*, *Hprt1*, *Rnase P*, *Rplp0*, *Tfr*) were determined calculating pairwise variations among reference genes using the GeNorm applet for Microsoft® Excel®. The sample set included cDNA samples from different SCLC and NSCLC cell lines synchronized at gap 1 (G1)-DNA synthesis (S) phase transition or gap 2 (G2)/mitosis (M) phase of the cell cycle which were collected at different time points (0 h, 2 h, 4 h, 6 h, 8 h, 10 h, 12 h, 24 h, 36 h, or 48 h) after release from the cell cycle arrest.

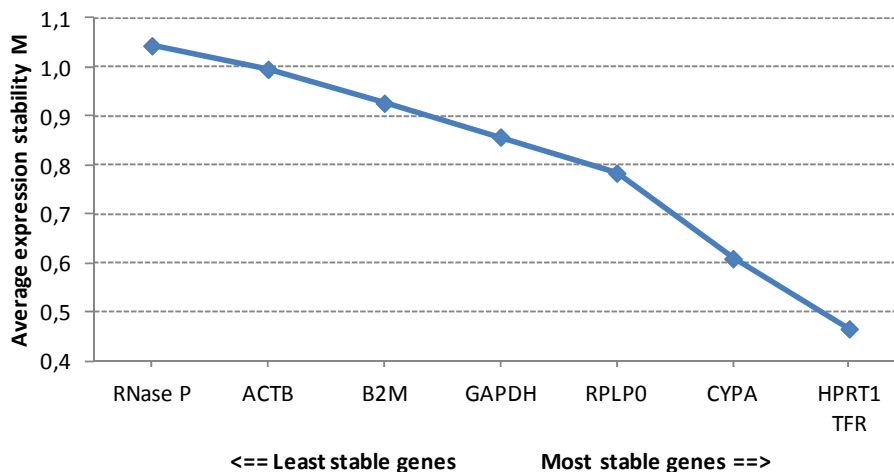


Figure 17: Reference genes *Hprt1*, *Tfr*, *Cypa*, and *Rplp0* are stably expressed in untreated or siRNA-transfected cells. Average expression instability values M of possible reference genes (*Actb*, *B2m*, *Cypa*, *Gapdh*, *Hprt1*, *Rnase P*, *Rplp0*, *Tfr*) were determined calculating pairwise variations among reference genes using the GeNorm applet for Microsoft® Excel®. The sample set included cDNA samples from different SCLC and NSCLC cell lines which had been treated with different *Gpr19* and *polo-like kinase 1 (Plk1)* siRNAs at various concentrations (up to 60 nM) collected on days 2 and 3 after transfection.

For different sample sets such as different cell lines, different siRNAs, different siRNA concentrations, or different synchronization conditions, the results for stable expression of possible reference genes discussed here varied slightly. However, all sample sets tested identified *Gapdh*, *Rnase P*, or *B2m* as unstable reference genes. They were therefore not used in RT-qPCR analyses. In contrast, *Actb*, *Cypa*, *Hprt1*, *Rplp0*, and *Tfr* were predominantly among the stably expressed reference genes. This was particularly true for sample sets that exclusively contained samples of the SCLC

cell line DMS 53 or the NSCLC cell line NCI-H1703 – the two major cell lines used for subsequent experimental studies.

Stable expression of reference genes is not the only criterion when choosing the genes for normalization of the genes of interest. **Similar assay efficiencies and low differences in quantification cycles (C_q) between reference genes and genes of interest are also crucial to obtain robust expression data.** A low difference in C_q values is equal to an expression of these genes at comparable levels. Generally speaking, *Rplp0*, *Hprt1*, and *Tfr* were found to be rather 'late' (non-abundantly expressed) reference genes in the samples tested, whereas *Cypa* and *Actb* were detected rather 'early'. Therefore, the final utilization of reference genes also considered a mix of genes from both these types. **The dynamic range and the PCR efficiency of a TaqMan® assay** had been determined for both reference gene and gene of interest assays by an input sample dilution series prior to any experimental application of these assays. These assay characteristics also influenced the final selection of reference genes, as both parameters should be similar for reference gene and gene of interest assays.

For reasons described above, both **reference genes *Cypa* and *Hprt1* were used for knockdown confirmations in subsequent *Gpr19* siRNA experiments. *Actb*, *Cypa*, *Hprt1*, and *Rplp0* were used when gene of interest expression over the course of the cell cycle and *Gpr19* expression in human NSCLC, SCLC, and normal lung RNA samples were examined.** Here, slight changes in gene expression are of greater importance than for the confirmation of a messenger ribonucleic acid (mRNA) knockdown – the reason why four reference genes were selected. This is in accordance with the suggestion by Vandesompele and coworkers: At least three reference genes should be used for RT-qPCR data normalization which are ideally not co-regulated, *i.e.*, whose gene products are involved in different cellular processes (Vandesompele *J et al.*, 2002).

2.2. Selection of *Gpr19*-targeting siRNAs

RNA interference⁷⁶ has become a popular technique for the induction of gene silencing (loss-of-function phenotype) since its discovery in *Caenorhabditis elegans* by Fire and coworkers (Fire *A et al.*, 1998). However, up-front crucial validation of different siRNAs destined to knock down a specific gene is imperative.

⁷⁶ The block of gene expression at the messenger ribonucleic acid (mRNA) level using sequence-specific double-stranded RNA molecules such as short interfering ribonucleic acids (siRNAs) is referred to as RNA interference. Transfected double-stranded RNA oligonucleotides are first cleaved into fragments of 21 to 23 nucleotides in length (with 3' overhangs of two nucleotides) by a ribonuclease III enzyme called Dicer or – in case they are already at the appropriate size – directly incorporated into a large cytoplasmic enzyme complex named the RNA-induced silencing complex (RISC). A small double-stranded RNA binding protein called R2D2 assists Dicer in the assembling of siRNA with RISC and both proteins are replaced by an Argonaute protein in the mature RISC that then includes only one siRNA strand. Complementary base-pairing guides the mature RISC to target mRNAs where cleavage is mediated by the Argonaute component of RISC with cleaved mRNAs being degraded by cytoplasmic exo- and endonucleases. A perfect complementarity between an siRNA and its target mRNA is required for mRNA cleavage whereas imperfect base-pairing only results in the repression of translation. The gene silencing effect induced by transfection of synthetic siRNAs is only transient with mRNA knockdown typically lasting for a couple of days (Downward J, 2004; Hammond SM, 2005; Sontheimer EJ, 2005; Sontheimer EJ and Carthew RW, 2005; Tomari Y and Zamore PD, 2005; Liu Q and Paroo Z, 2010).

Multiple siRNAs directed against *Gpr19* were purchased from Dharmacon (Thermo Fisher Scientific; Dh3) and Sigma Aldrich (Sig2, Sig3, Sig4, Sig5). They were assayed for their ability to knock down *Gpr19* on the mRNA level using RT-qPCR (relative to the reference genes *Cypa* and *Hprt1*) and for their effect on proliferation as determined by CloneSelect™ Imager well confluence measurement. NCI-H1703 cells (NSCLC) were siRNA-transfected using Lipofectamine® RNAiMAX (96 well culture plate; reverse transfection; 3,000 cells per well; 20 nM final siRNA concentration). Tested samples also included untreated, mock (transfection reagent only)-, and non-target siRNA-transfected cells. *Gpr19* mRNA levels were assessed on day 2 after transfection and confluence was recorded for six days at regular intervals starting 10 h after transfection. NCI-H1703 cells endogenously express *Gpr19* mRNA at a high level, which is specified later (figure 31).

Gpr19-targeting siRNAs Dh3, Sig2, Sig3, Sig4, and Sig5 were complementary to the *Gpr19* mRNA sequence (perfect matching). **Yet, only siRNAs Dh3, Sig4, and Sig5 but neither Sig2 nor Sig3 reduced the mRNA level of *Gpr19*** (figure 18). **Importantly, those siRNAs knocking down *Gpr19* also caused growth inhibition of transfected cells as their gain in well confluence over time was only modest (Dh3) or not existing (Sig4, Sig5;** figure 19). Cells transfected with *Gpr19* siRNAs Sig2 and Sig3 that did not cause *Gpr19* downregulation revealed a similar proliferative capacity as untreated, mock-, and non-target siRNA-treated controls.

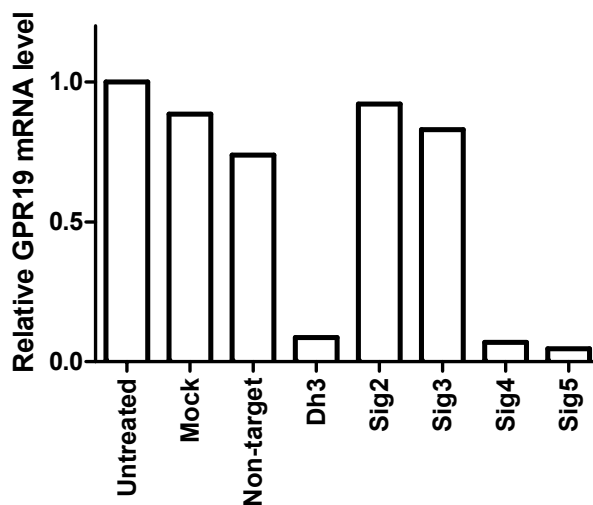


Figure 18: *Gpr19*-targeting siRNAs Dh3, Sig4, and Sig5 cause efficient knockdown of *Gpr19* mRNA. For each sample (triplicates), *Gpr19* mRNA knockdown in NCI-H1703 cells was assessed by RT-qPCR on day 2 after siRNA transfection (normalized against reference genes *Cypa* and *Hprt1*) and geometric mean values were calculated (untreated or mock (transfection reagent only)-transfected cells; cells treated with non-target siRNA or *Gpr19*-targeting siRNAs Dh3, Sig2, Sig3, Sig4, Sig5; 20 nM). Shown are the results from a representative experiment, two additional experiments gave concurrent results.

Those siRNAs that have proven their efficiency in silencing a target gene might nevertheless exhibit diverging phenotypic effects on the molecular or cellular level, which might be explained by so-called off-target effects not related to the knockdown of the target gene (Collinet C *et al.*, 2010). Using methods of

multiparametric data integration, this issue was addressed for *Gpr19*-targeting siRNAs Dh3, Sig4, and Sig5 that successfully silenced *Gpr19* and inhibited cell proliferation. NCI-H1703 cells were siRNA-transfected as described above and multiple parameters linked to the cytoskeleton of a cell derived from actin and tubulin staining (specified in the Methods section) were recorded on day 3 after transfection (high content screen (HCS) with the ArrayScan® VTI HCS reader). For characterization of the applied siRNAs, a **principal component analysis (PCA)** was performed reducing the dimensionality of the data to three variables (principal components; figure 20).

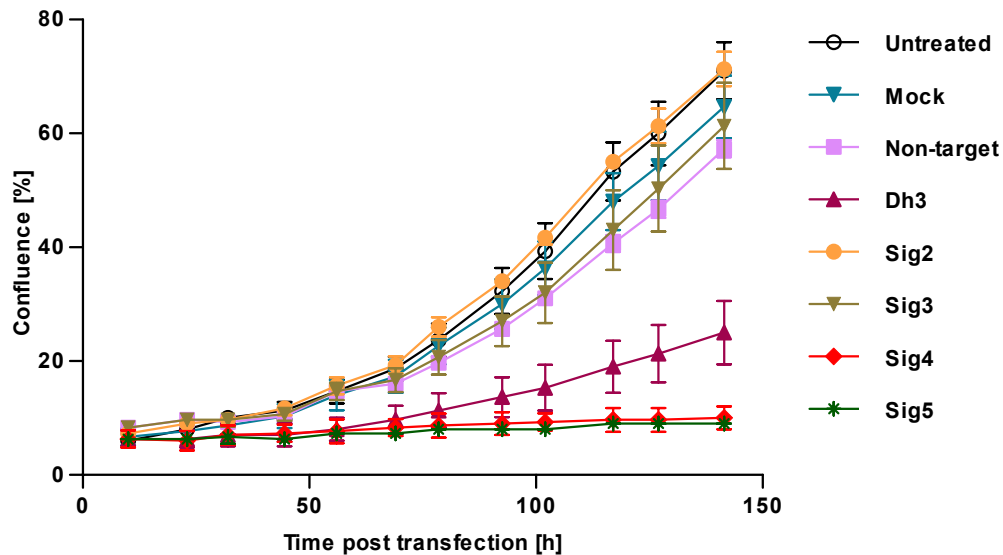


Figure 19: Cell proliferation (confluence) is inhibited by those siRNAs that cause *Gpr19* mRNA knockdown. Cell proliferation was determined by measuring confluence, i.e., % of total well area covered by cells. Shown is the time course after siRNA transfection (20 nM); data are mean values \pm standard deviation (error bars) of three wells per condition (96 well plate) from a representative experiment for untreated, mock (transfection reagent only)-, non-target siRNA-, and *Gpr19*-targeting (Dh3, Sig2, Sig3, Sig4, Sig5) siRNA-treated NCI-H1703 cells. Only siRNAs Dh3, Sig4, and Sig5 knocked down *Gpr19* message successfully (figure 18). Two additional experiments gave concurrent results.

Control cells (untreated, mock-treated) and cells treated with siRNAs that did not reduce *Gpr19* mRNA levels (non-target, Sig2, Sig3) showed similar actin and tubulin cytoskeleton characteristics as indicated by the close proximity of their principal components. However, the transfection of cells with Sig3 siRNA seemed to influence the cytoskeleton of these cells in a different way – this data point was most distant from the other controls. Therefore, **potential off-target effects were considered negligible only for the non-target and Sig2 siRNAs.**

The principal components for cells transfected with *Gpr19*-silencing siRNAs Dh3, Sig4, and Sig5, however, differed considerably from all controls not affecting *Gpr19* mRNA levels. Most notably, data points accounting for these three siRNAs were not only far from the control data points but also from each other. This indicates that they might mediate heterogeneous effects on the cytoskeleton.

In order to characterize these ambiguous consequences of *Gpr19*-targeting siRNAs Dh3, Sig4, and Sig5, their cellular effects were further examined in a second multiparameter study, for which siRNAs were applied at different concentrations and cells were harvested at different time points after transfection. NCI-H1703 cells were

transfected with 2 nM, 8 nM, 20 nM, or 60 nM of respective siRNAs and analyzed on days 1, 2, 3, and 4 after transfection by HCS. Multiple parameters derived from nuclear (deoxyribonucleic acid (DNA), Hoechst 33342) and cytoskeleton (actin) staining (specified in the Methods section) were recorded and subjected to **multidimensional scaling (MDS)** which reduced the dimensionality of the data to three variables (figure 21).

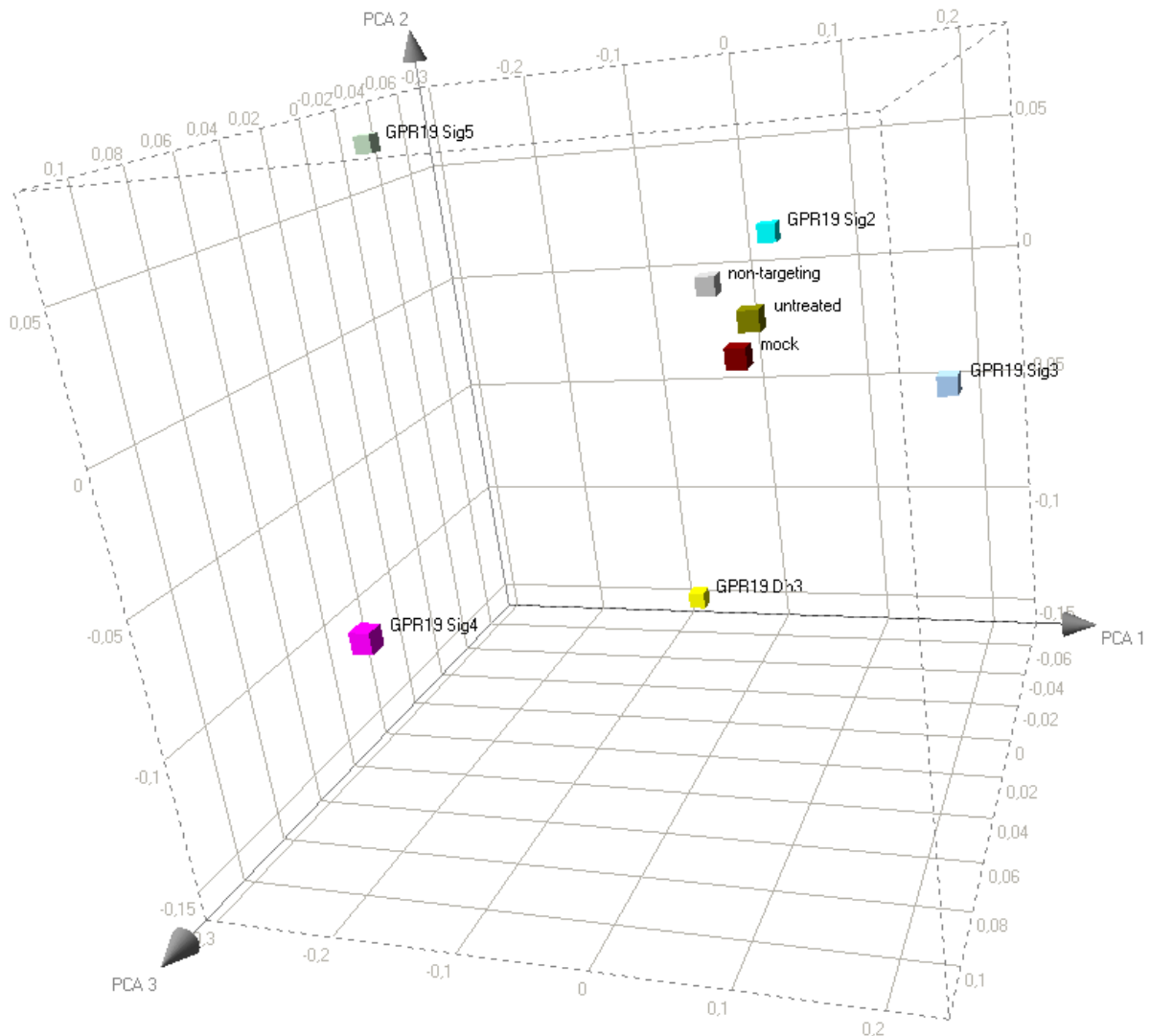


Figure 20: *Gpr19* silencing siRNAs differ in their effect on the cytoskeleton from controls that do not affect *Gpr19* mRNA levels. A principal component analysis (PCA) incorporating parameters from actin and tubulin stainings (high content screening) is shown for untreated, mock (transfection reagent only)-, non-target siRNA-, and *Gpr19*-targeting (Dh3, Sig2, Sig3, Sig4, Sig5) siRNA-treated NCI-H1703 cells (20 nM siRNA concentration, day 3 after transfection). The dimensionality of the data was reduced to three principal components (PCA 1, PCA 2, PCA 3) Only siRNAs Dh3, Sig4, and Sig5 knocked down *Gpr19* message successfully (figure 18).

MDS revealed similar influences on cellular parameters (nucleus, actin cytoskeleton) for siRNAs Sig4 and Sig5 in contrast to siRNA Dh3. **Data points of Sig4 and Sig5 moved into opposite directions with time relative to the data points of Dh3 for all siRNA**

concentrations examined. This discrimination was most obvious on days 3 and 4 after transfection.

The characterization of siRNAs directed against *Gpr19* led to the selection of the following oligonucleotides, which were used in subsequent RNA interference experiments: **For downregulation of *Gpr19* mRNA, oligonucleotides Sig4 and Sig5 were applied (they were termed GPR19 #1 and GPR19 #2, respectively). The pool of non-target siRNAs (termed CTL #1) served as transfection control sample. Oligonucleotide Sig2, which had been designed against *Gpr19* but did not cause *Gpr19* mRNA downregulation and behaved similarly to untreated, mock-, and non-target siRNA- treated samples in the PCA, was included as an additional control (CTL #2).**

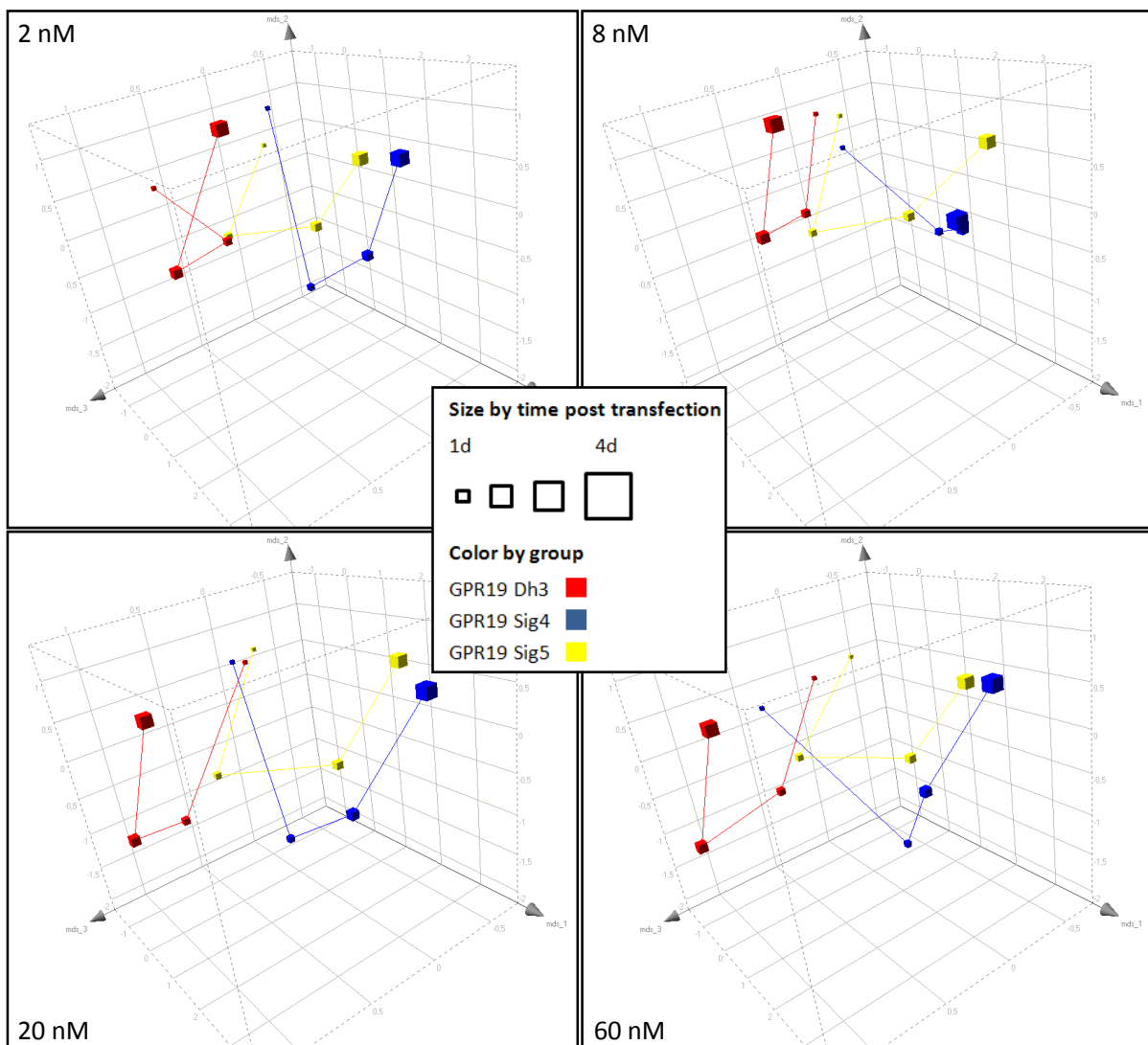


Figure 21: Sig4 and Sig5 siRNAs affect cellular parameters differently than Dh3. The results from multidimensional scaling (MDS) incorporating cellular parameters from nuclear and actin stainings (high content screening) are shown for NCI-H1703 cells transfected with *Gpr19*-targeting siRNAs Dh3 (red), Sig4 (blue), and Sig5 (yellow). siRNAs were applied at different concentrations (2 nM, 8 nM, 20 nM, 60 nM) and cells were analyzed on days 1, 2, 3, and 4 after transfection (indicated by the size of the cubes). The dimensionality of the data was reduced to three parameters (mds_1, mds_2, mds_3).

2.3. GPR19 antiserum validation

A prerequisite for the quantification of the GPR19 protein in Western Blot applications is its detection by a specific antiserum. In order to obtain GPR19-specific antisera, rabbits were immunized with GPR19-derived peptides as specified in the Materials and Methods sections. The Protean application of the Lasergene software was used for topological feature prediction of the GPR19 protein based on its primary sequence and assisted in the selection of peptides used for immunization (figure 22, table 11). Secondary structures ((amphipathic⁷⁷) alpha-helices, (amphipathic) beta-sheets, turn and coil regions) were identified using various algorithms according to Chou and Fasman (Chou PY and Fasman GD, 1978), Garnier and Robson (Garnier J *et al.*, 1978), or Eisenberg (Eisenberg D *et al.*, 1982). Besides, a Kyte-Doolittle hydrophobicity plot was utilized which aims at separating clusters of highly charged amino acids (mostly exposed to an aqueous environment) from strongly hydrophobic clusters (mostly found in transmembrane regions or in the interior of a protein; Kyte J and Doolittle RF, 1982). In fact, most regions with a positive hydrophobicity index were also called potential transmembrane regions by UniProt (see figure 6). According to Karplus and Schultz, flexible regions are more easily accessible as they are less likely found in the protein core and can be identified by local entropic energy potentials (Karplus PA and Schulz GE, 1985). Likewise, the surface probability of a protein region can be indicated by calculating the solvent accessibility of amino acid side chains (Emini EA *et al.*, 1985). The algorithm underlying the calculation of an antigenic index integrates many of these parameters originating from physicochemical properties of amino acids such as flexibility, hydrophathy, and surface/solvent accessibility (Jameson BA and Wolf H, 1988).

On the basis of this primary structure analysis, GPR19 peptides used for immunization of rabbits were chosen to lie near the amino- or carboxy-terminus, in the predicted intracellular loop regions 2 or 3, or in the predicted extracellular loop region 3 (table 11). These regions are characterized by high antigenicity and low hydrophobicity. Regions with high hydrophobicity (equal to transmembrane regions), however, were excluded from peptide selection.

The rabbit sera of the final bleeding were investigated for GPR19 detection on Western Blots after they had been affinity-purified using the peptides administered for immunization. Protein lysates from SCLC-derived cell lines DMS 53, NCI-H446, and SHP-77 were tested. Detection was either performed with unblocked purified serum, serum blocked with the GPR19 peptide used for purification, or serum blocked with an unspecific non-GPR19 peptide. As a representative example, the Western Blot signals resulting from the antiserum of animal #1 purified with one of the peptides used for immunization (AQLWHPHEQDYKKSSLVC) are shown in figure 23. All signals (bands) that were at an appropriate size (according to UniProt, the predicted molecular weight of GPR19 is 47.7 kilodaltons (kDa)) disappeared when the antiserum had been blocked with the GPR19 peptide. This was not the case when

⁷⁷ Amphipathic secondary protein structures project mainly hydrophilic residues on one surface and hydrophobic side chains on the opposite surface.

the antiserum had been blocked unspecifically. **Therefore, the purified antiserum might be utilized to detect the GPR19-containing peptide used for animal immunization on Western Blots.**

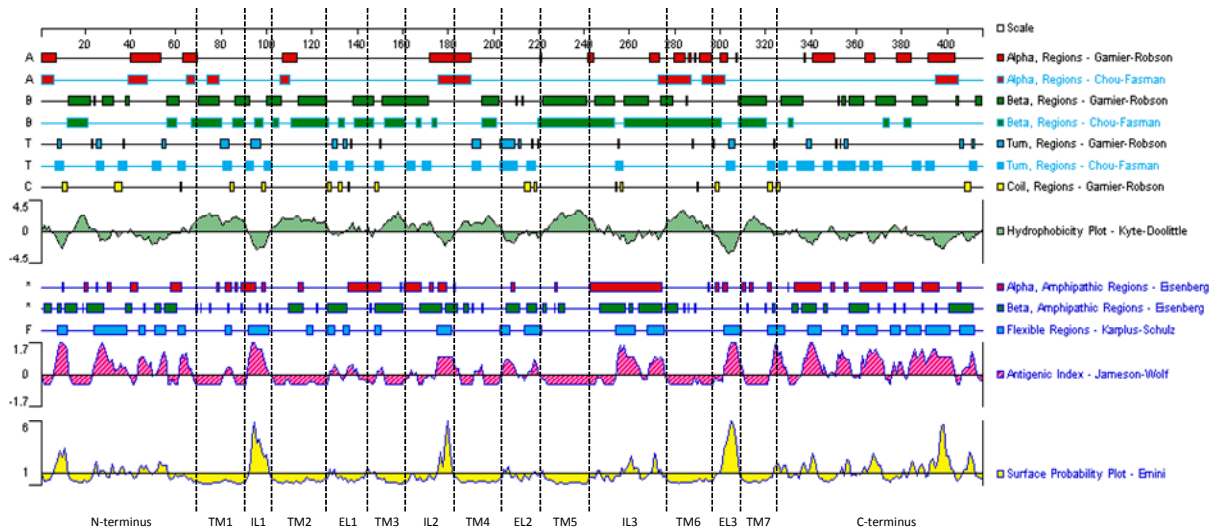


Figure 22: The GPR19 primary sequence (415 amino acids) shows regions with high antigenicity. Several algorithms (Garnier-Robson; Chou-Fasman; Eisenberg; Karplus-Schulz) as part of the Protean application (Lasergene, DNASTAR) were used to identify secondary structures such as (amphipathic) alpha-helices, (amphipathic) beta-sheets, turn or coil regions based on the amino acid sequence of GPR19. Additionally, the hydrophobicity (Kyte-Doolittle), antigenic index (Jameson-Wolf), and surface probability (Emini) of different GPR19 regions was predicted. High hydrophobicity indicated the presence of transmembrane regions (dotted lines separate the amino (N)-terminus, transmembrane (TM), intracellular loop (IL), and extracellular loop (EL) regions, and the carboxy (C)-terminus according to UniProt).

The specificity for GPR19 detection was assessed using lysates from human embryonic kidney (HEK)-293 cells that transiently overexpressed GPR19 (untagged or tagged with turbo green fluorescent protein (tGFP)). As specified later, untreated HEK-293 cells do virtually not express *Gpr19* mRNA (see figure 31). Signals were compared to the ones derived from cells that had been transfected with the empty vector backbone therefore only expressing tGFP. Transfected plasmids had been verified by sequencing. Various commercially available GPR19 antibodies offered for immunoblot and immunohistochemistry applications (table 9 in the Materials section) and purified GPR19 antisera from rabbit immunizations were tested for specific GPR19 detection on Western Blots (figure 24). Results for the GPR19 antiserum derived from animal #1, which had been purified with either of the two peptides used for immunization, are shown as a representative example.

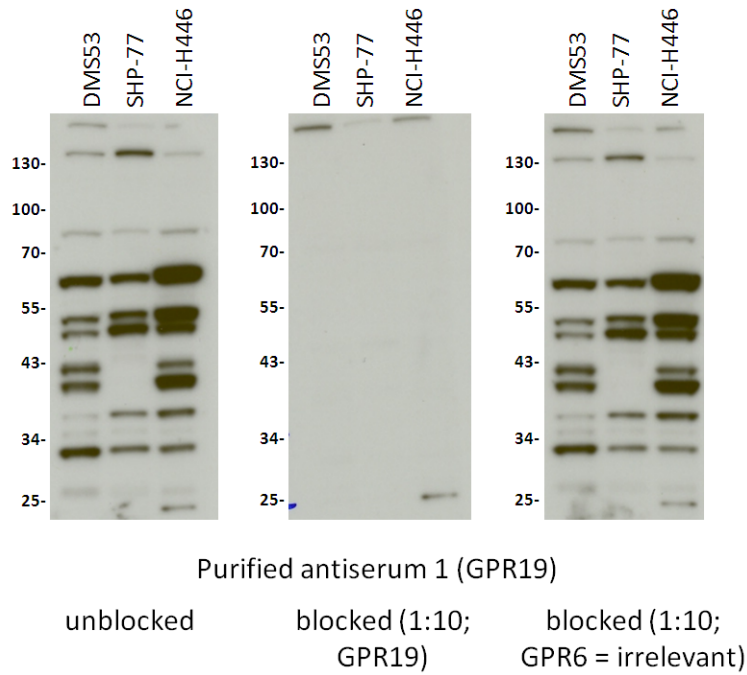


Figure 23: Purified GPR19 antiserum detects the GPR19 peptide used for immunization. For Western Blotting, protein lysates (30 μ g) from three lung cancer-derived cell lines (DMS 53, SHP-77, NCI-H446) were loaded onto lanes of a Criterion™ XT gel (18 well, 10% Bis-Tris, XT MOPS running buffer) and separated by sodium dodecyl sulfate (SDS)-polyacrylamide gel electrophoresis (PAGE). Primary antibody solutions were applied using either unblocked purified antiserum of animal #1, antiserum blocked with the GPR19 peptide used for purification (AQLWHPHEQDYKSSSLVC), or antiserum blocked with an unspecific non-GPR19 peptide (TAAGGPDTEGWGPPAAX, part of G protein-coupled receptor 6 (GPR6; irrelevant block) at an overall serum dilution of 1:1,500. High performance liquid chromatography (HPLC)-purified and lyophilized peptides were dissolved in dimethyl sulphoxide (DMSO) and incubated at 600 rounds per minute (rpm) for 1 h with the purified antiserum at a molar ratio of 1:10 (antiserum:peptide) assuming an average antibody weight of 150 kDa⁷⁸ (Chari RV, 2008). The predicted molecular weight of GPR19 is 47.7 kDa; the size marker is shown in kDa.

Except for GPR19 antibodies purchased from Abcam (ab75558) and Sigma Aldrich (SAB4501254), no differences in band signals were observed for any tested GPR19 antibody, regardless of whether lysates were obtained from GPR19, GPR19-tGFP, or tGFP-only overexpressing cells. This was also true for purified antisera which specifically detected GPR19 peptides in former blocking experiments. However, in lysates obtained from GPR19-tGFP overexpressing cells, ab75558 and SAB4501254 revealed signals that were not recovered in the tGFP-only control (mostly above 120 kDa). In addition, this high molecular weight pattern was recorded when an antibody directed against tGFP was applied for protein detection (figure 24A, lower row, seventh blot). Signals in the range of 120 to 250 kDa, that were absent in the control, were also observed in the lysates from GPR19 (true clone) overexpressing cells. But none of these signals could be attributed neither to a single GPR19 (the predicted molecular weight of GPR19 is 47.7 kDa) nor to a single GPR19-tGFP molecule (the predicted molecular weight of tGFP is 26 kDa; the fusion

⁷⁸ 1 Da = 1 g/mol.

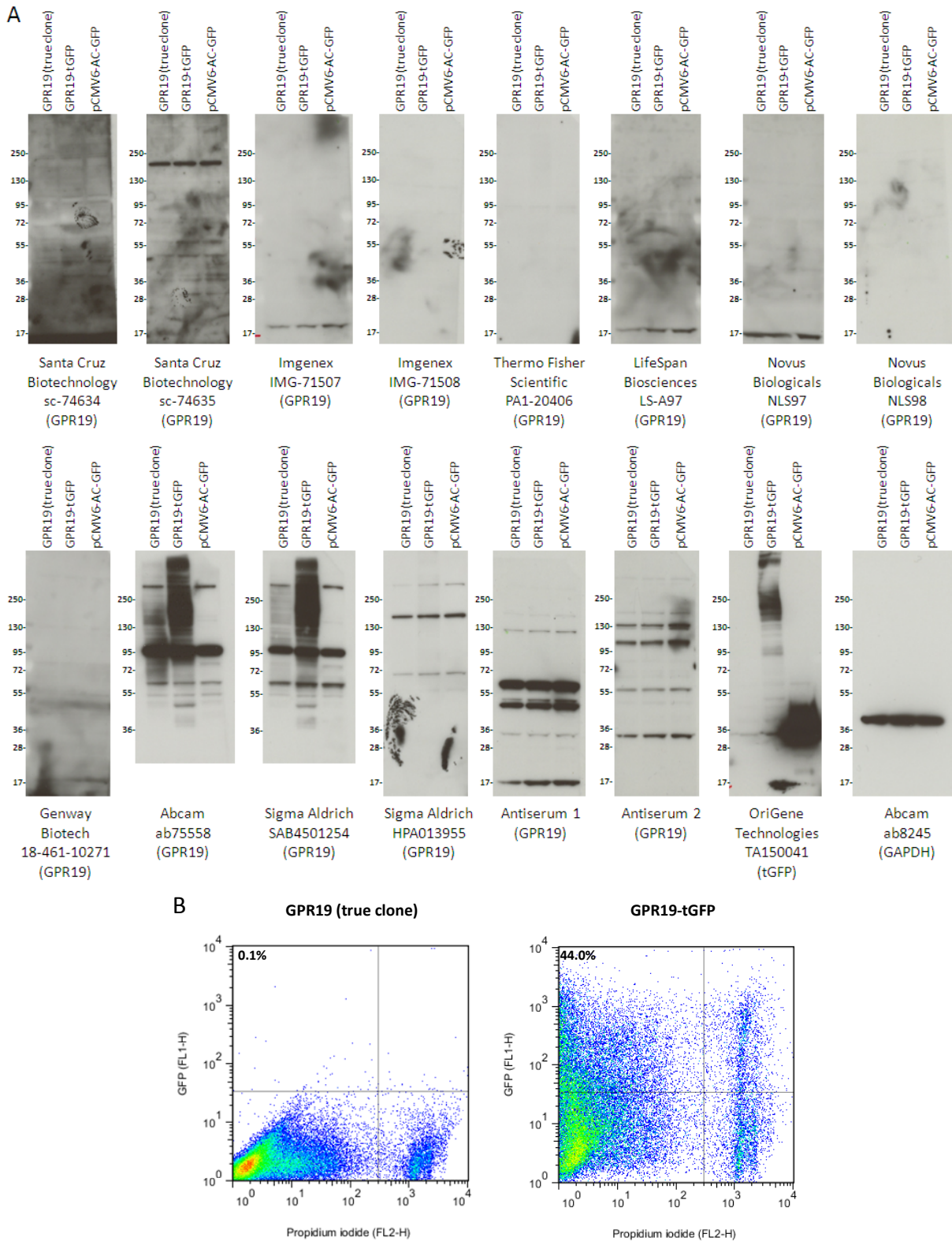


Figure 24: Most GPR19 signals from protein overexpression lysates are unspecific. (A) For Western Blotting, protein lysates (10 μ g) from HEK-293 cells transiently transfected with plasmids either encoding GPR19 (true clone), GPR19-tGFP (turbo green fluorescent protein), or tGFP-only (pCMV6-AC-GFP) harvested on day 2 after transfection were loaded onto lanes of a Criterion™ XT gel (18 well, 4-12% Bis-Tris, XT MOPS running buffer) and separated by SDS-PAGE. Primary antibody solutions containing commercially available GPR19, tGFP, or glyceraldehyde-3-phosphate dehydrogenase (GAPDH) antibodies (listed are manufacturers and product number) or purified GPR19 antisera (shown are antisera derived from animal # 1 (continued on next page)

after purification with either peptide AQLWHPHEQDYKKSSLVC (1) or KPTLYSIYNANFRRGMKETFC (2)) were used for protein detection (dilutions of antibodies are indicated in table 9 in the Materials section, purified GPR19 antisera were applied at a dilution of 1:500). The predicted molecular weight of GPR19 is 47.7 kDa, 26 kDa for tGFP, and 36 kDa for GAPDH (monomer; detection expected at 40 kDa according to the antibody manufacturer); the size marker is shown in kDa. **(B)** The transfection efficiency for GPR19-tGFP in comparison to GPR19 (true clone) was assessed on day 2 after transfection using flow cytometry (dot plot for tGFP (fluorescence channel 1 (FL1)-height (H)) and propidium iodide (fluorescence channel 2 (FL2)-H) signals, the data point density is reflected by different colors ranging from **blue** (low density, single data points) to **red** (high data point density); figures refer to the relative number of cells in the upper left quadrant (tGFP positive, propidium iodide negative)).

protein is therefore expected to have a molecular weight of 73.7 kDa). The loading of equal protein amounts was confirmed by GAPDH detection (comparable signal intensities for all conditions; figure 24A, lower row, last blot). Successful HEK-293 transfection was verified by flow cytometry (figure 24B) revealing 44% of successfully transfected and alive cells.

The GPR19 antibodies from Abcam (ab75558) and Sigma Aldrich (SAB4501254) were further evaluated for the detection of endogenous GPR19 in NCI-H1703 cells (Western Blot). This cell line was found to strongly express *Gpr19* mRNA as depicted later (figure 31). Further, Next Generation Sequencing identified no mutation in the gene encoding GPR19 in NCI-H1703 cells (proprietary Boehringer Ingelheim Next Generation Sequencing cell line genomic database; data not shown). In addition, *Gpr19* mRNA had been knocked down using *Gpr19*-targeting siRNAs. Endogenous GPR19 levels were examined in control siRNA-treated samples. Both antibodies showed a band pattern that – according to the predicted molecular weight of GPR19 of 47.7 kDa – might contain single bands reflecting the detection of GPR19 in control siRNA-treated samples (figure 25A). **However, these antibodies failed to detect GPR19 protein knockdown mediated by siRNAs that successfully diminished the *Gpr19* message as verified by RT-qPCR** (figure 25B): None of the detected signals showed a declined intensity. The loading of equal protein amounts was confirmed by GAPDH detection (comparable signal intensities for all conditions).

Taken together, validation experiments of various **commercially available antibodies against GPR19 were unable to detect GPR19 on Western Blots reliably**. In addition, rabbit **antisera raised against nine different GPR19 peptides located in the amino- or carboxy-terminus, predicted intracellular loop regions 2 or 3, or the predicted extracellular loop region 3 did not allow specific detection on Western Blots**, either. Due to the lack of an antibody detecting GPR19 protein, effective knockdown of *Gpr19* mRNA by *Gpr19*-targeting siRNAs was assessed by RT-qPCR in subsequent experiments.

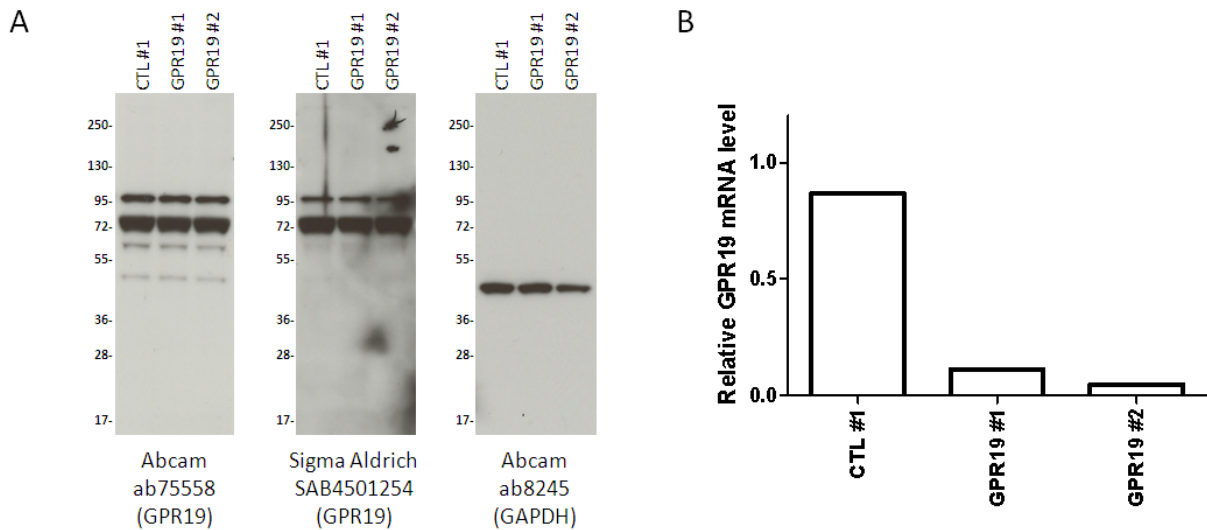


Figure 25: GPR19 antibodies do not detect GPR19 knockdown in NCI-H1703 cells. (A) For Western Blotting, protein lysates (10 μ g) from NCI-H1703 cells transfected with control (CTL #1) or GPR19 siRNAs #1 or #2 harvested on day 3 after transfection were loaded onto lanes of a Criterion™ XT gel (18 well, 4-12% Bis-Tris, XT MOPS running buffer) and separated by SDS-PAGE. Primary antibody solution containing GPR19 or glyceraldehyde-3-phosphate dehydrogenase (GAPDH) antibodies (listed are manufacturers and product number) were used for protein detection (dilutions of antibodies are indicated in table 9 in the Materials section). The predicted molecular weight of GPR19 is 47.7 kDa and 36 kDa for GAPDH (monomer; detection expected at 40 kDa according to the antibody manufacturer); the size marker is shown in kDa. (B) For each sample (triplicates), *Gpr19* mRNA knockdown was assessed by RT-qPCR on day 2 after siRNA transfection (normalized against reference genes *Cypa* and *Hprt1*) and geometric mean values were calculated relative to an untreated control sample (not included in the graph).

3. *Gpr19* gene expression

3.1. *Gpr19* mRNA levels are high in SCLC patient samples

Many GPCRs control signaling pathways that regulate cell growth, proliferation, and differentiation. It has long been known that tumor cells may express GPCRs in an aberrant or illegitimate fashion (Schorr I and Ney RL, 1971). In an unbiased approach, gene expression levels of genes encoding proteins with GPCR activity (GPCRs and GPCR-associated proteins) defined by the Gene Ontology (GO) number 0004930 were investigated in a series of human SCLC, NSCLC, and normal lung RNA samples. Patient samples were obtained from OriGene Technologies and sample details are listed in table 12 in the Methods section. They were analyzed by Affymetrix microarray analysis (Human Exon 1.0 ST Array). This survey also included the large GPCR subfamily of odorant receptors, because these may be expressed in tissues other than the olfactory epithelium and may have other functions than detecting odors (Spehr M and Munger SD, 2009); in fact, they can occur in neoplasms such as prostate cancers (Neuhaus EM *et al.*, 2009).

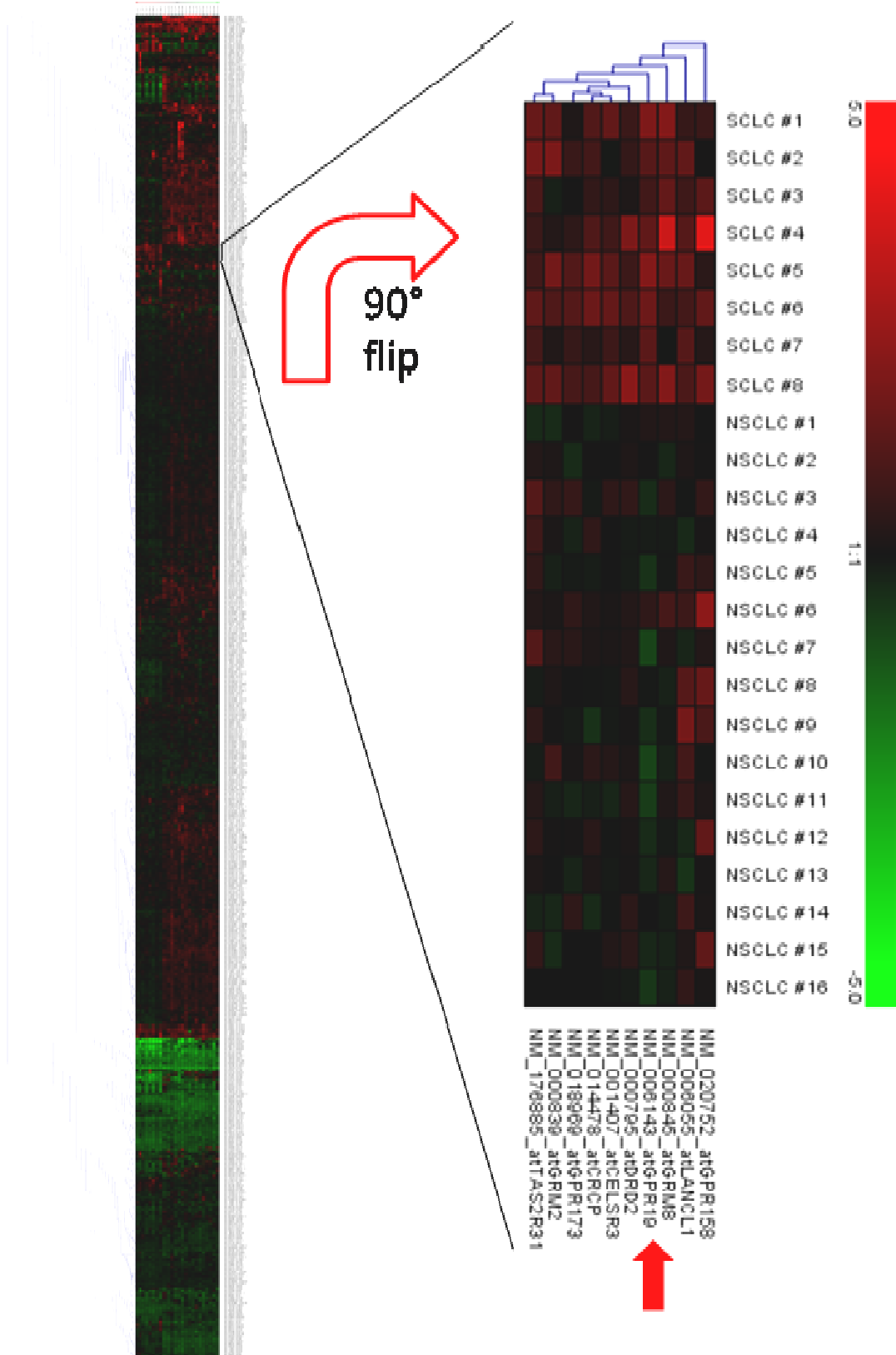


Figure 26: *Gpr19* clusters with other GPCRs overexpressed in samples from SCLC patients. Gene expression levels (Affymetrix GeneChip® Human Exon 1.0 ST Array) of genes encoding proteins with GPCR activity (Gene Ontology number 0004930) from SCLC and NSCLC patient-derived RNA tumor samples were normalized against expression levels of healthy controls (14 samples) and displayed in a heat map. Intensity values (pseudo color scale) were log₂-transformed and the enlargement shows the *Gpr19* (←)-containing cluster flipped at 90°. Cases are represented in columns (rows in the enlargement) and single genes in rows (columns in the enlargement).

Hierarchical clustering identified *Gpr19* among the mRNAs which encode proteins with GPCR activity showing a message overexpression mostly in SCLC but not in NSCLC samples relative to normal controls (figure 26). This cluster further included orphan GPCRs (G protein-coupled receptors 158 (GPR158) and 173 (GPR173)), metabotropic glutamate receptor family members 2 and 8 (GRM2, GRM8), the dopamine receptor D2 (DRD2), and a member of the taste receptor family involved in the perception of bitterness (taste receptor type 2 member 31 (TAS2R31)). In addition, non-classical GPCRs called by GO number 0004930 were also found in this cluster, e.g., the cadherin superfamily-assigned cadherin, epidermal growth factor (EGF) laminin A G-type seven-pass receptor 3 (CELSR3)⁷⁹ which could be involved in contact-mediated cellular communication. Apart from the above mentioned cluster, various other clusters existed in which mRNAs encoding proteins with GPCR activity were for example downregulated in both SCLC and NSCLC samples (**green** coloring, found in the lower part of the full heat map of figure 26, left panel).

High *Gpr19* mRNA levels in SCLC samples were verified by a direct comparison with those seen in samples from NSCLC and normal lung (figure 27, left panels). The same result was obtained through RT-qPCR analysis (figure 27, right panels). **Almost all individuals of the SCLC sample set showed high *Gpr19* expression relative to the NSCLC or normal lung controls.**

3.2. *Gpr19* is overexpressed in SCLC and pancreas islet cell carcinoma

The BioExpress® database (Gene Logic) was utilized for examination of *Gpr19* expression in various human normal and cancerous tissues. Two different Affymetrix array platforms (Human Genome U133A and Human Genome U133B array sets (figure 28); Human Genome U133 plus 2.0 array (figure 29)) were available.

Expression studies on both platforms revealed **high *Gpr19* mRNA expression predominantly in the central nervous system** (CNS; cerebral cortex, cerebellum, spinal cord). The CNS had been described before as the primary site of *Gpr19* expression (O'Dowd BF *et al.*, 1996; Vassilatis DK *et al.*, 2003; Hoffmeister-Ullerich SA *et al.*, 2004). In addition, ***Gpr19* mRNA levels were prominent in samples from SCLC and pancreas islet cell carcinoma.** Both these carcinoma types are mainly characterized by a neuroendocrine phenotype and the presence of neuroendocrine markers (Wiedenmann B *et al.*, 1986; Nakakura EK and Bergsland EK, 2007; Modlin IM *et al.*, 2010).

⁷⁹ CELSR3 (NCBI gene ID 1951; UniProt protein ID Q9NYQ7) is a member of the flamingo subfamily of the cadherin protein superfamily which is composed of non-classical-type cadherins. Its ectodomain contains nine cadherin domains (C), seven epidermal growth factor (EGF)-like repeats (E) and two laminin A G-type repeats (L). In addition, it harbors seven transmembrane domains (S) and is the third receptor assigned to this subfamily (R3; www.ncbi.nlm.nih.gov/gene/1951; www.uniprot.org/uniprot/Q9NYQ7).

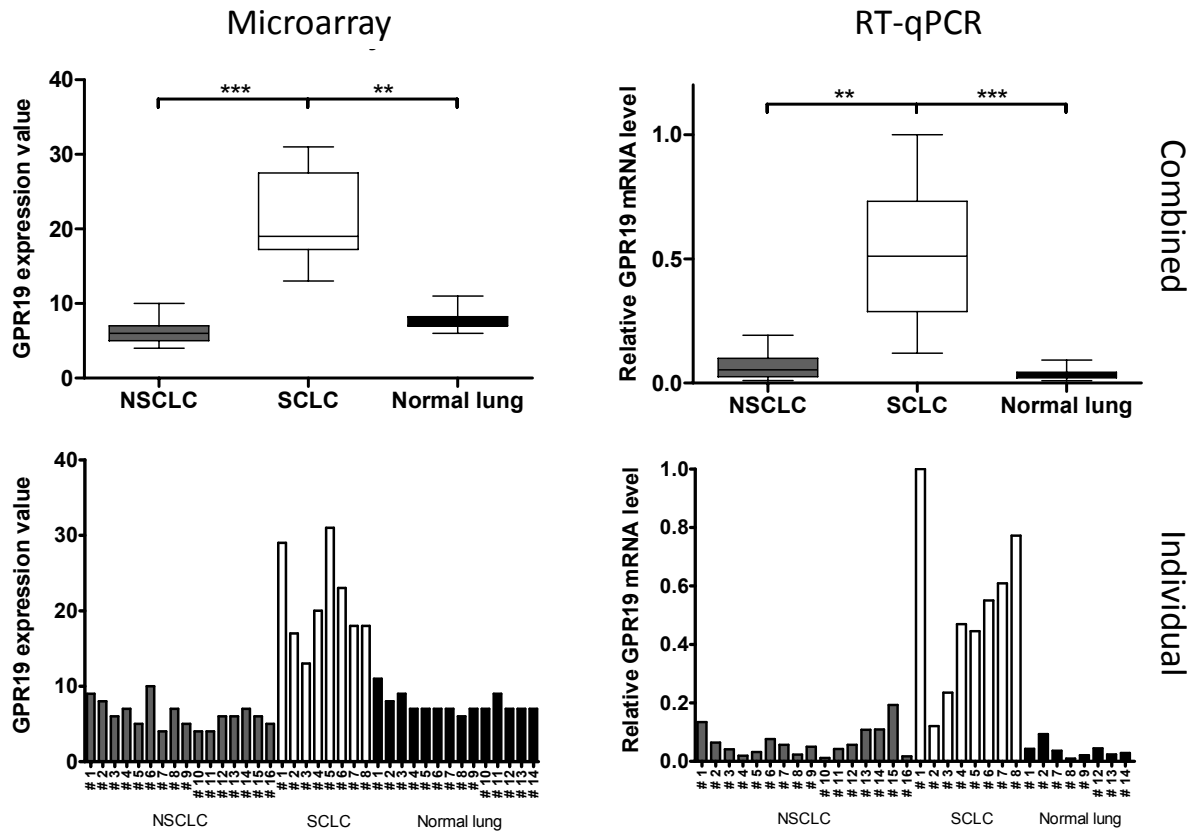


Figure 27: *Gpr19* is overexpressed in samples from SCLC patients. The results for *Gpr19* gene expression from Affymetrix GeneChip® analysis (Human Exon 1.0 ST Array; probe set NM_006143_at) and RT-qPCR analysis of human NSCLC, SCLC, and normal lung samples are shown per histological group. Expression data are either combined for all cases per group (upper panels; box (interquartile range; middle 50% of all expression values) and whiskers (minimum-maximum) plot with median (central bar)) or are shown for each individual sample (lower panels). RT-qPCR was performed for *Gpr19* normalized against reference genes *Actb*, *Cypa*, *Hprt1*, and *Rplp0* and geometric mean values were calculated. This analysis did not include all 14 normal lung samples due to sample limitations. Statistically significant differences were determined by a Kruskal-Wallis test followed by Dunn's multiple comparison (** $p < 0.01$; *** $p < 0.001$).

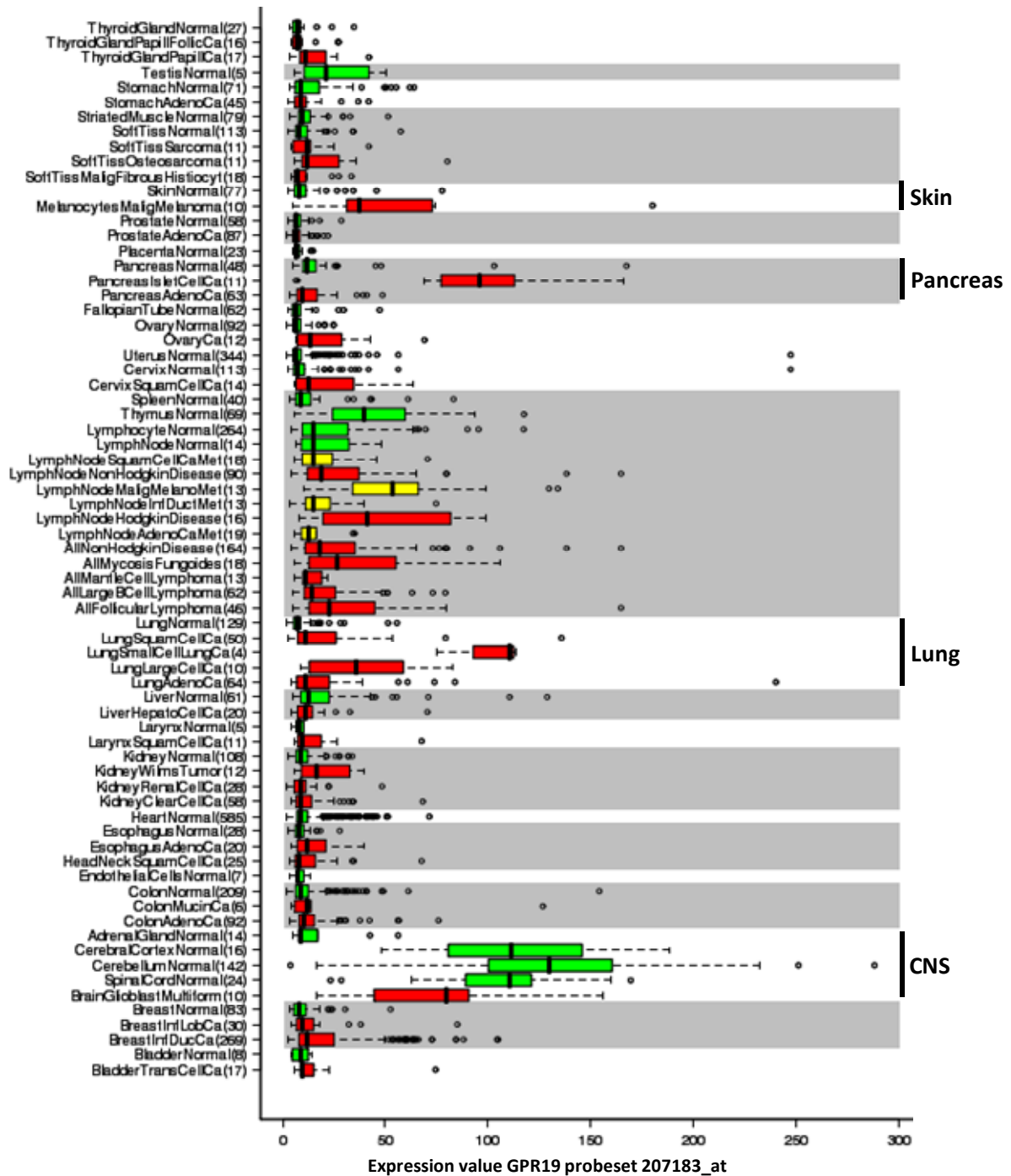


Figure 28: *Gpr19* expression is high in SCLC and pancreas islet cell carcinoma and in the central nervous system (CNS; part 1). *Gpr19* gene expression was determined by Affymetrix GeneChip® analysis (Human Genome U133A and Human Genome U133B array sets; probe set 207183_at) in human tissues (green = normal; red = cancer; yellow = metastasis). Expression data are represented as box (interquartile range; middle 50% of all expression values) and whiskers (extend to 1.5 times the interquartile range) plots with median (central bar) and outliers (open circles; expression values above and below the whisker limits). Sample numbers are indicated in brackets. Data were extracted from the BioExpress® database (Gene Logic).

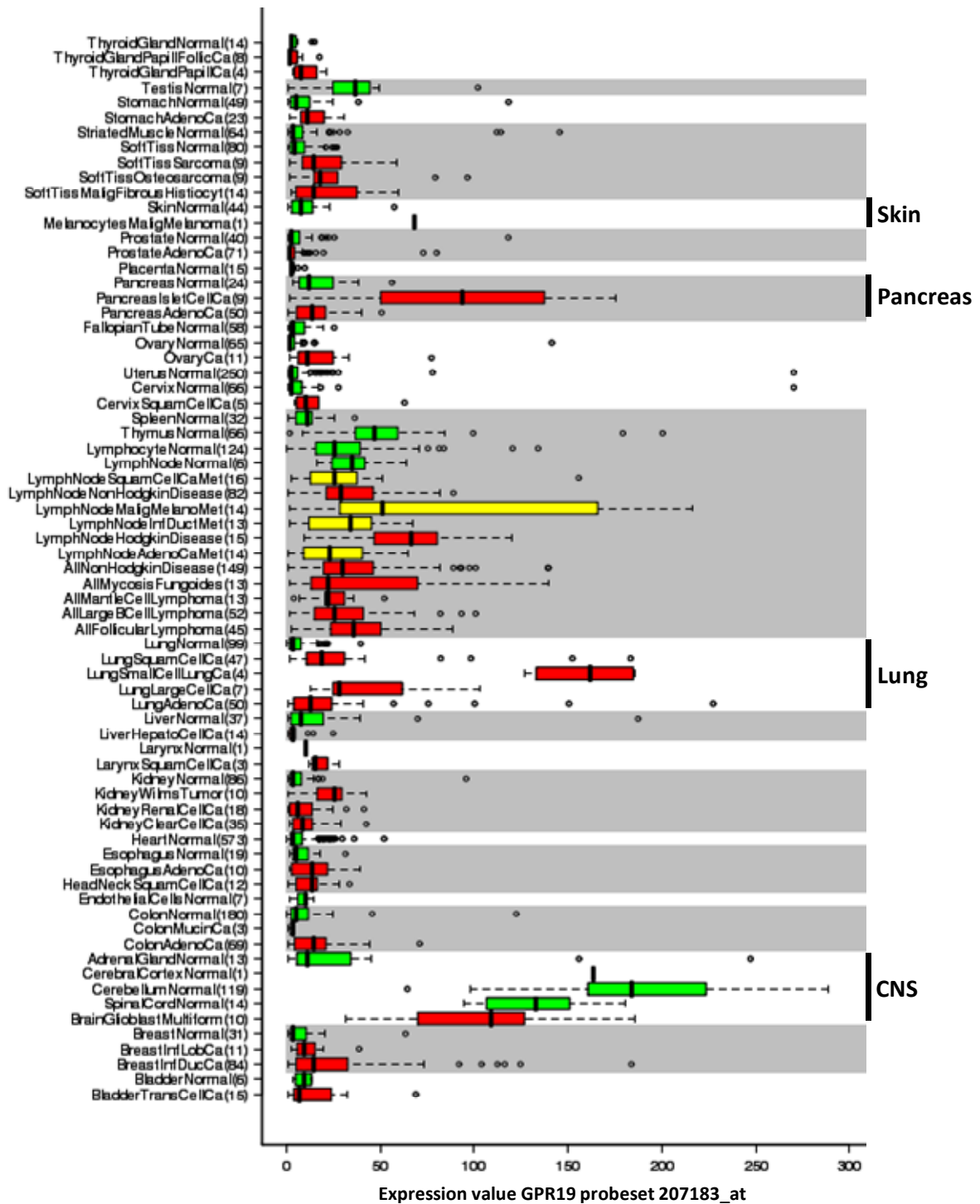


Figure 29: *Gpr19* expression is high in SCLC and pancreas islet cell carcinoma and in the central nervous system (CNS; part 2). *Gpr19* gene expression was determined by Affymetrix GeneChip® analysis (Human Genome U133 plus 2.0 array; probe set 207183_at) in human tissues (green = normal; red = cancer; yellow = metastasis). Data were extracted from the BioExpress® database (Gene Logic) and visualization was done as described in the legend of figure 28.

3.3. *Gpr19* mRNA expression is high in SCLC cell lines

In order to quantify *Gpr19* expression in lung-derived cell lines, the proprietary Boehringer Ingelheim cell line gene expression database was utilized. It contains expression data generated with Affymetrix GeneChip® technology (Human Exon 1.0 ST array) and data for 21 human SCLC and 45 human NSCLC cell lines were extracted (figure 30). Furthermore, *Gpr19* expression levels were measured by RT-qPCR in a partially overlapping set of NSCLC (3), SCLC (7), and normal lung (5)-derived cell lines and in HEK-293 cells (figure 31). Equal numbers of cells had been applied for RNA preparation.

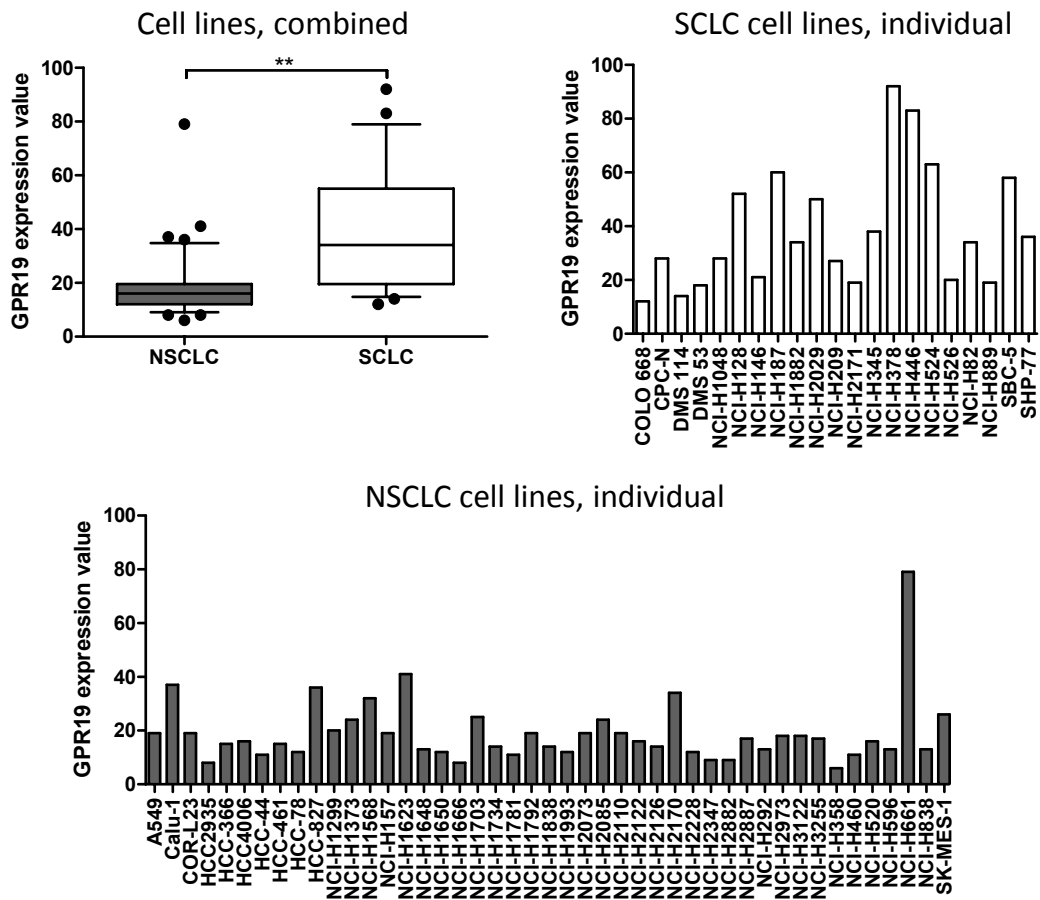


Figure 30: *Gpr19* expression in SCLC cell lines is higher than in NSCLC cell lines (microarray). *Gpr19* gene expression was determined by Affymetrix GeneChip® analysis (Human Exon 1.0 ST Array; probe set NM_006142_at) in various human SCLC and NSCLC cell lines. Expression data are either combined for all cases per histological group (upper left panel; box (interquartile range; middle 50% of all expression values) and whiskers (10 to 90 percentile) plot with median (central bar) and outliers (filled circles; expression values above and below the whisker limits) or are shown for each individual cell line (SCLC cell lines – upper right panel; NSCLC cell lines – lower panel). Statistically significant differences were determined by a t test with Welch's correction (**p < 0.01). These data are part of a proprietary Boehringer Ingelheim gene expression database.

In both methods, the expression pattern of *Gpr19* described in the analysis of SCLC-, NSCLC-, and normal lung-derived samples was recapitulated, i.e., **cell lines originating from SCLC** (such as NCI-H187, NCI-H378, or NCI-H446) **had higher *Gpr19***

expression levels than those derived from NSCLC (and from normal lung). However, high levels of *Gpr19* mRNA were also seen in some NSCLC cell lines (e.g., Calu-1, HCC-827, NCI-H1623, NCI-H1703, or NCI-H661) and an immortalized lung epithelial cell line derived from a cystic fibrosis patient (IB3-1). *Gpr19* expression was absent in HEK-293 cells.

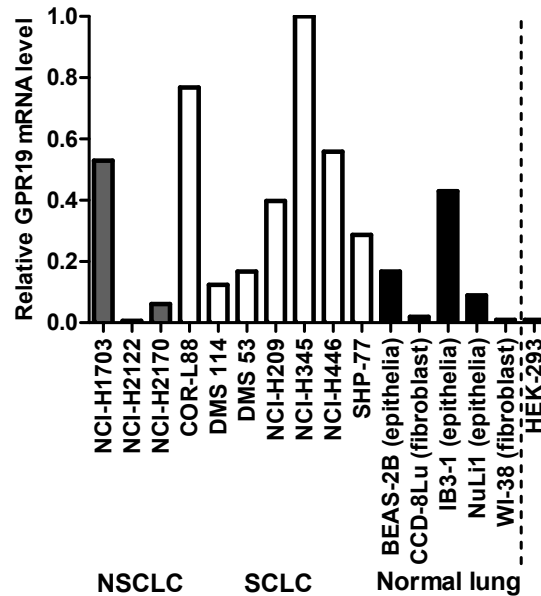


Figure 31: *Gpr19* expression is high in many SCLC cell lines (RT-qPCR). *Gpr19* gene expression was determined by RT-qPCR in various human NSCLC-, SCLC-, and normal lung-derived cell lines and in HEK-293 (cell line features are specified in table 10 in the Materials section). Expression values were normalized against reference genes *Actb*, *Cypa*, *Hprt1*, and *Rplp0* and geometric mean values were calculated.

One reason for increased gene expression could be a genomic amplification of the respective chromosomal area. Various SCLC and NSCLC cell lines were investigated for their copy number status of *Gpr19* (figure 32). These data are part of a proprietary Boehringer Ingelheim cell line database and were collected from the analysis of Affymetrix single nucleotide polymorphism (SNP) arrays. They do therefore not cover all cell lines examined for *Gpr19* gene expression (figure 30 and figure 31). Schematic representations of chromosome 12 for some cell lines investigated showing areas of genomic amplification or deletion are displayed in figure 33. A normal sample should harbor two copies per genomic region (except for sexual chromosomes X and Y in males). Cancer cells might have lost (copy number 0 or 1) or gained (copy number greater than 3) genomic DNA regions. Complexity is further increased as cancer cells are often not diploid (Hupé P *et al.*, 2004).

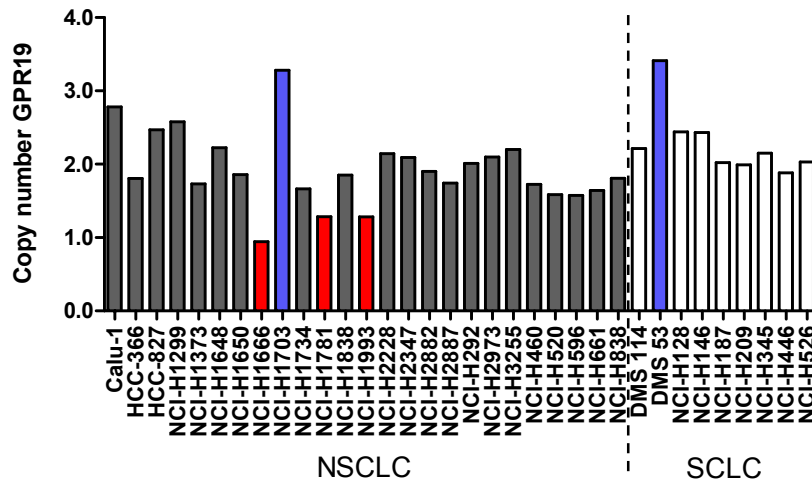


Figure 32: *Gpr19* copy numbers can vary in NSCLC and SCLC cell lines. Copy numbers for *Gpr19* in various SCLC and NSCLC cell lines are based on single nucleotide polymorphism (SNP) data from Affymetrix GeneChip® Human Mapping 250K Nsp arrays. These data are part of a proprietary Boehringer Ingelheim cell line database and cell line DNA copy numbers had been analyzed using the gain and loss analysis of DNA (GLAD) algorithm (Hupé P et al., 2004). Called deletions (red bars) and amplifications (blue bars) are highlighted.

Most lung cancer-derived cell lines showed a normal genomic copy number for *Gpr19*. However, the *Gpr19* copy number in SCLC cell line DMS 53 and NSCLC cell line NCI-H1703 was increased (figure 32 and figure 33), whereas it was decreased in NSCLC cell lines NCI-H1666, NCI-H1781, and NCI-H1993. This genomic amplification of the *Gpr19* locus in DMS 53 and NCI-H1703 cells could account for the *Gpr19* expression levels seen in these cell lines. On the other hand, *Gpr19* expression in NCI-H187 and NCI-H446 cells was very high (figure 30) but amplification of the *Gpr19* locus could not be detected (figure 32 and figure 33). **Genomic amplification of *Gpr19* might therefore contribute to *Gpr19* mRNA expression in lung cancer-derived cell lines but could not be considered the only cause for high *Gpr19* message levels.**

Finally, **Next Generation Sequencing did not retrieve mutations in the gene encoding GPR19 in any lung cancer-derived cell line**, which is included in the proprietary Boehringer Ingelheim Next Generation Sequencing cell line genomic database (data not shown). Among them are also NSCLC cell line NCI-H1703 and SCLC cell line DMS 53, the major cell lines used in subsequent studies.

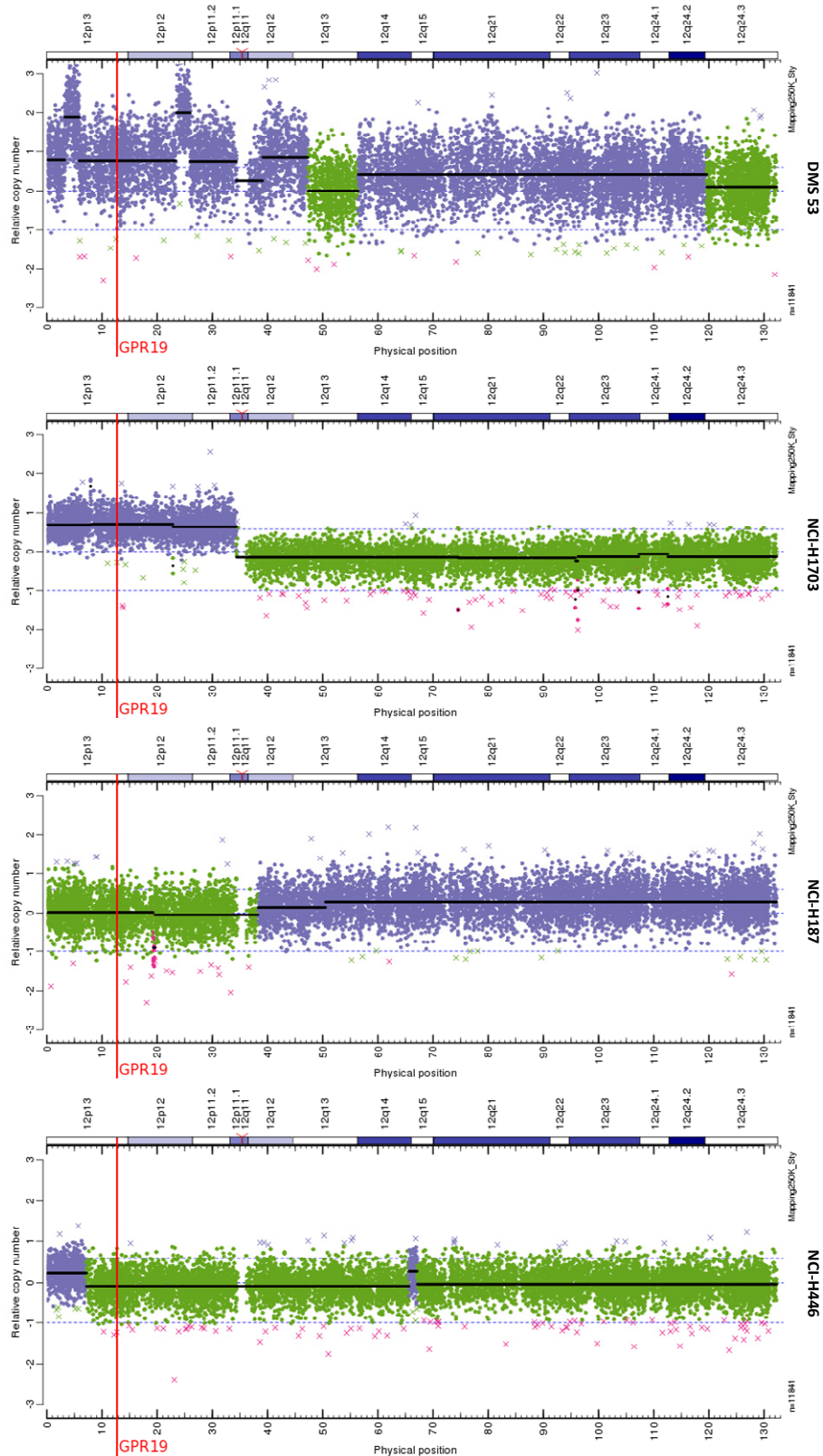


Figure 33: *Gpr19* can be located in chromosomal areas that had undergone amplification. The schematic representation shows the positions of single nucleotide polymorphisms (SNPs) covered by the Affymetrix GeneChip® Human Mapping 250K Nsp array on chromosome 12 for SCLC cell lines DMS 53, NCI-H187, and NCI-H446 and NSCLC cell line NCI-H1703. Filled circles represent a single SNP and are colored according to a normal (**green**) or higher than normal (**blue**) genomic copy number using the GLAD algorithm. Areas of normal or increased copy numbers were grouped, which is indicated by a **black** horizontal line. Filled circles in **red** (NCI-H187) indicate a focal deletion and crosses represent outliers. The chromosomal position of the *Gpr19* gene is shown by a **red** vertical line.

4. GPR19 localizes to the cytoplasmic membrane

As a member of the seven transmembrane (7TM)-spanning family of GPCRs, GPR19 is recruited to cellular membranes. This does not exclusively imply the cytoplasmic membrane of a cell, as GPCRs have been described to mediate signal transduction from intracellular compartments as well (e.g., G protein-coupled receptor 6 (GPR6; Padmanabhan S *et al.*, 2009; Prasad BM *et al.*, 2010)).

The subcellular localization of GPR19 was investigated by transient transfection of lung cancer-derived NCI-H2170 (NSCLC) and DMS 53 (SCLC) cells with an expression plasmid encoding a tGFP-tagged variant of GPR19. Transfected plasmids had been verified by sequencing. Confocal microscopy pictures were recorded on the first day after transfection clearly **indicating a distinct thin line signal for GPR19-tGFP, which might represent the plasma membrane** (figure 34A and B, middle panels). Additionally, some cells revealed a strong signal coming from an area lying close to the nucleus – a possible hint for the endoplasmic reticulum, the site for the generation of proteins that are later destined for sorting through the secretory pathway, for instance to the cytoplasmic membrane (figure 34A, middle panel). In contrast, the signals derived from the expression of tGFP-only (figure 34A and B, left hand panels) and tGFP-tagged GPR6 (figure 34A and B, right hand panels), a GPCR mostly found in intracellular membrane compartments, were distributed throughout the cell and not indicative of the cytoplasmic membrane (no thin line signal).

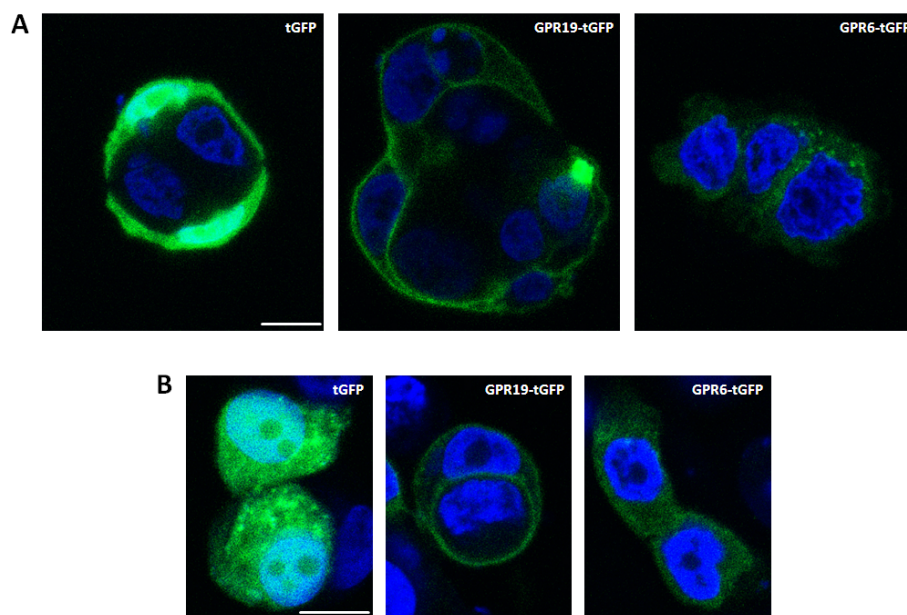


Figure 34: GPR19-tGFP expression indicates receptor localization to the plasma membrane. The NSCLC cell line NCI-H2170 (**A**) and the SCLC cell line DMS 53 (**B**) were transiently transfected with expression plasmids (0.2 µg per well of an 8 well chamber slide) encoding either turbo green fluorescent protein (tGFP)-only (pCMV6-AC-GFP; left hand panels; **green**), GPR19-tGFP (pCMV6-AC-GPR19-GFP; middle panels; **green**), or G protein-coupled receptor 6 (GPR6)-tGFP (pCMV6-AC-GPR6-GFP; right hand panel; **green**). Cells were fixed and mounted with DAPI-containing mounting medium (nuclear staining; **blue**) on the first day after transfection. Fluorescent signals were recorded by confocal microscopy at 60x magnification (bar represents 10 µm). Experiments were repeated yielding concurrent results.

In order to verify the potential subcellular localization of GPR19-tGFP to the plasma membrane, HEK-293 cells were transiently transfected with the GPR19-tGFP expression plasmid and sugar derivatives (N-acetyl glucosamine; N-acetyl neuraminic acid) mostly found on cell surface proteins were co-stained with Alexa Fluor® 647-conjugated wheat germ agglutinin (WGA; Prasad BM *et al.*, 2010) for confocal microscopy analysis the next day (figure 35A). **Merging of both the tGFP (GPR19; green) and the WGA (membrane; red) signal identified a clear overlay (yellow).** The same result was obtained when a plasmid encoding the murine enhanced yellow fluorescent protein (eYFP)-tagged corticotropin-releasing hormone receptor 1 (CRHR1), a GPCR that is known to localize to the cytoplasmic membrane (Aguilera G *et al.*, 2004), had been transfected into HEK-293 cells (figure 35B). Therefore, the conclusion that **transient overexpression of GPR19 leads to its localization to the cytoplasmic membrane** is justified.

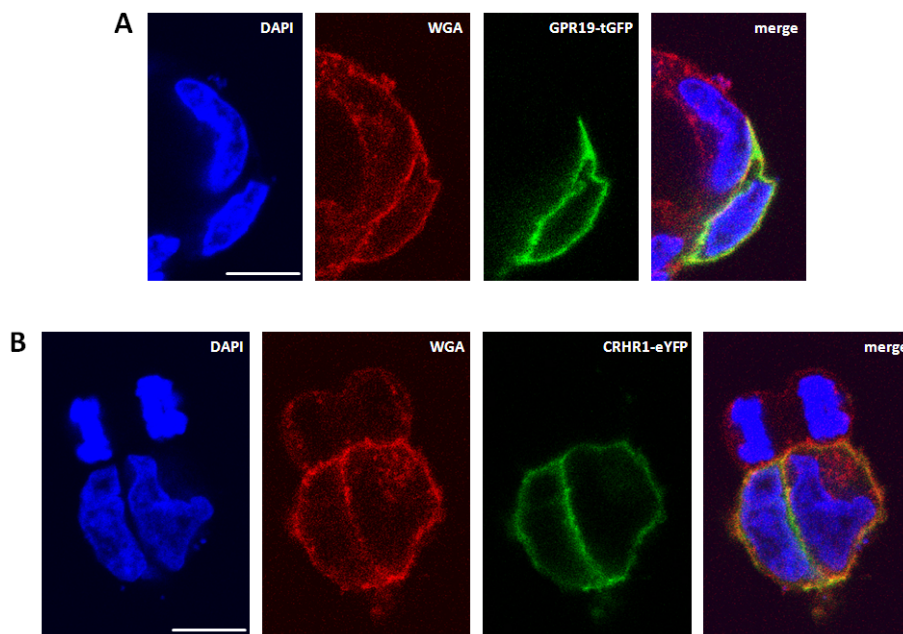


Figure 35: GPR19-tGFP colocalizes with WGA-stained plasma membrane proteins. HEK-293 cells were transiently transfected with expression plasmids (0.05 µg per well of an 8 well chamber slide) encoding either GPR19-tGFP (turbo green fluorescent protein; **A**; pCMV-AC-GPR19-GFP; **green**) or the murine CRHR1-eYFP (enhanced yellow fluorescent protein; **B**; pEYFP-N1-CRHR1; **green**). On the first day after transfection, cells were fixed, membrane-stained using wheat germ agglutinin (WGA; **red**), and mounted with DAPI-containing mounting medium (nuclear staining; **blue**). Fluorescent signals were recorded by confocal microscopy at 60x magnification (bar represents 10 µm). Merge panels combine signals from DAPI, WGA, and tGFP/eYFP, respectively. Experiments were repeated yielding concurrent results.

5. Proliferation

5.1. RNA interference-mediated knockdown of *Gpr19* reduces cell proliferation

The prominent expression of *Gpr19* in SCLC and in several lung cancer-derived cell lines suggested that this receptor might play a crucial role in cell proliferation and/or survival. Accordingly, the effect of *Gpr19* knockdown on proliferation in lung cancer-derived cell lines NCI-H1703 (NSCLC) and DMS 53 (SCLC) was investigated. These cell lines were chosen based on their well-detectable *Gpr19* mRNA expression (figure 31) and because they grew as monolayers. Most SCLC cell lines including COR-L88, NCI-H209, NCI-H345, NCI-H446, and SHP-77 that express *Gpr19* at high levels failed to grow as adherent monolayers but formed (floating) clusters. This growth behavior rendered them less amenable to experimental manipulations, in particular to transfection with siRNAs. GPR19 is an orphan receptor, its physiological ligand is not known and there is no antagonist. Hence, RNA interference was employed to examine the role of this receptor in supporting cell proliferation.

NCI-H1703 (3,500 cells) and DMS 53 (10,000 cells) were either treated with siRNAs targeting *Gpr19* mRNA for destruction (GPR19 #1, GPR19 #2), control siRNAs (CTL #1, CTL #2) or with transfection reagent only (mock) or left untreated. Additional positive controls included the cytotoxic anthracycline doxorubicin⁸⁰ and an siRNA directed against *Plk1*⁸¹ which were supposed to exhibit a dramatically reduced proliferation behavior (Fornari FA *et al.*, 1994; Spänkuch-Schmitt B, Wolf G *et al.*, 2002). The extent of well surface covered by adherently growing cells (confluence) was monitored to quantify cell proliferation. Images of wells covered by NCI-H1703 and DMS 53 cells were captured and analyzed at regular intervals after treatment using the CloneSelect™ Imager (figure 36). Well thumbnails (pictures of the well bottom and cellular detection by the selected detection algorithm) served as the basis for confluence calculation (figure 37, shown for NCI-H1703 cells). Measurements started

⁸⁰ Doxorubicin is frequently used as chemotherapeutic agent in the treatment of malignant diseases which is mainly based on two different modes of action. On the one hand, doxorubicin intercalates into DNA double strands therefore inhibiting DNA replication and gene transcription. In addition, it inhibits the enzyme topoisomerase II which is crucial for unwinding of supercoiled DNA structures during replication. Hence, the ligation of topoisomerase II-induced DNA strand breaks is prevented (Fornari FA *et al.*, 1994).

⁸¹ Polo-like kinases (PLKs) are highly conserved during evolution and play essential roles in the cell cycle. Four mammalian members (PLK1, PLK2, PLK3, and PLK4) have been described – all harbor an amino-terminal Ser/Thr-kinase domain and a carboxy-terminal polo-box domain (PBD; composed of one or two polo-boxes that can bind phosphorylated target proteins). They are involved in centrosome and centriole biogenesis, in the regulation of mitosis entry and mitotic chromosomes, and the promotion of mitotic exit and cytokinesis. Their activity can be regulated at different levels, e.g., via transcription, phosphorylation, proteasomal degradation, or protein interaction (Archambault V and Glover DM, 2009).

Human PLK1 (NCBI gene ID 5347; UniProt protein ID P53350) is found overexpressed in many cancers and is associated with tumorigenesis. Its expression and activity (phosphorylation at Thr210) is highest during mitosis and it localizes to different subcellular structures such as centrosomes (prophase), kinetochores (prometa-/metaphase), the central spindle (anaphase), or the mid-body (telophase). It primarily regulates the transition from meta- to anaphase (spindle assembly checkpoint, sister chromatid separation) and mitotic exit (initiation of cleavage furrow ingression) by phosphorylation of various target proteins such as CDC25, cyclin B1, the anaphase-promoting complex/cyclosome (APC/C), or proteins involved in microtubule dynamics (Strebhardt K and Ullrich A, 2006; Petronczki M *et al.*, 2008).

10 h after treatment and lasted until day 6 (right panels of figure 36 show results of three experiments at day 6). At this time point, untreated, mock-, and control siRNA-treated cells had already reached a high extent of confluence, *i.e.*, a plateau phase with more than 80% well confluence. *Plk1* siRNA-transfected and doxorubicin-treated cells did not grow (absent gain in confluence over time). **For cells transfected with either *Gpr19*-targeting siRNAs #1 or #2, the increase in well confluence was modest/not existing. This observation showed that cell proliferation was inhibited.**

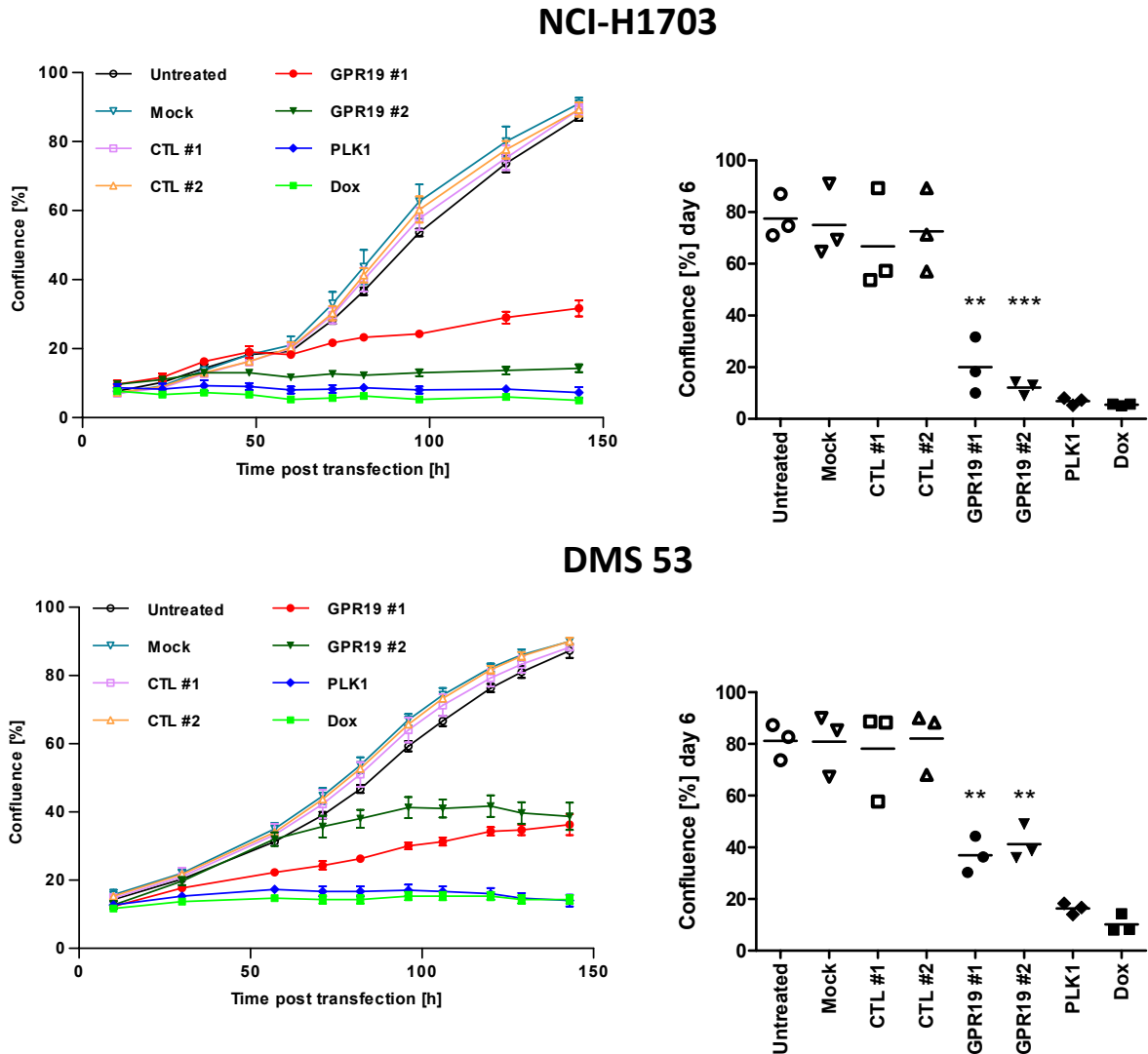


Figure 36: Cell proliferation is inhibited by *Gpr19*-targeting siRNAs (confluence measurement). Cell proliferation was determined by measuring confluence, *i.e.*, % of total well area covered by cells. Shown is the time course after siRNA transfection (20 nM) or addition of doxorubicin (1 μ M); data are mean values \pm standard deviation (error bars) of three wells per condition (96 well plate) from a representative experiment for untreated, mock (transfection reagent only)-, siRNA (CTL #1 and #2, *Gpr19*-targeting #1 and #2, *Plk1*-targeting)-, and doxorubicin (Dox)-treated NSCLC cell line NCI-H1703 and SCLC cell line DMS 53. Two additional experiments gave similar results. The right hand graphs illustrate the results from the last confluence measurement on day 6 after transfection from the three individual experiments (arithmetic mean values are indicated by the horizontal lines). Statistically significant differences across all experimental groups were determined by one way analysis of variance (ANOVA) followed by Tukey's test. GPR19 #1 and GPR19 #2 p values refer to the least significant one from the comparison with CTL #1 and CTL #2 (**p < 0.01; ***p < 0.001).

The negative influence on cell proliferation of *Gpr19*-targeting siRNAs could be confirmed using a second type of proliferation assay (alamarBlue® viability testing), which allows a correlation between the cells' metabolic activity and the number of living cells as an indication of cell proliferation. Cells had been transfected with siRNAs or treated with doxorubicin as described above and the metabolic activity of cells was determined three and six days later (figure 38). In order to minimize data variation, the time points of fluorescence intensity measurement after application of alamarBlue® on days 3 and 6 after treatment were comparable for repeated experiments and within the dynamic range of the assay. **There was a clear-cut reduction in metabolically active cells transfected with siRNAs targeting *Gpr19* compared to untreated, mock-, and control siRNA-treated samples.** Cells treated with *Plk1* siRNA or doxorubicin did not grow which was indicated by low numbers of metabolically active cells (low fluorescence intensity). In both cell lines, the effect was more pronounced on day 6 than on day 3.

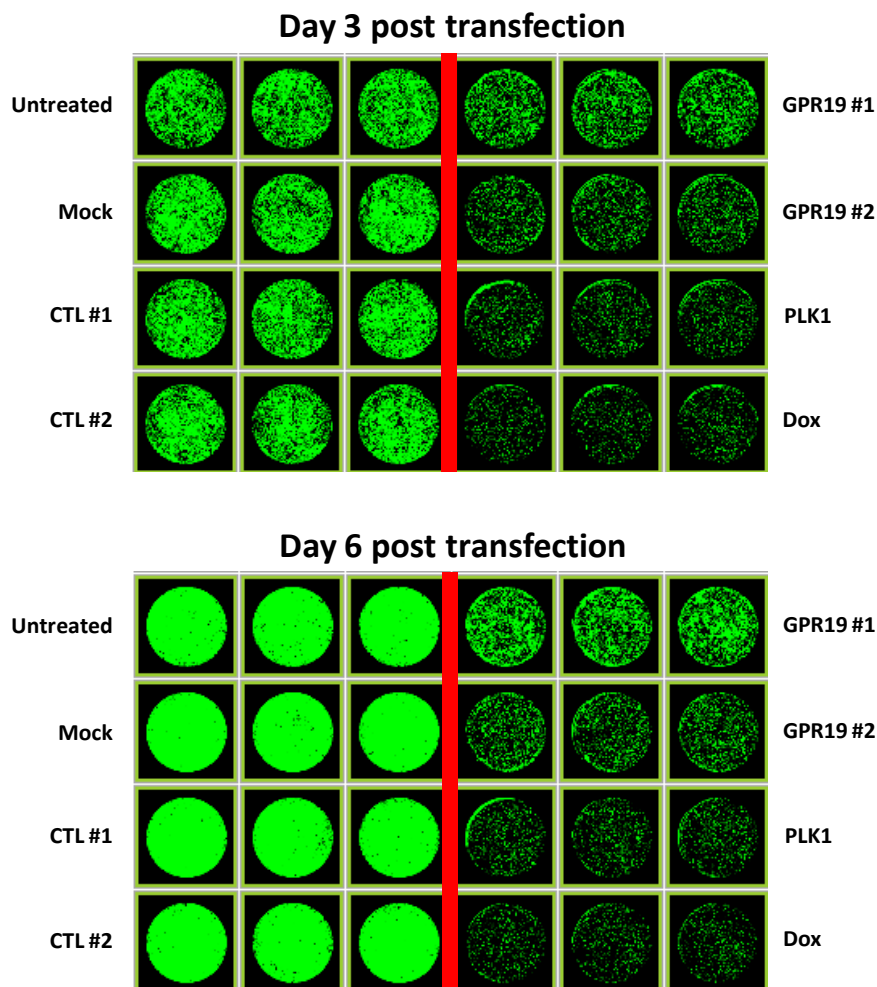


Figure 37: Cell proliferation is inhibited by *Gpr19*-targeting siRNAs indicated by confluence thumbnails. Confluence for NCI-H1703 cells (thumbnail visualization: Pictures of the well bottom and cellular detection by cell detection method 1) subjected to siRNA transfection (20 nM) or doxorubicin (Dox; 1 μ M) treatment as described in the legend of figure 36 was determined on days 3 and 6 after treatment.

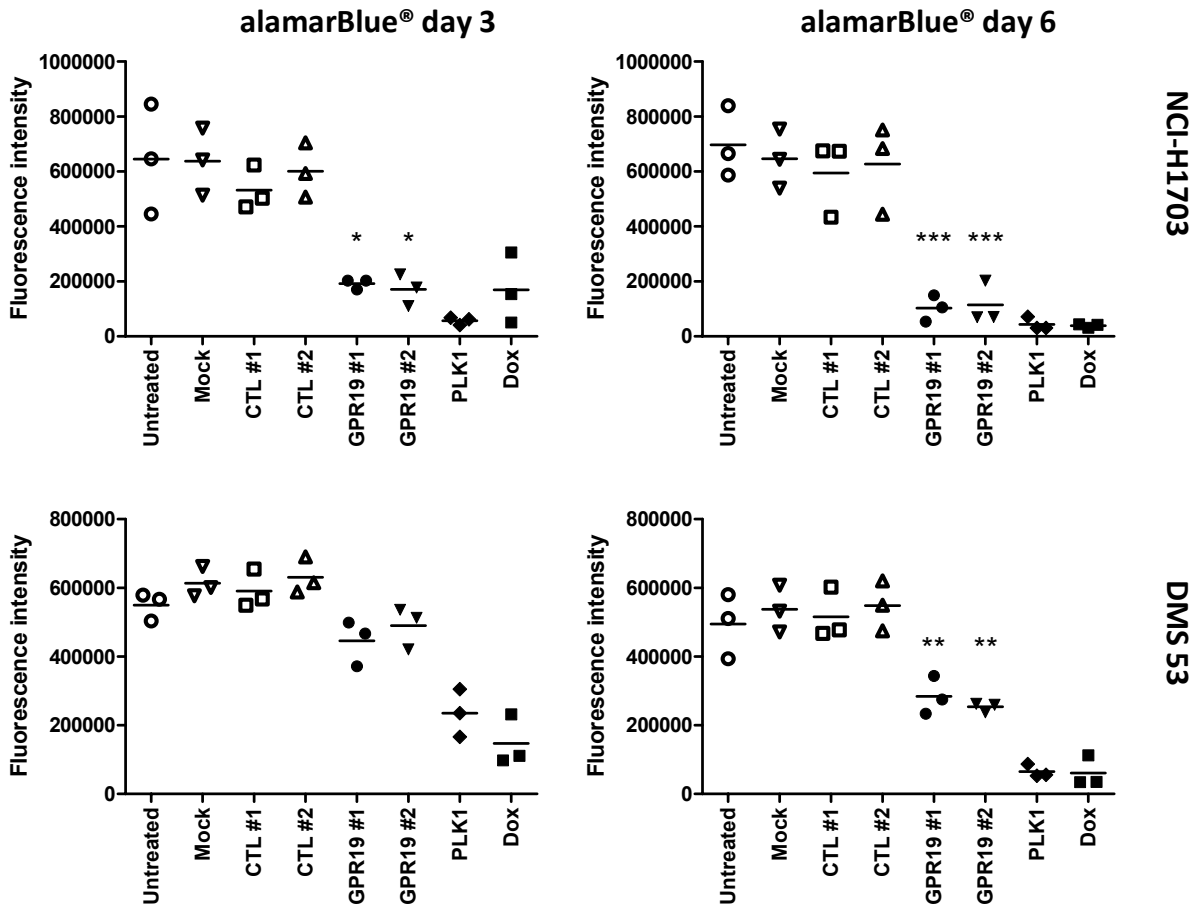
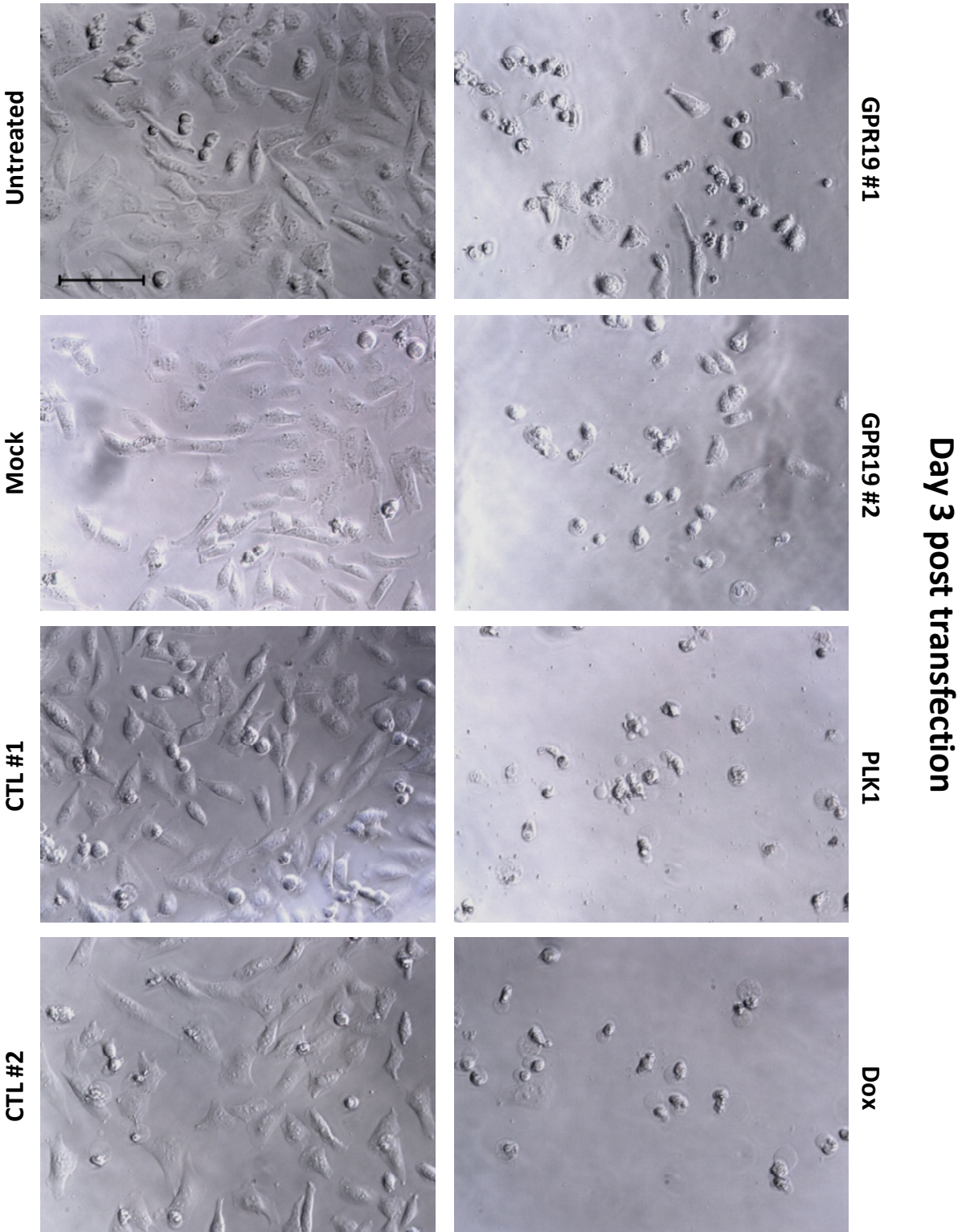


Figure 38: Cell proliferation is inhibited by *Gpr19*-targeting siRNAs (alamarBlue®). Cell proliferation was assessed by measuring cell viability with alamarBlue® on days 3 and 6 after siRNA transfection (20 nM) or doxorubicin (1 μ M) application for NCI-H1703 and DMS 53 cells treated as described in the legend of figure 36 in three independent experiments (data points are mean values of three wells per condition and experiment (96 well plate)); arithmetic mean values of results from all three experiments are indicated by the horizontal lines. Statistically significant differences across all experimental groups were determined by one way ANOVA followed by Tukey's test. GPR19 #1 and GPR19 #2 p values refer to the least significant one from the comparison with CTL #1 and CTL #2 (* $p < 0.05$; ** $p < 0.01$; *** $p < 0.001$).

In order to directly visualize the effect on proliferation, pictures of cells from all different experimental conditions were recorded on days 3 and 6 after treatment using phase contrast microscopy (figure 39). **NCI-H1703 showed a similar amount of dead cells upon *Gpr19* knockdown compared to *Plk1* knockdown and doxorubicin treatment. This was already the case on day 3 after treatment and became also apparent for DMS 53 cells on day 6.** In contrast, both mock-treated cells and cells treated with control siRNAs showed no obvious phenotypic effect relative to the untreated control. The effective knockdown of *Gpr19* mRNA by *Gpr19*-targeting siRNAs was verified using RT-qPCR for all these experiments (figure 40).

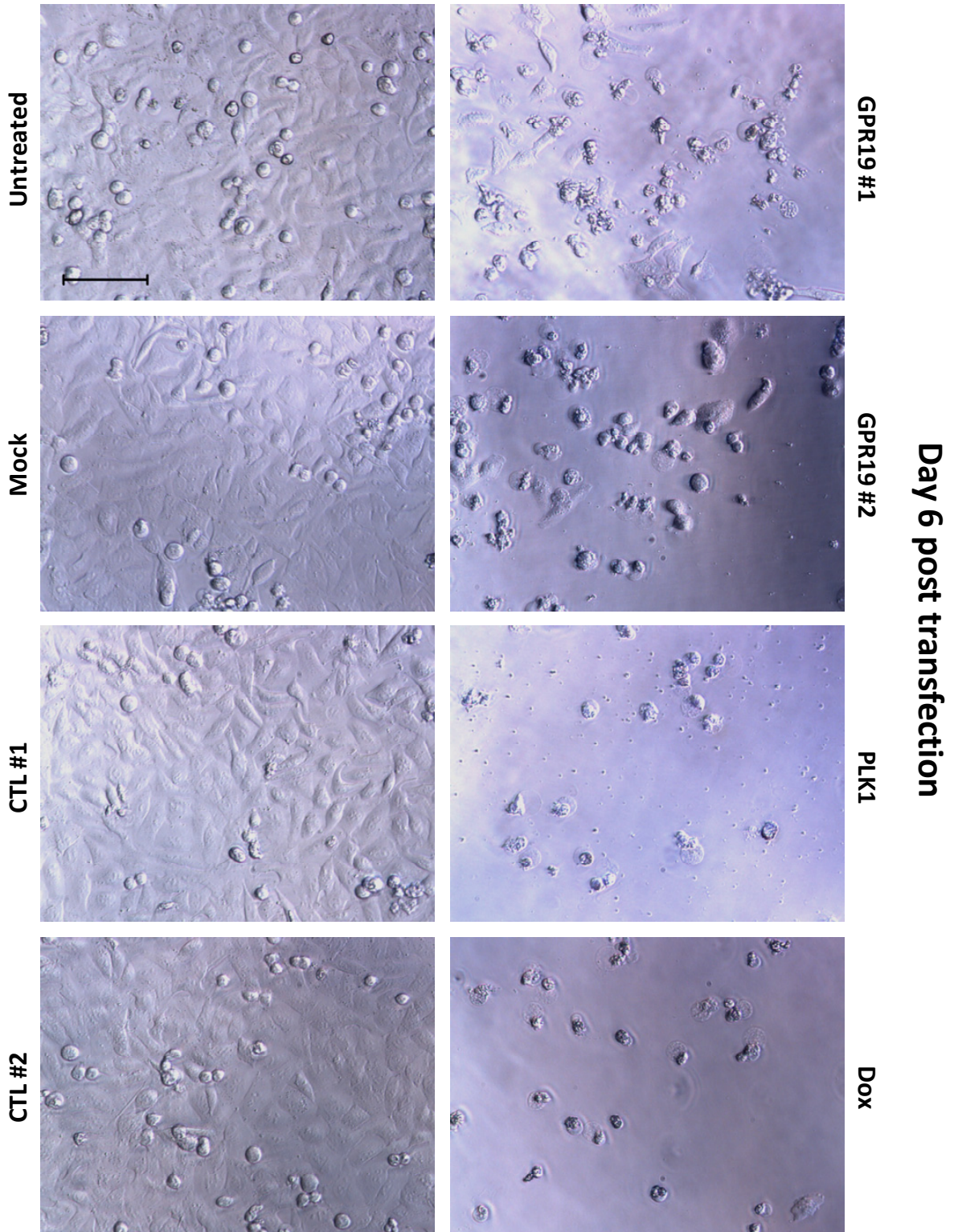
A

NCI-H1703



B

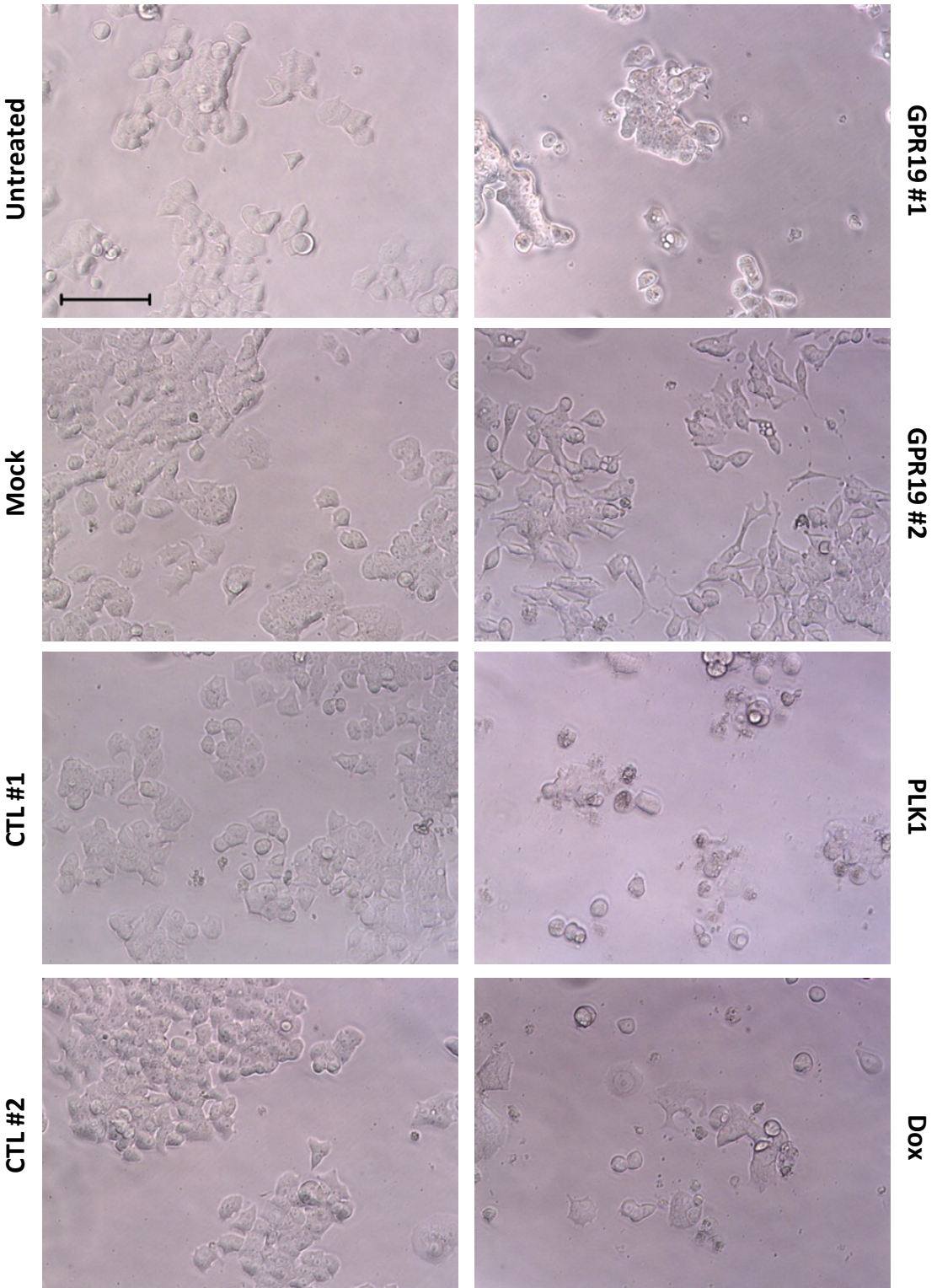
NCI-H1703



C

DMS 53

Day 3 post transfection



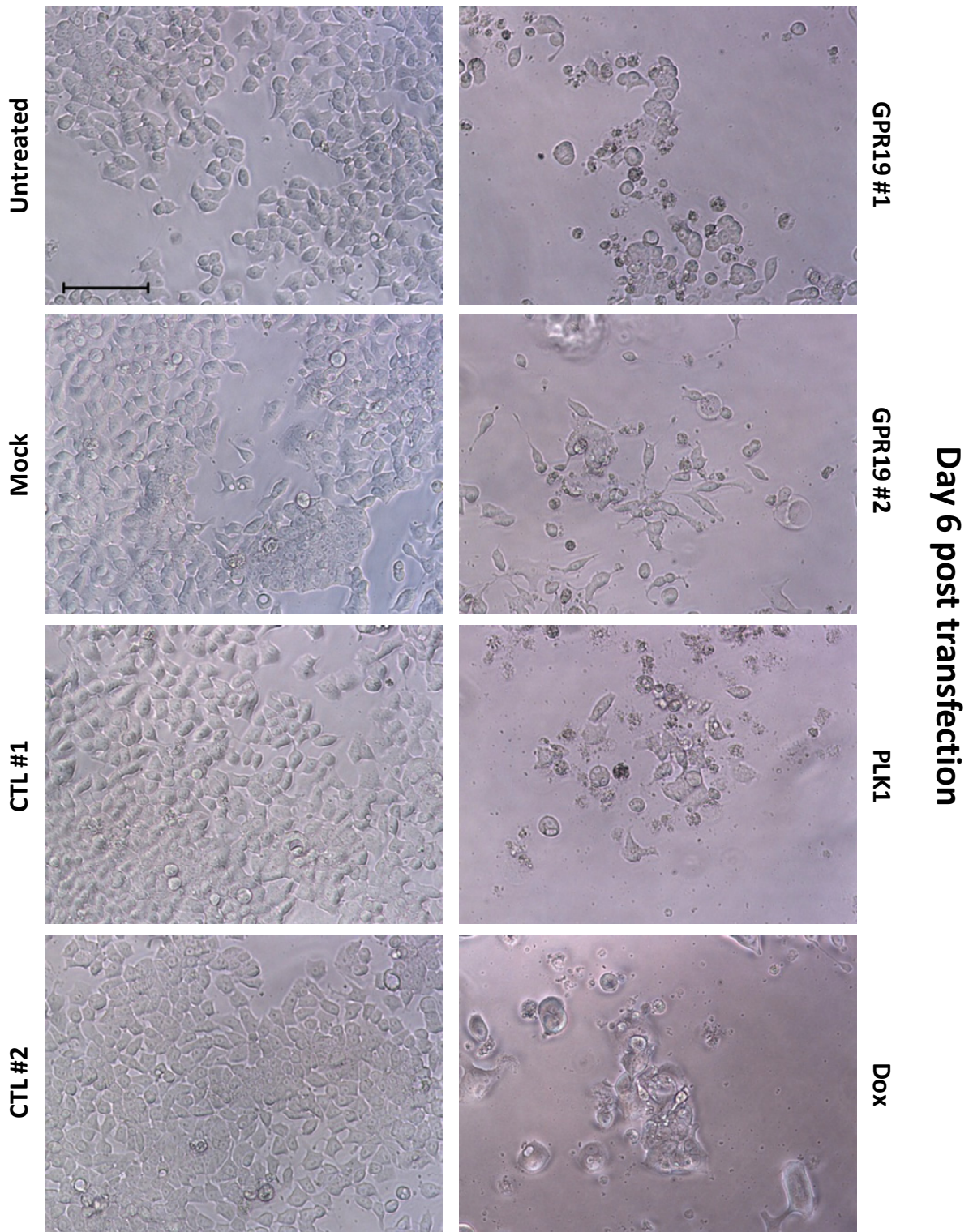
D**DMS 53**

Figure 39: Cell proliferation is inhibited by *Gpr19*-targeting siRNAs (microscopy). Phase contrast microscopy pictures (20x magnification) of NCI-H1703 (A, B) and DMS 53 (C, D) cells subjected to siRNA transfection (20 nM) or doxorubicin (Dox; 1 μ M) application as described in the legend of figure 36 were determined on days 3 (A, C) and 6 (B, D) after treatment (bar represents 100 μ m).

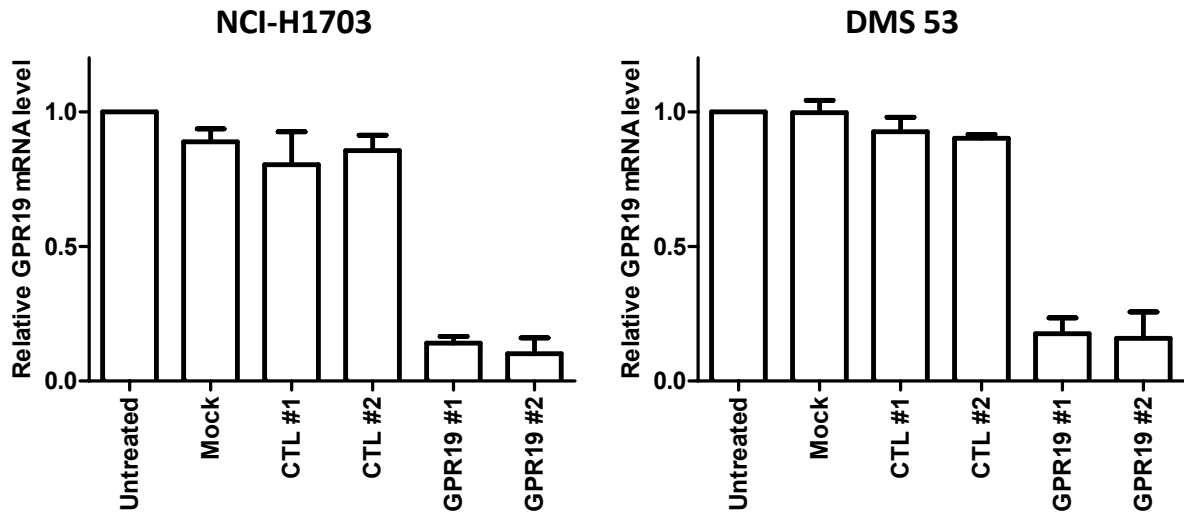


Figure 40: *Gpr19* knockdown is successful upon *Gpr19* siRNA treatment. *Gpr19* mRNA knockdown was assessed by RT-qPCR on day 3 after siRNA transfection (normalized against reference genes *Cypa* and *Hprt1*, geometric mean of triplicates per condition; data are mean values + standard deviation (error bar) of three experiments) for cells treated as described in the legend of figure 36.

5.2. Poly (adenosine diphosphate (ADP)-ribose) polymerase 1 (PARP1) cleavage reveals apoptosis induction upon *Gpr19* knockdown

The knockdown of *Gpr19* message inhibited cell proliferation and caused cell death in NCI-H1703 and DMS 53 cells. It was therefore examined whether siRNA-mediated *Gpr19* knockdown might lead to the induction of apoptosis in these cells.

NCI-H1703 and DMS 53 cells were either left untreated or transfected with control, *Gpr19*, or *Plk1* siRNAs. Protein lysates were harvested on days 2, 3, and 4 after transfection and investigated for PARP1 cleavage by Western Blot (figure 41A). The detection of cleaved PARP1 is indicative of apoptosis induction. PARP1 (116 kDa) is involved in DNA repair and its cleavage at the onset of apoptosis results from the activation of caspases 3 and 7 producing a carboxy-terminal 89 kDa fragment (Soldani C and Scovassi AI, 2002). ***Gpr19* knockdown by siRNAs resulted in the cleavage of PARP1 in both NCI-H1703 and DMS 53 cells. Apoptosis induction became more prominent with time.** Apoptosis was also induced upon *Plk1* message downregulation. The effective knockdown of *Gpr19* mRNA in both cell lines was confirmed by RT-qPCR (figure 41B).

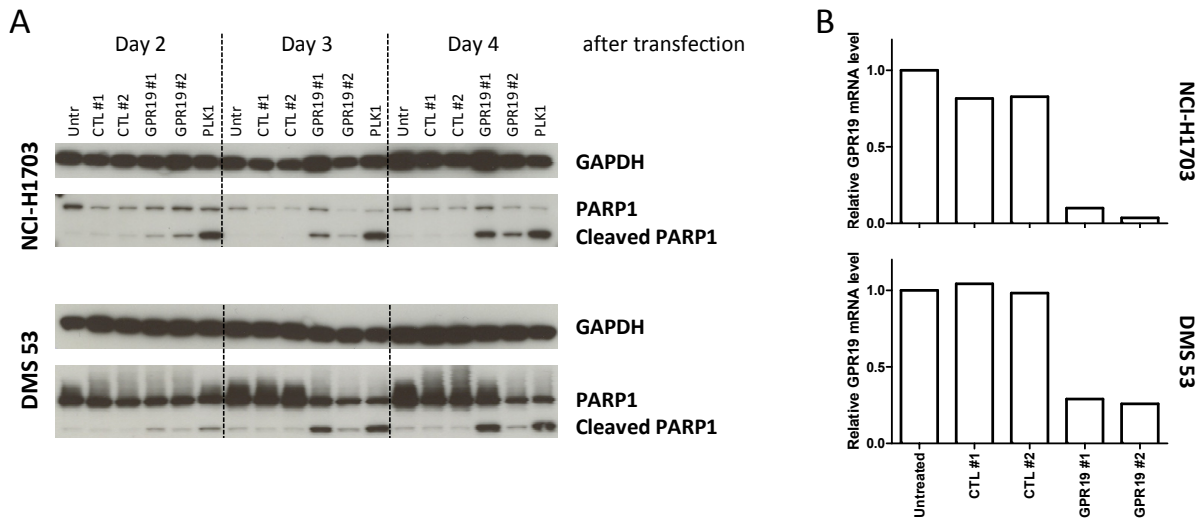


Figure 41: *Gpr19* knockdown induces apoptosis indicated by poly (ADP-ribose) polymerase 1 (PARP1) cleavage. (A) Protein lysates from untreated (Untr), control (CTL #1 and #2), *Gpr19* (GPR19 #1 and #2), or *Plk1* (PLK1) siRNA-transfected NCI-H1703 and DMS 53 cells were collected on days 2, 3, and 4 after transfection (20 nM final siRNA concentration). Proteins (10 μ g) were separated by SDS-PAGE (Criterion™ XT gel; 26 well, 10% Bis-Tris, XT MOPS (1x) running buffer) and primary antibody solutions containing either glyceraldehyde-3-phosphate dehydrogenase (GAPDH; loading control for equal protein amounts) or (cleaved) PARP1 antibodies were used for protein detection (dilutions of antibodies are indicated in table 9 in the Materials section). (B) For each sample (triplicates), *Gpr19* mRNA knockdown was assessed by RT-qPCR on day 2 after siRNA transfection (normalized against reference genes *Cypa* and *Hprt1*) and geometric mean values were calculated for NCI-H1703 (upper panel) and DMS 53 (lower panel) cells. The experiment was repeated yielding concurrent results.

5.3. Transient GPR19 overexpression does not influence cell proliferation

The anti-proliferative effect of *Gpr19* knockdown was unequivocal. It was therefore examined whether transient transfection of plasmids encoding GPR19 (GPR19 (true clone), GPR19 (codon-optimized), GPR19-tGFP) could provide an advantage to proliferation in HEK-293 cells, which had been characterized by the absence of *Gpr19* mRNA (figure 31). HEK-293 cells had been transfected in 6 well culture plates (3×10^5 cells per well) by forward plasmid transfection and 5,000 cells were seeded into wells of a poly-D-lysine-coated 96 well culture plate the next day. Non-GPR19 encoding plasmids (empty vector; tGFP only) as well as untreated, mock (transfection reagent only)- and doxorubicin-treated cells were included as controls. Expression plasmids had been verified by sequencing.

The proliferation of HEK-293 cells was assessed through the relative amount of well surface covered by these cells (confluence) which was recorded at regular intervals starting 24 h after transfection (8 h after seeding into wells of a 96 well culture plate). Measurements lasted until day 4 after transfection (figure 42A; the right hand panel shows the results of three experiments at the endpoint on day 4). At this time point, a plateau phase with more than 80% confluence had been reached by untreated

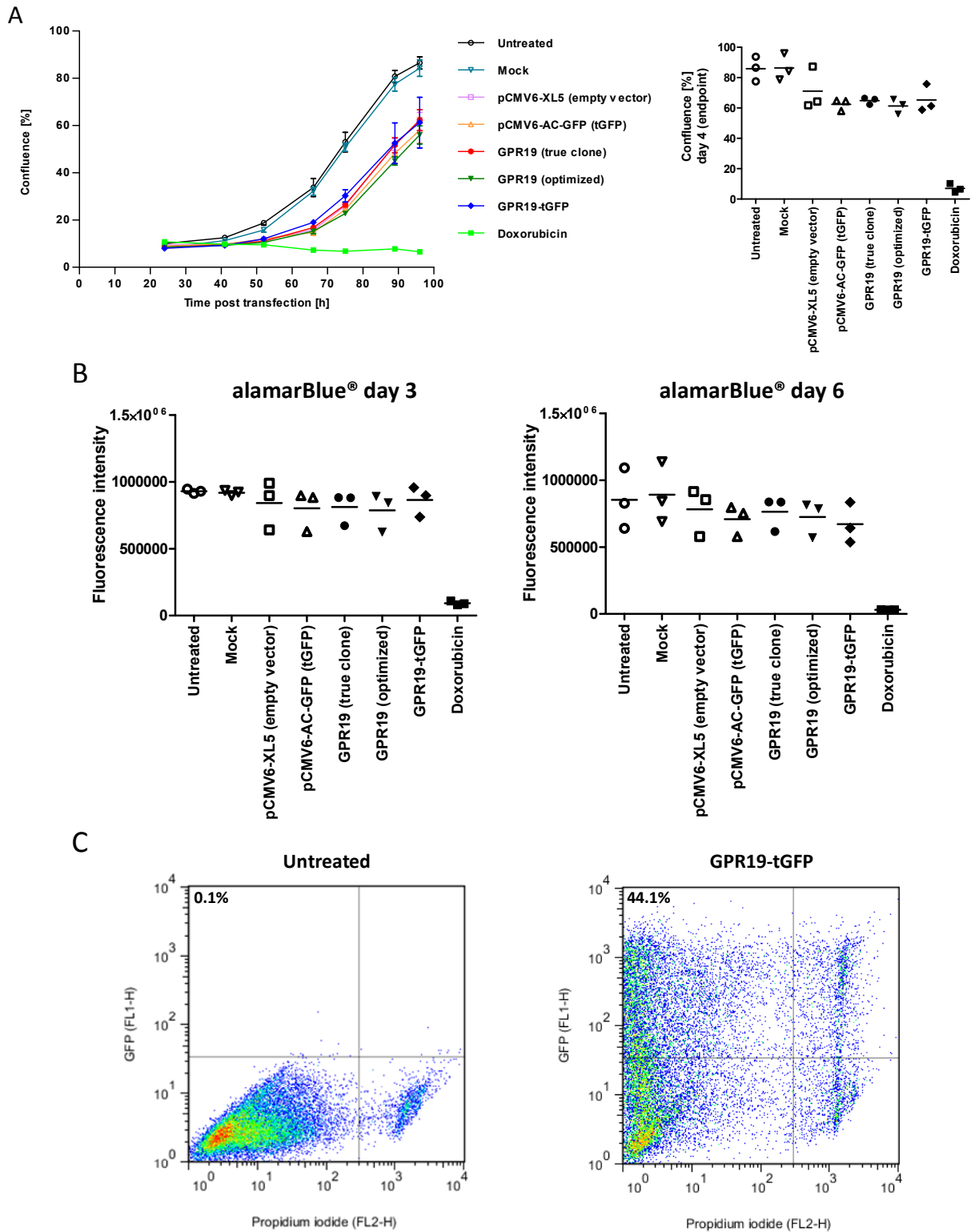


Figure 42: Transient overexpression of GPR19 does not provide an advantage to proliferation (HEK-293). (A) Cell proliferation was determined by confluence measurement. Shown is the time course after plasmid transfection (forward transfection) or addition of doxorubicin (1 μ M); data are mean values \pm standard deviation (error bars) of four wells per condition (96 well plate) from a representative experiment for untreated, mock (transfection reagent only)-, control plasmid (pCMV6-XL5 (empty vector), pCMV6-AC-GFP (turbo green fluorescent protein (tGFP))),- GPR19 plasmid (GPR19 (true clone), GPR19 (codon-optimized), GPR19-tGFP)-, or doxorubicin-treated HEK-293 cells. Two additional experiments gave similar results. The right hand graph illustrates the results from the last confluence measurement on day 4 after (continued on next page)

transfection from the three individual experiments (arithmetic mean values are indicated by the horizontal lines). **(B)** Cell proliferation in HEK-293 cells was assessed by measuring cell viability with alamarBlue® on days 3 and 6 after plasmid transfection or doxorubicin application in three independent experiments (data points are mean values of four wells per condition and experiment (96 well plate)); arithmetic mean values of results from all three experiments are indicated by the horizontal lines. Differences across all experimental groups **(A, right panel; B)** were determined by one way ANOVA followed by Tukey's test. Comparisons between GPR19 (true clone)/GPR19 (codon-optimized)/GPR19-tGFP- and empty vector/tGFP-transfected samples were statistically non-significant. **(C)** The transfection efficiency for GPR19-tGFP in comparison to untreated cells was assessed on day 2 after transfection using flow cytometry (dot plot for tGFP (fluorescence channel 1 (FL1)-height (H)) and propidium iodide (fluorescence channel 2 (FL2)-H) signals, the data point density is reflected by different colors ranging from blue (low density, single data points) to red (high data point density); figures refer to the relative number of cells in the upper left quadrant (tGFP positive, propidium iodide negative).

and mock-treated cells whereas doxorubicin-treated cells did not grow (absent gain in confluence over time). The gain in confluence for all the cells that had been transfected with expression plasmids was less prominent than for untreated or mock-treated cells and reached about 60% of the total well area. **There were no differences regarding the gain in confluence between cells transiently overexpressing GPR19 and cells that had been transfected with control plasmids.**

Similarly, when comparing confluence levels at the last time point examined from three individual experiments, minor differences between the results from cells transfected with either GPR19 or control plasmids were statistically non-significant.

The independence from GPR19 overexpression of HEK-293 proliferation could be confirmed by the alamarBlue® cell viability assay. Cells had been treated as described above and their metabolic activity was assessed on days 3 and 6 after treatment (figure 42B). Fluorescence intensity measurements were performed at comparable time points after alamarBlue® addition to prevent high data variation and measurements were within the dynamic range of the assay.

GPR19 overexpression did not result in increased metabolic and therefore proliferative activity of HEK-293 cells compared to untreated, mock-, or control plasmid-treated cells independent from the examined time point (day 3 and day 6) after transfection. The effective transfection of HEK-293 cells with expression plasmids was verified by flow cytometry detecting the tGFP-tagged version of GPR19. This method revealed 44.1% of successfully transfected and alive cells (figure 42C).

The results obtained from proliferation experiments in GPR19 overexpressing HEK-293 cells were verified in alamarBlue® assays using the NSCLC cell lines NCI-H1703 (figure 43), which was shown to express high levels of *Gpr19* mRNA (figure 31). Expression plasmids had been introduced into NCI-H1703 cells by electroporation: 2.5 µg of plasmid DNA had been applied to 5×10^5 cells and 4,000 cells had been seeded per well of a poly-D-lysine-coated 96 well culture plate.

As was the case for HEK-293 cells, **the number of metabolically active NCI-H1703 cells did not increase upon GPR19 overexpression neither on day 3 nor on day 6 after treatment** (figure 43A). In fact, the burden of plasmid transfection negatively affected cell proliferation in NCI-H1703 cells – untreated and mock-treated cells showed higher metabolic activity than cells transfected with any plasmid. The

transfection efficiency was again controlled by flow cytometry revealing 33.7% of successfully transfected and alive cells (figure 43B).

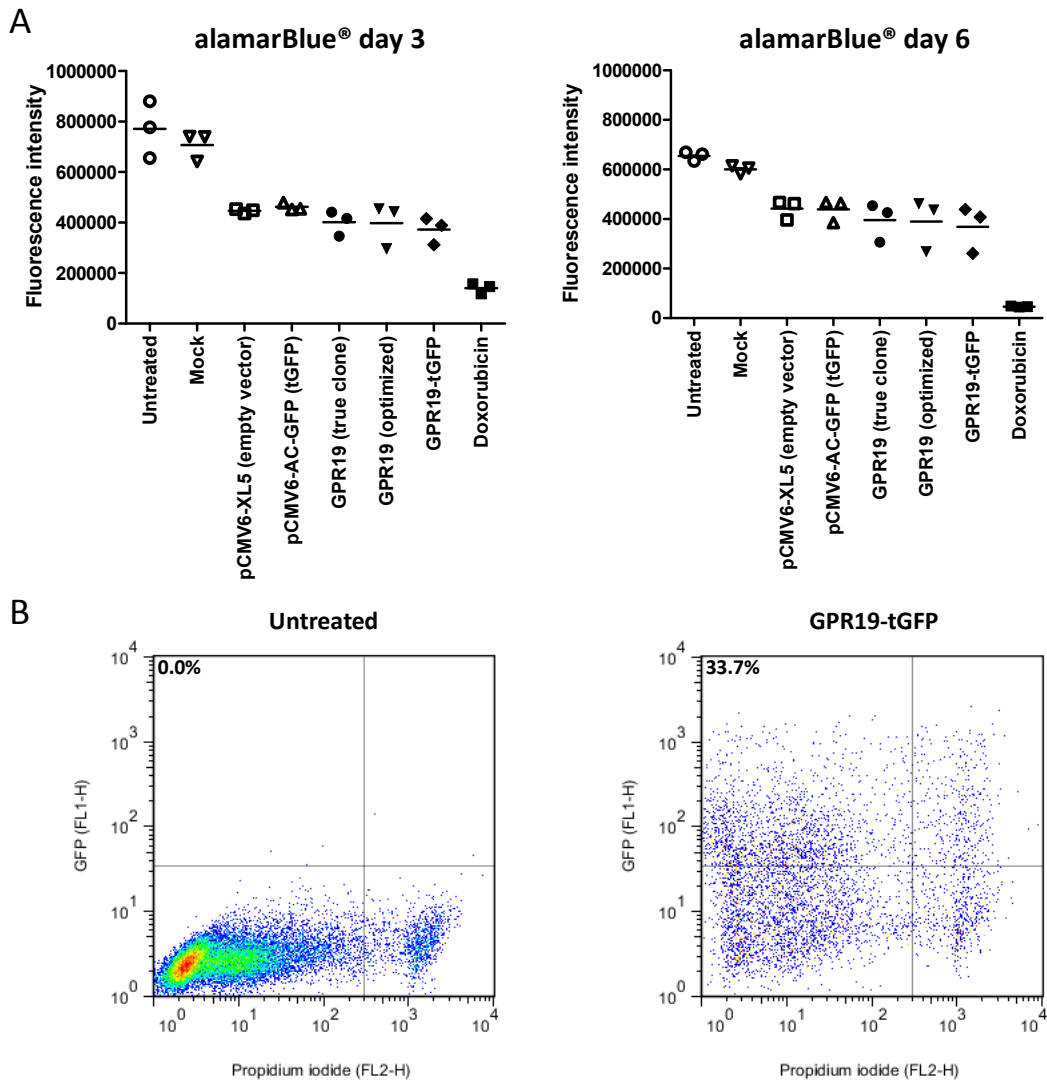


Figure 43: Transient overexpression of GPR19 does not provide an advantage to proliferation (NCI-H1703). (A) Cell proliferation in NCI-H1703 cells was assessed by measuring cell viability with alamarBlue® on days 3 and 6 after plasmid transfection (electroporation) or doxorubicin (1 μ M) application in three independent experiments as described in the legend of figure 42. Comparisons between GPR19 (true clone)/GPR19 (codon-optimized)/GPR19-tGFP (turbo green fluorescent protein)- and empty vector/tGFP-transfected samples were statistically non-significant. (B) The transfection efficiency for GPR19-tGFP in comparison to untreated cells was assessed on day 2 after transfection using flow cytometry as described in the legend of figure 42.

6. G protein coupling of GPR19

6.1. GPR19 does not couple to a pertussis toxin-sensitive G protein

The growth inhibitory action of *Gpr19*-directed siRNAs can be accounted for by two scenarios that are not necessarily mutually exclusive: (i) **When overexpressed GPR19 might display strong constitutive activity and engage its cognate G protein(s) in the absence of an agonist** (an activation mechanism discussed for GPCRs by Schütz and Freissmuth (Schütz W and Freissmuth M, 1992)). (ii) **GPR19-expressing cells might also synthesize and release the agonist; knockdown of the mRNA encoding the receptor would then disrupt the resulting autocrine loop.** GPR19 was described to couple to G_i (Bresnick JN *et al.*, 2003). Accordingly, its activation and onset of signal transduction would lead to the inhibition of adenylyl cyclase and therefore to reduced levels of cellular cyclic adenosine monophosphate (cAMP).

Both hypotheses described above were addressed using adenylyl cyclase assays which measure the amount of radioactively-labeled cAMP production upon cellular stimulation. HEK-293 cells seeded in 6 well culture plates (2.5×10^5 cells per well) were transiently transfected with expression plasmids encoding GPR19 (true clone) and/or the CRHR1⁸² (G_s -coupled) and/or the A1-adenosine receptor (A1R⁸³, G_i -coupled) and labeled with [3H]adenine the next day (figure 44). The transfection efficiency was controlled by visual inspection of a control well transfected with a GPR19-tGFP expression construct and plasmids had been verified by sequencing. Cells were starved and then subjected to stimulation with normal medium (Roswell Park Memorial Institute (RPMI) 1640 with GlutaMAX™, 10% fetal bovine serum (FBS)) or conditioned medium from either NCI-H1703 or NCI-H345 cells that highly express *Gpr19* mRNA (figure 31). Conditioned media were supernatants from cultured cells which had been cleared from cells and cellular debris by centrifugation ($250 \times g$, 5 min) and stored at -80°C . Stimulation conditions selectively contained the CRHR1 agonist corticotrophin-releasing hormone⁸⁴ (CRH; 100 nM) in order to stimulate cAMP production in CRHR1-transfected cells. Besides, the A1R agonists CCPA⁸⁵ and R-PIA⁸⁶

⁸² The corticotropin-releasing hormone receptor 1 (CRHR1; NCBI gene ID 1394, UniProt protein ID P34998) belongs to the secretin family of G protein-coupled receptors (GPCRs). It binds neuropeptides of the corticotropin-releasing hormone family and is mostly found in the brain (pituitary gland). Upon ligand-induced receptor activation, heterotrimeric G proteins (G_s) that activate adenylyl cyclase and therefore stimulate cyclic adenosine monophosphate (cAMP) production trigger signal transduction pathways leading to pituitary adrenocorticotropin hormone secretion which mainly regulates behavioral and autonomic responses to stress (Aguilera G *et al.*, 2004; Pioszak AA *et al.*, 2008; www.ncbi.nlm.nih.gov/gene/1394; www.uniprot.org/uniprot/P34998).

⁸³ The A1-adenosine receptor (A1R; NCBI gene ID 134, UniProt protein ID P30542) belongs to the rhodopsin family of G protein-coupled receptors (GPCRs) and is ubiquitously expressed with highest levels found in various regions of the brain. Upon receptor activation by adenosine, heterotrimeric G proteins (G_i) are recruited leading to the inhibition of adenylyl cyclase and therefore the attenuation of cyclic adenosine monophosphate (cAMP) formation (Wojcik M *et al.*, 2010; Wei CJ *et al.*, 2011; www.ncbi.nlm.nih.gov/gene/134; www.uniprot.org/uniprot/P30542).

⁸⁴ Corticotropin-releasing hormone is a neuropeptide composed of 41 amino acids with an amidated carboxy-terminus (Pioszak AA *et al.*, 2008).

⁸⁵ 2-chloro-N6-cyclopentyladenosine

⁸⁶ (-)-N6-(2-phenylisopropyl)adenosine

were included to inhibit cAMP production in A1R-transfected cells. Labeling, starvation, and stimulation solutions could further contain pertussis toxin⁸⁷ (PTX; 100 ng/ml) in order to inhibit the activity of $G_{i/o}$.

HEK-293 cells co-expressing CRHR1 and GPR19 did not decrease their cAMP level when treated with CRH and conditioned medium compared to CRH and normal medium (figure 44A, left and centerfold set of bars), which was independent of pertussis toxin. Normal medium alone resulted in barely detectable cAMP levels (with and without PTX). In contrast, pretreatment with pertussis toxin further augmented CRH-induced cAMP levels in these samples. This effect could be attributed to the CRHR1 as it also appeared when this receptor had been transfected into HEK-293 cells alone (figure 44B). This phenomenon could be explained by the fact that – at high agonist occupancy – CRHR1 also engages G_i (Milan-Lobo L *et al.*, 2009). However, A1R agonists CCPA and R-PIA elicited a prominent inhibition of CRH-induced cAMP production in cells co-expressing CRHR1 and A1R (figure 44A, right hand set of bars).

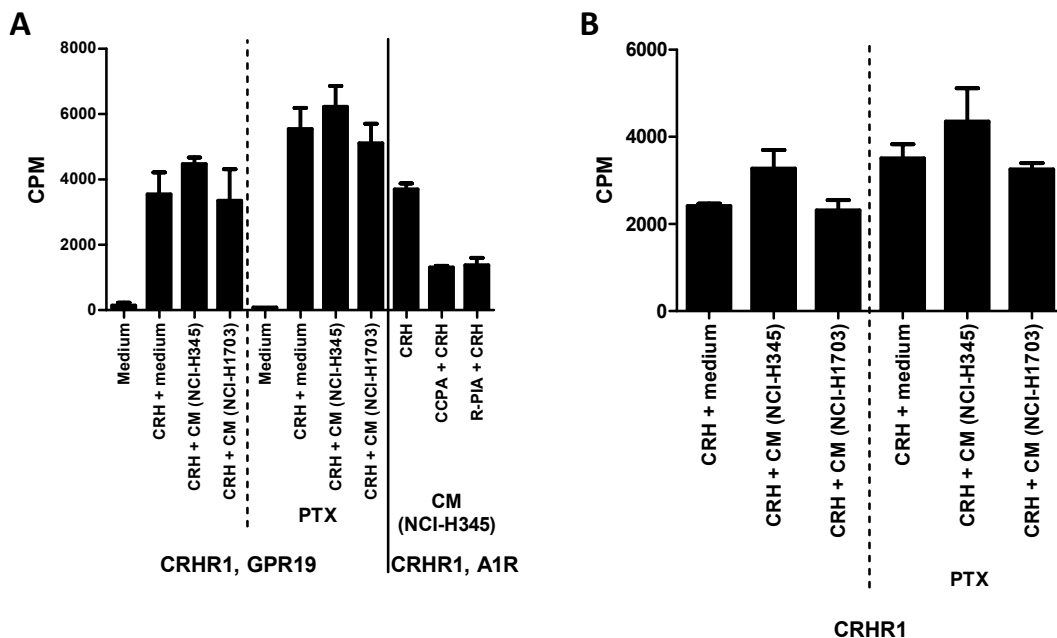


Figure 44: Conditioned medium does not affect cAMP levels in *Gpr19*-expressing HEK-293 cells. HEK-293 cells were transiently transfected with plasmids (0.5 μ g) driving the expression of (A) corticotrophin-releasing hormone receptor 1 (CRHR1; pEYFP-N1-CRHR1) and GPR19 (true clone) or the A1-adenosine receptor (A1R; pEYFP-N1-A1R) or (B) CRHR1 alone. Cells were subsequently labeled with [³H]adenine and treated with pertussis toxin (PTX; 100 ng/mL) for 16 h as indicated. Cells were stimulated with CRH (0.1 μ M) in the absence and presence of conditioned media (CM) from NCI-H345 and NCI-H1703 cells or control medium (medium; RPMI 1640 with GlutaMAX™, 10% FBS) for 30 min. As a positive control, CRH-induced cAMP accumulation was inhibited via stimulation of the co-expressed A1R by the agonists CCPA (1 μ M) and R-PIA (1 μ M). Data (counts per minute (CPM)) are mean values + standard deviation (error bar) of triplicates per condition. The absolute CPM in A and B are not comparable (different experiments). Experiments were repeated yielding concurrent results.

⁸⁷ Pertussis toxin (PTX) from *Bordetella pertussis* affects cellular adenylyl cyclase activity and potassium channels. It binds to the α -subunit of heterotrimeric G proteins (e.g., $G_{\alpha i}$ and $G_{\alpha o}$) and catalyzes ADP-ribosylation therefore blocking the G protein in the guanosine diphosphate (GDP)-bound, inactive state. Hence, these G proteins are unable to open potassium channels or to inhibit the activity of adenylyl cyclase which leads in turn to increased levels of cellular cyclic adenosine monophosphate (cAMP; Burns DL, 1988; www.sigmaaldrich.com/catalog/product/sigma/p7208?lang=de®ion=AT).

Pertussis toxin was also used to examine whether GPR19 could couple to G_i in a constitutive manner, when expressed in the NSCLC cell line NCI-H1703. Cells (3.5×10^5) were seeded in 6 well culture plates and labeled with [^3H]adenine 8 h later. They were starved and then subjected to stimulation with normal medium (RPMI 1640 with GlutaMAX™, 10% FBS) or conditioned medium from cultured NCI-H1703 cells. The stimulation medium selectively contained PTX or forskolin⁸⁸ (10 μM), an activator of adenylyl cyclase.

Inactivation of G_i and G_o proteins by pretreatment with pertussis toxin did not enhance forskolin-induced cAMP accumulation in NCI-H1703 cells, regardless of whether they were kept in fresh medium or challenged with conditioned medium (figure 45). ADP-ribosylation of $G_{\alpha i}/G_{\alpha o}$ by pertussis toxin prevents a receptor from accessing the G protein's carboxy-terminus (blocked interaction; Seifert R and Wieland T, 2006) and should have unmasked constitutive inhibition of cAMP accumulation through GPR19. In addition, conditioned medium did not affect cAMP levels compared to conditions in which cells were treated with normal medium (independent of PTX or forskolin).

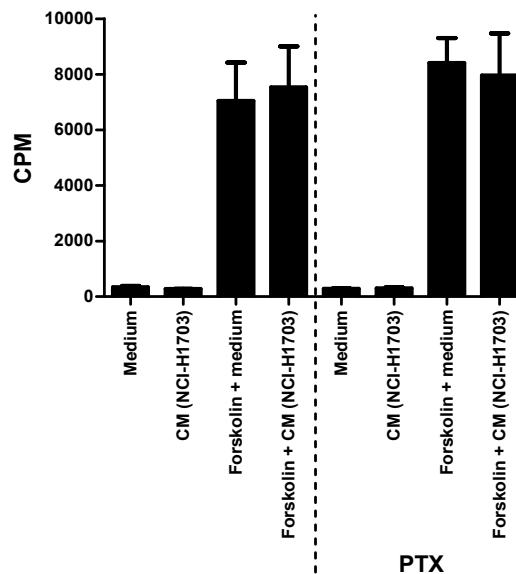


Figure 45: Pertussis toxin and conditioned medium do not affect cAMP levels in NCI-H1703 cells. NCI-H1703 cells were labeled with [^3H]adenine in the absence and presence of pertussis toxin (PTX; 100 ng/mL) for 16 h and subsequently stimulated with forskolin (10 μM) in the absence and presence of conditioned media (CM) from NCI-H1703 cells or control medium (medium; RPMI 1640 with GlutaMAX™, 10% FBS) for 30 min. Data (counts per minute (CPM)) are mean values + standard deviation (error bar) of triplicates per condition. Experiments were repeated yielding similar results.

Taken together, **conditioned medium did neither affect agonist- (i.e., CRH-)induced cAMP accumulation in HEK-293 cells that co-expressed GPR19 and the CRHR1 nor forskolin-mediated cAMP accumulation in NCI-H1703 cells which were found to express high levels of *Gpr19* mRNA.**

⁸⁸ The diterpene forskolin is found in the plant *Coleus forskohlii* and directly activates adenylyl cyclase independent of G_s leading to a rise in cellular cyclic adenosine monophosphate (cAMP) levels in a vast number of different cell types (Insel PA and Ostrom RS, 2003; www.mdidea.com/products/proper/proper00905.html).

7. Cell cycle effects of GPR19

7.1. The relative number of cells in gap 2 (G2)/mitosis (M) phase increases upon *Gpr19* knockdown (flow cytometry)

Knockdown of *Gpr19* reduced cell proliferation in NCI-H1703 and DMS 53 cells. However, it was unclear whether loss of *Gpr19* message could influence the progression of cells through the cell cycle and which phase would mainly be affected by the loss of *Gpr19* mRNA.

To address these issues, NCI-H1703 cells (3,500 cells per well of a 96 well culture plate) were either left untreated or transfected with control (CTL #1, CTL #2), *Gpr19* (#1, #2), or *Plk1* siRNAs. On days 2, 3, and 4 after transfection, cells were harvested (cells from replicate wells of three plates treated with the same conditions were pooled) and flow cytometry was done to analyze the distribution of cells in different stages of the cell cycle (figure 46A and B). Effective knockdown of *Gpr19* mRNA was confirmed by RT-qPCR (figure 46C). **The relative number of cells in G2/M phase increased over time when cells had been treated with *Gpr19* siRNAs in comparison to untreated or control siRNA-treated cells.** This increase in the G2/M population occurred at the expense of cells that were in DNA synthesis (S) phase while the proportion of cells in gap 1 (G1) phase was less affected. As anticipated, knockdown of *Plk1* caused a pronounced arrest of cells harboring a DNA content characteristic of the G2/M phase (Spänkuch-Schmitt B, Bereiter-Hahn J *et al.*, 2002; Liu X and Erikson RL, 2003). Here, the propidium iodide DNA staining analyzed by flow cytometry did not allow for the discrimination between cells in G2 or M phase.

This experiment was also performed in DMS 53 cells (10,000 cells per well of a 96 well culture plate) using untreated cells or cells transfected with control siRNA CTL #1, *Gpr19* siRNA GPR19 #2 (most effective depletion of *Gpr19* mRNA) or *Plk1* siRNA and cell cycle effects were investigated on day 3 after transfection (figure 47). The outcome here was similar to the result yielded with NCI-H1703 cells. Nevertheless, in comparison to results from NCI-H1703 cells, the changes in cell cycle populations were less prominent on day 3 after transfection (figure 47A and B). However, **the percentage of cells to which a G2/M phase DNA content had been assigned increased relative to the control sample.** Besides, the amount of cells in S and G1 phase was decreased. Effective *Gpr19* mRNA knockdown was again confirmed by RT-qPCR (figure 47C).

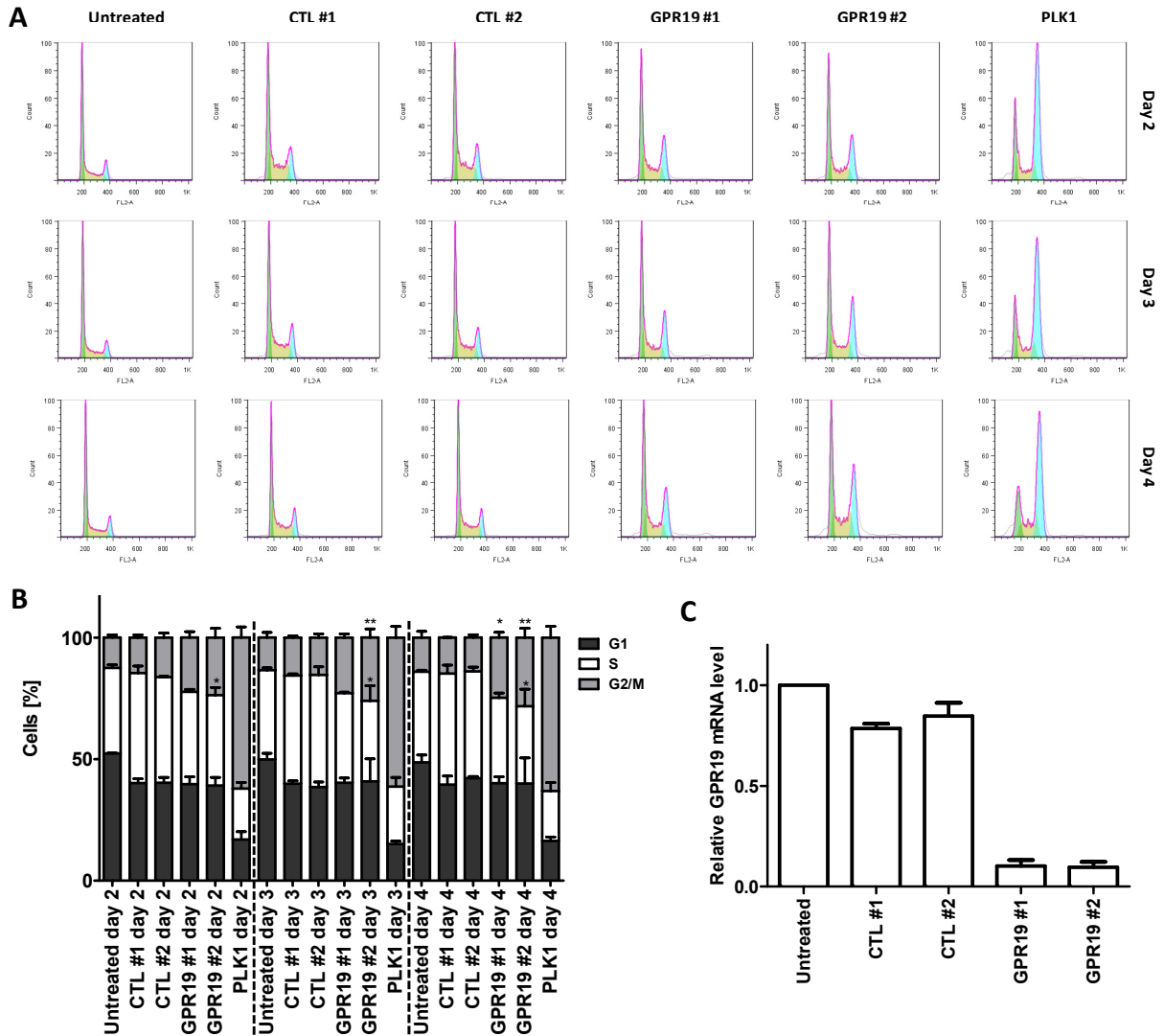


Figure 46: The relative number of NCI-H1703 cells with G2/M phase DNA content increases upon *Gpr19* knockdown (flow cytometry). (A, B) The cell cycle distribution (G1, S, G2/M phase) of NCI-H1703 cells (mean values + standard deviation (error bar) of three experiments) was determined staining the cellular DNA with propidium iodide and quantifying the distribution by flow cytometry on days 2, 3, and 4 after siRNA transfection (untreated cells; CTL #1 and #2, GPR19 #1 and #2, PLK1; 20 nM). Cellular debris had been excluded in a forward versus side scatter dot plot. The profiles of DNA content were analyzed using the cell cycle tool (Watson model) of FlowJo (A); this model approximates G1 (green) and G2/M (blue) phase populations with Gaussian curves and calculates the S phase population (yellow) exactly based on the DNA content histogram of propidium iodide (fluorescence channel 2 (FL2)-area (A)); the purple line represents the calculated sum of G1, S, and G2/M cells based on the Watson model). For each day and cell cycle phase, differences across all experimental groups were tested for significance using one way ANOVA followed by Tukey's test (B). GPR19 #1 and GPR19 #2 p values refer to the least significant one from the comparison with CTL #1 and CTL #2 (*p < 0.05; **p < 0.01). (C) Relative *Gpr19* mRNA levels on day 2 after transfection were determined by RT-qPCR (normalized against reference genes *Cypa* and *Hprt1*, geometric mean value of triplicates per condition; data are mean values + standard deviation (error bar) of three experiments).

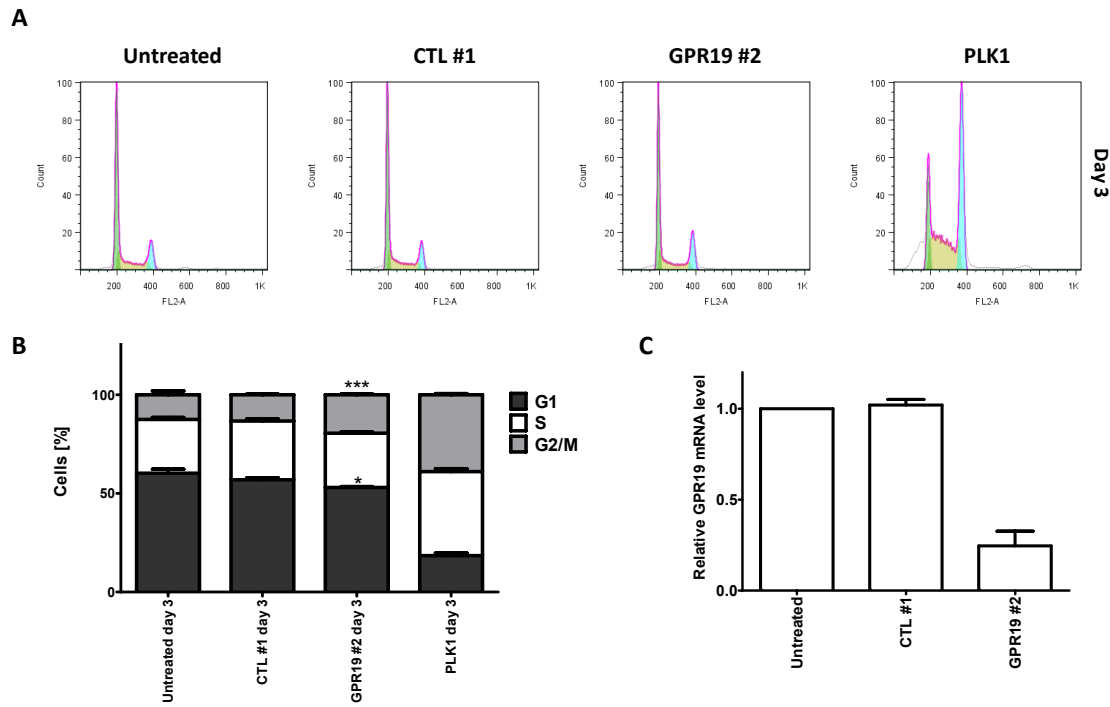


Figure 47: The relative number of DMS 53 cells with G2/M phase DNA content increases upon *Gpr19* knockdown (flow cytometry). (A, B) The cell cycle distribution (G1, S, G2/M phase) of DMS 53 cells (mean values + standard deviation (error bar) of three experiments) was determined staining the cellular DNA with propidium iodide and quantifying the distribution by flow cytometry on day 3 after siRNA transfection (untreated cells; CTL #1; GPR19 #2; PLK1; 20 nM). Cellular debris had been excluded in a forward versus side scatter dot plot. The profiles of DNA content were analyzed using the cell cycle tool (Watson model) of FlowJo as described in the legend of figure 46 (A). Differences across all experimental groups were tested for significance using one way ANOVA followed by Tukey's test. GPR19 #2 p values refer to the comparison with CTL #1 (*p < 0.05; ***p < 0.001). (C) Relative *Gpr19* mRNA levels on day 3 after transfection were determined by RT-qPCR (normalized against reference genes *Cypa* and *Hprt1*, geometric mean value of triplicates per condition; data are mean values + standard deviation (error bar) of three experiments).

7.2. The relative number of cells in G2/M phase increases upon *Gpr19* knockdown (high content screening)

The observations obtained from flow cytometry according to which cells treated with *Gpr19* siRNAs revealed an increased number of cells with a DNA content typical for the G2/M phase were verified by an independent approach that relied on HCS of cells. These experiments were only performed with NCI-H1703 cells because DMS 53 cells were not suitable for imaging with the ArrayScan® VTI HCS reader. They tend to grow in clusters at a certain cell density which made it difficult to detect single nuclei. NCI-H1703 cells (2,000 cells per well of a black poly-D-lysine-coated 96 well culture plate) were transfected with control (CTL #1, CTL #2), *Gpr19*- (#1, #2), or *Plk1*-targeting siRNAs or left untreated and analyzed on days 2, 3, and 4 after transfection. The number of detected cells per well was in the range of 300 to 1,000. However, for *Plk1* siRNA-transfected samples, this was only valid on day 2 after transfection due to the high cellular toxicity caused by the knockdown. For this

reason, data obtained from *Plk1* siRNA-treated samples were omitted in statistical analyses.

On the basis of Hoechst 33342 DNA staining, cell cycle analysis by HCS confirmed the results obtained by flow cytometry (figure 48). **Cell populations treated with *Gpr19* siRNA increased their fraction of cells with a DNA content characteristic of the G2/M phase over time** (figure 48A). Cell cycle profiles from HCS analysis reflected the population shifting in *Gpr19* siRNA-treated samples (figure 48B). Both the increase in relative cell number of G2/M and the decrease of G1 phase were significant for cells treated with *Gpr19* siRNA #2. This increasing number of cells in G2/M phase was not at the expense of the cells in S phase, which, however, was the case when shifts in

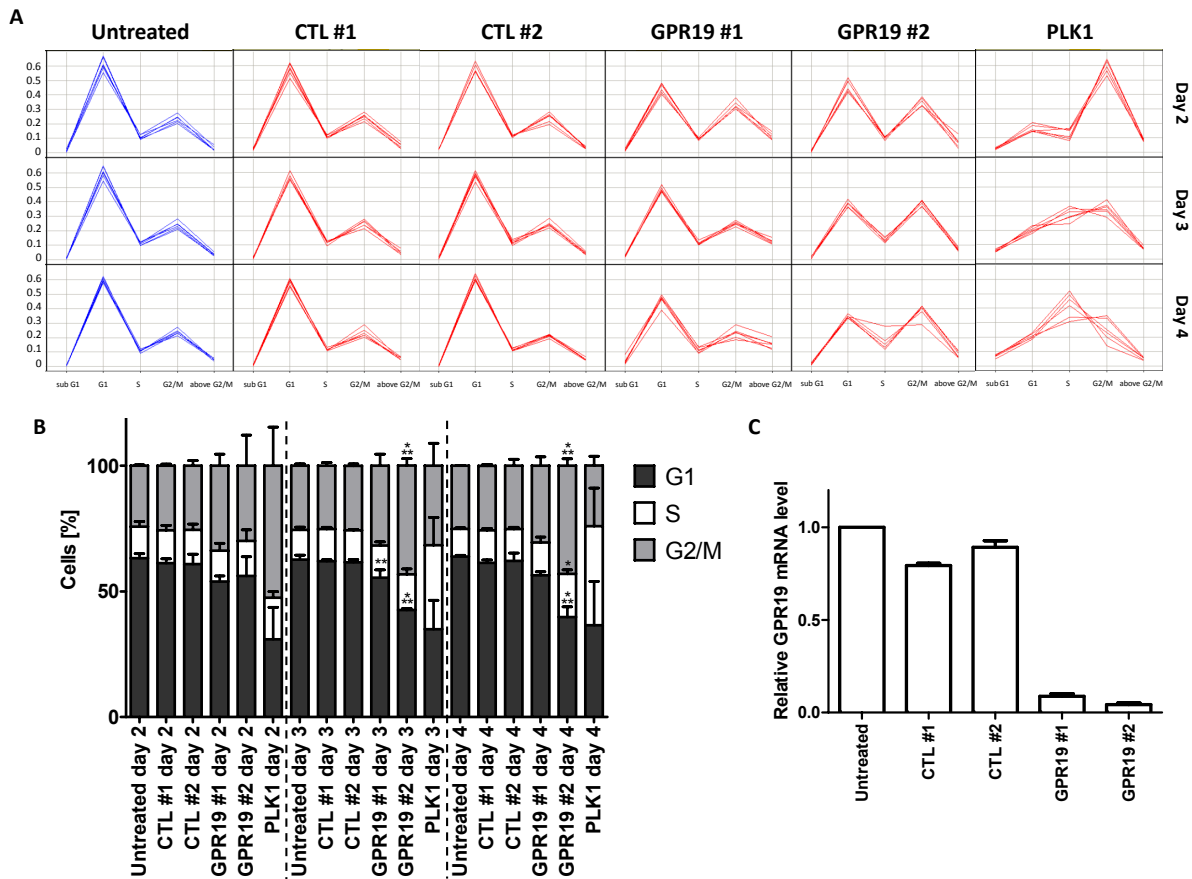


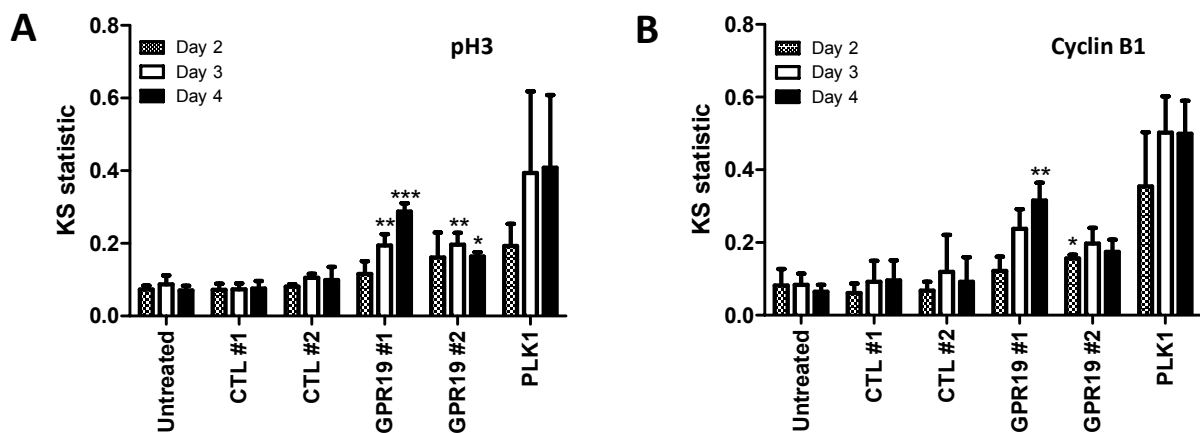
Figure 48: High content screening identifies an increased number of cells in G2/M phase upon *Gpr19* knockdown. (A) Visualization of cell cycle distribution analysis (sub G1, G1, S, G2/M, above G2/M) of NCI-H1703 cells on days 2, 3, and 4 after siRNA transfection (untreated cells (blue lines); CTL #1 and #2, GPR19 #1 and #2, PLK1 (red lines)) based on Hoechst 33342 DNA staining, ArrayScan® VTI analysis). One representative experiment out of three is shown. Data from each well of a 96 well culture plate are represented by a single line (six replicates per condition). (B) Relative number of cells with G1, S, and G2/M DNA content, data are mean values + standard deviation (error bar) of three experiments. For each day post transfection and cell cycle phase, differences across experimental groups – except for PLK1 (strong antimetabolic effect of the mRNA knockdown) were tested for significance using one way ANOVA followed by Tukey's test. GPR19 #1 and GPR19 #2 p values refer to the least significant one from the comparison with CTL #1 and CTL #2 (*p < 0.05; **p < 0.01; ***p < 0.001). (C) *Gpr19* mRNA knockdown was assessed by RT-qPCR on day 2 after siRNA transfection (normalized against reference genes *Cypa* and *Hprt1*, geometric mean value of triplicates per condition; data are mean values + standard deviation (error bar) of three experiments).

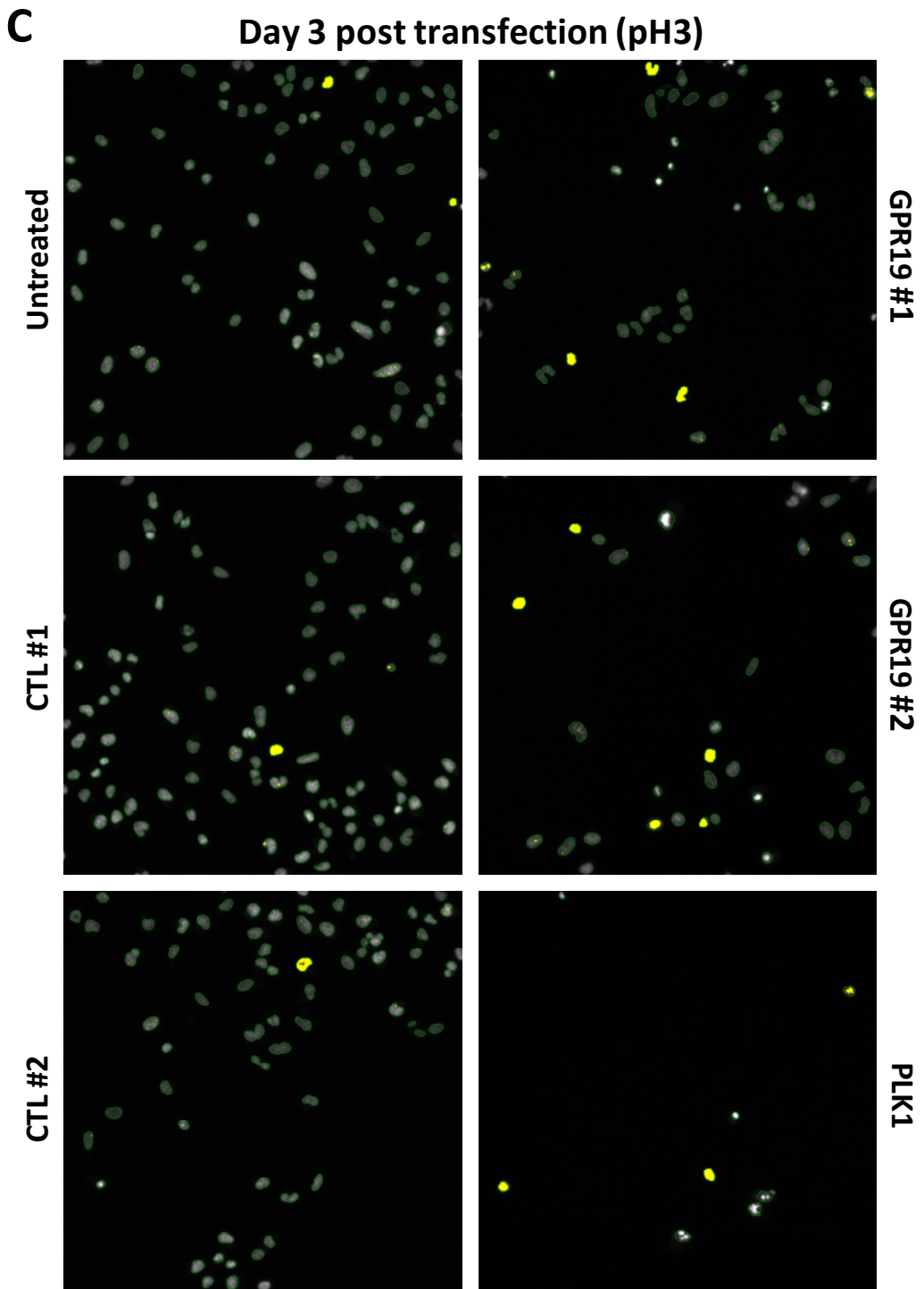
cell cycle population distributions had been determined by flow cytometry (figure 46C). The high variation for *Plk1* siRNA-treated samples might result partly from the fact that only few cells were left for HCS detection due to the high toxicity of the knockdown and subsequent washing-off during sample preparation. Knockdown of *Gpr19* mRNA by *Gpr19*-targeting siRNAs was effective as monitored by RT-qPCR (figure 48C).

7.3. Cells show increased levels of cyclin B1 and phosphorylated histone H3 upon *Gpr19* knockdown

The HCS approach for the investigation of cell cycle impairments caused by *Gpr19* knockdown further included the protein staining of cells for the G2/M phase marker cyclin B1 and the mitosis marker phosphorylated histone H3. A Kolmogorov-Smirnov (KS statistic) test was used to evaluate the distribution of cells that stained positive for phosphorylated histone H3 and cyclin B1 at each time point investigated after siRNA transfection. Cyclin B1 exerts its function in conjunction with cyclin-dependent kinase (CDK)1 during late G2 phase and early mitosis (Brown NR *et al.*, 2007). Histone H3 phosphorylation at Ser10 correlates with chromosome condensation during early mitosis with phosphorylation levels starting to rise in late G2 phase and dephosphorylation occurring in ana- and telophase (Hendzel MJ *et al.*, 1997).

This evaluation confirmed the increase in G2/M-arrested cells upon *Gpr19* knockdown (figure 49A and B). Figure 49C and D show representative pictures from the HCS based on Hoechst 33342 DNA staining and cells stained positive for phosphorylated histone H3 and cyclin B1, respectively, on day 3 after transfection. **The level of both immunoreactivity for phosphorylated histone H3 and cyclin B1 increased in cells upon *Gpr19* knockdown.** This effect was most prominent on days 3 and 4 after transfection. The G2/M block induced by the *Plk1* siRNA also resulted in increased levels of phosphorylated histone H3 and cyclin B1.





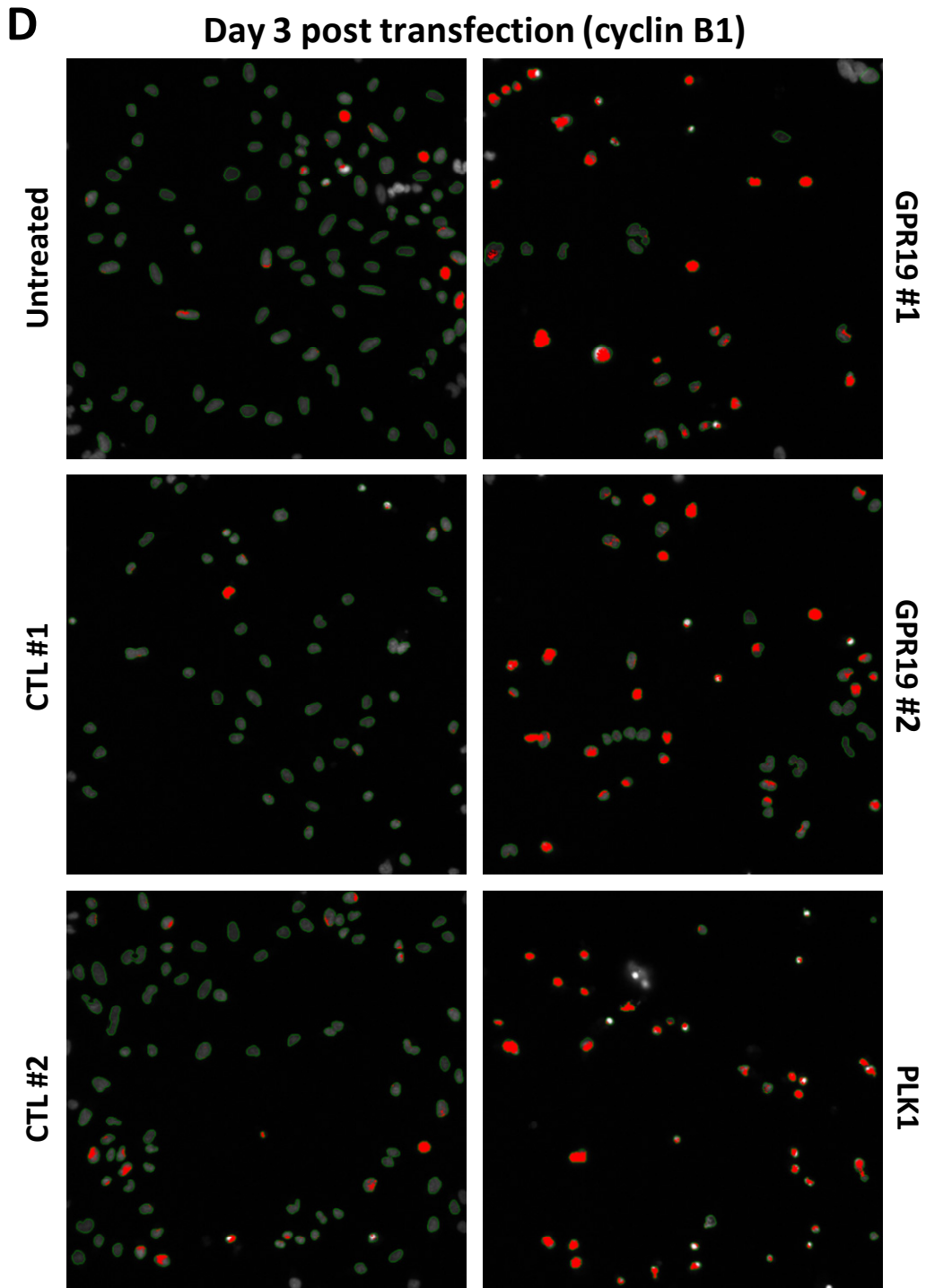


Figure 49: *Gpr19* knockdown increases immunoreactivity for phosphorylated histone H3 (pH3) and cyclin B1. The protein levels of cyclin B1 (marker for the G2/M phase) and of phosphorylated histone H3 (marker for mitosis) were determined by HCS (ArrayScan® VTI analysis) after siRNA transfection (untreated cells; CTL #1 and #2, GPR19 #1 and #2, PLK1; 20 nM). (A, B) Kolmogorov-Smirnov (KS) statistic for pH3- (A) and cyclin B1-positive (B) cellular staining on days 2, 3, and 4 after siRNA transfection (mean values + standard deviation (error bar) of three experiments). For each day, differences across experimental groups – except for PLK1 (strong antimitotic effect of the mRNA knockdown) – were tested for significance using one way ANOVA followed by Tukey's test. GPR19 #1 and GPR19 #2 p values refer to the least significant one from the comparison with CTL #1 and CTL #2 (*p < 0.05; **p < 0.01; ***p < 0.001). (C, D) Images of immunostaining for pH3 (C, yellow) and cyclin B1 (D, red) in one representative field of 36 (maximal) fields per well (96 well culture plate). Objects encircled in green represent cells which were detected based on Hoechst 33342 staining.

7.4. Cells show impairments in cell division upon *Gpr19* knockdown

Manipulations that interfere with transition of cells through G2/M phase might result in aberrant cell division. Accordingly, it was examined whether *Gpr19* knockdown elicited morphological changes that were consistent with impaired chromosomal segregation. HCS was indicative of abnormal DNA content in NCI-H1703 cells that had been treated with siRNAs directed against *Gpr19*. **Visual inspection revealed an excess of polylobed and binucleated cells upon *Gpr19* knockdown in comparison to untreated or control siRNA-treated cells** (figure 50).

7.5. High content screening data support inhibited proliferation upon *Gpr19* knockdown

In good agreement with results obtained from confluence measurements, alamarBlue® cell viability testing and morphological cell characterization by phase contrast microscopy (figure 36, figure 38, figure 39), **HCS identified inhibited proliferation of cells treated with *Gpr19* or *Pik1* siRNAs on days 3 and 4 after transfection** (figure 51A). The proliferation index parameter was based on the number of detected cells per field and analyzed by a KS statistic. On the other hand, the proliferation index for untreated or control siRNA-transfected cells was almost unaltered over time.

Through the combination of multiple parameters obtained from Hoechst 33342 nuclear DNA staining of cells (parameters are specified in the Methods section), the HCS approach also allowed for the calculation of an apoptotic index described as KS statistic (figure 51B). **NCI-H1703 cells transfected with siRNAs knocking down *Gpr19* were characterized by an increasing apoptotic index relative to their untreated or control siRNA-transfected counterparts on days 3 and 4 after transfection** – an effect also observed and expected in *Pik1* siRNA-treated cells (Spänkuch-Schmitt B, Bereiter-Hahn J *et al.*, 2002).

Day 3 post transfection (Hoechst 33342)

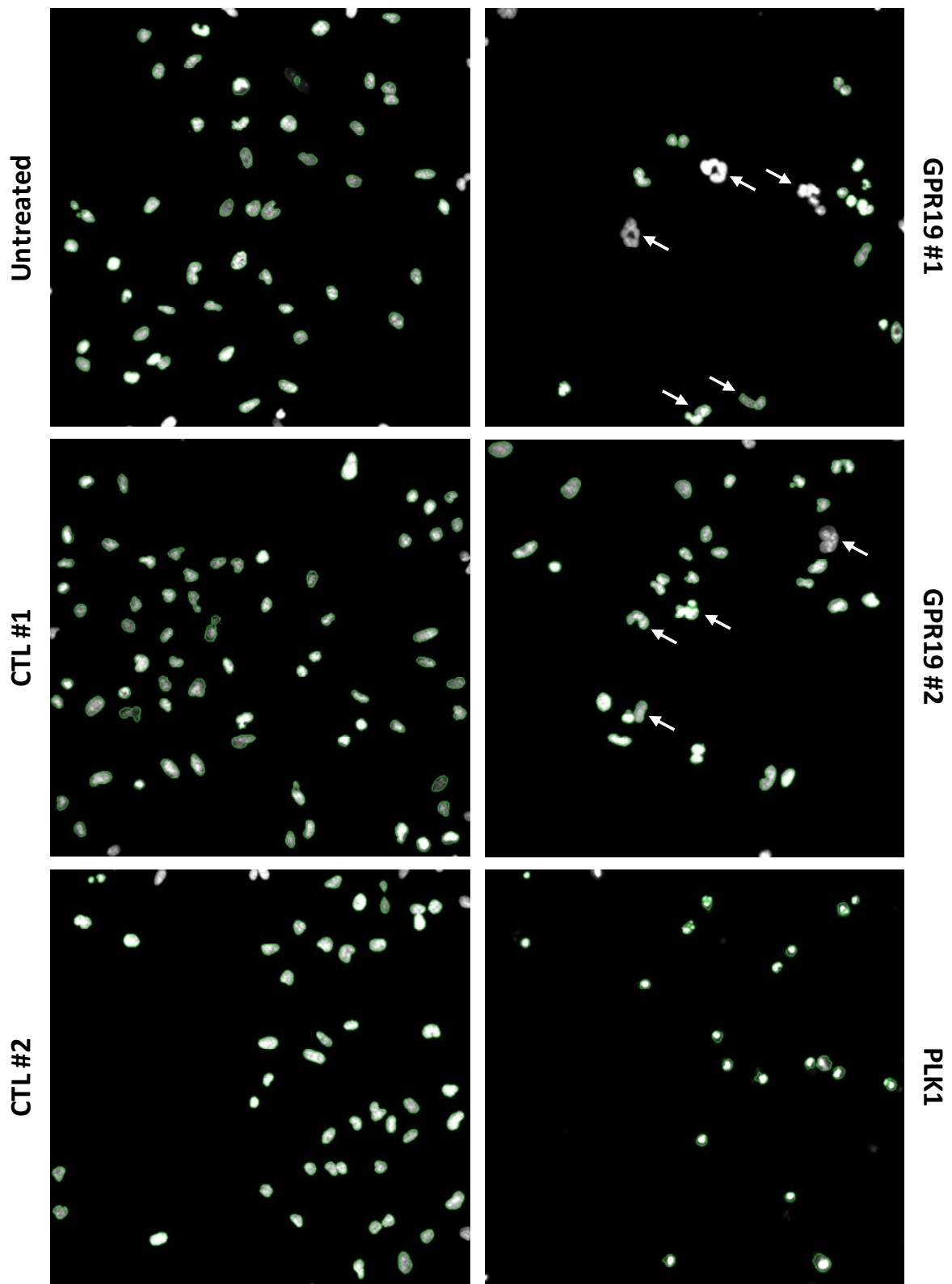


Figure 50: Binucleated and polylobed nuclei are detected in cells upon *Gpr19* knockdown. Nuclear morphology was determined by HCS 3 days after transfection with siRNA (untreated cells; CTL #1 and #2, GPR19 #1 and #2, PLK1; 20 nM); binucleated and polylobed nuclei-containing cells (white arrows) are highlighted. Objects encircled in **green** represent cells which were detected on the basis of DNA staining with Hoechst 33342. Many polylobed cells were automatically excluded from further analyses (indicated by the lack of **green** edge coloring).

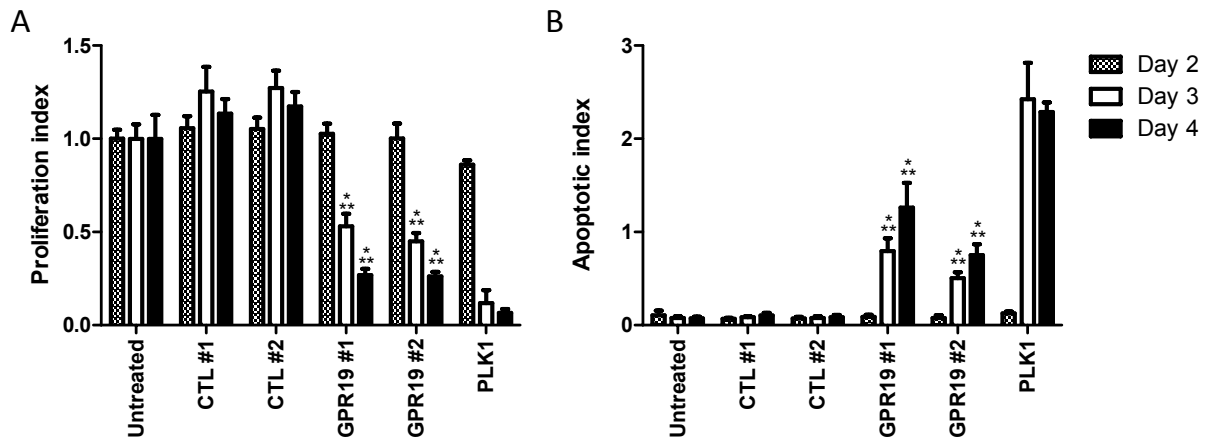


Figure 51: Cells treated with siRNAs knocking down *Gpr19* show a diminished proliferation index and an increased apoptotic index. Proliferation (A; cells per field) and apoptotic indices (B; multiple parameters specified in the Methods section) are based on the data from high content screening of NCI-H1703 cells transfected with siRNAs (untreated cells; CTL #1 and #2, GPR19 #1 and #2, PLK1; 20 nM) and described using a KS statistic on days 2, 3, and 4 after siRNA transfection (mean values + standard deviation (error bar) of six replicates from one representative experiment out of three). For each day, differences across experimental groups – except for PLK1 (strong antimetabolic effect of the mRNA knockdown) – were tested for significance using one way ANOVA followed by Tukey's test. GPR19 #1 and GPR19 #2 p values refer to the least significant one from the comparison with CTL #1 and CTL #2 (**p < 0.01). Two additional experiments gave similar results.

7.6. The distribution of cells in different phases of the cell cycle is unaltered upon transient GPR19 overexpression

The knockdown of *Gpr19* message resulted in an increased number of cells with a DNA content characteristic of the G2/M phase. Hence, it was investigated whether transient overexpression of GPR19 in HEK-293 cells, which do not express *Gpr19* mRNA endogenously (figure 31), might influence the relative distribution of cells in different stages of the cell cycle.

HEK-293 cells were either left untreated or transfected in 6 well poly-D-lysine-coated culture plates (2.5×10^5 cells per well) with plasmids encoding for GPR19 (GPR19 (true clone), GPR19 (codon-optimized), GPR19-tGFP) or control plasmids (empty vector, tGFP only). Expression plasmids had been verified by sequencing and cells were subjected to flow cytometric analysis on days 2, 3, and 4 after transfection (figure 52A and B). The effective transfection of HEK-293 cells with expression plasmids was verified detecting the tGFP-tagged version of GPR19 in non-fixed cells (figure 52C).

Cells that had been transfected with any plasmid showed a decreased relative number of S phase cells compared to untreated control cells. However, **there was no difference in cell cycle profiles between GPR19-overexpressing and control plasmid-transfected HEK-293 cells.** Hence, transient GPR19 overexpression did not influence the distribution of cells in different phases of the cell cycle at any time point examined.

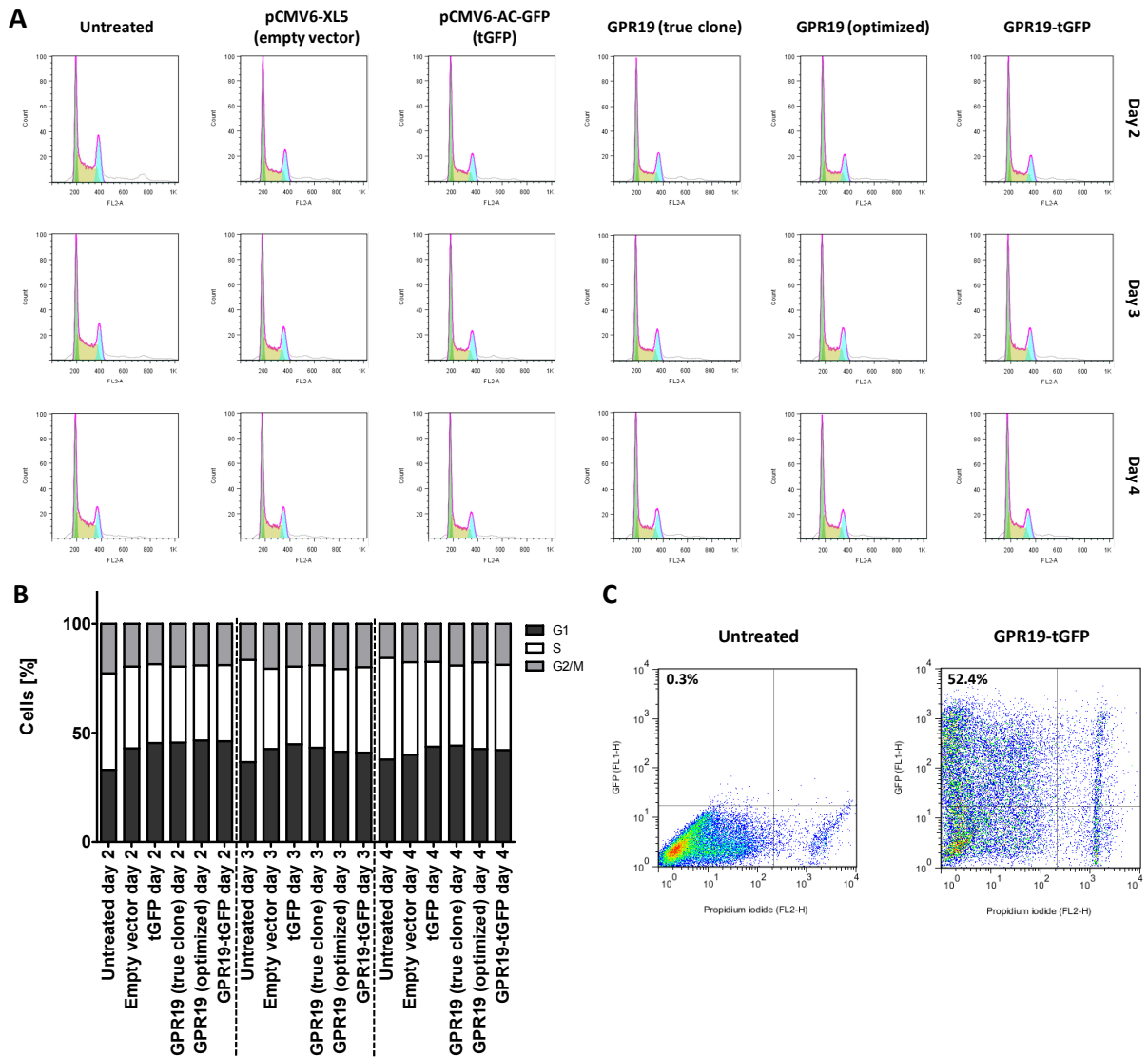


Figure 52: Transient overexpression of GPR19 does not influence the distribution of cells in the cell cycle phases (HEK-293). (A, B) The cell cycle distribution (G1, S, G2/M phase) of HEK-293 cells was determined staining the cellular DNA with propidium iodide and quantifying the distribution by flow cytometry on days 2, 3, and 4 after plasmid transfection (untreated, mock (transfection reagent only)-, control plasmid (pCMV6-XL5 (empty vector), pCMV6-AC-GFP (turbo green fluorescent protein (tGFP))),- or GPR19 plasmid (GPR19 (true clone), GPR19 (codon-optimized), GPR19-tGFP)-treated cells). Cellular debris had been excluded in a forward versus side scatter dot plot. The profiles of DNA content were analyzed using the cell cycle tool (Watson model) of FlowJo as described in the legend of figure 46. (C) The transfection efficiency for GPR19-tGFP in comparison to untreated cells was assessed on day 2 after transfection using flow cytometry (dot plot for tGFP (fluorescence channel 1 (FL1)-height (H)) and propidium iodide (fluorescence channel 2 (FL2)-H) signals, the data point density is reflected by different colors ranging from blue (low density, single data points) to red (high data point density); figures refer to the relative number of cells in the upper left quadrant (tGFP positive, propidium iodide negative). The experiment was repeated yielding concurrent results.

This experiment was also performed with the NSCLC cell line NCI-H1703. Unlike HEK-293 cells, NCI-H1703 cells revealed high endogenous levels of *Gpr19* mRNA (figure 31). Electroporation was used for the transfer of expression plasmids into NCI-H1703 cells (6×10^5 cells; $2.5 \mu\text{g}$ of plasmid DNA) and 1.5×10^5 cells were seeded into wells of a 6 well culture plate. On days 2, 3, and 4, cells were harvested for flow

cytometric analysis (figure 53A and B) and the transfection efficiency was again controlled using non-fixed cells (figure 53C).

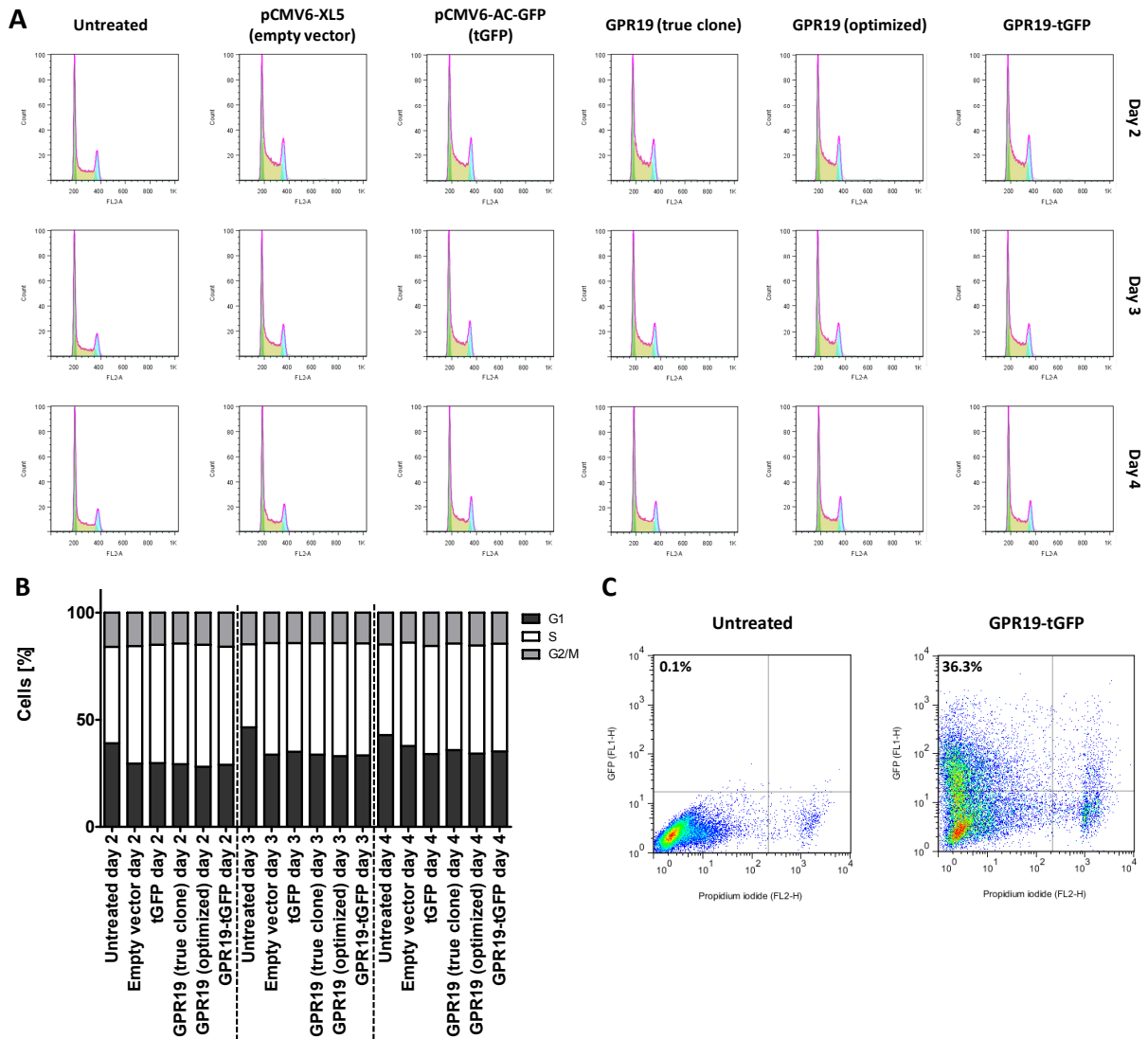


Figure 53: Transient overexpression of GPR19 does not influence the distribution of cells in the cell cycle phases (NCI-H1703). (A, B) The cell cycle distribution (G1, S, G2/M phase) of NCI-H1703 cells was determined staining the cellular DNA with propidium iodide and quantifying the distribution by flow cytometry on days 2, 3, and 4 after plasmid transfection (untreated, mock (transfection reagent only)-, control plasmid (pCMV6-XL5 (empty vector), pCMV6-AC-GFP (turbo green fluorescent protein (tGFP))), or GPR19 plasmid (GPR19 (true clone), GPR19 (codon-optimized), GPR19-tGFP)-treated cells) as described in the legends of figure 46 and figure 52. (C) The transfection efficiency for GPR19-tGFP in comparison to untreated cells was assessed on day 2 after transfection as described in the legend of figure 52. The experiment was repeated yielding concurrent results.

In accordance with the results obtained from plasmid-transfected HEK-293 cells, **plasmid-transfected NCI-H1703 cells did not differ in their cell cycle profiles, either – regardless of whether they overexpressed any form of GPR19 or had been transfected with a control plasmid.** Thus, no influence of transient GPR19 overexpression on the cell cycle profile of these cells was observed on days 2, 3, or 4 after plasmid transfection. In contrast, all plasmid-transfected NCI-H1703 cells showed an increased relative number of cells in S phase compared to their untreated counterparts.

8. Cell cycle-dependent expression of *Gpr19* mRNA

8.1. *Gpr19* mRNA expression peaks during S phase

Proteins involved in cell cycle progression – cyclins and CDKs are among the most prominent representatives – can be functionally regulated by various means such as phosphorylation, subcellular localization, interaction with other proteins, or *de novo* synthesis (Ohtsubo M *et al.*, 1995; Brown NR *et al.*, 2007). Observations from *Gpr19* mRNA knockdown experiments are consistent with the hypothesis that this GPCR might play a role during the G2/M phase of the cell cycle. Therefore, the potential differential expression of *Gpr19* mRNA during the course of the cell cycle was investigated using cell synchronization⁸⁹. Different incubation times and concentrations of all chemical agents applied in subsequently described experiments had been optimized in order to guarantee minimal toxicity to cells and sufficient release from the induced arrest.

DMS 53 and NCI-H1703 cells were treated with hydroxyurea for 24 h to synchronize them at the G1-S transition⁹⁰. Samples were taken at various time points after release from cell cycle arrest for DNA content analysis by flow cytometry. Upon removal of hydroxyurea, DMS 53 (figure 54, upper panel) and NCI-H1703 cells (figure 55, upper panel) moved subsequently through the cell cycle in an essentially synchronous fashion: The number of cells in S phase rapidly accumulated and the DNA content shifted from 2n (G1 phase, G1/S boundary) to 4n (G2/M phase) within 10 h. After 12 h, the vast majority of cells had reached the G2/M phase of the cell cycle. At later time points (24 h, 36 h, and 48 h), the effect of hydroxyurea was lost and the cell cycle distribution in the population approached that seen in an asynchronously growing culture. RNA was also extracted at these time points and the message levels

⁸⁹ Cells can be arrested at different stages of the cell cycle using tools that trigger various cell cycle control/checkpoint mechanisms. This so-called synchronization of cultured cells is often reversible. A well-synchronized cell population is characterized by its uniform movement through the cell cycle for a short period of time (hours) when culture conditions have been set back to normal. However, the synchronization effect on cells strongly depends on the synchronization method but also on the tissue type from which a cell line was derived and on the individual cell line used. When using chemical agents, different concentrations and incubation times can influence the characteristics of arrested cells. They can further exhibit adverse cellular consequences apart from synchronizing the culture of cells such as induction of replication stress or DNA damage responses. On the other hand, non-invasive synchronization methods, e.g., serum deprivation or contact inhibition, can be controlled less strictly. Moreover, cancer cells are less amenable to these methods and metabolic perturbations can occur. In any case, whole-culture synchronization methods can only result in the majority of cells being cell cycle-arrested (Davis PK *et al.*, 2001; Cooper S *et al.*, 2006; Darzynkiewicz Z *et al.*, 2011).

⁹⁰ Hydroxyurea blocks cells in the S phase of the cell cycle and they accumulate at the G1-S transition (Davis PK *et al.*, 2001). It functions as an inhibitor of DNA synthesis by interfering with ribonucleoside diphosphate reductase – a rate-limiting enzyme in deoxyribonucleoside triphosphate (dNTP) synthesis (Hendricks SP and Mathews CK, 1998). This enzyme's catalytically essential free tyrosyl radical at its active site gets quenched by hydroxyurea (Lassmann G *et al.*, 1992; Yarbro JW, 1992). The conversion of ribonucleoside diphosphates into dNTPs is stalled and cells are stuck in G1/S phase. Synchronized cells can be released from G1/S arrest upon removal of hydroxyurea from the growth medium (www.cancer.gov/drugdictionary/?Cdrid=40685; www.hiv.ch/rubriken/therapie/medikamente/hydra.htm).

The fact that hydroxyurea can directly cause apoptosis and interfere with DNA repair is of major therapeutical interest (Gui CY *et al.*, 1997). It also keeps cells in a radiation-sensitive pre-DNA synthesis stage rendering them more susceptible towards irradiation. For this reason, hydroxyurea has shown efficiency in the treatment of melanoma, chronic myelocytic leukemia, or squamous cell carcinoma of the head and neck (www.drugs.com/pro/hydroxyurea.html; www.nlm.nih.gov/medlineplus/druginfo/meds/a682004.html).

of several genes were determined by RT-qPCR (figure 54 and figure 55, lower panels). The levels of mRNA encoding cyclin E1⁹¹ were elevated while cells were at the G1/S boundary and subsequently declined to reach a nadir after 12 h in both DMS 53 and NCI-H1703 cells. In contrast, a peak in *cyclin B1*⁹² mRNA expression was seen after 12 h, *i.e.*, coincident with the accumulation of cells in the G2/M phase of the cell cycle. These results were anticipated as *cyclin B1* and *cyclin E1* show a known cyclic pattern of mRNA expression over the course of the cell cycle. Expression levels of *E-type cyclins* are highest prior to S phase entry, fall during S phase, and remain low during G2/M phase (Ohtsubo M *et al.*, 1995; Maity A *et al.*, 1997; Penelova A *et al.*, 2005) whereas *cyclin B1* message is low in G1 phase, rises during S phase, and peaks at G2/M phase (Maity A *et al.*, 1995; Maity A *et al.*, 1997). Both patterns were recapitulated here.

The mRNA of *ribosomal protein L32 (Rpl32)*⁹³ encodes a ribosomal protein and does not vary through the cell cycle (Maity A *et al.*, 1995; Maity A *et al.*, 1997). Accordingly, *Rpl32* was used as an internal control. In addition, the cell cycle-dependent changes in mRNAs encoding two different GPCRs, namely the *lysophosphatidic acid receptor 1 (Lpar1)*⁹⁴ for NCI-H1703 cells and the *muscarinic cholinergic receptor 3 (Chrm3)*⁹⁵ for DMS 53 cells were examined. The expression of

⁹¹ Cyclin E1 (CCNE1; NCBI gene ID 898; UniProt protein ID P24864) is involved in the regulation of the G1-S transition of cells. It forms a complex with cyclin-dependent kinase 2 (CDK2) leading to autophosphorylation and therefore activation of the kinase function. The activated kinase is required for G1-S transition of the cell cycle. Cyclin E1 accumulates at the G1/S boundary due to its cell cycle-dependent transcription profile and it is rapidly degraded by ubiquitination when cells progress through S phase. Two distinct isoforms exist which arise from alternatively spliced transcript variants (Ohtsubo M *et al.*, 1995; Geng Y *et al.*, 1996; Won KA and Reed SI, 1996; www.ncbi.nlm.nih.gov/gene/898; www.uniprot.org/uniprot/P24864).

⁹² Cyclin B1 (CCNB1; NCBI gene ID 891, UniProt protein ID P14635) is involved in the regulation of mitosis. It is part of the maturation-promoting factor (MPF) upon binding to CDK1 allowing the kinase to become active. This complex is translocated to the nucleus where phosphorylation reactions necessary for mitotic onset are performed. Levels of cyclin B1 accumulate during G2 phase and are rapidly destroyed in late mitosis. Two transcripts (alternative transcription start sites) encoding cyclin B1 exist. One is constitutively expressed whereas expression of the other one is cell cycle-regulated with message accumulation during G2/mitosis (Pines J and Hunter T, 1989; Castedo M *et al.*, 2002; Porter LA and Donoghue DJ, 2003; www.ncbi.nlm.nih.gov/gene/891; www.uniprot.org/uniprot/P14635).

⁹³ Protein synthesis takes place at ribosomes. Eukaryotic ribosomes are composed of a small 40 S and a large 60 S subunit. About 80 proteins and 4 RNA species make up for an entire ribosome. The ribosomal protein L32 (RPL32; NCBI gene ID 6161; UniProt protein ID P62910) belongs to the L32E ribosomal protein family and is a member of the 60 S subunit. An identical primary sequence is encoded by alternatively spliced transcript variants (www.ncbi.nlm.nih.gov/gene/6161; www.uniprot.org/uniprot/P62910).

⁹⁴ The most common forms of lysophosphatidic acid (LPA) produced from membrane phospholipids are 16:0, 18:0, 18:1, and 20:4-LPA. These bioactive lipid molecules can bind to and activate GPCRs of the rhodopsin-like LPA receptor subfamily such as lysophosphatidic acid receptor 1 (LPAR1; NCBI gene ID 1902; UniProt protein ID Q92633). LPA receptors differ in their tissue distribution with LPAR1 being ubiquitously expressed in humans. Receptor activation leads to the coupling of $G_{i/o}$, $G_{q/11}$, or $G_{12/13}$ proteins finally resulting in cellular proliferation and survival as well as cytoskeletal rearrangements and migration. LPAR1 stimulation has been shown to promote tumor progression in gastrointestinal cancer and further evidence also points to a role in breast and ovarian cancer (Aziziyeh Al *et al.*, 2009; www.ncbi.nlm.nih.gov/gene/1902; www.uniprot.org/uniprot/Q92633).

⁹⁵ The muscarinic cholinergic receptor 3 (CHRM3; NCBI gene ID 1131; UniProt protein ID P20309) belongs to the muscarinic acetylcholine (ACh) receptor subfamily within rhodopsin G protein-coupled receptors (GPCRs). Members of this subfamily mediate responses to their prototypical ligand ACh mainly in the central and peripheral nervous system. On a cellular level, they inhibit adenylyl cyclase, break down phosphoinositides, and modulate potassium channels upon ligand-induced activation. CHRM3 itself plays a physiological role in the
(continued on next page)

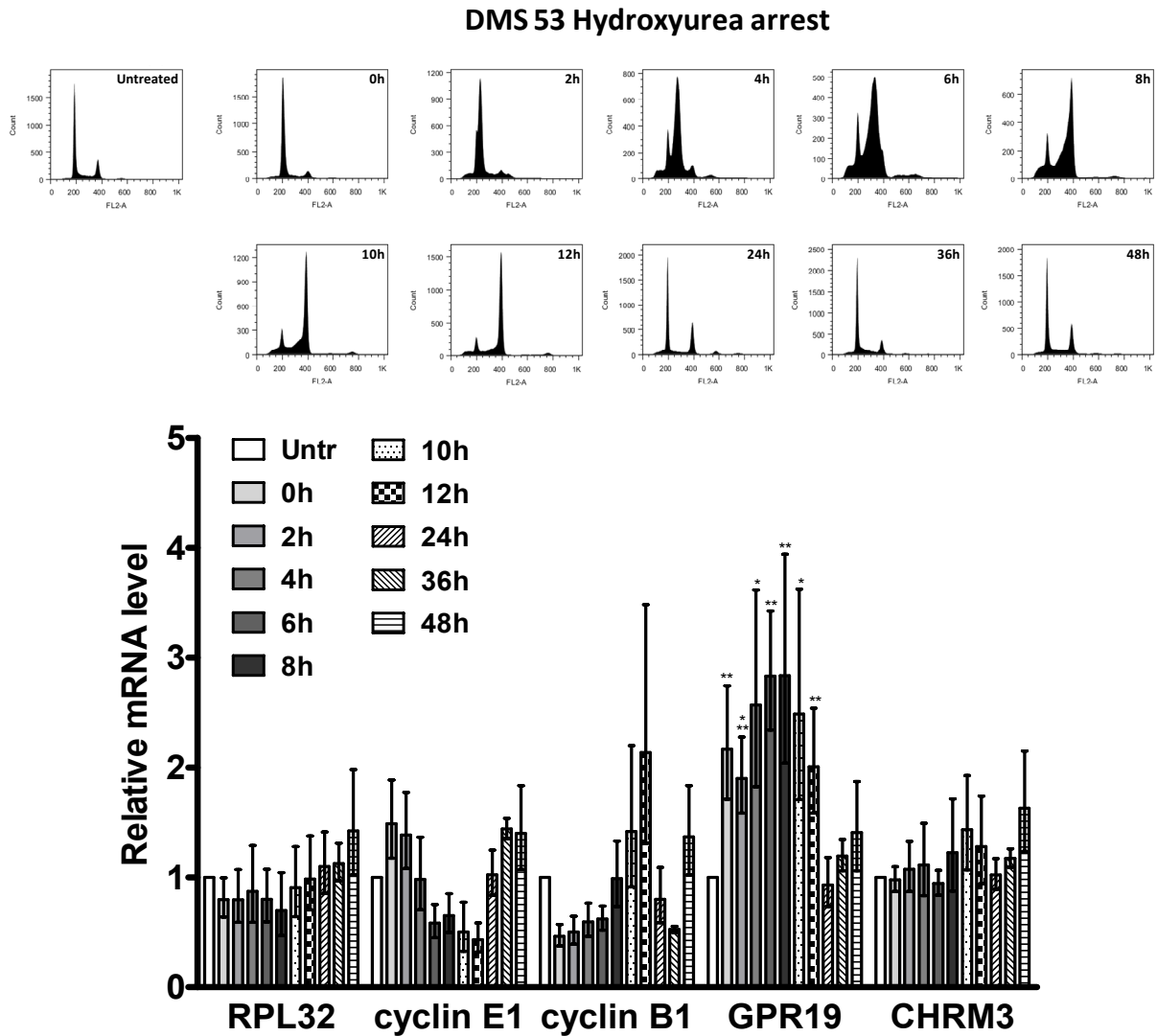


Figure 54: *Gpr19* mRNA is differentially expressed over the course of the cell cycle and peaks during S phase (hydroxyurea arrest) in DMS 53 cells. DMS 53 cells were treated with hydroxyurea (1 mM) for 24 h and therefore arrested at the G1-S transition. Following release of the block, the DNA content was determined at regular time points by propidium iodide staining and flow cytometry (upper panel; fluorescence channel 2 (FL2)-area (A) histogram) and the corresponding expression profiles of the indicated genes (encoding the ribosomal protein L32 (RPL32), cyclin E1, cyclin B1, and the GPCRs GPR19 and muscarinic cholinergic receptor 3 (CHRM3)) were determined by RT-qPCR (lower panel). The gene of interest mRNA expression was normalized against four reference genes (*Actb*, *Cypa*, *Hprt1*, *Rplp0*). Gene expression plots show mRNA levels (geometric mean value) relative to control samples (untreated (Untr) cells) with error bars indicating 95% confidence intervals. *Gpr19* mRNA expression at each time point post release was compared to the mRNA expression of non-differentially expressed *Rpl32* using a t test with Welch's correction (* $p < 0.05$; ** $p < 0.01$; *** $p < 0.001$). The experiment was repeated yielding concurrent results.

Lpar1 in DMS 53 cells and *Chrm3* in NCI-H1703 cells was either not detectable or only present at high quantification cycles (> 37 Cq) rendering these data error-prone. These mRNAs remained essentially constant over time – with some limitations at few

secretion of glandular tissue and the contraction of smooth muscle tissue. Besides, activation of the muscarinic ACh receptor family in general and CHRM3 in particular was proposed to contribute to colon carcinogenesis (Belo A *et al.*, 2011; www.ncbi.nlm.nih.gov/gene/1131; www.uniprot.org/uniprot/P20309).

time points assessed – therefore serving as undifferentially expressed controls. **The expression of *Gpr19* mRNA, however, was cell cycle-dependent: *Gpr19* mRNA levels rose when the synchronized cells moved through S phase, peaked after 6 to 8 h, and started to decline as cells reached G2/M phase, i.e., after 10 h** (figure 54 and figure 55, lower panels). At later time points (24 h, 36 h, and 48 h), mRNA levels did not differ appreciably from those seen in untreated control cells (open bar in the lower panels of figure 54 and figure 55), regardless of which mRNA was examined. This is consistent with the fact that the cell population grew again asynchronously at this stage.

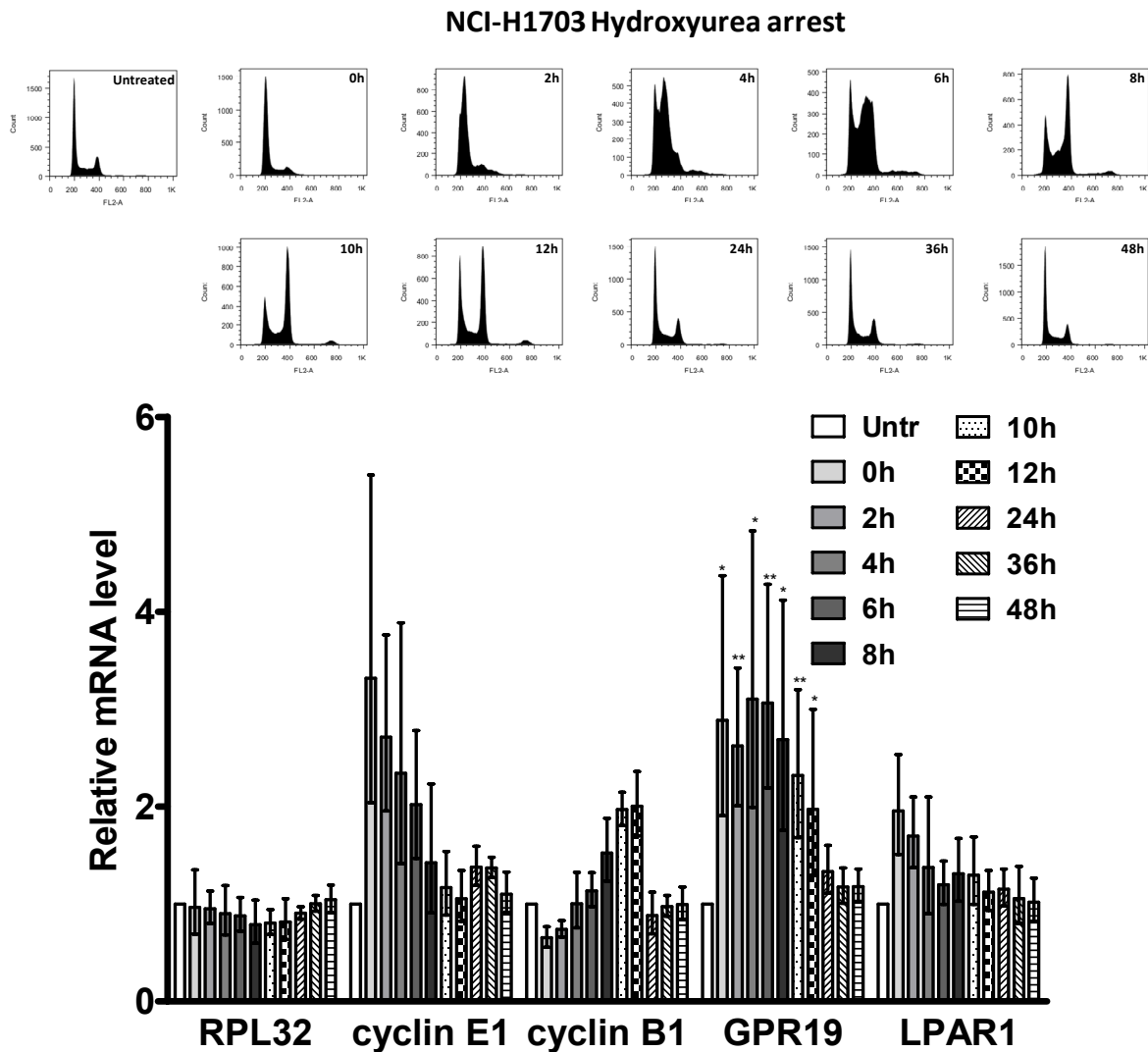


Figure 55: *Gpr19* mRNA is differentially expressed over the course of the cell cycle and peaks during S phase (hydroxyurea arrest) in NCI-H1703 cells. NCI-H1703 cells were treated with hydroxyurea (1 mM) for 24 h and therefore arrested at the G1-S transition. Following release of the block, the DNA content was determined at regular time points by propidium iodide staining and flow cytometry (upper panel; fluorescence channel 2 (FL2)-area (A) histogram) and the corresponding expression profiles of the indicated genes (encoding the ribosomal protein L32 (RPL32), cyclin E1, cyclin B1, and the GPCRs GPR19 and lysophosphatidic acid receptor 1 (LPAR1)) were determined by RT-qPCR (lower panel). Data analysis was performed as outlined in the legend of figure 54 (* $p < 0.05$; ** $p < 0.01$). The experiment was repeated yielding concurrent results.

The possibility was addressed that differential *Gpr19* mRNA expression was due to the chemical treatment of cells with hydroxyurea, *i.e.*, an off-target effect unrelated to its effect on the cell cycle. The expression study was therefore repeated with DMS 53 cells using the DNA replication inhibitor aphidicolin⁹⁶ that also causes cells to arrest at the G1-S transition (Pedrali-Noy G *et al.*, 1980).

Cell cycle profiles and the degree of synchronization resembled those of hydroxyurea-treated cells (figure 56, upper panel). The amount of cells in S phase was also highest at 2, 4, 6, and 8 h after release and returned back to normal at 24, 36, and 48 h. Similarly, mRNA profiles were also comparable (figure 56, lower panel). **Most importantly, following aphidicolin-induced synchronization, the time-dependent changes in *Gpr19* mRNA levels recapitulated those seen in hydroxyurea-treated cells.** Expression of *cyclin B1* and *cyclin E1* mRNAs over the course of the cell cycle followed their expected patterns, *Rpl32* and *Chrm3* expressions were unaltered.

Hydroxyurea and aphidicolin allowed the synchronous passage of cells from the G1-S transition over S and G2/M phases finally reaching a normal cell cycle population profile. In order to better compare *Gpr19* expression levels between cells in G1 and G2/M phase, NCI-H1703 and DMS 53 cells were arrested during mitosis using nocodazole⁹⁷ (figure 57). Samples of untreated cells and cells at 0, 4, 24, and 48 h after nocodazole block release were examined. Cells arrested with nocodazole harbored a DNA content characteristic of the G2/M phase and did not go through another round of synchronous cell cycling. Instead, the G2/M population declined with time at the expense of a rising G1 population (figure 57A and B, upper panels). ***Gpr19*, *Rpl32*, *Lpar1*, and *Chrm3* mRNA levels remained almost unaltered at all time points after nocodazole-induced cell cycle block release compared to the respective untreated control sample** (figure 57A and B, lower panels). Expression of *cyclin E1* was decreased when cells were found with a DNA content characteristic of the G2/M phase, whereas *cyclin B1* expression was increased here. Message levels

⁹⁶ Aphidicolin is a diterpene fungal metabolite from *Nigrospora sphaerica* which targets the cellular DNA replication process by inhibition of α and δ -polymerases. Cultured cells are prevented from entering S phase and accumulate at the G1-S transition or are blocked in S phase. Aphidicolin does not hinder the synthesis of neither deoxyribonucleoside triphosphates (dNTPs) nor DNA polymerases. Hence, a quick recovery and onset of synchronous cell cycle progression is favored upon removal of this cell cycle block-inducing agent from the culture medium (Pedrali-Noy G *et al.*, 1980; www.enzolifesciences.com/fileadmin/reports/els_b56aaf7f2b.pdf).

⁹⁷ The anti-neoplastic agent nocodazole exerts its biological effects by interaction with tubulin heterodimers and by increasing tubulin guanosine triphosphatase (GTPase) activity four- to fivefold and therefore affecting microtubule dynamics (Mejillano MR *et al.*, 1996). Cells exposed to nocodazole exhibit suppressed dynamic instability of microtubules with reduced elongation and shortening velocities and a net decrease in turnover. Microtubules enter a so-called attenuated or paused state with little overall change in length (Vasquez RJ *et al.*, 1997). Besides their role in controlling the movement of cellular organelles and vesicles, correct microtubule function and dynamics is a prerequisite for cells to coordinate the arrangement of chromosomes during mitosis. Treatment with nanomolar concentrations of nocodazole causes an arrest of cells in mitosis (metaphase) typically detected by a G2/M phase-specific DNA content upon propidium iodide DNA staining in flow cytometry. The mitotic checkpoint, which ensures that chromosomes are properly attached to the mitotic spindle before anaphase can occur, is triggered. These effects are reversible by ablation of nocodazole (Samson F *et al.*, 1979; Zieve GW *et al.*, 1980; Jordan MA *et al.*, 1992; Burke DJ, 2000). In contrast, there are also reports that nocodazole-treated cells lack some features of synchronized cultures such as a narrow cell size range, for instance (Cooper S *et al.*, 2006).

of cyclin *B1* declined back to their initial levels (untreated cells) when the mitosis-arrested cell population shifted towards a normal cell cycle profile.

Taken together, the examination of *Gpr19* mRNA expression over the course of the cell cycle revealed a peak in expression when most cells were in S phase.

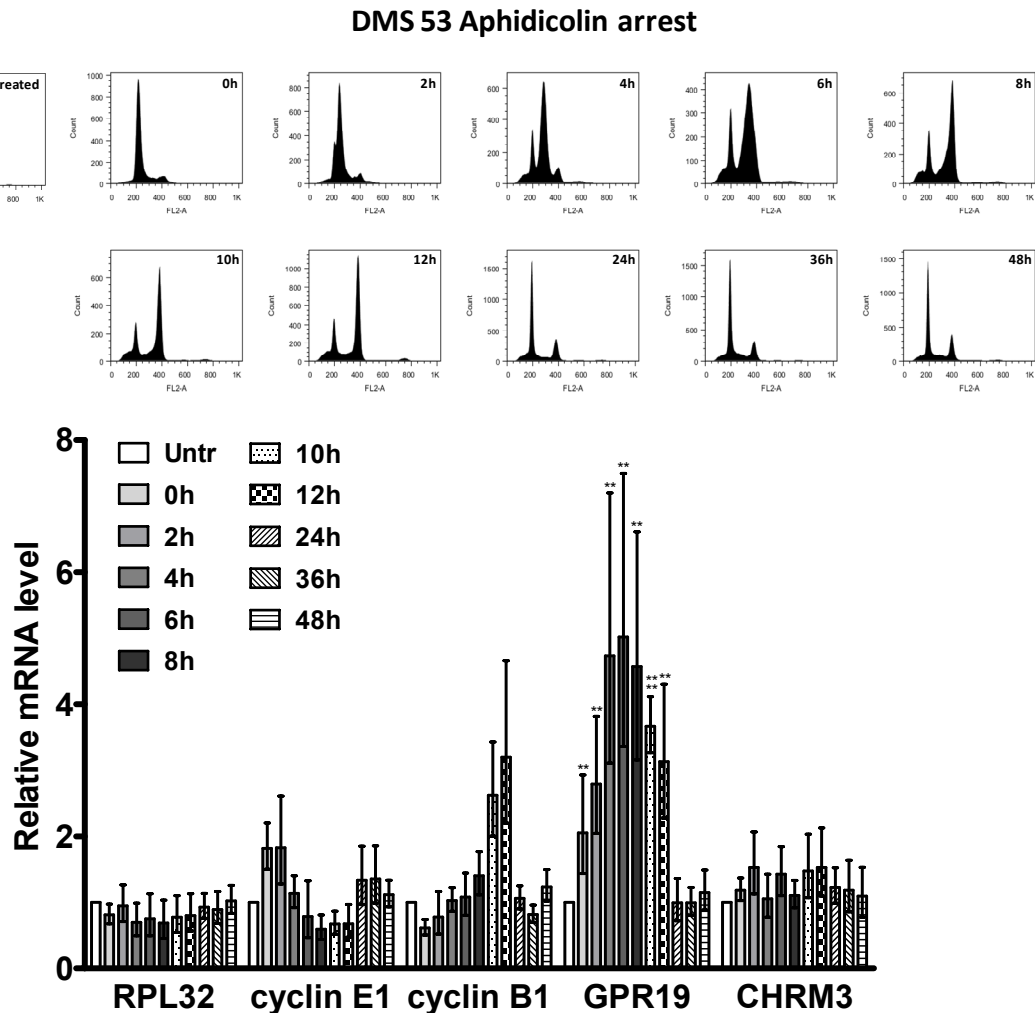


Figure 56: *GPR19* mRNA is differentially expressed over the course of the cell cycle and peaks during S phase (aphidicolin arrest) in DMS 53 cells. DMS 53 cells were treated with aphidicolin ($3 \mu\text{M}$) for 24 h and therefore arrested at the G1-S transition. Following release of the block, the DNA content was determined at regular time points by propidium iodide staining and flow cytometry (upper panel; fluorescence channel 2 (FL2)-area (A) histogram) and the corresponding expression profiles of the indicated genes (encoding the ribosomal protein L32 (RPL32), cyclin E1, cyclin B1, and the GPCRs *GPR19* and muscarinic cholinergic receptor 3 (CHR3)) were determined by RT-qPCR (lower panel). Data analysis was performed as outlined in the legend of figure 54 (** $p < 0.01$; *** $p < 0.0001$). The experiment was repeated yielding concurrent results.

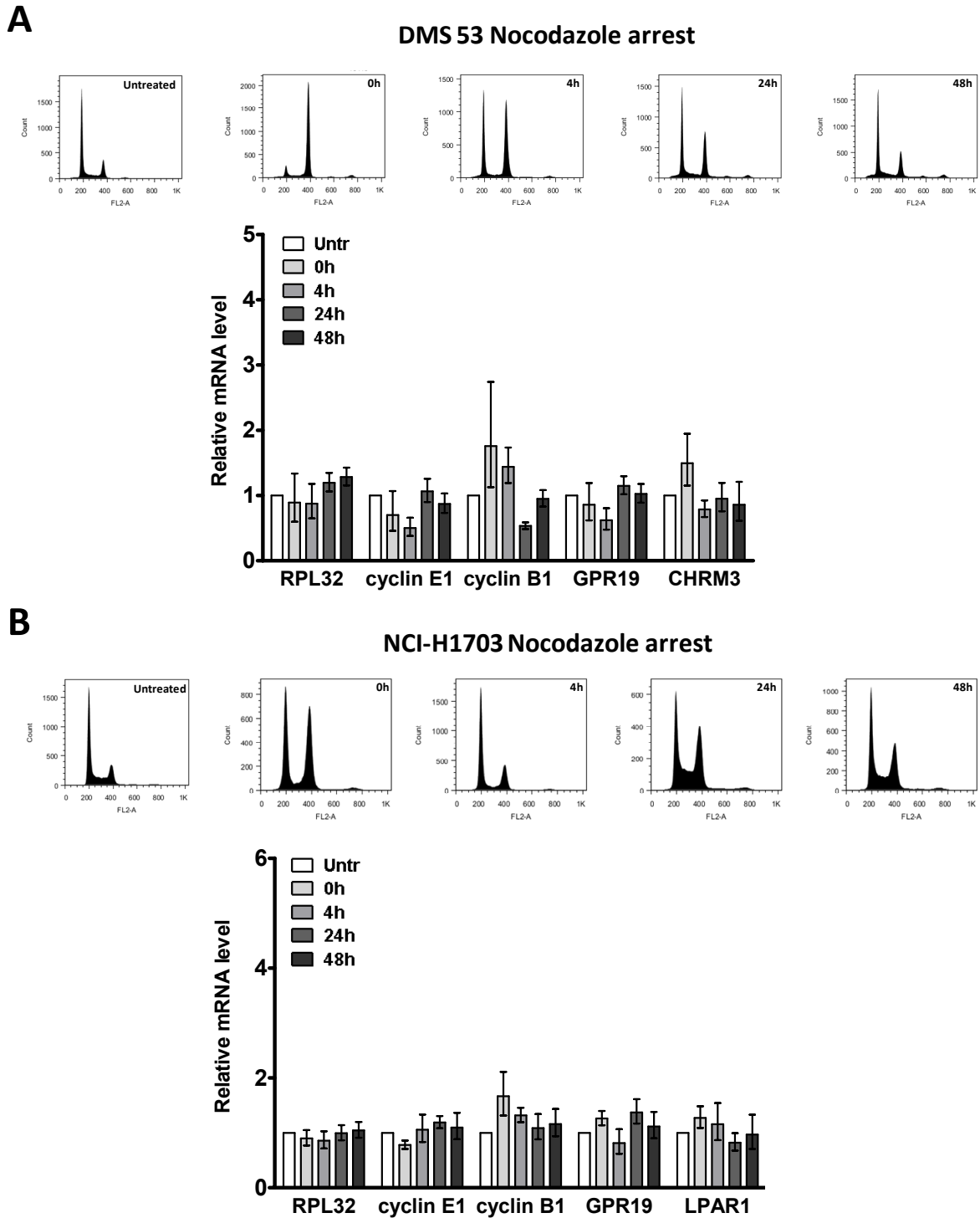


Figure 57: *Gpr19* mRNA expression is nearly unaltered during G1 and G2/M phase (nocodazole arrest). DMS 53 (A) and NCI-H1703 (B) cells were treated with nocodazole (300 nM) for 24 h and therefore arrested during mitosis. Following release of the block, the DNA content was determined at regular time points by propidium iodide staining and flow cytometry (upper panels; fluorescence channel 2 (FL2)-area (A) histogram) and the corresponding expression profiles of the indicated genes (encoding the ribosomal protein L32 (RPL32), cyclin E1, cyclin B1, and the GPCRs GPR19, lysophosphatidic acid receptor 1 (LPAR1), or muscarinic cholinergic receptor 3 (CHRM3)) were determined by RT-qPCR (lower panels). The gene of interest mRNA expression was normalized against four reference genes (*Actb*, *Cypa*, *Hprt1*, *Rplp0*). Gene expression plots show mRNA levels (geometric mean value) relative to control samples (untreated (Untr) cells) with error bars indicating 95% confidence intervals. Experiments were repeated yielding concurrent results.

8.2. Relative *Gpr19* mRNA levels correlate with the amount of cells in S phase

Gpr19 expression levels at various time points after hydroxyurea block release were further examined for correlation with the relative number of cells in G1, S, and G2/M phase for both DMS 53 and NCI-H1703 cells (figure 58). The proportion of cells at different stages of the cell cycle was determined using the Watson curve fitting model from FlowJo. As hydroxyurea arrested cells at the G1-S transition, it was impossible to precisely discriminate between G1 and S phase populations at 0 h and 2 h after release of the hydroxyurea-induced block. These data points were therefore omitted. In both cell lines, ***Gpr19* message levels correlated with the relative number of cells in S phase. Conversely, *Gpr19* mRNA levels were inversely related to the fraction of G1 cells.** In contrast, no correlation could be observed between the amount of cells in G2/M phase and *Gpr19* mRNA expression.

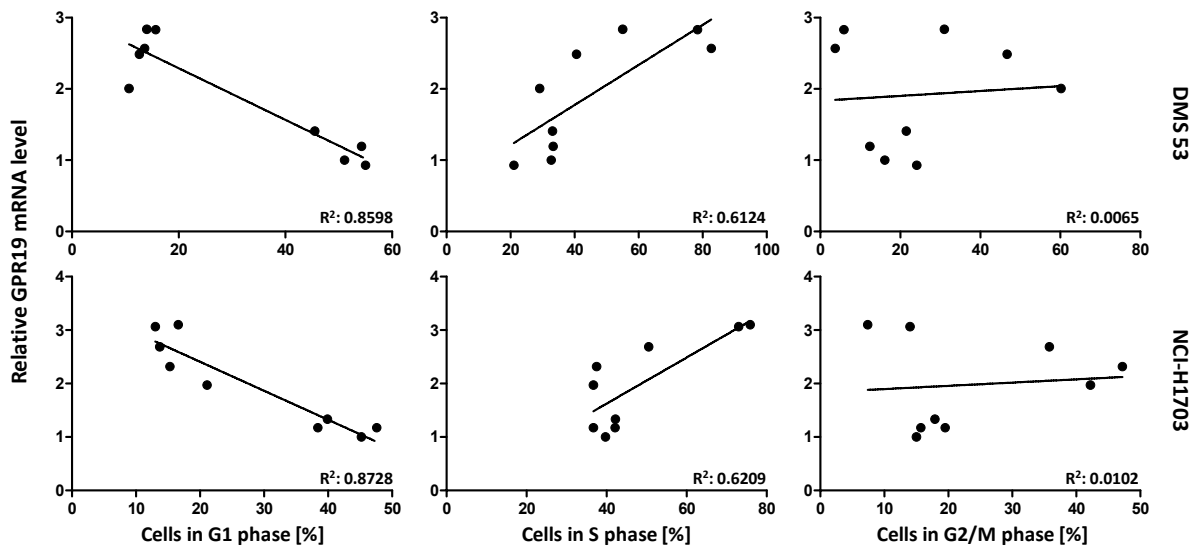


Figure 58: Relative *Gpr19* mRNA levels correlate with the amount of cells in S phase. The correlation analysis incorporated *Gpr19* expression levels determined over the course of the cell cycle from hydroxyurea-arrested DMS 53 and NCI-H1703 cells (see figure 54 and figure 55) plotted as a function of the relative number of cells in G1, S, and G2/M phase. Data from untreated cells and cells at 4 h, 6 h, 8 h, 10 h, 12 h, 24 h, 36 h, and 48 h after hydroxyurea-induced block release were included. Shown are the results of linear regressions; squared correlation coefficient values (R^2) are given for each plot.

9. *Gpr19* gene regulation

9.1. *In silico* analysis of the *Gpr19* promoter reveals E2 promoter binding factor (E2F) binding

The data from cell cycle-dependent *Gpr19* expression analysis suggested that accumulation of the mRNA encoding *Gpr19* was initiated as soon as cells progressed from G1 to S phase. Members of the E2F family of transcription factors are known to boost transcription from E2F-targeted promoter sites during late G1 or early S phase (Wells J *et al.*, 2000), e.g., the component of the pre-replicative complex *cell division cycle 6* (*Cdc6*; Brown KC *et al.*, 2010) and *Myc* (myelocytomatosis oncogene; Rabinovich A *et al.*, 2008). As *Gpr19* mRNA expression was shown to peak during S phase, the possible involvement of the E2F family of transcription factors in regulating its expression was investigated.

The *Gpr19* promoter region (5 kilobases (kb) of the 5' upstream sequence ahead of the open reading frame (ORF)) was examined for potential E2F binding sites *in silico* using ConSite⁹⁸ and the University of California, Santa Cruz (UCSC) genome browser⁹⁹. The consensus DNA recognition sequence for E2F transcription factors is 5'-T-T-T-G/C-G/C-C-G-C-3' (Rabinovich A *et al.*, 2008). Results from both databases were based on computational data and had not been biologically verified.

Four potential E2F binding sites (-15 (5'-T-T-T-A-G-C-G-C-3'), -185 (5'-T-T-T-G-C-T-G-C-3'; reverse strand), -3184 (5'-T-T-T-G-G-C-C-C-3'), and -3769 base pairs (bp; 5'-T-T-T-G-G-C-T-C-3') upstream of the *Gpr19* ORF) were retrieved from the ConSite search and only the one at position -15 was called by the UCSC genome browser search. However, these hypothetical E2F binding sites did not strictly follow the consensus DNA recognition sequence for E2F transcription factors. When investigating the same promoter region (5 kb of the 5' upstream sequence ahead of the ORF) of *Gpr19* in *Macaca mulatta*, *Mus musculus*, *Pan troglodytes*, and *Xenopus tropicalis* for binding of E2F transcription factors using ConSite, at least one possible binding site was retrieved in all these species (assuming the validity of the human E2F consensus DNA recognition site).

In addition to the E2F family, the UCSC database depicted the theoretical binding of the POU¹⁰⁰ family of transcription factors to the promoter region of *Gpr19* at position -875 (reverse strand) strictly following the consensus DNA recognition sequence 5'-A-T-G-C-A-A-A-T-3' (Cook AL and Sturm RA, 2008). An excerpt of the *Gpr19* promoter sequence (1,000 bases upstream of the *Gpr19* ORF) is shown in the Appendix section.

⁹⁸ asp.ii.uib.no:8090/cgi-bin/CONSITE/consite

⁹⁹ genome.ucsc.edu

¹⁰⁰ Transcription factors containing the POU (*Pit1/Oct2/unc-86*) domain are ubiquitously expressed proteins that function either in the regulation of housekeeping genes or in determining developmental or cell type-specific cell fate decisions (Cook AL and Sturm RA, 2008).

9.2. Chromatin immunoprecipitation (ChIP) determines the recruitment of transcription factors E2F-1, E2F-2, E2F-3, and E2F-4 to the *Gpr19* promoter

ChIP analyses were performed with 5 µg of respective E2F antibodies as described in the Materials and Methods sections (Schebesta A *et al.*, 2007). Genomic DNA was sheared by multiple rounds of sonication (30 sec pulse – 30 sec pause; DMS 53: four cycles at 75% intensity; NCI-H1703: eight cycles at 100% intensity; NCI-H446: four cycles at 100% intensity; SHP-77: two cycles at 100% intensity). Sonication typically resulted in chromatin fragments of 250 to 600 bp (figure 59, shown for NCI-H1703 cells).

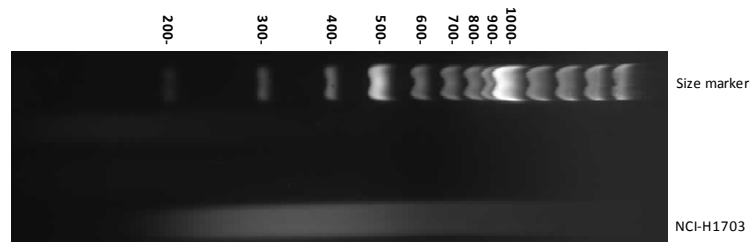


Figure 59: Chromatin fragmentation after sonication results in DNA fragments of 250 to 600 base pairs (bp). Shown is the result from agarose gel electrophoresis of an NCI-H1703 cell lysate (1:20 dilution) for ChIP analysis sonicated with eight times 30 sec pulses at 100% intensity. The size marker is shown in bp.

ChIP PCR was performed for 32 (NCI-H1703; NCI-H446), 33 (DMS 53), or 36 (SHP-77) cycles depending on the cell line examined. In any case, an overamplification of the PCR signal was avoided by sampling a dilution series of the unprecipitated genomic input material together with the precipitated DNA fragments.

ChIP assays identified the binding of E2F-1, E2F-2, E2F-3, and E2F-4 to the promoter region of *Gpr19* in NCI-H1703, DMS 53, NCI-H446 and SHP-77 cells (figure 60). They were either recruited to binding site -15 or -185 or to both of them. As typical chromatin fragmentation after sonication resulted in DNA fragments of 250 to 600 bp (figure 59), it was not possible to distinguish E2F binding on these two predicted binding sites from each other. However, **E2Fs were not recruited to the suggested E2F binding sites at positions -3184 or -3769.** Primer pairs for PCR amplification of all predicted E2F binding sites were chosen in a way that the PCR product did not contain any other site – except for primer pair GPR19 (-15; -185). With this primer pair, the resulting PCR product covered both these predicted E2F binding sites of the *Gpr19* promoter. The expected binding of E2Fs to the promoter region of *Cdc6* served as positive control and could be recapitulated. Indeed, no binding of E2Fs to the coding sequence of *Gpr19* or the promoter region of *albumin* was also confirmed (Wells J *et al.*, 2000). Full-length agarose gels for NCI-H1703 are presented in figure 61. PCR primer sequences are listed in table 6 (Materials section).

These data seem to argue that *Gpr19* expression might be regulated by some members of the E2F family of transcription factors. Several facts suggest that the binding of E2F-1, E2F-2, E2F-3, and E2F-4 to the promoter sites at position -15 and/or -185 of the *Gpr19* gene were specific: (i) Immunoprecipitation of these E2F-family

members did neither pull down the coding sequence of *Gpr19* nor (ii) the promoter region of albumin. (iii) Several E2F-family members with repressor activity (E2F-5, E2F-6, E2F-7; Polager S and Ginsberg D, 2008; Chen HZ *et al.*, 2009) did not pull down the *Gpr19* promoter, either.

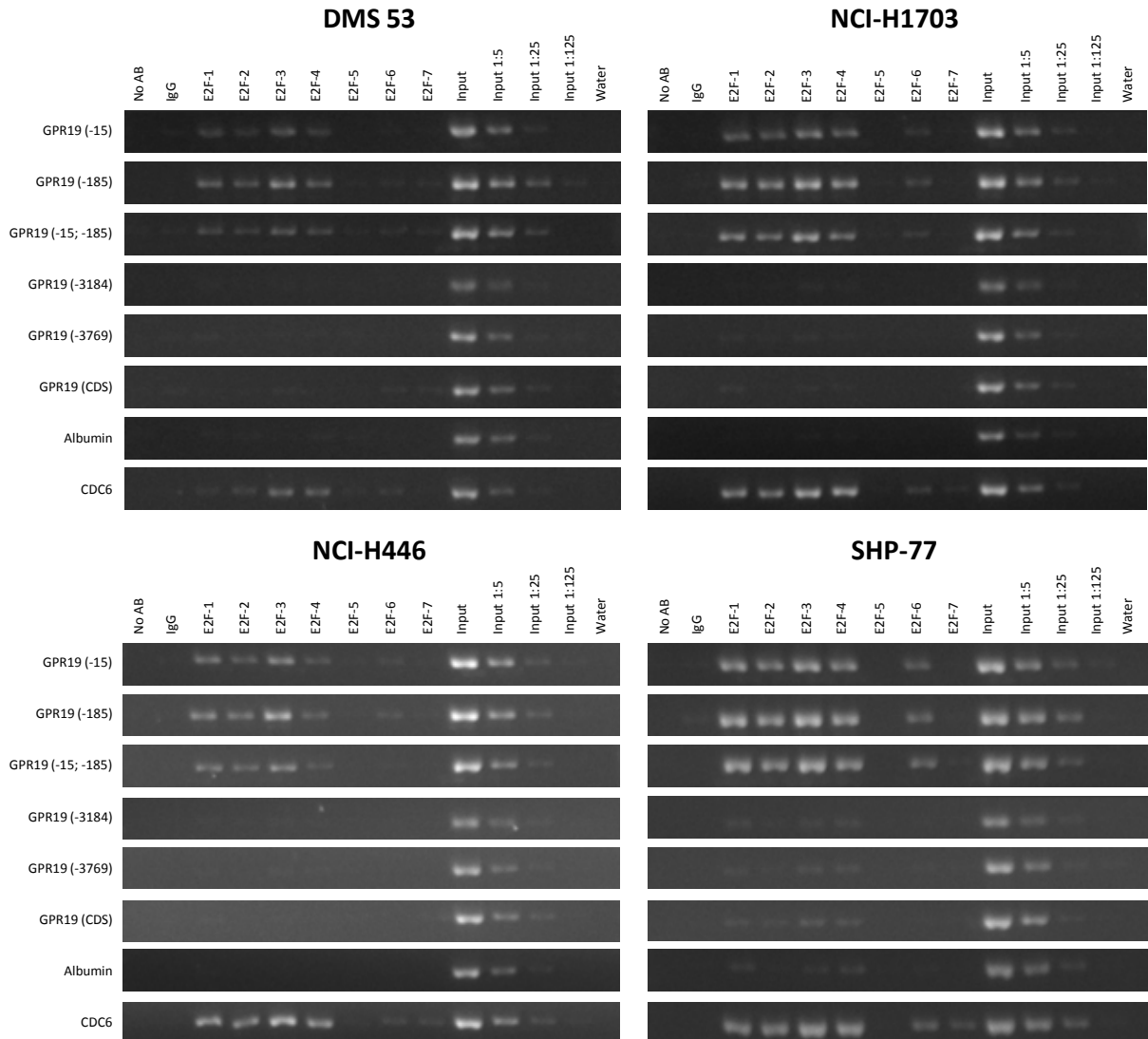


Figure 60: E2F family members 1 to 4 bind to the promoter of *Gpr19*. Chromatin immunoprecipitation (ChIP) was performed with antibodies against E2F family members (E2F-1, 2, 3, 4, 5, 6, and 7) and immunoglobulin G isotype control (IgG) assayed for binding to different *Gpr19* promoter regions predicted to contain putative E2F binding sites (-15, -185, -3184, and -3769 bp upstream of the *Gpr19* open reading frame (ORF)) in DMS 53, NCI-H1703, NCI-H446, and SHP-77 cells. As an additional negative control, the immunoprecipitation was done in the absence of any antibody (no AB). DNA from the sheared chromatin input was serially diluted with nuclease-free water (undiluted, 1:5, 1:25, 1:125, water only). Internal controls also included amplification of the promoter of a known E2F target gene (*cell division cycle* (*Cdc6*)) and of an E2F-independent gene (*albumin*) as well as of a region lying in the coding sequence (CDS) of *Gpr19*. Forward and reverse primer sequences are listed in table 6 (Materials section). Primer pair GPR19 (-15; -185) covered both predicted E2F binding sites of the *Gpr19* promoter in the PCR product (primers 15rev1, 185fow1). Shown are the amplicons from a representative experiment, which was repeated twice with concurrent results.

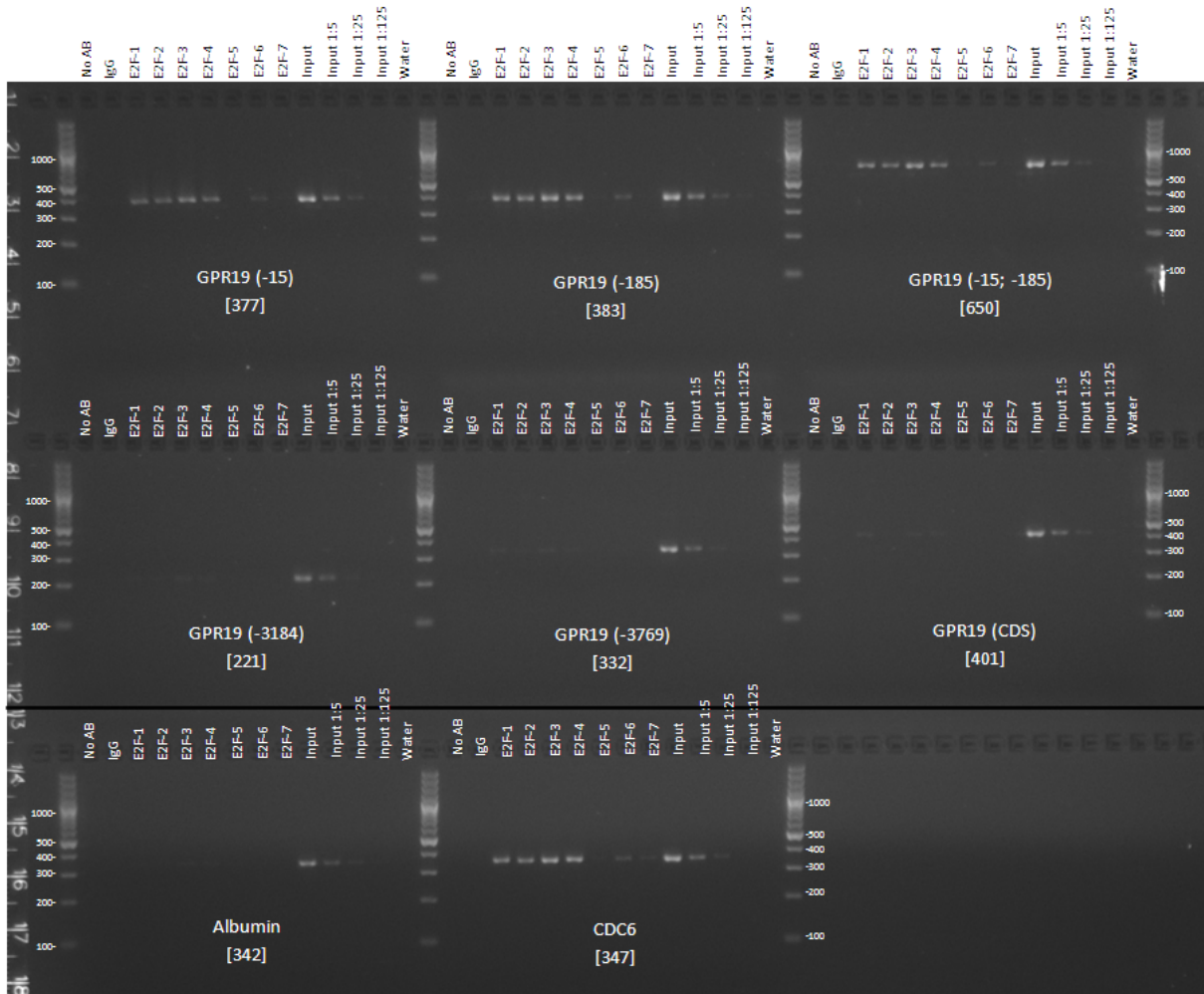


Figure 61: E2F family members 1 to 4 bind to the promoter of *Gpr19*. ChIP was done with antibodies against E2F family members (E2F-1, 2, 3, 4, 5, 6, and 7) as described in the legend of figure 60. Full-length agarose gel electrophoresis data for NCI-H1703 cells are shown and numbers in squared brackets indicate PCR product size (bp). The size marker is shown in bp.

9.3. Both E2F binding sites at positions -15 and -185 of the *Gpr19* promoter are crucial for luciferase reporter gene expression

Fragments of the *Gpr19* promoter (300 or 1,000 bp upstream of the *Gpr19* ORF) were introduced upstream of a firefly luciferase reporter gene in order to evaluate their influence on gene expression (figure 62). In addition, the putative E2F transcription factor binding sites at positions -15 and/or -185 had been selectively removed in the pGL3-Basic-300GPR19-miniTK construct. Constructs are schematically shown in figure 62B. All constructs had been verified by sequencing. An excerpt of the *Gpr19* promoter sequence (1,000 bases upstream of the *Gpr19* ORF) is shown in the Appendix section.

Expression plasmids had been introduced into DMS 53, HEK-293, and NCI-H1703 cells by electroporation: 3 μ g (5 μ g for HEK-293 cells) of plasmid DNA had been applied to 5×10^5 cells and 10,000 cells had been seeded per well of a poly-D-lysine-coated 96 well culture plate. Cells were subjected to luciferase assay 14 h (DMS 53), 13 h (HEK-

293), and 26 h (NCI-H1703) later. HEK-293 cells had been characterized to not express *Gpr19* endogenously (figure 31).

The transfection of the pGL3-Basic-CMV-miniTK construct was used as an assay control and resulted in the massive expression of luciferase: Relative light units were 50 to 100 times higher than for any *Gpr19* promoter fragment-containing luciferase construct (data not shown). **All constructs bearing fragments of the *Gpr19* promoter were able to drive luciferase reporter gene expression in DMS 53, HEK-293, and NCI-H1703 cells** (figure 62A). The long promoter fragment of *Gpr19* (1,000 bp) increased the light signal relative to the shorter fragment that contained only 300 bp in all cell lines. The removal of the putative E2F binding site at position -15 alone or in combination with the one at position -185 negatively affected reporter gene expression clearly in HEK-293 and NCI-H1703 cells, as a decrease in the light signal was observed (figure 62A, left and centrefold graphs). However, luciferase expression was not completely abolished. In contrast, the knockout of the putative E2F binding site at position -185 alone did not diminish luciferase expression in HEK-293 and NCI-H1703 cells. The opposite was true for DMS 53 cells: The predicted E2F binding site at position -185 was more important for luciferase reporter gene expression here (figure 62A, right graph). Removal of the E2F consensus site at position -185 from the *Gpr19* promoter sequence diminished luciferase expression. This signal reduction was further enhanced when the E2F consensus site at position -15 had also been erased. Again, eradication of E2F consensus sites from the *Gpr19* promoter did not completely abolish luciferase expression.

Hence, the consensus motif for the recruitment of E2F transcription factors to the promoter of *Gpr19* at both positions -15 and -185 upstream of the *Gpr19* ORF seemed to be important for luciferase reporter gene expression. The preferred usage might be cell line-dependent. However, based on the remaining basal expression levels observed with mutated E2F binding sites, E2F transcription factors might not be exclusively responsible for *Gpr19* gene expression.

9.4. The expression levels of *E2f-1*, *E2f-2*, and *E2f-3* are increased in SCLC patient samples relative to normal lung controls

The recovery of the *Gpr19* promoter in ChIP assays using E2F-1 to E2F-4 antibodies and the results from *Gpr19* promoter fragment-controlled luciferase reporter expression indicated a cause-and-effect relation between the action of E2F transcription factors and the expression of *Gpr19*. This association is further fostered by gene expression data of *E2f-1*, *E2f-2*, and *E2f-3* in samples from SCLC patients in comparison to samples from NSCLC patients and normal lung controls analyzed by Affymetrix microarray analysis (figure 63; Human Exon 1.0 ST Array; samples were obtained from OriGene Technologies, details are listed in table 12). High levels of *Gpr19* expression had been shown in SCLC samples (figure 27; figure 63, upper left panel). **Likewise, the expression of *E2f-1*, *E2f-2*, and *E2f-3* followed the pattern observed for *Gpr19*: Expression levels were highest in patient samples derived from SCLC.**

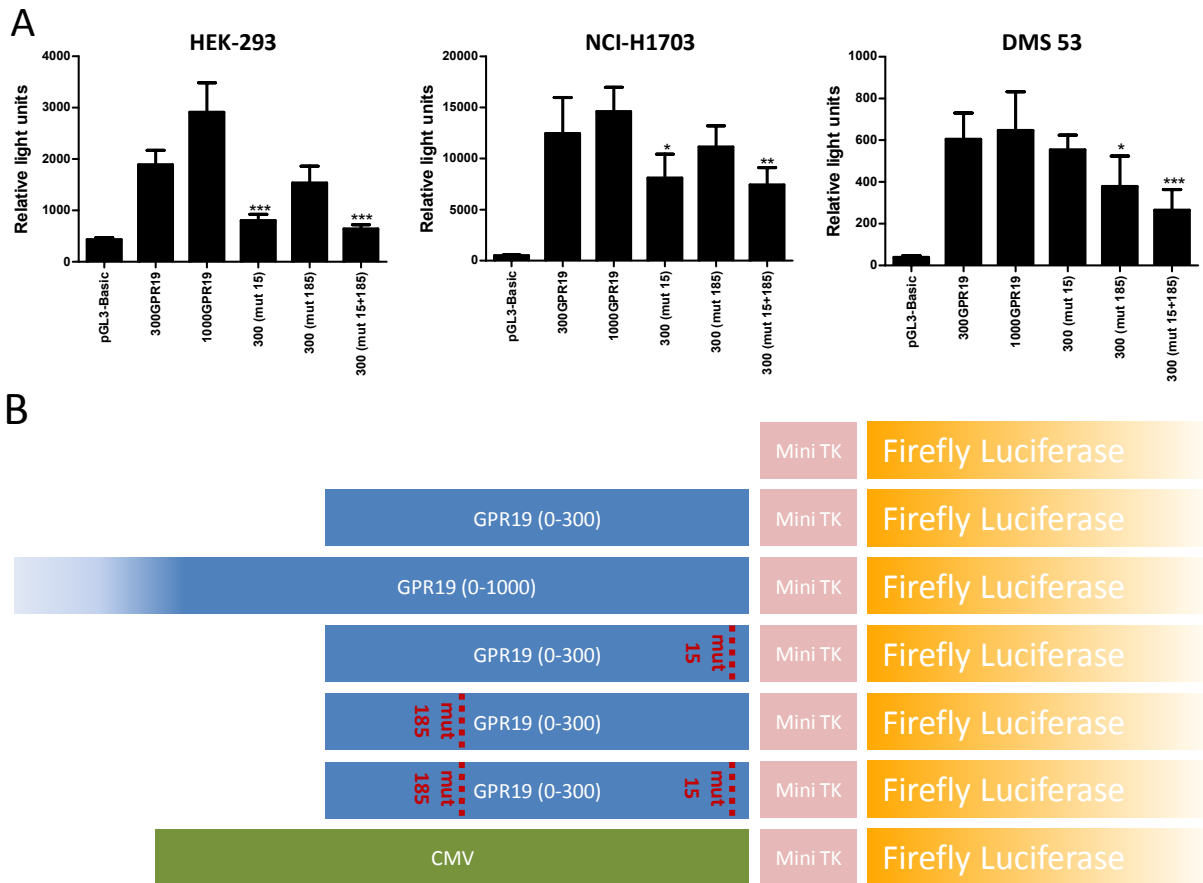


Figure 62: Both E2F binding sites in the *Gpr19* promoter at position -15 and -185 upstream of the *Gpr19* open reading frame (ORF) are important for luciferase reporter gene expression. (A) HEK-293, NCI-H1703, and DMS 53 cells were transiently transfected with control (pGL3-Basic-miniTK) or *Gpr19* promoter fragment-containing luciferase reporter constructs (pGL3-Basic-300GPR19-miniTK, pGL3-Basic-1000GPR19-miniTK (300/1,000 bp of the *Gpr19* promoter upstream of the *Gpr19* ORF)). Besides, cells were transfected with constructs in which the putative E2F transcription factor binding sites at position -15 and/or -185 upstream of the *Gpr19* ORF had been eliminated (pGL3-Basic-300GPR19-miniTK (mut 15), pGL3-Basic-300GPR19-miniTK (mut 185), pGL3-Basic-300GPR19-miniTK (mut 15+185)). A schematic representation of all constructs is given in **B**. Cells were harvested for luciferase assay 13 h (HEK-293), 26 h (NCI-H1703), and 14 h (DMS 53) after transfection. Data are mean values + standard deviation (error bar) of six replicates per condition (96 well plate) from a representative experiment. Differences across all experimental groups were determined by one way ANOVA followed by Tukey's test. P values of GPR19-mutated constructs 15 and/or 185 refer to the comparison with the non-mutant promoter construct pGL3-Basic-300GPR19-miniTK (*p < 0.05; **p < 0.01; ***p < 0.001). The experiments were repeated yielding concurrent results. CMV – cytomegalovirus; Mini TK – minimal thymidine kinase promoter.

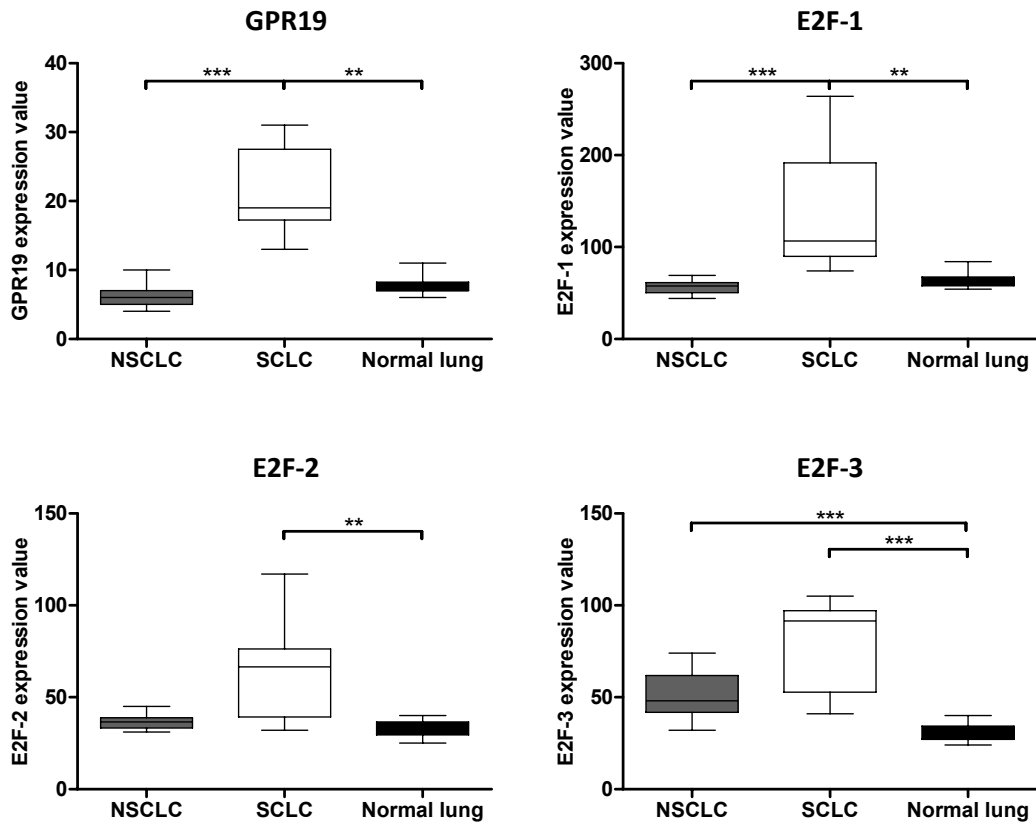


Figure 63: *Gpr19*, *E2f-1*, *E2f-2*, and *E2f-3* are overexpressed in samples from SCLC patients. The results for *Gpr19*, *E2f-1*, *E2f-2*, and *E2f-3* gene expression from Affymetrix GeneChip® analysis (Human Exon 1.0 ST Array; probe sets NM_006143_at (*Gpr19*), NM_005225_at (*E2f-1*), NM_004091_at (*E2f-2*), NM_001949_at (*E2f-3*)) of human NSCLC, SCLC, and normal lung samples are shown per histological group. Expression data were combined for all cases per group (box (interquartile range; middle 50% of all expression values) and whiskers (minimum-maximum) plot with median (central bar)). Detailed sample information is listed in table 12. Statistically significant differences were determined by a Kruskal-Wallis test followed by Dunn's multiple comparison (**p < 0.01; ***p < 0.001).

VII. Discussion

1. G protein-coupled receptor 19 (GPR19) – an exceptional GPCR difficult to pigeonhole

GPR19 is a member of the family of G protein-coupled receptors (GPCRs) and predicted to harbor a seven transmembrane (7TM) structure. **When transmembrane core sequences of human GPCRs had been compared for receptor classification, GPR19 was assigned to the rhodopsin family of GPCRs** (Vassilatis DK *et al.*, 2003). In fact, the search for paralogs of this receptor (full-length amino acid sequence) in *Homo sapiens* identified only members of the rhodopsin family as its GPCR relatives (figure 14). However, those relatives did not seem to be very close. **Its classification into the rhodopsin family was therefore not confirmed when full-length receptor sequences had been applied for GPCR classification – GPR19 was not assigned to any of the five GRAFS (glutamate – rhodopsin – adhesion – frizzled/taste2 – secretin) GPCR families** (Fredriksson R *et al.*, 2003). Moreover, GPR19 lacks features characteristic for each of these five families: It does neither harbor a strict E/DRY motif at the boundary of transmembrane (TM) region 3 and intracellular loop region 2 nor a strict NPxxY-motif at the boundary of TM region 7 and the intracellular carboxy-terminus characteristic for rhodopsin family members (figure 6; Krishnan A *et al.*, 2012). Further, it lacks a very long amino-terminus not to mention any structural protein domains therein – features that would support its classification into the adhesion, secretin, glutamate, or frizzled/taste2 family. In addition, the GPR19 amino-terminus does not contain multiple Cys residues seen in most glutamate or secretin family receptors (Lagerström MC and Schiöth HB, 2008; Krishnan A *et al.*, 2012).

Thus, **the search for relatives in various species identified GPR19 as a highly conserved GPCR**. Orthologs were found in euarchontoglires (supra-primates) as well as many species that are evolutionary very distant to mammals like the sea anemone, sea urchin, lancelet, or the fly (figure 13). The fact that many diverse species are equipped with GPR19 points towards an important role for this receptor in multicellular organisms, it is likely required to perform an important cellular function. Further, GPR19 might have been present in the genome of common ancestor species during the times of their evolutionary differentiation (Lipman DJ *et al.*, 2002).

Phylogenetic analyses within one species can be used to determine the closest relatives of a protein within a larger protein family. It might therefore be possible to narrow down the nature of a putative ligand for a receptor. **GPR19 was found to have closest GPCR paralogs in receptors activated by biogenic amines and peptides in phylogenetic analyses performed with complete receptor primary sequences** (table 14). Similar results were obtained in five different species: *Homo sapiens*, *Pan troglodytes*, *Macaca mulatta*, *Mus musculus*, and *Danio rerio* (figure 14 and figure 15). However, GPR19 was mostly found on branches that separated both these receptor subtypes or very distant from any other GPCR. **When the transmembrane core of GPCRs had been used for sequence alignment, GPR19 was found within a bigger cluster of peptide-activated GPCRs and its designated ligand was therefore proposed to be a peptide** (Vassilatis DK *et al.*, 2003). Sequence

similarities were reported between GPR19 and the dopamine D2 and neuropeptide Y GPCRs. Yet, as GPR19 is deficient in both an Asp residue within TM region 3 as well as two conserved Ser residues within TM region 5, which, on the other hand, are characteristic features for functional catecholaminergic receptors (Ji TH *et al.*, 1998), its endogenous ligand is unlikely to be aminergic. Neither dopamine nor serotonin nor epinephrine (among other biogenic amines) affected adenylyl cyclase activity in GPR19-transfected COS (short for 'C_V-1 origin, Simian Virus (SV)40-immortalized') cells (O'Dowd BF *et al.*, 1996). In contrast, GPR19 does not harbor a DxxCR motif in the extracellular loop region 1 which is highly conserved among peptidergic GPCRs (Peeters MC *et al.*, 2011).

Thus, the plethora of potential ligands described to act on GPCRs might be narrowed down for GPR19 to biogenic amines and peptides on the basis of various phylogenetic analyses. However, GPR19 often seemed to lie on the interconnection between these two groups of GPCRs. Nevertheless, the data underlying the phylogenetic analysis of GPCR transmembrane domains might justify a tendency towards a peptide ligand for GPR19 (Vassilatis DK *et al.*, 2003).

When transiently overexpressed, GPR19 localized to the plasma membrane in HEK-293, NCI-H2170 (non-small cell lung cancer (NSCLC)), and DMS 53 (small cell lung cancer (SCLC)) cells (figure 34 and figure 35). In some cells, the GPR19-derived signal was also found in an area lying next to the nucleus. This could likely indicate its secretion and maturation through the secretory pathway to the plasma membrane employing the endoplasmic reticulum and the Golgi apparatus. Most GPCRs are in fact found at the plasma membrane where they engage their ligand(s) and initiate downstream signaling cascades upon activation (Achour L *et al.*, 2008). Whether localization to the plasma membrane in general or to specialized areas within the plasma membrane is important for ligand binding/activation of GPR19 remains elusive. Some GPCRs are known to preferentially remain in lipid microdomains such as membrane rafts or caveolae (Drake MT *et al.*, 2006; Paila YD and Chattopadhyay A, 2010). As many signaling components of multiple protein interaction pathways are present and pre-organized in rafts/caveolae, GPCRs can rapidly convey extracellular signals into the activation of downstream signaling cascades (Patel HH *et al.*, 2008). The fact that GPR19 harbors a strict cholesterol consensus motif might argue in favor of its preferred homing to these cholesterol-rich microdomains (Hanson MA *et al.*, 2008).

The resolution of GPCR structures as well as the production of high affinity antibodies against GPCRs is very challenging (Peeters MC *et al.*, 2011). Sources of conformational heterogeneity include glycosylation, phosphorylation, and highly flexible loops next to the transmembrane regions causing an equilibrium of different conformations in GPCRs – one reason why the availability of highly purified GPCR preparations and antibodies against GPCRs is limited (Rosenbaum DM *et al.*, 2009; Peeters MC *et al.*, 2011).

In addition, the immunogenicity of GPCRs is low. Most of them are highly glycosylated and – generally speaking – they share a high degree of sequence homology among each other and among different species (Gupta A *et al.*, 2008).

These characteristics could prevent the generation of high and specific serum titers. Nevertheless, the most successful strategy pursued to circumvent this problem uses short peptides coupled to antigenicity-increasing carrier proteins for immunization. Here, peptide sequences of the amino- or carboxy-terminus or the third intracellular loop region have revealed most promising results as these regions are highly diverse among different receptors and even receptor subtypes (Gupta A *et al.*, 2008).

This strategy for the production of a GPCR-specific antiserum was also followed for GPR19 (peptides used for immunization were located in the amino- or carboxy-terminus, predicted intracellular loop regions 2 or 3, or the predicted extracellular loop region 3; table 11). However, **purified antisera raised against GPR19 peptides and commercially available GPR19 antibodies failed to specifically detect this receptor in lysates from both HEK-293 cells transfected with *Gpr19* expression plasmids and the NSCLC cell line NCI-H1703 on Western Blots** (figure 24 and figure 25). Besides, the exact molecular weight of GPR19 was hard to predict due to likely posttranslational modifications (O'Dowd BF *et al.*, 1996). HEK-293 cells did not express *Gpr19* messenger ribonucleic acid (mRNA) which allowed for the evaluation of unspecific signals seen in receptor-transfected cells. Endogenous *Gpr19* mRNA expression was high in NCI-H1703 cells (figure 31) and short interfering ribonucleic acid (siRNA)-mediated *Gpr19* knockdown should have unmasked GPR19 detection (expected signal decline), which was not the case. Nevertheless, the decay in gene message by RNA interference might not strictly correlate with an equally reduced protein level (Alemán LM *et al.*, 2007). **Yet, as an undisputed decision for the specific detection of GPR19 on Western Blots could not be made, this method was not pursued in subsequent experiments.** The proprietary Boehringer Ingelheim Next Generation Sequencing cell line database retrieved a wildtype *Gpr19* gene status for NCI-H1703 cells, which excludes the possibility that non-synonymous single nucleotide polymorphisms (SNPs) in GPR19 might account for the lack of antisera specificity.

2. High *Gpr19* mRNA expression is associated with malignant diseases

Gpr19 was first described to be expressed in the central nervous system (CNS; O'Dowd BF *et al.*, 1996; Hoffmeister-Ullerich SA *et al.*, 2004). In the present work, it was shown that **GPR19 can also be associated with lung cancer**. This conclusion is based on (i) an unbiased approach that found *Gpr19* specifically overexpressed in SCLC, (ii) database mining comparing *Gpr19* expression levels in normal and malignant tissues and (iii) the presence of high *Gpr19* mRNA levels in several human lung cancer-derived cell lines. Illegitimately high expression of GPCRs in tissues different from their primary sites of expression suggests that they may have more diversified cell-biological roles (Deshpande DA *et al.*, 2010).

When comparing gene expression ratios between SCLC and NSCLC patients relative to normal lung samples, a cluster analysis revealed various expression signatures for the members of the vast family of GPCRs. Different clusters existed indicating that some of these GPCRs were either up- or downregulated in either SCLC or NSCLC.

***Gpr19* formed part of a subcluster in which proteins with GPCR activity showed a high message upregulation in SCLC patient samples whereas their mRNA levels were rather unaltered in NSCLC samples compared to normal lung controls** (figure 26).

This general specificity – high *Gpr19* expression in SCLC but not in NSCLC patient samples or samples from normal lung – was further confirmed by a database mining approach utilizing the BioExpress® database that allowed for comparisons of gene expression profiles in various human normal and cancerous tissues. **High levels of *Gpr19* mRNA were not only detectable in SCLC patient samples but also in samples from patients suffering from pancreas islet cell carcinoma** (figure 28 and figure 29). Both these carcinoma types are often characterized by the presence of neuroendocrine markers, e.g., chromogranin A or synaptophysin (Wiedenmann B *et al.*, 1986; Nakakura EK and Bergsland EK, 2007; Modlin IM *et al.*, 2010). This is also true for subsets of NSCLC called large cell neuroendocrine carcinoma (LCNEC; Beasley MB *et al.*, 2005) and NSCLC with neuroendocrine features (Rekhtman N, 2010). In fact, a slight increase in *Gpr19* message could also be observed in large cell lung carcinoma (comprising both neuroendocrine and non-neuroendocrine cancers) relative to normal lung samples when utilizing the BioExpress® database (figure 28 and figure 29). Moreover, the correct classification of lung cancers into SCLC or NSCLC is sometimes disputable. An exemplary study revealed approximately 30% of SCLC-classified cancers which were in fact associated with NSCLC elements (Nicholson SA *et al.*, 2002). Among other human NSCLC-derived cell lines, NCI-H1703 also showed high levels of *Gpr19* mRNA expression. It is not clear whether this reflects either misclassification, a neuroendocrine phenotype, or *de novo* illegitimate expression. Thus, the discrimination between *Gpr19* high and *Gpr19* low expression lung cancers might not strictly follow histological boundaries. Whether GPR19 might serve as additional neuroendocrine marker in these malignancies would require further elucidation. Therefore, its expression status in other neuroendocrine carcinomas such as medullary thyroid carcinoma would be of interest (Adams MS and Bronner-Fraser M, 2009). Additionally, the detection of high levels of GPR19 protein using immunohistochemistry would argue in favor of its expression (and also functionality) being a crucial hallmark for these types of *Gpr19*-overexpressing carcinomas.

High *Gpr19* expression seen in SCLC patient-derived samples was also reflected on the cell line level. *Gpr19* expression was not evenly distributed among lung-derived cell lines. **Moreover, an on average bias towards higher *Gpr19* expression was observed in SCLC- versus NSCLC- or normal lung-derived cells** (figure 30 and figure 31). A few cell lines such as the SCLC cell line DMS 53 and the NSCLC cell line NCI-H1703 could be characterized by a genomic amplification of the chromosomal region covering the *Gpr19* gene locus (figure 32). Thus, genomic abnormalities are unlikely to be the sole cause of *Gpr19* overexpression as some of the cell lines showing highest *Gpr19* mRNA levels (e.g., NCI-H187 or NCI-H446) had no amplification of the *Gpr19* locus in their genome. In addition, the amplification of *Gpr19* detected in DMS 53 and NCI-H1703 cells was not a focal event as huge parts of the chromosome were found amplified (figure 33).

When comparing gene expression profiles of primary and metastatic melanoma, former reports had found *Gpr19* to be overexpressed in the metastases (Li S *et al.*, 2005; Riker AI *et al.*, 2008). Samples from metastatic melanoma patients were not included in the sample panel from the BioExpress® database. **However, samples from malignant melanoma did show a higher *Gpr19* mRNA expression when compared to samples from normal skin (figure 28 and figure 29).** These findings are further supported by many melanoma-derived cell lines being part of the proprietary Boehringer Ingelheim cell line gene expression database which highly expressed *Gpr19* mRNA (data not shown). Besides, *Gpr19* expression in melanoma fosters the notion of the cell type-specific expression of this receptor in neuroendocrine tumors (Takeda K *et al.*, 2007).

3. GPR19 is involved in proliferation and cell cycle regulation

3.1. GPR19 contributes to cell proliferation in human lung cancer-derived cell lines

Investigations on the role of GPR19 in lung cancer cell proliferation conferred a growth advantage in these cells. **Regardless of the histological classification of the cell line (SCLC or NSCLC), knockdown of *Gpr19* mRNA depressed cell proliferation and induced apoptosis.** These effects were assessed by the use of different experimental techniques such as confluence measurement, determination of metabolic cell activity, examination of cell morphology, and poly (adenosine diphosphate (ADP)-ribose) polymerase 1 (PARP1) cleavage (figure 36, figure 38, figure 39, and figure 41). Additionally, they were supported by proliferation and apoptotic indices which had been calculated on the basis of a multiple cellular parameter analysis (high content screening (HCS); figure 51). The validation of different *Gpr19*-targeting siRNAs was a prerequisite for these experiments, as the transfection of siRNAs can cause off-target effects not related to the knockdown of the gene of interest (Collinet C *et al.*, 2010).

These findings were consistent with earlier observations that proposed a role for GPR19 in cellular proliferation. **During mouse embryogenesis, in particular in the developing brain, high levels of *Gpr19* mRNA were initially observed in germ cell layers of the embryo** (neuroepithelium, neural plate) as determined by *in situ* hybridization. Subsequently, *Gpr19* mRNA accumulated in the neural plate, the subventricular zone, and other sites of cellular proliferation, from which neuronal cells emerge in the differentiating CNS. After embryogenesis, overall *Gpr19* signals in the adult mouse brain declined (Hoffmeister-Ullerich SA *et al.*, 2004). Additionally, **spermatogonia stem cells** – the type of proliferating cells in the testes that account for the constant production of sperms – **were proposed as a source of *Gpr19* expression** (Hoffmeister-Ullerich SA *et al.*, 2004). High *Gpr19* expression was also assigned to human embryonic stem cells (hESC; Assou S *et al.*, 2007).

Tumors can be considered as heterogeneous 'organs' as they do not only harbor malignant cells but also stromal cells such as tumor fibroblasts, cells of the immune system such as inflammatory cells as well as endothelial cells that form the inner lining of blood vessels needed for a tumor's blood supply. This heterogeneity can be partly modeled *in vitro* using 3-dimensional (3D) cell culture techniques (e.g., spheroid culture) that include the co-cultivation of cancer-associated fibroblasts (CAFs). With regards to the cellular phenotype, migration, signal transduction, and gene expression, cells grown as a 3D culture might differ from their counterparts growing adherently on the bottom of a culture plate (2D). Here, the modulation of the cytoskeleton might account for changes in signal transduction affecting in turn cell growth, migration, or apoptosis. Hence, a 3D culture would resemble the real situation *in vivo* more closely where cells interact with their surrounding neighbors and the extracellular matrix (Smalley KS *et al.*, 2006; Fischbach C *et al.*, 2007; Dolznig H *et al.*, 2011).

Gpr19 knockdown reduced proliferation in lung cancer cells growing adherently in 2D. However, many SCLC-derived cell lines formed floating clusters and did not attach to the culture plate bottom (e.g., NCI-H209, NCI-H345). Studies using 3D cell cultures combined with GPR19 loss of function (e.g., achieved via inducible *Gpr19* knockdown techniques) might assist in characterizing the contribution of this GPCR to the formation and proliferation of 3D tumor spheroids in the future. Additionally, the enclosed use of (cancer-associated) fibroblasts might help to unravel a potential involvement of the tumor stroma in this respect.

3.2. GPR19 plays a role during cell cycle progression in gap 2 (G₂)/mitosis (M) phase and is the first GPCR to show differential mRNA expression over the course of the cell cycle

In the NSCLC cell line NCI-H1703 and the SCLC cell line DMS 53, the involvement of GPR19 not only in proliferation but also in cell cycle regulation could be demonstrated with the help of RNA interference. GPCRs control signaling pathways that are typically associated with the recruitment of quiescent cells into the cell cycle (gap 0 (G₀)-gap 1 (G₁) phase transition) or with accelerated progression through G₁ (Dorsam RT and Gutkind JS, 2007; Spiegelberg BD and Hamm HE, 2007). Surprisingly, **knockdown of *Gpr19* affected progression through the cell cycle at a later stage, namely in G₂/M**. The conclusion that GPR19 might play a role during the G₂/M phase of the cell cycle is based on two independent lines of evidence, namely (i) the determination of deoxyribonucleic acid (DNA) content by flow cytometry and high content screening and (ii) the quantification of the G₂/M phase marker cyclin B1 and the mitosis marker phosphorylated histone H3 by immunocytochemistry. The mechanistic link between a GPCR and cell division during G₂/M phase is not intuitively evident. It is, however, worth pointing out that heterotrimeric G proteins of the G_i/G_o-subfamily are involved in the control of the mitotic spindle; they are thought to regulate the mitotic force generator and thus to promote chromosomal segregation (Wilkie TM and Kinch L, 2005). Furthermore, the CXC chemokine receptor 3 (CXCR3) was found to exhibit a differential protein

expression pattern during the cell cycle in primary cultures of human microvascular endothelial cells (HMVECs) with peaking protein levels in late DNA synthesis (S)/G2/M phases and this GPCR directly controlled cell proliferation (Romagnani P *et al.*, 2001).

The fact that **Gpr19 siRNA-treated cell populations showed increased numbers of cells with a DNA content characteristic for the G2/M phase** points towards a role of GPR19 in late stage cell cycle checkpoint control or cellular division. The population of cells in G2/M phase was found to be increased in both HCS and flow cytometry studies (figure 46, figure 47, and figure 48). Yet, in the HCS, NCI-H1703 cell population shiftings towards the G2/M phase were mostly at the expense of cells in G1 phase, whereas flow cytometry identified a diminished S phase population. Discrepancies in accompanying effects on G1 and S phase populations might be due to different detection methods used for discriminating cells in different cell cycle phases between HCS and flow cytometry. DNA content data (propidium iodide staining) obtained by flow cytometry were allocated to different cell cycle phases using a curve-fitting model for G1, S, and G2/M phase populations. In contrast, HCS analysis (Hoechst 33342 DNA staining) assigned cells to either sub G1, G1, S, G2/M, or above G2/M phase based on clear-cut phase discrimination of cell cycle phases from a control population (untreated cells).

In this context, it is of note that **in both methods (HCS and flow cytometry), incompletely separated cells had been excluded at best from subsequent analyses.**

Multiparametric HCS analysis allowed the exclusion of nuclei from further analyses when they were too large/too close together/overlapping (e.g., cells with a polylobed nuclear phenotype; figure 50). The exclusion of cells bearing a 4n DNA content inspite of not being in the G2/M phase of the cell cycle due to improper cell separation could also be achieved by flow cytometry. Here, cell doublets corresponding to data points with an untypical fluorescence signal in the propidium iodide area versus width graph allowed for their exclusion from the contribution to the G2/M phase cell population. Nevertheless, it is possible that some binucleated cells could not be excluded efficiently enough in order to rule out their contribution to the population of cells in G2/M phase in both HCS and flow cytometry. This is particularly true for cells treated with *Gpr19* siRNAs which resulted in the occurrence of binucleated and polylobed cells (figure 50).

The less prominent effect on the G2/M cell population seen upon *Gpr19* siRNA treatment in DMS 53 in comparison to NCI-H1703 cells might be due to the less efficient knockdown of *Gpr19* in DMS 53 cells (figure 46 and figure 47). This explanation is further fostered by the fact that *polo-like kinase 1 (Plk1)* siRNA-induced increases in the relative number of cells with a G2/M DNA content in flow cytometry were also more pronounced in NCI-H1703 than in DMS 53 cells. When the siRNA-mediated knockdown of *Plk1* had been examined on the message level, remaining *Plk1* levels in DMS 53 cells were higher compared to those in NCI-H1703 cells on day 2 after transfection (data not shown). Hence, **DMS 53 cells might in general be less amenable to siRNA transfection than NCI-H1703 cells** – at least regarding the optimized transfection procedure used in these studies.

In addition to an increased number of cells with G2/M phase DNA content, **cell populations treated with *Gpr19* siRNAs contained more cells that could be stained**

positively for the G2/M phase marker cyclin B1 and the mitosis marker phosphorylated histone H3 (figure 49). Cyclin B1 – together with its preferred binding partner cyclin-dependent kinase (CDK)1 – accounts for the regulation of proteins during late G2 phase and early mitosis (Brown NR *et al.*, 2007). The phosphorylation of histone H3 at Ser10 starts during late G2 phase but is mainly observed during mitosis when chromosome condensation occurs (Hendzel MJ *et al.*, 1997). Thus, these observations are consistent with a model where GPR19 impinges on checkpoint controls that allow for the transition through G2 and entry into mitosis (checkpoint for G2-M transition) or for the initiation of the separation of daughter cells (metaphase-to-anaphase transition; spindle assembly checkpoint).

However, the fact that the mitosis marker phosphorylated histone H3 was present in cells upon *Gpr19* knockdown might argue in favor of a role for this receptor during mitosis. It further supports the notion that the *Gpr19* knockdown-mediated increase in G2/M cells observed by flow cytometry and HCS might actually be a block of these cells in mitosis. Both flow cytometry and HCS could not allow for an accurate discrimination between cells in the G2 phase and cells in mitosis. Furthermore, as *Gpr19* knockdown induced cell death in lung cancer cells, these cells might undergo a mitotic-linked form of cell death called mitotic catastrophe which could result from the premature or inappropriate entry of cells into mitosis (Vakifahmetoglu H *et al.*, 2008). Indeed, *Gpr19* knockdown resulted in polylobed cells, and these nuclear aberrations could indicate the induction of mitotic catastrophe (Vakifahmetoglu H *et al.*, 2008; Caruso R *et al.*, 2011). Yet, the elucidation of the exact mode of cell death would require more detailed cell/nuclear morphology and biochemical characterizations.

Earlier findings also suggested that GPR19 might play a role in cell division. High *Gpr19* expression was found in murine spermatogonia stem cells of the testes (Hoffmeister-Ullerich SA *et al.*, 2004) and in spermatocytes undergoing meiotic cell division (Rossi P *et al.*, 2004)¹⁰¹. Besides, a meta-analysis comparing the transcriptome from human embryonic stem cells with differentiated cells found *Gpr19* to be upregulated in hESC (Assou S *et al.*, 2007). In a genome-wide siRNA screen, *Gpr19* was identified as a potential cell division gene (Neumann B *et al.*, 2010). Henrietta Lacks (HeLa) cells treated with two out of five siRNAs directed against *Gpr19* showed a binuclear or polylobed nuclear phenotype. However, it is of note that the proprietary Boehringer Ingelheim cell line gene expression database reported only a very weak expression of *Gpr19* in HeLa cells (data not shown). Nevertheless, similar nuclear phenotypic changes were also seen in the HCS analysis when NCI-H1703 cells highly expressing *Gpr19* had been treated with *Gpr19* siRNAs (figure 50). But a reliable automated detection and quantification of these cells was unsuccessful due to the limited accuracy of available algorithms for HCS data procession with regards to this specific problem.

As GPR19 is part of the GPCR protein family, its knockdown is supposed to interfere with an early stage of signal transduction. In contrast, the knockdown of *Plk1*, which

¹⁰¹ The sperm maturation process consists of spermatogonia undergoing mitotic cell division, spermatocytes undergoing meiotic cell division and spermatids undergoing differentiation into mature sperms (Rossi P *et al.*, 2004).

was included as positive control for an increase in the number of cells with a G2/M phase-specific DNA content, directly interferes with an essential downstream effector kinase that has various roles in M phase progression control (Petronczki M *et al.*, 2008). The depletion or knockdown of *Plk1* results in metaphase arrest but does not induce G2 arrest (Liu X and Erikson RL, 2003). This difference in pathway intervention might account for the more prominent effects (e.g., the increase in the cell population with a (G2/)M phase-specific DNA content and the increase in (G2/)M protein marker expression) seen with *Plk1* compared to *Gpr19* siRNAs (figure 46, figure 47, figure 48, and figure 49). **Hence, in contrast to the pleiotropic effects of PLK1 during the cell cycle, GPR19 might have a more focused function in cell cycle regulation.**

Proteins involved in cell cycle progression can be functionally regulated by various means such as subcellular location, posttranslational modification, protein-protein interaction, or *de novo* synthesis (Ohtsubo M *et al.*, 1995; Brown NR *et al.*, 2007). The family of cyclins represents the classical example of proteins involved in cell cycle regulation. They interact specifically with CDKs and owe their name to their differential expression patterns throughout the cell cycle. When investigating *Gpr19* mRNA expression over the course of the cell cycle, a similar differential expression pattern was observed for this GPCR. **The expression levels of the mRNA encoding GPR19 peaked when most cells were in S phase** (figure 54, figure 55, and figure 56). Rising levels of *Gpr19* mRNA could further be correlated with the increase in the relative numbers of cells in S phase and the decrease of the G1 population (figure 58). Besides, the known differential expression patterns of the mRNAs encoding cyclin B1 and cyclin E1 could be recapitulated (Maity A *et al.*, 1995; Ohtsubo M *et al.*, 1995; Maity A *et al.*, 1997; Penelova A *et al.*, 2005). The use of multiple stably expressed reference genes for data normalization as well as different cell synchronization agents further contributed to the validity of this method. Synchronization of NCI-H1703 cells with nocodazole was only partially successful (the propidium iodide histogram peaks reflecting cells in G1 and G2/M phase were almost evenly high after nocodazole treatment) which could therefore explain only subtle changes observed for the control expression patterns of *cyclin B1* and *cyclin E1* here (figure 57). This finding provides additional – albeit circumstantial – evidence for a role of GPR19 in the regulation of the cell cycle.

For soluble proteins, the observed mRNA expression pattern (peak expression in S phase) typically implies that the proteins are required for S phase transition. However, overexpression of GPR19 revealed that this receptor localizes to the plasma membrane (figure 34 and figure 35). Members of the GPCR family must mature through the secretory pathway to reach their presumed site of action where receptor activation leads to the initiation of a downstream signaling cascade (Dong C *et al.*, 2007; Achour L *et al.*, 2008). Transcription and translation are rapid processes (less than 1 min for a protein of 400 amino acids), but folding in the endoplasmic reticulum imposes a time lag of up to several hours (Hebert DN and Molinari M, 2007). Besides, subsequent trafficking through and maturation steps in the secretory pathway result in an additional delay prior to insertion of the protein into the cell membrane. While there are no concrete estimates for GPR19, pharmacochaperone-

triggered folding of the A1-adenosine receptor suggests that more than 5 hours are required for this receptor to reach the cell surface (Málaga-Diéguez L *et al.*, 2010). Thus, **assuming the validity of these underlying features for GPR19, a delay of several hours is to be anticipated between induction of mRNA expression and accumulation of GPR19 at the cell surface.** Given this inherent delay from mRNA translation to effector function, the expression of the GPR19 protein from *Gpr19* mRNA (peak expression during S phase) is timely for a membrane protein required for the G2/M phase.

GPR19 is not the only GPCR whose expression is cell cycle-dependent. **In primary cultures of HMVECs, the protein level of the chemokine receptor CXCR3 was found to be highest when cells exited S phase and entered G2/M** (Romagnani P *et al.*, 2001). However, the data shown in the present study refer to mRNA levels of *Gpr19* rather than accumulation of the protein at the cell surface. CXCR3 was also shown to be directly involved in the proliferation of endothelial cells: Engagement of its ligands interferon- γ -inducible protein of 10 kDa (IP-10) and monokine induced by interferon- γ (MIG) stalled cell proliferation in HMVECs. This effect could be reversed by a CXCR3-specific antibody.

Another example of cell cycle-dependent receptor expression was attributed to the cell surface nerve growth factor (NGF) receptors tropomyosin-related kinase A (TrkA) and p75 neurotrophin receptor (p75^{NTR}) in PC-12 cells derived from a rat adrenal medulla tumor (Urdiales JL *et al.*, 1998). TrkA protein expression started to rise during mitosis and peaked during early G1 phase. In contrast, the protein levels of p75^{NTR} declined at these stages of the cell cycle. The NGF-elicited cell cycle-dependent responses were proposed to be linked to the differential expression pattern of these receptors. Differentiation of PC-12 cells into cells with a neuronal phenotype was promoted by NGF stimulation during G1 phase (attributed to the action of TrkA). When added at subsequent stages of the cell cycle, NGF promoted progression through the cell cycle, attributed to its action on p75^{NTR}.

3.3. Overexpression of GPR19 influences neither proliferation nor cell cycle progression

In contrast to the inhibition of proliferation observed upon *Gpr19* message knockdown in both the SCLC cell line DMS 53 and the NSCLC cell line NCI-H1703, **neither HEK-293 nor NCI-H1703 cells were conferred an advantage regarding proliferation when they had been transiently transfected with GPR19 expression plasmids** compared to control cells (figure 42 and figure 43). This was true for both the gain in confluence (investigated only in HEK-293 cells) and the metabolic activity of these cells indicative of cell proliferation. The effects of transient receptor overexpression are thought to be most striking at early time points after transfection – transient gene expression usually bursts after 0.5 to 3 days (Colosimo A *et al.*, 2000). Upon cell division, the expression plasmids encoding for GPR19 are expected to be excluded from genomic duplication and subjected to subsequent loss. Therefore, a potential gain-of-function effect resulting from transient GPR19 overexpression might

not be detectable for multiple days after transfection. Overall effects were not expected to be as prominent as if these cells had been forced to overexpress GPR19 from a genome-integrated vector (permanent overexpression; stable transfection). Moreover, the transfection efficiency for both NCI-H1703 and HEK-293 cells was below 50% (turbo green fluorescent protein (tGFP) positive, propidium iodide negative cells). Hence, only less than half the cells in the whole cell population would be allowed to exhibit an altered proliferative phenotype at early time points after GPR19 expression plasmid transfection. Here, a possible pro-proliferative effect might be unraveled by the combination of stable GPR19 expression and 3D organotypic cultures in the future.

Transient plasmid transfection slightly influenced proliferation negatively in both HEK-293 and NCI-H1703 cells compared to untreated cells or cells treated only with transfection reagent but without any plasmid (figure 42 and figure 43). This effect was more prominent in NCI-H1703 cells and independent of whether the transfected vectors encoded any sort of GPR19 or tGFP or none of the above. Cells consume high amounts of energy when they are obliged to express proteins at high levels by genetic engineering. The energy needed for the artificial expression of proteins is taken away from the energy needed for cell growth and proliferation. Therefore, those cells often exhibit a slower than normal growth rate¹⁰².

Similarly, **neither HEK-293 nor NCI-H1703 cells showed impairments in cell cycle phase progression upon transient transfection with GPR19 expression plasmids** in comparison to control plasmid-transfected cells (figure 52 and figure 53). Again – as it was argued for the investigation of proliferation – the gain-of-function effects resulting from transient receptor overexpression (the transfection efficiency (relative number of tGFP positive, propidium iodide negative cells) for HEK-293 cells was 52.4% and for NCI-H1703 cells 36.3%) were not expected to be as evident as if gene overexpression had been achieved from a genome-integrated vector source. Nevertheless, cell cycle effects due to GPR19 overexpression could have been detected at early time points (e.g., day 2) after transfection when the transfected plasmids had not yet been subjected to serious dilution caused by non-propagation during cell division or nuclease-mediated degradation. However, this was not the case. The above mentioned impairments in energy homeostasis through the forced protein expression from a transfected plasmid might in turn have also affected the relative distribution of cells during the cell cycle.

The knockdown of *Gpr19* message mostly ablated the receptor and therefore diminished its designated signaling function in any case, either upon ligand binding or as a scaffolding protein, for instance. Overexpression of the receptor, however, did not necessarily need to result in its overactivation – unless the receptor could be rendered constitutively active. A GPCR at the cell surface might rather require other functional members of the receptor activation apparatus (e.g., putative ligand(s), GPCR-interacting proteins (GIPs), potential heteromerization partners, etc.) in order to execute its designated downstream signaling resulting in phenotypical changes. These prerequisites might have not been fully accounted for by the sole overexpression of GPR19. In addition, overexpression of a GPCR could interfere with

¹⁰² www.korambiotech.com/upload/bbs/2/tb07.pdf

signal transduction of other GPCRs and might therefore lead to the attenuation of their signaling action (Tubio MR *et al.*, 2010). **These results might further argue against GPR19 being a constitutively active receptor.**

4. E2 promoter binding factor (E2F) family members might regulate *Gpr19* gene expression in human lung cancer-derived cell lines

Gpr19 revealed a differential expression pattern during the course of the cell cycle in both the SCLC cell line DMS 53 and the NSCLC cell line NCI-H1703 with peaking mRNA levels during S phase. The regulation of gene expression essentially involves the recruitment of transcription factors to the promoter region, which in turn can engage other factors necessary for the initiation of gene transcription.

E2F transcription factors are known to activate the expression of genes at the G1-S transition crucial for cell cycle progression (Wells J *et al.*, 2000; Polager S and Ginsberg D, 2008; Poznic M, 2009) and could therefore account for cellular proliferation (Chen HZ *et al.*, 2009). A high number of genes whose involvement in cell cycle progression was shown are in fact E2F targets (Chen HZ *et al.*, 2009). Among the genes with an E2F target sequence in their promoter are genes involved in DNA synthesis (e.g., *DNA polymerase α* (Gorgoulis VG *et al.*, 2002), *dihydrofolate reductase*, or *thymidine kinase* (Wells J *et al.*, 2000)) and cell cycle control (e.g., *cell division cycle (Cdc)6* and *Cdc25* (Brown KC *et al.*, 2010), *E* and *A-type cyclins*, *cyclin-dependent kinase inhibitor 2a (Cdkn2a)*, and *Cdk2/4* (Gorgoulis VG *et al.*, 2002)) as well as transcription factors (e.g., the proto-oncogene *Myc* (Rabinovich A *et al.*, 2008), *E2f-1*, or *E2f-2* (Gorgoulis VG *et al.*, 2002)).

Based on an *in silico* approach, the promoter region of the gene encoding GPR19 in *Homo sapiens* was found to contain several candidate binding sites for E2F transcription factors. In concurrence with the situation in *Homo sapiens*, potential E2F binding sites within the *Gpr19* promoter region could also be detected in *Pan troglodytes*, *Macaca mulatta*, *Mus musculus*, and *Xenopus tropicalis*. **Chromatin immunoprecipitation (ChIP) performed with antibodies against E2F family members 1, 2, 3, and 4 allowed for the recovery of the *Gpr19* promoter in human lung cancer-derived cell lines DMS 53 (SCLC), NCI-H1703 (NSCLC), NCI-H446 (SCLC), and SHP-77 (SCLC; figure 60).** Hence, these results provide conclusive evidence that at least one of the predicted E2F binding sites – namely at position -15 and/or -185 upstream of the *Gpr19* open reading frame (ORF) – was in fact occupied by E2F-1, E2F-2, E2F-3, and E2F-4 in these cells. Binding sites for E2F-1 and E2F-4 were shown to lie mostly within 2 kilobases (kb) of a transcription start site (Xu X *et al.*, 2007) and this was also true for the E2Fs binding to the *Gpr19* promoter. Further, the cloning of *Gpr19* promoter fragments of different length with and without E2F binding site integrity at positions -15 and/or -185 upstream of a luciferase reporter identified the E2F consensus sequence at -15 to be predominantly important for sustained gene expression in HEK-293 and NCI-H1703 cells. In contrast, the E2F binding site at position -185 was more important for reporter gene expression in DMS 53 cells (figure 62). It

might be possible that both E2F binding sites are in use for the activation of *Gpr19* gene expression in a cell-specific manner. In all three cell lines tested, the combined abolition (positions -15 and -185) led to the most pronounced reduction of luciferase reporter expression. Nevertheless, reporter gene expression was not completely attenuated when these positions had been removed from the promoter fragment indicating the involvement of yet unknown additional transcriptional regulators in *Gpr19* gene expression.

HEK-293 cells did not express *Gpr19* endogenously (figure 31). Nevertheless, a similar luciferase expression pattern as observed in NCI-H1703 cells was recovered when HEK-293 cells had been transiently transfected with *Gpr19* promoter fragment-containing luciferase reporter plasmids. This could be due to the fact that transcription factors might unrestrictedly engage a promoter region on plasmids whereas chromatin structures induced by histone tail methylation and acetylation patterns, for instance, might normally render the same promoter region inaccessible.

The regulation of gene expression by transcription factors is very complex as their pure binding to the promoter region of a gene does not necessarily account for its expression. Transcription factors can be regulated by interaction with heteromerization partners, activators, or repressors; their action depends on chromatin structure or the presence of enhancer elements. Besides, the binding of different transcription factors to the same promoter region or even the same consensus sequence may mediate different effects on gene transcription (Paranjape SM *et al.*, 1994; Boyd KE and Farnham PJ, 1999).

Apart from the confirmed binding of E2F transcription factors to the promoter region of *Gpr19*, **additional transcription factors might be involved in the regulation of *Gpr19* gene expression**. In the murine striatum and hippocampus, *Gpr19* mRNA expression was linked to the functional presence of **cyclic adenosine monophosphate (cAMP)-responsive element modulator (CREM) and cAMP-responsive element binding protein (CREB**; Lemberger T *et al.*, 2008). CREM and CREB are classically activated by phosphorylation through kinases upon cellular stimulation with cAMP, Ca²⁺, or growth factor signals (De Cesare D *et al.*, 1999). They bind with high affinity to the **cAMP-responsive element (CRE)** on a palindromic 5'-T-G-A-C-G-T-C-A-3' site and with lower affinity to the so-called **half-CRE site** (consensus sequence 5'-C-G-T-C-A-3'). However, gene transcription can be fostered by the recruitment of the CREB-binding protein (CBP; Piera-Velazquez S *et al.*, 2007). This co-activator of transcription possesses histone acetyltransferase activity rendering the local chromatin more accessible to its self-mediated recruitment of the general transcription machinery (De Cesare D *et al.*, 1999). **The *Gpr19* promoter also harbors a half-CRE site at position -587 upstream of exon 1**, whose contribution to the regulation of gene expression might be explained by the attenuation of *Gpr19* transcription when CREM and CREB had been inactivated (Lemberger T *et al.*, 2008). CBP was further described to interact with E2F-1 and to function as its co-activator (Trouche D *et al.*, 1996).

In addition, theoretical binding of the Pit1/Oct2/unc-86 (**POU**) family of transcription factors to the *Gpr19* promoter at position -875 upstream of the *Gpr19* ORF was retrieved by the University of California, Santa Cruz (UCSC) genome browser *in silico* search. Those transcription factors are ubiquitously-expressed and were assigned

diverse cellular roles such as the regulation of housekeeping genes or the determination of developmental or cell type-specific cell fate decisions. They are expressed in many different cancer tissues and one family member, BRN2, was shown to be involved in melanoma cell proliferation. Their contribution to tumorigenesis is likely mediated by direct or downstream transcriptional targets (Cook AL and Sturm RA, 2008). POU proteins have further shown their ability to interact with the p300/CBP co-activators of transcription (Sugihara TM *et al.*, 2001; Cook AL and Sturm RA, 2008).

The hypothesis that the E2F family of transcription factors is not exclusively responsible for *Gpr19* gene expression is fostered by results obtained from the luciferase reporter study in which the reporter gene was set under the control of *Gpr19* promoter fragments (figure 62). The first 300 base pairs (bp) of the *Gpr19* promoter, which contain potential E2F binding sites (positions -15 and -185), were sufficient for reporter gene expression in HEK-293, NCI-H1703 and DMS 53 cells. However, the larger promoter fragment (1,000 bp) augmented this expression. This 1,000 bp fragment not only harbors both predicted E2F binding sites but also the hypothesized half-CRE (position -587) and POU (position -875) binding sites. **Thus, in addition to the action of E2F family members, a synergistic role of both the CREM/CREB/CBP-recruiting half-CRE site and a potential POU binding site in the promoter of *Gpr19* might be conceivable.** ChIP assays as well as reporter gene expression using *Gpr19* promoters deficient for these respective transcription factor binding sites would shed more light on their involvement in *Gpr19* gene expression regulation.

The family of E2F transcription factors can be subdivided into activators (E2F-1, E2F-2, and E2F-3) and repressors (E2F-4, E2F-5, E2F-6, E2F-7, and E2F-8) of gene transcription – a classification also reflected by their primary structure (Polager S and Ginsberg D, 2008; Chen HZ *et al.*, 2009). Transactivation and repression result from interactions with different cofactors. E2F-4 and E2F-5 are recruited to promoters during G0 and early G1 phase. They prevent quiescent and differentiated cells from entering the cell cycle or progressing through G1 phase (Chen HZ *et al.*, 2009). Upon mitogenic stimulation, E2F-1, E2F-2, and E2F-3 accumulate in late G1 phase and cause a pattern of gene expression that drives cells into S phase. Their combined loss induces cell cycle arrest and an oncogenic role has been described for them in many cancers (Attwooll C *et al.*, 2004; Chen HZ *et al.*, 2009). During late S phase, these cell cycle-promoting signals are attenuated by E2F-6, E2F-7, and E2F-8 (Chen HZ *et al.*, 2009). Classification of E2Fs into activators and repressors of gene transcription is an oversimplification, because some isoforms can mediate both transactivation and repression. Another level of complexity and target promoter specificity is added by the heterodimerization of E2F members E2F-1 to E2F-6 with dimerization partner proteins (DP1, DP2, DP3, and DP4; E2F-7 and E2F-8 only form homodimers or E2F-7–E2F-8 heterodimers; Polager S and Ginsberg D, 2008). However, **ChIP results documented the binding of three activating E2F isoforms (E2F-1, E2F-2, and E2F-3) to the *Gpr19* promoter** in unsynchronized cell populations of human lung cancer-derived cell lines (figure 60). Binding of the repressor E2F-4 might reflect its recruitment to the *Gpr19* promoter during early G1 phase and subsequent displacement with activator E2Fs in late G1 and early S phase leading to *Gpr19* transcription. Besides,

E2f-1, *E2f-2*, and *E2f-3* expression levels in SCLC patient samples were equally high as observed for *Gpr19* compared to NSCLC samples and samples from normal lung controls (figure 63). **Thus, it appears justified to conclude that there might be a cause-and-effect relation between E2F binding to the *Gpr19* promoter and the observed accumulation of the mRNA coding for GPR19 during S phase.**

E2Fs can be regulated by the retinoblastoma (RB) protein family (retinoblastoma-associated protein 1 (RB1), retinoblastoma-like protein 1 (p107), and retinoblastoma-like protein 2 (p130)). Activator E2Fs (E2F-1, E2F-2, and E2F-3) are preferentially bound by RB1 which inhibits their transcription-activating ability. This is abrogated when RB1 gets hyperphosphorylated (Chen HZ *et al.*, 2009). E2Fs mediating transcriptional repression when bound to a promoter either associate with all three RB family proteins (E2F-4) or preferentially interact with p130 (E2F-5) leading to the recruitment of co-repressors such as histone deacetylases and gene silencing. The activity of E2F-6, E2F-7, and E2F-8 is presumably not regulated by RB proteins (Attwooll C *et al.*, 2004; Chen HZ *et al.*, 2009).

Inactivation of the RB1 regulatory pathway – the main regulator of E2F activity at the G1-S transition of the cell cycle – was described to happen in most lung cancers (Wikenheiser-Brokamp KA, 2006). Both overexpression of activator E2Fs and loss of RB1 protein function occur very frequently in SCLC (Kitamura H *et al.*, 2008; Pleasance ED *et al.*, 2010). In NSCLC, however, RB1 is preferentially rendered inactive due to accelerated phosphorylation by CDK4 or CDK6 whose upstream regulator CDKN2A (p16 family member) is often inactivated. Besides, cyclin D1, the coactivator of CDK4 and CDK6, was found overexpressed in many NSCLC cases (Wikenheiser-Brokamp KA, 2006; Kitamura H *et al.*, 2008).

DMS 53 (SCLC) and NCI-H1703 (NSCLC) cells harbor no mutation in the *Rb1* gene which is the result from Next Generation Sequencing approaches on cancer cell lines (proprietary Boehringer Ingelheim Next Generation Sequencing cell line genomic database; data not shown). However, elements upstream of RB1 could render it inactive. All these events would equip a lung cancer cell with increased levels of free activator E2Fs destined to drive proliferation by selective gene expression. As activator E2Fs, which are mainly linked to G1-S specific gene transcription, were shown to bind to the promoter region of *Gpr19*, the paradigm of *Gpr19* expression being regulated by E2Fs in lung cancer cells is fostered.

The observation that *Gpr19* mRNA was present at high levels in the immortalized cell line IB3-1 further supports the conclusion that *Gpr19* was under the control of the RB1-E2F regulatory pathway (figure 31). This cell line was derived from the lung epithelium of a patient suffering from cystic fibrosis with the help of a hybrid virus. Accordingly, IB3-1 cells contain high levels of SV40 large T antigen (Zeitlin PL *et al.*, 1991), which inactivates RB1 and therefore derepresses E2F-dependent transcription (Jha KK *et al.*, 1998).

Hence, RB1- and E2F-dependent transcription may not only regulate S phase-specific genes but also control the expression of genes that are required at later stages, e.g., during G2/M phase. This might be particularly true for membrane proteins subjected to intracellular trafficking like GPR19.

5. GPR19 might exhibit different functional characteristics in the central nervous system than in lung cancer

Various parts and cell types of the CNS have been described to be the predominant site of *Gpr19* expression (O'Dowd BF *et al.*, 1996; Hoffmeister-Ullerich SA *et al.*, 2004). This could also be confirmed by *Gpr19* gene expression data from normal and cancerous tissue samples as part of the BioExpress® database (figure 28 and figure 29). Further, GPR19 was associated with proliferation in lung cancer-derived cell lines as *Gpr19* message abrogation by RNA interference caused growth inhibition and cell death. In contrast, **the CNS is not characterized by the presence of highly proliferating cells**; the potential of neurons to regenerate after tissue injury is rather limited as observed in many neurodegenerative diseases such as stroke, spinal cord injury, or amyotrophic lateral sclerosis (Cavallucci V and D'Amelio M, 2011). Further, the expression of *Gpr19* in glioblastoma was slightly reduced in comparison to normal tissues of the CNS (figure 28 and figure 29). What seems to be contradictory at first glance might be explained by the action of different types of transcription factors in different tissues. In lung cancer-derived cells, the expression of *Gpr19* was found to be differentially regulated during the course of the cell cycle with a peak expression during S phase which is likely mediated by some members of the E2F family of transcription factors acting during G1-S transition. However, **in cells of the CNS, different promoter regions of *Gpr19* and therefore different transcription factors might be in preferential use for the expression of this GPCR**. Disparities among different tissues in promoter usage for gene expression have been demonstrated (Mahendroo MS *et al.*, 1993; Sun H *et al.*, 2011).

On the other hand, **lineage-specific effects have also been shown for E2F family members in the CNS and the roles of E2F-1 and E2F-3 differ in the developing and in the adult brain**. During CNS development, proliferating cells were found to express *E2f-1*, *E2f-2*, and *E2f-5*, whereas only differentiated cells allowed for the detection of *E2f-4* expression (Swiss VA and Casaccia P, 2010). Differential *E2f* expression patterns might further account for the differences in *Gpr19* expression seen in the developing and adult murine CNS (Hoffmeister-Ullerich SA *et al.*, 2004).

In addition, **GPR19 might have cellular functions different from the regulation of proliferation and cell cycle progression observed in lung cancer-derived cell lines**. These functions might be more important in cells of the adult CNS. They might therefore repress the proliferation-promoting action of GPR19 through the use of different transcriptional regulators or through proteins that counteract this function, for instance. Hence, differences in GPCR phosphorylation can occur in a tissue-specific manner leading in turn to the employment of different signaling pathways and receptor regulatory features (Tobin AB *et al.*, 2008).

6. GPR19 ligand engagement and G protein coupling remain elusive

Gpr19 knockdown by siRNAs resulted in growth inhibition of human lung cancer cell lines. The expression of a GPCR does not *per se* render a cell susceptible to regulation by the receptor – the ligand must also be present. It might therefore be possible that GPR19-expressing cells could also synthesize and release its agonist which could lead to an autocrine receptor stimulation loop. Alternatively, the receptor could have a high level of basal activity and engage its cognate G protein(s) in the absence of an agonist (Freissmuth M *et al.*, 1991; Schütz W and Freissmuth M, 1992). GPR19 was previously proposed to couple to G_i therefore inhibiting adenylyl cyclase because it engaged a chimeric fusion protein comprised of G_{α_q} and the last five amino acids of G_{α_i} (Bresnick JN *et al.*, 2003). **In an attempt to verify G_i -dependent inhibition of cAMP formation via GPR19, it was not possible to detect an effect of pertussis toxin on cAMP accumulation in NCI-H1703 cells** (figure 45). As the pertussis toxin-catalyzed carboxy-terminal ADP-ribosylation of $G_{\alpha_i}/G_{\alpha_o}$ blocks the access of receptors to these G proteins, this manipulation ought to have unmasked constitutive inhibition of cAMP accumulation (Seifert R and Wieland T, 2006). The pertussis toxin-induced increase in cAMP accumulation observed in HEK-293 cells transfected only with CRHR1 proves that constitutive G protein coupling of GPR19 ought to have been detectable, if it had occurred. Furthermore, pertussis toxin has been described to abolish A1R-mediated inhibition of cAMP accumulation (Waldhoer M *et al.*, 1999). Similarly, **conditioned medium (supernatants from cell lines NCI-H1703 and NCI-H345 which were found to highly express *Gpr19* mRNA) did not have any effect on cAMP accumulation in HEK-293 cells that had been transfected with GPR19 expression plasmids** (figure 44). Either the putative ligand of GPR19 was not present in conditioned media or GPR19 does not couple to a G protein with modulating effects on cellular cAMP levels.

Thus, **it appears unlikely that the action of GPR19 in the G2/M phase of the cell cycle could arise from coupling to G_i/G_o** . Here, the examination of different second messengers such as inositol-1,4,5-trisphosphate (IP3) might help to unmask the coupling of GPR19 to different G proteins than G_i/G_o in the future. Further progress in this area is contingent on the identification of the cognate agonist(s) of GPR19. Finally, **a function different from direct signaling via G proteins might also be conceivable for GPR19**, e.g., recruiting G protein-independent pathways via β -arrestins (Shukla AK *et al.*, 2011), via direct binding of tyrosine kinases (Venema RC *et al.*, 1998), exchange factors for small G proteins (Gsandtner I *et al.*, 2005), or lipid kinases (Bousquet C *et al.*, 2006), or by acting as a scaffold protein (Schmid MC *et al.*, 2011). Based on its primary sequence, GPR19 harbors a type I PSD-95/DLP/ZO-1 (PDZ)-binding motif at its carboxy-terminus (figure 6; Liu M and Horowitz A, 2006). This motif could serve as a ligand for proteins containing a PDZ domain leading to their recruitment to GPR19 and subsequent G protein-independent signaling (Bockaert J *et al.*, 2004).

7. GPR19 – a receptor applicable for targeted cancer therapy

Chemotherapy plays a major role in the treatment of multiple types of cancer. However, many long-serving agents lack tumor specificity. They interfere with the ability of cells to proliferate and divide. Among them are for example topoisomerase inhibitors (e.g., topotecan, etoposide), DNA intercalating agents (e.g., cisplatinum), anti-mitotic substances (e.g., paclitaxel), or anti-metabolites (e.g., methotrexate). Hence, proliferating cancer cells are preferentially hit by these compounds but their cytotoxic potential also affects non-transformed cells and can cause severe side effects (Chari RV, 2008).

These indiscriminating cell killing strategies are more and more replaced by **targeted tumor therapy** in which tumor-associated features resulting from genetic changes are hit by pharmaceutical agents (Sharma SV and Settleman J, 2010). This concept promises to allow for a better therapeutic effect as normal cells would be affected less severely. Examples in which targeted tumor therapy has been applied to inhibit the enzymatic activity of a kinase include epidermal growth factor receptor (EGFR)-targeting in NSCLC patients with EGFR mutation (Yoshida T *et al.*, 2010), targeting of the fusion protein kinase BCR-ABL1 (short for 'breakpoint cluster region' on chromosome 22 and 'Abelson murine leukemia viral oncogene homolog 1' on chromosome 9) prevalent in chronic myeloid leukemia (CML; Maekawa T *et al.*, 2007), or B-Raf (rapidly accelerated fibrosarcoma isoform B)-targeting in melanoma patients with B-Raf mutation (Wellbrock C and Hurlstone A, 2010), for instance. Another strategy aims at targeting cell surface markers specific for or overexpressed in tumors with antibodies to which cytotoxic drugs are conjugated (Chari RV, 2008). Further, antisense molecules such as siRNAs could interfere specifically with the expression of oncogenes to which a tumor has become addicted (Wacheck V and Zangemeister-Wittke U, 2006).

Much of the expected success of targeted tumor therapy is linked to the concept of **oncogene addiction**, which describes the dependence of a cancer cell on the sustained activity of one or a few genes for the maintenance of its malignant phenotype (Weinstein IB and Joe A, 2008). Hence, many approaches in targeted tumor therapy aim at specifically inhibiting the activity of an oncogene. When the *Gpr19* message in *Gpr19*-expressing lung cancer-derived cell lines was attenuated by the use of RNA interference, proliferation of these cells was diminished eventually leading to cell death (figure 36, figure 38, figure 39, and figure 41). Thus, it seems justified to speak of **GPR19 as a vulnerable target**, which – when overexpressed in lung cancer cells – is involved in cell proliferation. However, *Gpr19* expression did not result in any gain of proliferation in neither HEK-293 nor NCI-H1703 cells transiently transfected with GPR19 expression plasmids. These studies have not been performed in non-malignant cells, but they indicate that GPR19 might lack the ability to transform cells into a malignant phenotype. In very few lung cancer-derived cell lines examined (including DMS 53 and NCI-H1703), the overexpression of *Gpr19* could be explained by amplification of the *Gpr19*-containing chromosomal region. None of the lung cancer-derived cell lines listed in the proprietary Boehringer Ingelheim Next Generation Sequencing cell line database had any mutation in the gene encoding GPR19. These findings might argue against the strict categorization of *Gpr19* as an

oncogene (Croce CM, 2008). Instead, its overexpression particularly seen in human lung cancer-derived cell lines and SCLC patient samples might be accounted for by the deregulated action of members of the E2F family of transcription factors, which is very often observed in lung cancer (Wikenheiser-Brokamp KA, 2006; Kitamura H *et al.*, 2008).

The present work highlights GPR19 as a potential drug target for the treatment of a subset of *Gpr19*-overexpressing lung cancers.

Although mainly SCLC and not NSCLC patient samples exhibited high levels of *Gpr19* mRNA in this study, all experiments conducted in both the SCLC cell line DMS 53 and the NSCLC cell line NCI-H1703 led to concordant results. Hence, individual screening of lung cancer patients for *Gpr19* expression status might be an important necessity regardless of histological typing.

The CNS is the predominant tissue where high *Gpr19* expression was found in healthy individuals. Due to the existence of the **blood-brain-barrier**, the limited accessibility of the CNS for the delivery of pharmaceutical compounds is often a problem when their site of action lies in the CNS (Witt KA and Davis TP, 2006). Here, this physical and enzymatic barrier could be made use of to protect the CNS from drugs targeting GPR19 in cancerous tissues.

When looking at target identification and validation programs for the treatment of cancer patients, the main focus of research falls into the area of elucidating the contributions of effector kinases and membrane-spanning receptor tyrosine kinases to tumorigenesis (Sharma SV and Settleman J, 2010). The large family of human G protein-coupled receptors with more than 800 predicted members, however, seems to be left aside here. Though some GPCRs have revealed their potential as well-druggable targets for the treatment of various diseases (Schlyer S and Horuk R, 2006; Lundstrom K, 2009) – a fact that is generating growing interest in GPCRs when searching for novel therapeutic strategies also in oncology. The results described in this work strongly support the notion of GPR19 as a specific drug target when overexpressed in lung cancer.

8. Summary

Taken together, the described observations point to a role for GPR19 in cellular proliferation of human lung cancer cells which overexpress *Gpr19* mRNA. They further argue in favor of a contribution of GPR19 in cell cycle regulation – possibly at late stages of the G2 phase but more likely during mitosis – as *Gpr19* mRNA levels peak during S phase. This cell cycle-dependent expression pattern is likely to be mediated by E2F transcription factors. To the best of knowledge, GPR19 is the first GPCR whose mRNA has been shown to be expressed in a cell cycle-dependent manner and to impinge on G2/M transition in human tumor cells. It can hereby be called a '**cycloceptor**'. However, insights into signal transduction mechanisms that account for its proliferation and cell cycle regulatory effects as well as a physiological ligand for this orphan receptor remain to be determined. So far, only little is known about possible effector activation pathways of GPR19. Finally, the insights from this work could also be of relevance to understand the physiological role of GPR19 during embryogenesis and brain development.

VIII. Appendix

1. *Gpr19* genomic sequence

The National Center for Biotechnology Information (NCBI) gene identification number for human *Gpr19* is 2842 and the Ensembl gene identification number is ENSG00000183150. *Gpr19* is located on the reverse strand of chromosome 12 (short arm; 12p12.3) at the position 12,849,121 to 12,813,995 and the exon-intron structure is shown in table 15.

Table 15: The gene structure of human *Gpr19*. *Gpr19* is composed of four exons (**purple**; coding sequence (CDS) in **black**) spaced by three introns (**blue**). The table further includes the end of the 5' upstream and the beginning of the 3' downstream sequence (**green**). This gene structure is adopted from Ensembl.

Exon / Intron	Start	End	Length	Sequence
5' upstream sequence			gtttgcatgcatgctctggctcatcatttttagcgcgcaaaagtttcaaaa
ENSE00001806684	12,849,121	12,848,999	123	CTTTCGCCCTAGTCAGAGCCGGTCCGATTTCGCCCTTGGGGAGTGTCCGTCGCCGTTGATC TCATGCATTACGTTACACAAACCACATTCTATGAGATTTTCGACGCCAAAAGTCCACAAG CTC
Intron 1-2	12,848,998	12,848,446	553	gtatggtcatcccttctttccggtt.....aatctgacctctttttgtctctcag
ENSE00001791213	12,848,445	12,848,393	53	GATATATGGGACACCTGCCACCGGCATTGGATTTCGCCCCGCAACATCTTAAAG
Intron 2-3	12,848,392	12,837,442	10,951	gtaccaccaaacacctgaagtgtct.....cagcgtcatctgtctccctaacag
ENSE00001294881	12,837,441	12,837,285	157	GAAGCAGGCTCTGAGCCAAGGGGAAGCCAGGACAGAAATGAATGTCTTTCCAGGCTTT CCTGGTGGTTTATGCCATTCTCCAACTCCTATGCAAGGGCTATTCTGACCAAGAAGAT CTAAACGAAACGCTCTCTGAAATCAAGTCGGATGAAG
Intron 3-4	12,837,284	12,815,405	21,880	gtatgtagataggatcccttggat.....cttcattcttcttttccccaccag
ENSE00001322526	12,815,404	12,813,995	1,410	AATTAAACAGAAAAAAGTCAATATGGTTTTTGCCTCACAGAAATGGATAACAGCAAGCCACA TTTGATTATTCCTACACTTCTGGTCCCTCCAAAACCCGACGCTGCATGAAAACAGCCAC ACCTCTGCCAAGCCAAATCCTGATGGAATTAAGTGAGGAGCACAGTTGGATGAGCAACCA AACAGACCTTCACTATGTGCTGAAACCCGGGAAAGTGGCCACAGCCAGCATCTTCTTTGG GATTCGTGGTTGTTTTCTATCTTCGCCAATTCCTGGTTTGTTCGTCATCCATAGGAG TAGGAGGACTCAGTCTACCACCAACTACTTTTGTGGTCTCCATGGCATGTGCTGACCTTCT CATCAGCGTTGCCAGCAGCCCTTTGCTCCTGCTCCAGTTCACCCTGCAAGGTGGACGCT GGTACTGCAACGTGCAAGGTTGTCGGATATTTCAATATCTCACTCCAGGTGCCAGAT CTACGTTCTCCTCCTCATCTGCATAGACCGGTTCTACACCATCGTCTATCCTCTGAGGCT CAAGCTGTCCACAGAAAAAGCCAAAGAAATGATTGGGCATCGTGGCTCTTGTATGCCAGG CTTTGTGACCCCTGTGCTCTTTTTCTATGGCTCCAACTGGGACAGTCAATGTAACATTT CCTCCCTCCTCTGGGAAGGCACTGCCTACACTGTCTCCACTTCTTGGTGGGCTTTGT GATTCATCTGCTCCTATAATTTTTATTTACCAAAAAGGTCATAAAAATATATTTGGAGAA AGCCACAGATGCCCAACCGGTGAGGAGCAAAATGAACATTTCCCTCCGCAAAAAGTGA AACTATCAAGATGTTCCCTCAATTTAAATCTGTTGTTTTGCTCTCCTGGCTGCCCTTTCA TGAGCTCAGCTATGGCACCCCATGAACAAGACTATAAGAAAAGTTCCTTGTTTTCAC AGCTATCACATGGATATCCTTTAGTTCTTCAGCCTCTAAACCTACTCTGATTTCAATTTA TAATGCCAATTTTCGGAGAGCGATGAAAGAGACTTTTTGCATGCTCTCTATGAAATGTTA CCGAAAGCAATGCCATATACTATCACAAAGTTCAAGGATGCCCAAAAAAACTACGTTGG CATTTCCAGAAATCCCTTCCATGGCCAAAATATTACCAAGACTCGATCTATGACTCAT TGACAGAGAACCAAGCAAAAAAGCTTCTTGGCCATTAACTCAAATCCACCAAAATAC TTTTGCTAAAGTCTCATTCTTTCAATTGTTATGCCACAGAGATTA AAAAGCTTTAACTA TAAAAACAGAACTATTTACATATTTGTTTTCACTCAACTTTCCAGGAAATGTTTTAT TTTGTAAAATGCATTCATTGTTTACTGTA
3' downstream sequence				gtttttgtgggttttattttacttgctttttatgttttagggaaaagcgtt.....

2. *Gpr19* messenger ribonucleic acid (mRNA) sequence

The NCBI accession number for the mRNA (5' to 3' direction) of human *Gpr19* is NM_006143. It is composed of four exons (exon 1: position 1 to 123; exon 2: 124 to 176; exon 3: 177 to 333; exon 4: 334 to 1743) and the coding sequence lies entirely in exon 4 (356 to 1603, **bold**). This accession number encodes the GPR19 protein variant with Ile at amino acid position 189 (A at transcript position 920; see non-synonymous single nucleotide polymorphisms (SNPs) in table 16).

```

1 CUUUCCGCCU AGUGAGAGGC GGUCCGAUUU GGCCCUUGGG GAGUGUCCGU CGCGUUGAUC
61 UGAUGGAUUC ACGUACACAA CACCACAUUC UAUGAGAUUU UGCAGGCAAA AGUCCACAAG
121 CUCGAUUAU GGGACACCUG CACCGGCAUU GGAUUUGGCC CCGCAACAUC UUAAAGGAAG
181 CAGGCUGUGA GCCAAGGGGA AGGCAGAGGA CAGAAAUGAA UGUGUUUCCA GGCUUUCCUG
241 GUGGUUUUUG GCAUUCUCCA AACUCCUAUG CAAGGGCUAU UCCUGACCAA GAAGAUCUAA
301 AGAGAACGUC UCUGAAAUCA AGUCCGGAUG AAGAAUUAAG AGAAAAAAG UGAAUAUGGU
361 UUUUGCUCAC AGAAUGGAUA ACAGCAAGCC ACAUUUGAUU AUUCCUACAC UUCUGGUGCC
421 CCUCCAAAAC CGCAGCUGCA CUGAAACAGC CACACCUCUG CCAAGCCAAU ACCUGAUGGA
481 AUUAAGUGAG GAGCACAGUU GGAUGAGCAA CCAAACAGAC CUUCACUAUG UGCUGAAACC
541 CGGGGAAGUG GCCACAGCCA GCAUCUUCUU UGGGAUUCUG UGGUUGUUUU CUAUCUUCGG
601 CAAUCCUG GUUUGUUUGG UCAUCCAAG GAGUAGGAGG ACUCAGUCUA CCACCAACUA
661 CUUUGUGGUC UCCAUGGCAU GUGCUGACCU UCUCAUCAGC GUUGCCAGCA CGCCUUUCGU
721 CCUGCUCAG UUCACCACUG GAAGGUGGAC GCUGGGUAGU GCAACGUGCA AGGUUGUGCG
781 AUAUUUCAA UAUCUCACUC CAGGUGUCCA GAUCUACGUU CUCCUCUCCA UCUGCAUAGA
841 CCGGUUCUAC ACCAUCGUCU AUCCUCUGAG CUUCAAGGUG UCCAGAGAAA AAGCCAAGAA
901 AAUGAUUGCG GCAUCGUGGA UCUUUGAUGC AGGCUUUGUG ACCCCUGUGC UCUUUUUCUA
961 UGGCUCCAAC UGGGACAGUC AUUGUAACUA UUUCCUCCCC UCCUCUUGGG AAGGCACUGC
1021 CUACACUGUC AUCCACUUCU UGGUGGGCUU UGUGAUUCCA UCUGUCCUCA UAAUUUUUUU
1081 UUACCAAAG GUCAUAAAAU AUAUUUGGAG AAUAGGCACA GAUGGCCGAA CGGUGAGGAG
1141 GACAAUGAAC AUUGUCCUC GGACAAAAGU GAAAACUAUC AAGAUGUUC UCAUUUUAAA
1201 UCUGUUGUUU UUGCUCUCCU GGCUGCCUUU UCAUGUAGCU CAGCUAUGGC ACCCCCAUGA
1261 ACAAGACUAV AAGAAAAGUU CCCUUGUUUU CACAGCUAUC ACAUGGAUAV CCUUUAGUUC
1321 UUCAGCCUCU AAACCUACUC UGUUAUCAAU UUAUAAUGCC AAUUUUCGGA GAGGGAUGAA
1381 AGAGACUUUU UGCAUGUCCU CUAUGAAAUG UUACCGAAGC AAUGCCUAUA CUAUCACAAC
1441 AAGUUAAGG AUGGCCAAA AAAACUACGU UGGCAUUUCA GAAAUCCUUC CCAUGGCCAA
1501 AACUAUUACC AAAGACUCGA UCUAUGACUC AUUUGACAGA GAAGCCAAGG AAAAAAAGCU
1561 UGCUGGCCC AUUAACUCAA AUCCACCAA UACUUUUGUC UAAAGUUCUCA UUCUUUCAAU
1621 UGUUAUGCAC CAGAGAUUAA AAAGCUUUAA CUAUAAAAAC AGAAGCUAUU UACAUUUUG
1681 UUUUCACUCA ACUUUCCAAG GGAAAUGUUU UAUUUUGUAA AAUGCAUUCA UUUGUUUACU
1741 GUA

```

3. *Gpr19* codon-optimized coding sequence (mRNA)

The codon-optimized *Gpr19* coding sequence (5' to 3' direction) was introduced in the pcDNA3.1 (+) expression vector downstream of a cytomegalovirus (CMV) promoter for the expression of GPR19 (see table 5).

```

1  AUGGUGUUCG CCCACCGGAU GGACAACAGC AAGCCCCACC UGAUCAUCCC CACCCUGCUG
61  GUGCCCCUGC AGAACAGAAG CUGCACCGAG ACAGCCACCC CCCUGCCCAG CCAGUACCUG
121 AUGGAACUGA GCGAGGAACA CAGCUGGAUG AGCAACCAGA CCGACCUGCA CUACGUGCUG
181 AAGCCCGGCG AAGUGGCUAC CGCCAGCAUC UUUUUCGGCA UCCUGUGGCU GUUCAGCAUC
241 UUCGGCAACA GCCUCGUGUG CCUGGUCAUC CACAGAUCUC GGC GGACCCA GAGCACCACC
301 AACUACUUCG UGGUGUCCAU GGCCUGCGCC GACCUGCUGA UCAGCGUGGC CAGCACCCCC
361 UUCGUGCUGC UGCAGUUCAC CACAGGCCGG UGGACACUGG GCAGCGCCAC CUGUAAAGUC
421 GUGCGGUACU UUCAGUACCU GACCCUGGC GUGCAGAUUC ACGUGCUGCU GAGCAUCUGC
481 AUCGACCGGU UCUACACCAU CGUGUACCCC CUGAGCUUCA AGGUGUCCCG CGAGAAGGCC
541 AAGAAGAUGA UCGCCGCCAG CUGGGUGUUC GACGCCGGCU UUGUGACCCC CGUGCUGUUC
601 UUCUACGGCA GCAACUGGGA CAGCCACUGC AACUACUUUC UGCCUAGCAG CUGGGAGGGC
661 ACCGCCUACA CCGUGAUCCA CUUUCUGUG GGCUUCGUGA UCCCCAGCGU GCUGAUCAUC
721 CUGUUCUACC AGAAAGUGAU CAAGUACAUC UGGCGGAUCG GCACCGACGG CCGGACCGUG
781 CGGCGGACCA UGAACAUCGU GCCCCGGACC AAAGUCAAGA CCAUCAAGAU GUUUCUGAUC
841 CUGAACCGC UGUUCCUGCU GAGCUGGCUG CCCUCCACG UGGCCAGCU GUGGCACCCC
901 CACGAGCAGG ACUACAAGAA AAGCAGCCUG GUGUUCACCG CCAUCACCUG GAUCAGCUUC
961 AGCAGCAGCG CCUCCAAGCC CACCCUGUAC AGCAUCUACA ACGCCAACUU CAGACGGGGG
1021 AUGAAGGAAA CCUUCUGCAU GAGCAGCAUG AAGUGCUACA GAAGCAACGC UUACACCAUC
1081 ACCACCAGCA GCCGGAUGGC CAAGAAAAAC UACGUGGGCA UCAGCGAGAU CCCCAGCAUG
1141 GCCAAGACAA UCACCAAGGA CUCCAUCUAC GACAGCUUCG ACAGAGAGGC CAAAGAGAAG
1201 AAGCUGGCCU GGCCCAUCAA UAGCAACCCC CCCAACACCU UCGUGUGA

```

4. GPR19 protein sequence

The UniProt identification number for human GPR19 is Q15760. The NCBI protein reference sequence is NP_006134.1 (protein variant V189I). The sequence is arranged from the amino- to the carboxy-terminus.

```

      10      20      30      40      50      60
MVFAHRMDNS KPHLIPTLL VPLQNRSCTE TATPLPSQYL MELSEEHSWM SNQTDLHYVL
      70      80      90     100     110     120
KPGEVATASI FFGILWLFSI FGNSLVCLVI HRSRRTQSTT NYFVVSMACA DLLISVASTP
      130     140     150     160     170     180
FVLLQFTTGR WTLGSATCKV VRYFQYLTPG VQIYVLLSIC IDRFTYTIYYP LSFKVSREKA
      190     200     210     220     230     240
KKMIAASWVF DAGFVTPVLF FYGSNWDSHC NYFLPSSWEG TAYTVIHFLV GFVIPSVLII
      250     260     270     280     290     300
LFYQKVIKYI WRIGTDGRTV RRTMNIVPRT KVKTIKMFLI LNLLFLLSWL PFHVAQLWHP
      310     320     330     340     350     360
HEQDYKKSSL VFTAITWISF SSSASKPTLY SIYNANFRRG MKETFCMSSM KCYRSNAYTI
      370     380     390     400     410
TTSSRMAKKN YVGISEIPSM AKTITKDSIY DSFDREAKEK KLAWPINSNP PNTFV

```

According to Ensembl¹⁰³, 24 SNPs exist within the coding sequence of *Gpr19*. Twelve SNPs do not affect the protein sequence (synonymous), whereas the other twelve cause an amino acid substitution (non-synonymous). The latter ones are listed in table 16.

Table 16: Non-synonymous SNPs in the *Gpr19* coding sequence according to Ensembl. Only those SNPs listed in the NCBI SNP database¹⁰⁴ were included. The feature-specified positions of amino acid substitutions (external amino (N)-terminus, cytoplasmic carboxy (C)-terminus, transmembrane (TM), or intracellular loop (IL) regions) are hypothetical and refer to the UniProt human GPR19 protein ID Q15760 (figure 6). Amino acid substitutions that were considered to be deleterious (*i.e.*, affecting protein function) are shown in **red** (Sorting Intolerant From Tolerant (SIFT) score ≤ 0.05).

Identification number	Amino acid substitution	Allele (transcript position)	Frequency [%]	SIFT ¹⁰⁵
rs143657544	S27N (N-terminus)	G435A	0.022	0
rs148944358	S48I (N-terminus)	G498T	0.022	0.05
rs41276680	V116I (TM2)	G701A	1.203	0.46
rs139420660	V155I (TM3)	G818A	0.022	0.08

¹⁰³ useast.ensembl.org/Homo_sapiens/Gene/Variation_Gene/Table?g=ENSG00000183150;r=12:12813825-12849141#NON_SYNONYMOUS_CODING_tablePanel

¹⁰⁴ www.ncbi.nlm.nih.gov/snp

¹⁰⁵ The Sorting Intolerant From Intolerant (SIFT) algorithm evaluates the effect of non-synonymous SNPs on protein function. Based on sequence homology of the protein of interest to related protein family members, amino acid substitutions are judged according to their position in the protein and their effect on physicochemical properties. The SIFT score indicates the normalized probability that the amino acid substitution caused by the SNP does not affect protein function (Ng PC and Henikoff S, 2003).

Identification number	Amino acid substitution	Allele (transcript position)	Frequency [%]	SIFT ¹⁰⁵
rs115836857	V168I (IL2)	G857A	0.519	0.51
rs4763862	V189I (TM4)	G920A	13.444	0.93
rs147196823	T224A (TM5)	A1025G	0.022	0.84
rs149524125	V272L (IL3)	G1169C	0.022	0.08
rs140470262	K351R (C-terminus)	A1407G	0.022	0.24
rs145071913	V372A (C-terminus)	T1470C	0.022	0
rs138857972	K398R (C-terminus)	A1548G	0.198	0.25
rs61733942	P411T (C-terminus)	C1586A	1.389	0.01

5. *Gpr19* promoter sequence

The first 1,000 bases (5' to 3' direction) of the *Gpr19* promoter (located on the reverse strand of chromosome 12 (short arm; 12p12.3) at the position 12,850,121 to 12,849,122) are listed below. Potential E2 promoter binding factor (E2F), Pit1/Oct2/unc-86 (POU), and half-cyclic adenosine monophosphate (cAMP)-responsive element (CRE) transcription factor binding sites as explained in the Results and Discussion sections are highlighted.

```

1 GCATGGCTGC TTTTTTTTTT TTTTTTTTTT TTTTACTTCG CTTCAAGAGT CAGTCTTAAA
61 TCATGTAGGT TTTGCTTGAG GTTTGCTCGA GCAAGAGGAC CTTAGGTTTG GTCTTATTTG
POU (-875)
121 CATTTTTTACC ATAACTAGGC CTACATTCTA AATAAGTAAC TAAATGCCAC CTATGAGTTT
181 CATTAACTGT GGCTGCTTGC CACTTTTTTAG TTCTGGTTAG GGTGGTGCTA TTGTTTTCCCT
241 CAGGTTTCATT AGAAACATCT TCCGTGACAG CTCTGACGCG GCACCGATTT CTGAGTGTC
301 AGTGTTTTCC CTACCATTAT TTTCTTTGGT CTGAAGTTGA CACTTAAACT GTCCAGTTTT
361 AAACCTCCGA TCCGTGTTCC CAAATGAAAA CATGACTTTC ATTACGAATT ACACCGTCAAG
halfCRE (-587)
421 GGAGCAAACC AAGGCGCTCG GGGCGGCGAG AACCGCGACA CAGCGCTTCG CCTGGACTGG
481 TAAACAAACC GCCGCGCAGG CGCAATGGCA ACAGGACGGT AACCTGGGTA GCCGCCAATG
541 GGCTTTTTTCG TAGAGTGAAA AGCGGAAAAG CCAAACAAAA CGCTGGTTCC AAGGTGATAA
601 ACTGGCTGAC TTCCTCTATT TTTACTTTTT TAAAAAATTT TGTTTCTGAA GAAGTAGTTG
661 TGCGGCCTTC TGGGCCTCGC AGAGATCTTC TTCGTGGAAT TCCTCGGCCC CAGAGAAATG
721 CCGCTAGCCT GTCGGCTAGT TATATTAGCC TAATTTTTTTG TCTTGATCTT TTTCATTTGA
781 CTGCAGCACT AATCCTAATC CACTGGGGCA GCAAAAAAAA AAAAAAAAAA AAAAAAAAAA
E2F (-185)
841 AAAAAAAGG GCGGGTGGGA TCTCAACGCC ACGGAAAACC TTCATACTAG CCGGCCATCA
901 CCAAACCACG CGAGATCTGC CTGAGGAGAA GCGCCACCCC GGGAGTGCAC GTTTGCGCAT
961 GCGTCTGGCT CATCATTTT AGCGCGCAAA AGTTTCAAAA CTTTCCGCCT AGTGAGAGGC
E2F (-15) Start of exon 1

```

IX. References

- Abeloff MD**, Eggleston JC, Mendelsohn G, Ettinger DS, Baylin SB. Changes in morphologic and biochemical characteristics of small cell carcinoma of the lung. A clinicopathologic study. *Am J Med.* 1979;66:757-64.
- Achour L**, Labbé-Jullié C, Scott MG, Marullo S. An escort for GPCRs: implications for regulation of receptor density at the cell surface. *Trends Pharmacol Sci.* 2008;29:528-35.
- Adams MS**, Bronner-Fraser M. Review: the role of neural crest cells in the endocrine system. *Endocr Pathol.* 2009;20:92-100.
- Aguilera G**, Nikodemova M, Wynn PC, Catt KJ. Corticotropin releasing hormone receptors: two decades later. *Peptides.* 2004;25:319-29.
- Alemán LM**, Doench J, Sharp PA. Comparison of siRNA-induced off-target RNA and protein effects. *RNA.* 2007;13:385-95.
- American Cancer Society.** Cancer Facts & Figures 2012. Atlanta: American Cancer Society; 2012. p.1, p.37.
- Archambault V**, Glover DM. Polo-like kinases: conservation and divergence in their functions and regulation. *Nat Rev Mol Cell Biol.* 2009;10:265-75.
- Arora P**, Ricks TK, Trejo J. Protease-activated receptor signalling, endocytic sorting and dysregulation in cancer. *J Cell Sci.* 2007;120:921-8.
- Assou S**, Le Carrouer T, Tondeur S, Ström S, Gabelle A, Marty S, Nadal L, Pantesco V, Réme T, Hugnot JP, Gasca S, Hovatta O, Hamamah S, Klein B, De Vos J. A meta-analysis of human embryonic stem cells transcriptome integrated into a web-based expression atlas. *Stem Cells.* 2007;25:961-73.
- Attwooll C**, Lazzerini Denchi E, Helin K. The E2F family: specific functions and overlapping interests. *EMBO J.* 2004;23:4709-16.
- Aziziyeh AI**, Li TT, Pape C, Pampillo M, Chidiac P, Possmayer F, Babwah AV, Bhattacharya M. Dual regulation of lysophosphatidic acid (LPA1) receptor signalling by Ral and GRK. *Cell Signal.* 2009;21:1207-17.
- Ballesteros JA**, Weinstein H. Integrated methods for the construction of three-dimensional models and computational probing of structure-function relations in G protein-coupled receptors. *Methods Neurosci.* 1995;25:366-428.
- Beasley MB**, Brambilla E, Travis WD. The 2004 World Health Organization classification of lung tumors. *Semin Roentgenol.* 2005;40:90-7.
- Beasley MB**, Lantuejoul S, Abbondanzo S, Chu WS, Hasleton PS, Travis WD, Brambilla E. The P16/cyclin D1/Rb pathway in neuroendocrine tumors of the lung. *Hum Pathol.* 2003;34:136-42.
- Beisser PS**, Lavreysen H, Bruggeman CA, Vink C. Chemokines and chemokine receptors encoded by cytomegaloviruses. *Curr Top Microbiol Immunol.* 2008;325:221-42.
- Belo A**, Cheng K, Chahdi A, Shant J, Xie G, Khurana S, Raufman JP. Muscarinic receptor agonists stimulate human colon cancer cell migration and invasion. *Am J Physiol Gastrointest Liver Physiol.* 2011;300:G749-60.
- Bockaert J**, Fagni L, Dumuis A, Marin P. GPCR interacting proteins (GIP). *Pharmacol Ther.* 2004;103:203-21.

- Borensztajn KS**, Spek CA. Protease-activated receptors, apoptosis and tumor growth. *Pathophysiol Haemost Thromb*. 2008;36:137-47.
- Bousquet C**, Guillermet-Guibert J, Saint-Laurent N, Archer-Lahlou E, Lopez F, Fanjul M, Ferrand A, Fourmy D, Pichereaux C, Monsarrat B, Pradayrol L, Estève JP, Susini C. Direct binding of p85 to sst2 somatostatin receptor reveals a novel mechanism for inhibiting PI3K pathway. *EMBO J*. 2006;25:3943-54.
- Boyd KE**, Farnham PJ. Coexamination of site-specific transcription factor binding and promoter activity in living cells. *Mol Cell Biol*. 1999;19:8393-9.
- Brambilla E**, Travis WD, Colby TV, Corrin B, Shimosato Y. The new World Health Organization classification of lung tumours. *Eur Respir J*. 2001;18:1059-68.
- Bresnick JN**, Skynner HA, Chapman KL, Jack AD, Zamiara E, Negulescu P, Beaumont K, Patel S, McAllister G. Identification of signal transduction pathways used by orphan G protein-coupled receptors. *Assay Drug Dev Technol*. 2003;1:239-49.
- Brough R**, Frankum JR, Costa-Cabral S, Lord CJ, Ashworth A. Searching for synthetic lethality in cancer. *Curr Opin Genet Dev*. 2011;21:34-41.
- Brown KC**, Witte TR, Hardman WE, Luo H, Chen YC, Carpenter AB, Lau JK, Dasgupta P. Capsaicin displays anti-proliferative activity against human small cell lung cancer in cell culture and nude mice models via the E2F pathway. *PLoS One*. 2010;5:e10243.
- Brown NR**, Lowe ED, Petri E, Skamnaki V, Antrobus R, Johnson LN. Cyclin B and cyclin A confer different substrate recognition properties on CDK2. *Cell Cycle*. 2007;6:1350-9.
- Burger JA**, Kipps TJ. CXCR4: a key receptor in the crosstalk between tumor cells and their microenvironment. *Blood*. 2006;107:1761-7.
- Burger JA**, Stewart DJ, Wald O, Peled A. Potential of CXCR4 antagonists for the treatment of metastatic lung cancer. *Expert Rev Anticancer Ther*. 2011;11:621-30.
- Burke DJ**. Complexity in the spindle checkpoint. *Curr Opin Genet Dev*. 2000;10:26-31.
- Burns DL**. Subunit structure and enzymic activity of pertussis toxin. *Microbiol Sci*. 1988;5:285-7.
- Bustin SA**, Benes V, Garson JA, Hellemans J, Huggett J, Kubista M, Mueller R, Nolan T, Pfaffl MW, Shipley GL, Vandesompele J, Wittwer CT. The MIQE guidelines: minimum information for publication of quantitative real-time PCR experiments. *Clin Chem*. 2009;55:611-22.
- Cannon M**. The KSHV and other human herpesviral G protein-coupled receptors. *Curr Top Microbiol Immunol*. 2007;312:137-56.
- Capani F**, Deerinck TJ, Ellisman MH, Bushong E, Bobik M, Martone ME. Phalloidin-eosin followed by photo-oxidation: a novel method for localizing F-actin at the light and electron microscopic levels. *J Histochem Cytochem*. 2001;49:1351-61.
- Carey GB**, Donjerković D, Mueller CM, Liu S, Hinshaw JA, Tonnetti L, Davidson W, Scott DW. B-cell receptor and Fas-mediated signals for life and death. *Immunol Rev*. 2000;176:105-15.
- Caruso R**, Fedele F, Lucianò R, Branca G, Parisi C, Paparo D, Parisi A. Mitotic catastrophe in malignant epithelial tumors: the pathologist's viewpoint. *Ultrastruct Pathol*. 2011;35:66-71.
- Castedo M**, Perfettini JL, Roumier T, Kroemer G. Cyclin-dependent kinase-1: linking apoptosis to cell cycle and mitotic catastrophe. *Cell Death Differ*. 2002;9:1287-93.

- Catty P**, Pfister C, Bruckert F, Deterre P. The cGMP phosphodiesterase-transducin complex of retinal rods. Membrane binding and subunits interactions. *J Biol Chem*. 1992;267:19489-93.
- Cavallucci V**, D'Amelio M. Matter of life and death: the pharmacological approaches targeting apoptosis in brain diseases. *Curr Pharm Des*. 2011;17:215-29.
- Chari RV**. Targeted cancer therapy: conferring specificity to cytotoxic drugs. *Acc Chem Res*. 2008;41:98-107.
- Chen CH**, Chen RJ. Prevalence of telomerase activity in human cancer. *J Formos Med Assoc*. 2011;110:275-89.
- Chen HZ**, Tsai SY, Leone G. Emerging roles of E2Fs in cancer: an exit from cell cycle control. *Nat Rev Cancer*. 2009;9:785-97.
- Cho RW**, Clarke MF. Recent advances in cancer stem cells. *Curr Opin Genet Dev*. 2008;18:48-53.
- Chou PY**, Fasman GD. Prediction of the secondary structure of proteins from their amino acid sequence. *Adv Enzymol Relat Areas Mol Biol*. 1978;47:45-148.
- Clarke PR**, Allan LA. Cell-cycle control in the face of damage – a matter of life or death. *Trends Cell Biol*. 2009;19:89-98.
- Clayton PE**, Banerjee I, Murray PG, Renehan AG. Growth hormone, the insulin-like growth factor axis, insulin and cancer risk. *Nat Rev Endocrinol*. 2011;7:11-24.
- Collinet C**, Stöter M, Bradshaw CR, Samusik N, Rink JC, Kenski D, Habermann B, Buchholz F, Henschel R, Mueller MS, Nagel WE, Fava E, Kalaidzidis Y, Zerial M. Systems survey of endocytosis by multiparametric image analysis. *Nature*. 2010;464:243-9.
- Colosimo A**, Goncz KK, Holmes AR, Kunzelmann K, Novelli G, Malone RW, Bennett MJ, Gruenert DC. Transfer and expression of foreign genes in mammalian cells. *Biotechniques*. 2000;29:314-31.
- Cook AL**, Sturm RA. POU domain transcription factors: BRN2 as a regulator of melanocytic growth and tumorigenesis. *Pigment Cell Melanoma Res*. 2008;21:611-26.
- Cooper CS**, Nicholson AG, Foster C, Dodson A, Edwards S, Fletcher A, Roe T, Clark J, Joshi A, Norman A, Feber A, Lin D, Gao Y, Shipley J, Cheng SJ. Nuclear overexpression of the E2F3 transcription factor in human lung cancer. *Lung Cancer*. 2006;54:155-62.
- Cooper S**, Iyer G, Tarquini M, Bissett P. Nocodazole does not synchronize cells: implications for cell-cycle control and whole-culture synchronization. *Cell Tissue Res*. 2006;324:237-42.
- Cooray SN**, Chan L, Webb TR, Metherell L, Clark AJ. Accessory proteins are vital for the functional expression of certain G protein-coupled receptors. *Mol Cell Endocrinol*. 2009;300:17-24.
- Cotton M**, Claing A. G protein-coupled receptors stimulation and the control of cell migration. *Cell Signal*. 2009;21:1045-53.
- Coulson JM**, Ocejó-García M, Woll PJ. Neuroendocrine phenotype of small cell lung cancer. *Methods Mol Med*. 2003;74:61-73.
- Croce CM**. Oncogenes and cancer. *N Engl J Med*. 2008;358:502-11.

- Darzynkiewicz Z**, Halicka HD, Zhao H, Podhorecka M. Cell synchronization by inhibitors of DNA replication induces replication stress and DNA damage response: analysis by flow cytometry. *Methods Mol Biol.* 2011;761:85-96.
- Davies MA**, Samuels Y. Analysis of the genome to personalize therapy for melanoma. *Oncogene.* 2010;29:5545-55.
- Davis PK**, Ho A, Dowdy SF. Biological methods for cell-cycle synchronization of mammalian cells. *Biotechniques.* 2001;30:1322-31.
- De Cesare D**, Fimia GM, Sassone-Corsi P. Signaling routes to CREM and CREB: plasticity in transcriptional activation. *Trends Biochem Sci.* 1999;24:281-5.
- DeBerardinis RJ**, Lum JJ, Hatzivassiliou G, Thompson CB. The biology of cancer: metabolic reprogramming fuels cell growth and proliferation. *Cell Metab.* 2008;7:11-20.
- Deshpande DA**, Wang WC, McIlmoyle EL, Robinett KS, Schillinger RM, An SS, Sham JS, Liggett SB. Bitter taste receptors on airway smooth muscle bronchodilate by localized calcium signaling and reverse obstruction. *Nat Med.* 2010;16:1299-304.
- Dolznic H**, Rupp C, Puri C, Haslinger C, Schweifer N, Wieser E, Kerjaschki D, Garin-Chesa P. Modeling colon adenocarcinomas *in vitro* a 3D co-culture system induces cancer-relevant pathways upon tumor cell and stromal fibroblast interaction. *Am J Pathol.* 2011;179:487-501.
- Dolznic H**, Schweifer N, Puri C, Kraut N, Rettig WJ, Kerjaschki D, Garin-Chesa P. Characterization of cancer stroma markers: *in silico* analysis of an mRNA expression database for fibroblast activation protein and endosialin. *Cancer Immun.* 2005;5:10.
- Dong C**, Filipeanu CM, Duvernay MT, Wu G. Regulation of G protein-coupled receptor export trafficking. *Biochim Biophys Acta.* 2007;1768:853-70.
- Dorsam RT**, Gutkind JS. G-protein-coupled receptors and cancer. *Nat Rev Cancer.* 2007;7:79-94.
- Dowell JE**. Small cell lung cancer: are we making progress? *Am J Med Sci.* 2010;339:68-76.
- Downward J**. Use of RNA interference libraries to investigate oncogenic signalling in mammalian cells. *Oncogene.* 2004;23:8376-83.
- Drake MT**, Shenoy SK, Lefkowitz RJ. Trafficking of G protein-coupled receptors. *Circ Res.* 2006;99:570-82.
- Eisenberg D**, Weiss RM, Terwilliger TC. The helical hydrophobic moment: a measure of the amphiphilicity of a helix. *Nature.* 1982;299:371-4.
- Elliott JA**, Osterlind K, Hirsch FR, Hansen HH. Metastatic patterns in small-cell lung cancer: correlation of autopsy findings with clinical parameters in 537 patients. *J Clin Oncol.* 1987;5:246-54.
- Emini EA**, Hughes JV, Perlow DS, Boger J. Induction of hepatitis A virus-neutralizing antibody by a virus-specific synthetic peptide. *J Virol.* 1985;55:836-9.
- Fire A**, Xu S, Montgomery MK, Kostas SA, Driver SE, Mello CC. Potent and specific genetic interference by double-stranded RNA in *Caenorhabditis elegans*. *Nature.* 1998;391:806-11.
- Fischbach C**, Chen R, Matsumoto T, Schmelzle T, Brugge JS, Polverini PJ, Mooney DJ. Engineering tumors with 3D scaffolds. *Nat Methods.* 2007;4:855-60.

- Fischer B**, Marinov M, Arcaro A. Targeting receptor tyrosine kinase signalling in small cell lung cancer (SCLC): what have we learned so far? *Cancer Treat Rev.* 2007;33:391-406.
- Fornari FA**, Randolph JK, Yalowich JC, Ritke MK, Gewirtz DA. Interference by doxorubicin with DNA unwinding in MCF-7 breast tumor cells. *Mol Pharmacol.* 1994;45:649-56.
- Franco OE**, Shaw AK, Strand DW, Hayward SW. Cancer associated fibroblasts in cancer pathogenesis. *Semin Cell Dev Biol.* 2010;21:33-9.
- Franco R**, Casadó V, Cortés A, Ferrada C, Mallol J, Woods A, Lluís C, Canela EI, Ferré S. Basic concepts in G-protein-coupled receptor homo- and heterodimerization. *ScientificWorldJournal.* 2007;7:48-57.
- Fredriksson R**, Lagerström MC, Lundin LG, Schiöth HB. The G-protein-coupled receptors in the human genome form five main families. Phylogenetic analysis, paralogon groups, and fingerprints. *Mol Pharmacol.* 2003;63:1256-72.
- Freissmuth M**, Selzer E, Schütz W. Interactions of purified bovine brain A1-adenosine receptors with G-proteins. Reciprocal modulation of agonist and antagonist binding. *Biochem J.* 1991;275:651-6.
- Ganjavi H**, Malkin D. Genetics of childhood cancer. *Clin Orthop Relat Res.* 2002;401:75-87.
- Garnier J**, Osguthorpe DJ, Robson B. Analysis of the accuracy and implications of simple methods for predicting the secondary structure of globular proteins. *J Mol Biol.* 1978;120:97-120.
- Geng Y**, Eaton EN, Picón M, Roberts JM, Lundberg AS, Gifford A, Sardet C, Weinberg RA. Regulation of cyclin E transcription by E2Fs and retinoblastoma protein. *Oncogene.* 1996;12:1173-80.
- Giuliano KA**, Chen YT, Taylor DL. High-content screening with siRNA optimizes a cell biological approach to drug discovery: defining the role of P53 activation in the cellular response to anticancer drugs. *J Biomol Screen.* 2004;9:557-68.
- Glatf S**, Halbauer D, Heindl S, Wernitznig A, Kozina D, Su KC, Puri C, Garin-Chesa P, Sommergruber W. hGPR87 contributes to viability of human tumor cells. *Int J Cancer.* 2008;122:2008-16.
- Göhlmann H**, Talloen W. Gene expression studies using Affymetrix Microarrays. London: Chapman & Hall/CRC; 2009. p.244.
- Gorgoulis VG**, Zacharatos P, Mariatos G, Kotsinas A, Bouda M, Kletsas D, Asimacopoulos PJ, Agnantis N, Kittas C, Papavassiliou AG. Transcription factor E2F-1 acts as a growth-promoting factor and is associated with adverse prognosis in non-small cell lung carcinomas. *J Pathol.* 2002;198:142-56.
- Grivennikov SI**, Greten FR, Karin M. Immunity, inflammation, and cancer. *Cell.* 2010;140:883-99.
- Gruber CW**, Muttenthaler M, Freissmuth M. Ligand-based peptide design and combinatorial peptide libraries to target G protein-coupled receptors. *Curr Pharm Des.* 2010;16:3071-88.
- Gsandtner I**, Charalambous C, Stefan E, Ogris E, Freissmuth M, Zezula J. Heterotrimeric G protein-independent signaling of a G protein-coupled receptor. Direct binding of ARNO/cytohesin-2 to the carboxyl terminus of the A2A adenosine receptor is necessary for sustained activation of the ERK/MAP kinase pathway. *J Biol Chem.* 2005;280:31898-905.

- Gugger M**, White R, Song S, Waser B, Cescato R, Rivière P, Reubi JC. GPR87 is an overexpressed G-protein coupled receptor in squamous cell carcinoma of the lung. *Dis Markers*. 2008;24:41-50.
- Gui CY**, Jiang C, Xie HY, Qian RL. The apoptosis of HEL cells induced by hydroxyurea. *Cell Res*. 1997;7:91-7.
- Guinee DG Jr**, Fishback NF, Koss MN, Abbondanzo SL, Travis WD. The spectrum of immunohistochemical staining of small-cell lung carcinoma in specimens from transbronchial and open-lung biopsies. *Am J Clin Pathol*. 1994;102:406-14.
- Gupta A**, Heimann AS, Gomes I, Devi LA. Antibodies against G-protein coupled receptors: novel uses in screening and drug development. *Comb Chem High Throughput Screen*. 2008;11:463-7.
- Hammond SM**. Dicing and slicing: the core machinery of the RNA interference pathway. *FEBS Lett*. 2005;579:5822-9.
- Hanahan D**, Weinberg RA. Hallmarks of cancer: the next generation. *Cell*. 2011;144:646-74.
- Hanson MA**, Cherezov V, Griffith MT, Roth CB, Jaakola VP, Chien EY, Velasquez J, Kuhn P, Stevens RC. A specific cholesterol binding site is established by the 2.8 Å structure of the human beta2-adrenergic receptor. *Structure*. 2008;16:897-905.
- Hanyaloglu AC**, von Zastrow M. Regulation of GPCRs by endocytic membrane trafficking and its potential implications. *Annu Rev Pharmacol Toxicol*. 2008;48:537-68.
- Hebert DN**, Molinari M. In and out of the ER: protein folding, quality control, degradation, and related human diseases. *Physiol Rev*. 2007;87:1377-408.
- Hendricks SP**, Mathews CK. Differential effects of hydroxyurea upon deoxyribonucleoside triphosphate pools, analyzed with vaccinia virus ribonucleotide reductase. *J Biol Chem*. 1998;273:29519-23.
- Henzel MJ**, Wei Y, Mancini MA, Van Hooser A, Ranalli T, Brinkley BR, Bazett-Jones DP, Allis CD. Mitosis-specific phosphorylation of histone H3 initiates primarily within pericentromeric heterochromatin during G2 and spreads in an ordered fashion coincident with mitotic chromosome condensation. *Chromosoma*. 1997;106:348-60.
- Hochegger H**, Takeda S, Hunt T. Cyclin-dependent kinases and cell-cycle transitions: does one fit all? *Nat Rev Mol Cell Biol*. 2008;9:910-6.
- Hoffmeister-Ullerich SA**, Süsens U, Schaller HC. The orphan G-protein-coupled receptor GPR19 is expressed predominantly in neuronal cells during mouse embryogenesis. *Cell Tissue Res*. 2004;318:459-63.
- Hoppe-Seyler F**, Hoppe-Seyler K. Emerging topics in human tumor virology. *Int J Cancer*. 2011;129:1289-99.
- Hua H**, Li M, Luo T, Yin Y, Jiang Y. Matrix metalloproteinases in tumorigenesis: an evolving paradigm. *Cell Mol Life Sci*. 2011;68:3853-68.
- Hupé P**, Stransky N, Thiery JP, Radvanyi F, Barillot E. Analysis of array CGH data: from signal ratio to gain and loss of DNA regions. *Bioinformatics*. 2004;20:3413-22.
- Hurst JH**, Hooks SB. Regulator of G-protein signaling (RGS) proteins in cancer biology. *Biochem Pharmacol*. 2009;78:1289-97.

- Insel PA**, Ostrom RS. Forskolin as a tool for examining adenylyl cyclase expression, regulation, and G protein signaling. *Cell Mol Neurobiol.* 2003;23:305-14.
- Irizarry RA**, Hobbs B, Collin F, Beazer-Barclay YD, Antonellis KJ, Scherf U, Speed TP. Exploration, normalization, and summaries of high density oligonucleotide array probe level data. *Biostatistics.* 2003;4:249-64.
- Jackman DM**, Johnson BE. Small-cell lung cancer. *Lancet.* 2005;366:1385-96.
- Jalink K**, Moolenaar WH. G protein-coupled receptors: the inside story. *Bioessays.* 2010;32:13-6.
- Jameson BA**, Wolf H. The antigenic index: a novel algorithm for predicting antigenic determinants. *Comput Appl Biosci.* 1988;4:181-6.
- Jarrous N**, Reiner R. Human RNase P: a tRNA-processing enzyme and transcription factor. *Nucleic Acids Res.* 2007;35:3519-24.
- Jha KK**, Banga S, Palejwala V, Ozer HL. SV40-Mediated immortalization. *Exp Cell Res.* 1998;245:1-7.
- Ji TH**, Grossmann M, Ji I. G protein-coupled receptors. I. Diversity of receptor-ligand interactions. *J Biol Chem.* 1998;273:17299-302.
- Johnson RA**, Salomon Y. Assay of adenylyl cyclase catalytic activity. *Methods Enzymol.* 1991;195:3-21.
- Jordan MA**, Thrower D, Wilson L. Effects of vinblastine, podophyllotoxin and nocodazole on mitotic spindles. Implications for the role of microtubule dynamics in mitosis. *J Cell Sci.* 1992;102:401-16.
- Karplus PA**, Schulz GE. Prediction of chain flexibility in proteins: a tool for the selection of peptide antigens. *Naturwissenschaften.* 1985;72:212-3.
- Kim JI**, Chakraborty P, Wang Z, Daaka Y. G-protein coupled receptor kinase 5 regulates prostate tumor growth. *J Urol.* 2012;187:322-9.
- Kitamura H**, Yazawa T, Okudela K, Shimoyamada H, Sato H. Molecular and genetic pathogenesis of lung cancer: differences between small-cell and non-small-cell carcinomas. *Open Pathol J.* 2008;2:106-14.
- Koppenol WH**, Bounds PL, Dang CV. Otto Warburg's contributions to current concepts of cancer metabolism. *Nat Rev Cancer.* 2011;11:325-37.
- Krishna G**, Weiss B, Brodie BB. A simple, sensitive method for the assay of adenylyl cyclase. *J Pharmacol Exp Ther.* 1968;163:379-85.
- Krishnan A**, Almén MS, Fredriksson R, Schiöth HB. The origin of GPCRs: identification of mammalian like Rhodopsin, Adhesion, Glutamate and Frizzled GPCRs in fungi. *PLoS One.* 2012;7:e29817.
- Kyte J**, Doolittle RF. A simple method for displaying the hydropathic character of a protein. *J Mol Biol.* 1982;157:105-32.
- Lagerström MC**, Schiöth HB. Structural diversity of G protein-coupled receptors and significance for drug discovery. *Nat Rev Drug Discov.* 2008;7:339-57.

- Lambert LA**, Mitchell SL. Molecular evolution of the transferrin receptor/glutamate carboxypeptidase II family. *J Mol Evol.* 2007;64:113-28.
- Lappano R**, Maggiolini M. G protein-coupled receptors: novel targets for drug discovery in cancer. *Nat Rev Drug Discov.* 2011;10:47-60.
- Larsson LG**, Henriksson MA. The Yin and Yang functions of the Myc oncoprotein in cancer development and as targets for therapy. *Exp Cell Res.* 2010;316:1429-37.
- Lassmann G**, Thelander L, Gräslund A. EPR stopped-flow studies of the reaction of the tyrosyl radical of protein R2 from ribonucleotide reductase with hydroxyurea. *Biochem Biophys Res Commun.* 1992;188:879-87.
- Lemberger T**, Parkitna JR, Chai M, Schütz G, Engblom D. CREB has a context-dependent role in activity-regulated transcription and maintains neuronal cholesterol homeostasis. *FASEB J.* 2008;22:2872-9.
- Lemmon MA**, Schlessinger J. Cell signaling by receptor tyrosine kinases. *Cell.* 2010;141:1117-34.
- Li S**, Huang S, Peng SB. Overexpression of G protein-coupled receptors in cancer cells: involvement in tumor progression. *Int J Oncol.* 2005;27:1329-39.
- Lipman DJ**, Souvorov A, Koonin EV, Panchenko AR, Tatusova TA. The relationship of protein conservation and sequence length. *BMC Evol Biol.* 2002;2:20.
- Liu M**, Horowitz A. A PDZ-binding motif as a critical determinant of Rho guanine exchange factor function and cell phenotype. *Mol Biol Cell.* 2006;17:1880-7.
- Liu Q**, Paroo Z. Biochemical principles of small RNA pathways. *Annu Rev Biochem.* 2010;79:295-319.
- Liu X**, Erikson RL. Polo-like kinase (Plk)1 depletion induces apoptosis in cancer cells. *Proc Natl Acad Sci U S A.* 2003;100:5789-94.
- Liu Y**, Dean DC. Tumor initiation via loss of cell contact inhibition versus Ras mutation: do all roads lead to EMT? *Cell Cycle.* 2010;9:897-900.
- Livak KJ**, Schmittgen TD. Analysis of relative gene expression data using real-time quantitative PCR and the 2⁻(Delta Delta C(T)) Method. *Methods.* 2001;25:402-8.
- Lu Y**, Cai Z, Galson DL, Xiao G, Liu Y, George DE, Melhem MF, Yao Z, Zhang J. Monocyte chemotactic protein-1 (MCP-1) acts as a paracrine and autocrine factor for prostate cancer growth and invasion. *Prostate.* 2006;66:1311-8.
- Lu Y**, Cai Z, Xiao G, Liu Y, Keller ET, Yao Z, Zhang J. CCR2 expression correlates with prostate cancer progression. *J Cell Biochem.* 2007;101:676-85.
- Lu Y**, Chen Q, Corey E, Xie W, Fan J, Mizokami A, Zhang J. Activation of MCP-1/CCR2 axis promotes prostate cancer growth in bone. *Clin Exp Metastasis.* 2009;26:161-9.
- Luker KE**, Luker GD. Functions of CXCL12 and CXCR4 in breast cancer. *Cancer Lett.* 2006;238:30-41.
- Lum AM**, Wang BB, Beck-Engeser GB, Li L, Channa N, Wabl M. Orphan receptor GPR110, an oncogene overexpressed in lung and prostate cancer. *BMC Cancer.* 2010;10:40.
- Lundstrom K**. An overview on GPCRs and drug discovery: structure-based drug design and structural biology on GPCRs. *Methods Mol Biol.* 2009;552:51-66.

Luttrell DK, Luttrell LM. Not so strange bedfellows: G-protein-coupled receptors and Src family kinases. *Oncogene*. 2004;23:7969-78.

Madeo A, Maggiolini M. Nuclear alternate estrogen receptor GPR30 mediates 17beta-estradiol-induced gene expression and migration in breast cancer-associated fibroblasts. *Cancer Res*. 2010;70:6036-46.

Maekawa T, Ashihara E, Kimura S. The Bcr-Abl tyrosine kinase inhibitor imatinib and promising new agents against Philadelphia chromosome-positive leukemias. *Int J Clin Oncol*. 2007;12:327-40.

Mahendroo MS, Mendelson CR, Simpson ER. Tissue-specific and hormonally controlled alternative promoters regulate aromatase cytochrome P450 gene expression in human adipose tissue. *J Biol Chem*. 1993;268:19463-70.

Maity A, McKenna WG, Muschel RJ. Cyclin A message stability varies with the cell cycle. *Cell Growth Differ*. 1997;8:311-8.

Maity A, McKenna WG, Muschel RJ. Evidence for post-translational regulation of cyclin B1 mRNA in the cell cycle and following irradiation in HeLa cells. *EMBO J*. 1995;14:603-9.

Maksym RB, Tarnowski M, Grymula K, Tarnowska J, Wysoczynski M, Liu R, Czerny B, Ratajczak J, Kucia M, Ratajczak MZ. The role of stromal-derived factor-1-CXCR7 axis in development and cancer. *Eur J Pharmacol*. 2009;625:31-40.

Málaga-Diéguez L, Yang Q, Bauer J, Pankevych H, Freissmuth M, Nanoff C. Pharmacochaperoning of the A1 adenosine receptor is contingent on the endoplasmic reticulum. *Mol Pharmacol*. 2010;77:940-52.

Malumbres M, Barbacid M. Cell cycle, CDKs and cancer: a changing paradigm. *Nat Rev Cancer*. 2009;9:153-66.

Malvezzi M, Bertuccio P, Levi F, La Vecchia C, Negri E. European cancer mortality predictions for the year 2012. *Ann Oncol*. 2012;23:1044-52.

Mansur NR, Meyer-Siegler K, Wurzer JC, Sirover MA. Cell cycle regulation of the glyceraldehyde-3-phosphate dehydrogenase/uracil DNA glycosylase gene in normal human cells. *Nucleic Acids Res*. 1993;21:993-8.

Marchese A, Paing MM, Temple BR, Trejo J. G protein-coupled receptor sorting to endosomes and lysosomes. *Annu Rev Pharmacol Toxicol*. 2008;48:601-29.

Margolskee RF. Molecular mechanisms of bitter and sweet taste transduction. *J Biol Chem*. 2002;277:1-4.

Marshall FH, Jones KA, Kaupmann K, Bettler B. GABAB receptors – the first 7TM heterodimers. *Trends Pharmacol Sci*. 1999;20:396-9.

Martin D, Gutkind JS. Human tumor-associated viruses and new insights into the molecular mechanisms of cancer. *Oncogene*. 2008;27:S31-42.

Mejillano MR, Shivanna BD, Himes RH. Studies on the nocodazole-induced GTPase activity of tubulin. *Arch Biochem Biophys*. 1996;336:130-8.

Micke P, Ostman A. Exploring the tumour environment: cancer-associated fibroblasts as targets in cancer therapy. *Expert Opin Ther Targets*. 2005;9:1217-33.

- Milan-Lobo L**, Gsandtner I, Gaubitzer E, Rünzler D, Buchmayer F, Köhler G, Bonci A, Freissmuth M, Sitte HH. Subtype-specific differences in corticotropin-releasing factor receptor complexes detected by fluorescence spectroscopy. *Mol Pharmacol*. 2009;76:1196-210.
- Modlin IM**, Gustafsson BI, Moss SF, Pavel M, Tsolakis AV, Kidd M. Chromogranin A – biological function and clinical utility in neuro endocrine tumor disease. *Ann Surg Oncol*. 2010;17:2427-43.
- Montpetit A**, Sinnott D. Physical mapping of the G-protein coupled receptor 19 (GPR19) in the chromosome 12p12.3 region frequently rearranged in cancer cells. *Hum Genet*. 1999;105:162-4.
- Mougiakakos D**, Choudhury A, Lladser A, Kiessling R, Johansson CC. Regulatory T cells in cancer. *Adv Cancer Res*. 2010;107:57-117.
- Nakakura EK**, Bergsland EK. Islet cell carcinoma: neuroendocrine tumors of the pancreas and periampullary region. *Hematol Oncol Clin North Am*. 2007;21:457-73; viii.
- Neuhaus EM**, Zhang W, Gelis L, Deng Y, Noldus J, Hatt H. Activation of an olfactory receptor inhibits proliferation of prostate cancer cells. *J Biol Chem*. 2009;284:16218-25.
- Neumann B**, Walter T, Hériché JK, Bulkescher J, Erfle H, Conrad C, Rogers P, Poser I, Held M, Liebel U, Cetin C, Sieckmann F, Pau G, Kabbe R, Wünsche A, Satagopam V, Schmitz MH, Chapuis C, Gerlich DW, Schneider R, Eils R, Huber W, Peters JM, Hyman AA, Durbin R, Pepperkok R, Ellenberg J. Phenotypic profiling of the human genome by time-lapse microscopy reveals cell division genes. *Nature*. 2010;464:721-7.
- Ng PC**, Henikoff S. SIFT: Predicting amino acid changes that affect protein function. *Nucleic Acids Res*. 2003;31:3812-4.
- Nguyen DX**, Bos PD, Massagué J. Metastasis: from dissemination to organ-specific colonization. *Nat Rev Cancer*. 2009;9:274-84.
- Nicholson SA**, Beasley MB, Brambilla E, Hasleton PS, Colby TV, Sheppard MN, Falk R, Travis WD. Small cell lung carcinoma (SCLC): a clinicopathologic study of 100 cases with surgical specimens. *Am J Surg Pathol*. 2002;26:1184-97.
- Nijman SM**. Synthetic lethality: general principles, utility and detection using genetic screens in human cells. *FEBS Lett*. 2011;585:1-6.
- O'Dowd BF**, Nguyen T, Lynch KR, Kolakowski LF Jr, Thompson M, Cheng R, Marchese A, Ng G, Heng HH, George SR. A novel gene codes for a putative G protein-coupled receptor with an abundant expression in brain. *FEBS Lett*. 1996;394:325-9.
- Ohtsubo M**, Theodoras AM, Schumacher J, Roberts JM, Pagano M. Human cyclin E, a nuclear protein essential for the G1-to-S phase transition. *Mol Cell Biol*. 1995;15:2612-24.
- Padmanabhan S**, Myers AG, Prasad BM. Constitutively active GPR6 is located in the intracellular compartments. *FEBS Lett*. 2009;583:107-12.
- Paila YD**, Chattopadhyay A. Membrane cholesterol in the function and organization of G-protein coupled receptors. *Subcell Biochem*. 2010;51:439-66.
- Paila YD**, Tiwari S, Chattopadhyay A. Are specific nonannular cholesterol binding sites present in G-protein coupled receptors? *Biochim Biophys Acta*. 2009;1788:295-302.
- Paranjape SM**, Kamakaka RT, Kadonaga JT. Role of chromatin structure in the regulation of transcription by RNA polymerase II. *Annu Rev Biochem*. 1994;63:265-97.

- Patel HH**, Murray F, Insel PA. G-protein-coupled receptor-signaling components in membrane raft and caveolae microdomains. *Handb Exp Pharmacol*. 2008;186:167-84.
- Pedrali-Noy G**, Spadari S, Miller-Faurès A, Miller AO, Kruppa J, Koch G. Synchronization of HeLa cell cultures by inhibition of DNA polymerase alpha with aphidicolin. *Nucleic Acids Res*. 1980;8:377-87.
- Peeters MC**, van Westen GJ, Li Q, IJzerman AP. Importance of the extracellular loops in G protein-coupled receptors for ligand recognition and receptor activation. *Trends Pharmacol Sci*. 2011;32:35-42.
- Penelova A**, Richman L, Neupert B, Simanis V, Kühn LC. Analysis of the contribution of changes in mRNA stability to the changes in steady-state levels of cyclin mRNA in the mammalian cell cycle. *FEBS J*. 2005;272:5217-29.
- Percherancier Y**, Berchiche YA, Slight I, Volkmer-Engert R, Tamamura H, Fujii N, Bouvier M, Heveker N. Bioluminescence resonance energy transfer reveals ligand-induced conformational changes in CXCR4 homo- and heterodimers. *J Biol Chem*. 2005;280:9895-903.
- Perlman ZE**, Slack MD, Feng Y, Mitchison TJ, Wu LF, Altschuler SJ. Multidimensional drug profiling by automated microscopy. *Science*. 2004;306:1194-8.
- Petit-Bertron AF**, Machavoine F, Defresne MP, Gillard M, Chatelain P, Mistry P, Schneider E, Dy M. H4 histamine receptors mediate cell cycle arrest in growth factor-induced murine and human hematopoietic progenitor cells. *PLoS One*. 2009;4:e6504.
- Petronczki M**, Lénárt P, Peters JM. Polo on the Rise – from Mitotic Entry to Cytokinesis with Plk1. *Dev Cell*. 2008;14:646-59.
- Piera-Velazquez S**, Hawkins DF, Whitecavage MK, Colter DC, Stokes DG, Jimenez SA. Regulation of the human SOX9 promoter by Sp1 and CREB. *Exp Cell Res*. 2007;313:1069-79.
- Pin JP**, Kniazeff J, Liu J, Binet V, Goudet C, Rondard P, Prézeau L. Allosteric functioning of dimeric class C G-protein-coupled receptors. *FEBS J*. 2005;272:2947-55.
- Pines J**. Cubism and the cell cycle: the many faces of the APC/C. *Nat Rev Mol Cell Biol*. 2011;12:427-38.
- Pines J**, Hunter T. Isolation of a human cyclin cDNA: evidence for cyclin mRNA and protein regulation in the cell cycle and for interaction with p34cdc2. *Cell*. 1989;58:833-46.
- Pioszak AA**, Parker NR, Suino-Powell K, Xu HE. Molecular recognition of corticotropin-releasing factor by its G-protein-coupled receptor CRFR1. *J Biol Chem*. 2008;283:32900-12.
- Pleasant ED**, Stephens PJ, O'Meara S, McBride DJ, Meynert A, Jones D, Lin ML, Beare D, Lau KW, Greenman C, Varela I, Nik-Zainal S, Davies HR, Ordoñez GR, Mudie LJ, Latimer C, Edkins S, Stebbings L, Chen L, Jia M, Leroy C, Marshall J, Menzies A, Butler A, Teague JW, Mangion J, Sun YA, McLaughlin SF, Peckham HE, Tsung EF, Costa GL, Lee CC, Minna JD, Gazdar A, Birney E, Rhodes MD, McKernan KJ, Stratton MR, Futreal PA, Campbell PJ. A small-cell lung cancer genome with complex signatures of tobacco exposure. *Nature*. 2010;463:184-90.
- Poehlmann A**, Roessner A. Importance of DNA damage checkpoints in the pathogenesis of human cancers. *Pathol Res Pract*. 2010;206:591-601.
- Polager S**, Ginsberg D. E2F – at the crossroads of life and death. *Trends Cell Biol*. 2008;18:528-35.

- Porter LA**, Donoghue DJ. Cyclin B1 and CDK1: nuclear localization and upstream regulators. *Prog Cell Cycle Res.* 2003;5:335-47.
- Poznic M**. Retinoblastoma protein: a central processing unit. *J Biosci.* 2009;34:305-12.
- Prasad BM**, Hollins B, Lambert NA. Methods to detect cell surface expression and constitutive activity of GPR6. *Methods Enzymol.* 2010;484:179-95.
- Puglisi M**, Dolly S, Faria A, Myerson JS, Popat S, O'Brien ME. Treatment options for small cell lung cancer – do we have more choice? *Br J Cancer.* 2010;102:629-38.
- Puntoni M**, Decensi A. The rationale and potential of cancer chemoprevention with special emphasis on breast cancer. *Eur J Cancer.* 2009;45 Suppl 1:346-54.
- Pylayeva-Gupta Y**, Grabocka E, Bar-Sagi D. RAS oncogenes: weaving a tumorigenic web. *Nat Rev Cancer.* 2011;11:761-74.
- Qian BZ**, Pollard JW. Macrophage diversity enhances tumor progression and metastasis. *Cell.* 2010;141:39-51.
- Rabinovich A**, Jin VX, Rabinovich R, Xu X, Farnham PJ. E2F *in vivo* binding specificity: comparison of consensus versus nonconsensus binding sites. *Genome Res.* 2008;18:1763-77.
- Ramachandran J**. A new simple method for separation of adenosine 3',5'-cyclic monophosphate from other nucleotides and its use in the assay of adenyl cyclase. *Anal Biochem.* 1971;43:227-39.
- Rekhtman N**. Neuroendocrine tumors of the lung: an update. *Arch Pathol Lab Med.* 2010;134:1628-38.
- Rieder CL**, Khodjakov A. Mitosis through the microscope: advances in seeing inside live dividing cells. *Science.* 2003;300:91-6.
- Rigau M**, Morote J, Mir MC, Ballesteros C, Ortega I, Sanchez A, Colás E, Garcia M, Ruiz A, Abal M, Planas J, Reventós J, Doll A. PSGR and PCA3 as biomarkers for the detection of prostate cancer in urine. *Prostate.* 2010;70:1760-7.
- Riker AI**, Enkemann SA, Fodstad O, Liu S, Ren S, Morris C, Xi Y, Howell P, Metge B, Samant RS, Shevde LA, Li W, Eschrich S, Daud A, Ju J, Matta J. The gene expression profiles of primary and metastatic melanoma yields a transition point of tumor progression and metastasis. *BMC Med Genomics.* 2008;1:13.
- Ritter SL**, Hall RA. Fine-tuning of GPCR activity by receptor-interacting proteins. *Nat Rev Mol Cell Biol.* 2009;10:819-30.
- Romagnani P**, Annunziato F, Lasagni L, Lazzeri E, Beltrame C, Francalanci M, Uguccioni M, Galli G, Cosmi L, Maurenzig L, Baggiolini M, Maggi E, Romagnani S, Serio M. Cell cycle-dependent expression of CXC chemokine receptor 3 by endothelial cells mediates angiostatic activity. *J Clin Invest.* 2001;107:53-63.
- Rose AA**, Siegel PM. Emerging therapeutic targets in breast cancer bone metastasis. *Future Oncol.* 2010;6:55-74.
- Rosenbaum DM**, Rasmussen SG, Kobilka BK. The structure and function of G-protein-coupled receptors. *Nature.* 2009;459:356-63.

- Rossi P**, Dolci S, Sette C, Capolunghi F, Pellegrini M, Loiarro M, Di Agostino S, Paronetto MP, Grimaldi P, Merico D, Martegani E, Geremia R. Analysis of the gene expression profile of mouse male meiotic germ cells. *Gene Expr Patterns*. 2004;4:267-81.
- Rovati GE**, Capra V, Neubig RR. The highly conserved DRY motif of class A G protein-coupled receptors: beyond the ground state. *Mol Pharmacol*. 2007;71:959-64.
- Rozenfeld R**, Devi LA. Exploring a role for heteromerization in GPCR signalling specificity. *Biochem J*. 2011;433:11-8.
- Rozenfeld R**, Devi LA. Receptor heteromerization and drug discovery. *Trends Pharmacol Sci*. 2010;31:124-30.
- Rozengurt E**. Mitogenic signaling pathways induced by G protein-coupled receptors. *J Cell Physiol*. 2007;213:589-602.
- Salomon Y**, Londos C, Rodbell M. A highly sensitive adenylylate cyclase assay. *Anal Biochem*. 1974;58:541-8.
- Samson F**, Donoso JA, Heller-Bettinger I, Watson D, Himes RH. Nocodazole action on tubulin assembly, axonal ultrastructure and fast axoplasmic transport. *J Pharmacol Exp Ther*. 1979;208:411-7.
- Schebesta A**, McManus S, Salvagiotto G, Delogu A, Busslinger GA, Busslinger M. Transcription factor Pax5 activates the chromatin of key genes involved in B cell signaling, adhesion, migration, and immune function. *Immunity* 2007;27:49-63.
- Schlyer S**, Horuk R. I want a new drug: G-protein-coupled receptors in drug development. *Drug Discov Today*. 2006;11:481-93.
- Schmid MC**, Avraamides CJ, Dippold HC, Franco I, Foubert P, Ellies LG, Acevedo LM, Manglicmot JR, Song X, Wrasidlo W, Blair SL, Ginsberg MH, Cheresh DA, Hirsch E, Field SJ, Varner JA. Receptor tyrosine kinases and TLR/IL1Rs unexpectedly activate myeloid cell PI3ky, a single convergent point promoting tumor inflammation and progression. *Cancer Cell*. 2011;19:715-27.
- Schorr I**, Ney RL. Abnormal hormone responses of an adrenocortical cancer adenylyl cyclase. *J Clin Invest*. 1971;50:1295-300.
- Schröder R**, Janssen N, Schmidt J, Kebig A, Merten N, Hennen S, Müller A, Blättermann S, Mohr-Andrä M, Zahn S, Wenzel J, Smith NJ, Gomeza J, Drewke C, Milligan G, Mohr K, Kostenis E. Deconvolution of complex G protein-coupled receptor signaling in live cells using dynamic mass redistribution measurements. *Nat Biotechnol*. 2010;28:943-9.
- Schütz W**, Freissmuth M. Reverse intrinsic activity of antagonists on G protein-coupled receptors. *Trends Pharmacol Sci*. 1992;13:376-80.
- Seifert R**, Wieland T. G protein-coupled receptors as drug targets. Weinheim: WILEY-VCH; 2006. p.81, p.135.
- Sharma SV**, Settleman J. Exploiting the balance between life and death: targeted cancer therapy and "oncogenic shock". *Biochem Pharmacol*. 2010;80:666-73.
- Shukla AK**, Xiao K, Lefkowitz RJ. Emerging paradigms of β -arrestin-dependent seven transmembrane receptor signaling. *Trends Biochem Sci*. 2011;36:457-69.
- Siegel R**, Naishadham D, Jemal A. Cancer statistics, 2012. *CA Cancer J Clin*. 2012;62:10-29.

- Smalley KS**, Lioni M, Herlyn M. Life isn't flat: taking cancer biology to the next dimension. *In Vitro Cell Dev Biol Anim.* 2006;42:242-7.
- Soldani C**, Scovassi AI. Poly(ADP-ribose) polymerase-1 cleavage during apoptosis: an update. *Apoptosis.* 2002;7:321-8.
- Sontheimer EJ**. Assembly and function of RNA silencing complexes. *Nat Rev Mol Cell Biol.* 2005;6:127-38.
- Sontheimer EJ**, Carthew RW. Silence from within: endogenous siRNAs and miRNAs. *Cell.* 2005;122:9-12.
- Spänkuch-Schmitt B**, Bereiter-Hahn J, Kaufmann M, Strebhardt K. Effect of RNA silencing of polo-like kinase-1 (PLK1) on apoptosis and spindle formation in human cancer cells. *J Natl Cancer Inst.* 2002;94:1863-77.
- Spänkuch-Schmitt B**, Wolf G, Solbach C, Loibl S, Knecht R, Stegmüller M, von Minckwitz G, Kaufmann M, Strebhardt K. Downregulation of human polo-like kinase activity by antisense oligonucleotides induces growth inhibition in cancer cells. *Oncogene.* 2002;21:3162-71.
- Spehr M**, Munger SD. Olfactory receptors: G protein-coupled receptors and beyond. *J Neurochem.* 2009;109:1570-83.
- Spiegelberg BD**, Hamm HE. Roles of G-protein-coupled receptor signaling in cancer biology and gene transcription. *Curr Opin Genet Dev.* 2007;17:40-4.
- Stievano L**, Piovan E, Amadori A. C and CX3C chemokines: cell sources and physiopathological implications. *Crit Rev Immunol.* 2004;24:205-28.
- Strebhardt K**, Ullrich A. Targeting polo-like kinase 1 for cancer therapy. *Nat Rev Cancer.* 2006;6:321-30.
- Sturn A**, Quackenbush J, Trajanoski Z. Genesis: cluster analysis of microarray data. *Bioinformatics.* 2002;18:207-8.
- Sugihara TM**, Kudryavtseva EI, Kumar V, Horridge JJ, Andersen B. The POU domain factor Skin-1a represses the keratin 14 promoter independent of DNA binding. A possible role for interactions between Skn-1a and CREB-binding protein/p300. *J Biol Chem.* 2001;276:33036-44.
- Sun H**, Wu J, Wickramasinghe P, Pal S, Gupta R, Bhattacharyya A, Agosto-Perez FJ, Showe LC, Huang TH, Davuluri RV. Genome-wide mapping of RNA Pol-II promoter usage in mouse tissues by ChIP-seq. *Nucleic Acids Res.* 2011;39:190-201.
- Suzuki K**, Matsubara H. Recent advances in p53 research and cancer treatment. *J Biomed Biotechnol.* 2011;2011:978312.
- Swiss VA**, Casaccia P. Cell-context specific role of the E2F/Rb pathway in development and disease. *Glia.* 2010;58:377-90.
- Takeda K**, Takahashi NH, Shibahara S. Neuroendocrine functions of melanocytes: beyond the skin-deep melanin maker. *Tohoku J Exp Med.* 2007;211:201-21.
- Thiery JP**, Sleeman JP. Complex networks orchestrate epithelial-mesenchymal transitions. *Nat Rev Mol Cell Biol.* 2006;7:131-42.
- Tobin AB**, Butcher AJ, Kong KC. Location, location, location...site-specific GPCR phosphorylation offers a mechanism for cell-type-specific signalling. *Trends Pharmacol Sci.* 2008;29:413-20.

- Tomari Y**, Zamore PD. Perspective: machines for RNAi. *Genes Dev.* 2005;19:517-29.
- Touge H**, Chikumi H, Igishi T, Kurai J, Makino H, Tamura Y, Takata M, Yoneda K, Nakamoto M, Suyama H, Gutkind JS, Shimizu E. Diverse activation states of RhoA in human lung cancer cells: contribution of G protein coupled receptors. *Int J Oncol.* 2007;30:709-15.
- Trouche D**, Cook A, Kouzarides T. The CBP co-activator stimulates E2F1/DP1 activity. *Nucleic Acids Res.* 1996;24:4139-45.
- Tsao AS**, Kim ES, Hong WK. Chemoprevention of cancer. *CA Cancer J Clin.* 2004;54:150-80.
- Tubio MR**, Fernandez N, Fitzsimons CP, Copsel S, Santiago S, Shayo C, Davio C, Monczor F. Expression of a G protein-coupled receptor (GPCR) leads to attenuation of signaling by other GPCRs: experimental evidence for a spontaneous GPCR constitutive inactive form. *J Biol Chem.* 2010;285:14990-8.
- Urdiales JL**, Becker E, Andrieu M, Thomas A, Jullien J, van Grunsven LA, Menut S, Evan GI, Martín-Zanca D, Rudkin BB. Cell cycle phase-specific surface expression of nerve growth factor receptors TrkA and p75^{NTR}. *J Neurosci.* 1998;18:6767-75.
- Vakifahmetoglu H**, Olsson M, Zhivotovsky B. Death through a tragedy: mitotic catastrophe. *Cell Death Differ.* 2008;15:1153-62.
- Vandesompele J**, De Preter K, Pattyn F, Poppe B, Van Roy N, De Paepe A, Speleman F. Accurate normalization of real-time quantitative RT-PCR data by geometric averaging of multiple internal control genes. *Genome Biol.* 2002;3:RESEARCH0034.
- Vasquez RJ**, Howell B, Yvon AM, Wdsworth P, Cassimeris L. Nanomolar concentrations of nocodazole alter microtubule dynamic instability *in vivo* and *in vitro*. *Mol Biol Cell.* 1997;8:973-85.
- Vassilatis DK**, Hohmann JG, Zeng H, Li F, Ranchalis JE, Mortrud MT, Brown A, Rodriguez SS, Weller JR, Wright AC, Bergmann JE, Gaitanaris GA. The G protein-coupled receptor repertoires of human and mouse. *Proc Natl Acad Sci U S A.* 2003;100:4903-8.
- Venema RC**, Venema VJ, Eaton DC, Marrero MB. Angiotensin II-induced tyrosine phosphorylation of signal transducers and activators of transcription 1 is regulated by Janus-activated kinase 2 and Fyn kinases and mitogen-activated protein kinase phosphatase 1. *J Biol Chem.* 1998;273:30795-800.
- Wacheck V**, Zangemeister-Wittke U. Antisense molecules for targeted cancer therapy. *Crit Rev Oncol Hematol.* 2006;59:65-73.
- Waizenegger IC**, Hauf S, Meinke A, Peters JM. Two distinct pathways remove mammalian cohesin from chromosome arms in prophase and from centromeres in anaphase. *Cell.* 2000;103:399-410.
- Waldhoer M**, Wise A, Milligan G, Freissmuth M, Nanoff C. Kinetics of ternary complex formation with fusion proteins composed of the A(1)-adenosine receptor and G protein alpha-subunits. *J Biol Chem.* 1999;274:30571-9.
- Watson JV**, Chambers SH, Smith PJ. A pragmatic approach to the analysis of DNA histograms with a definable G1 peak. *Cytometry.* 1987;8:1-8.
- Wei CJ**, Li W, Chen JF. Normal and abnormal functions of adenosine receptors in the central nervous system revealed by genetic knockout studies. *Biochim Biophys Acta.* 2011;1808:1358-79.

- Weinstein IB**, Joe A. Oncogene addiction. *Cancer Res.* 2008;68:3077-80.
- Wellbrock C**, Hurlstone A. BRAF as therapeutic target in melanoma. *Biochem Pharmacol.* 2010;80:561-7.
- Wells J**, Boyd KE, Fry CJ, Bartley SM, Farnham PJ. Target gene specificity of E2F and pocket protein family members in living cells. *Mol Cell Biol.* 2000;20:5797-807.
- Weng J**, Wang J, Cai Y, Stafford LJ, Mitchell D, Ittmann M, Liu M. Increased expression of prostate-specific G-protein-coupled receptor in human prostate intraepithelial neoplasia and prostate cancers. *Int J Cancer.* 2005;113:811-8.
- White AA**, Zenser TV. Separation of cyclic 3',5'-nucleoside monophosphates from other nucleotides on aluminum oxide columns. Application to the assay of adenyl cyclase and guanyl cyclase. *Anal Biochem.* 1971;41:372-96.
- Wiedenmann B**, Franke WW, Kuhn C, Moll R, Gould VE. Synaptophysin: a marker protein for neuroendocrine cells and neoplasms. *Proc Natl Acad Sci U S A.* 1986;83:3500-4.
- Wikenheiser-Brokamp KA**. Retinoblastoma regulatory pathway in lung cancer. *Curr Mol Med.* 2006;6:783-93.
- Wilkie TM**, Kinch L. New roles for Galpha and RGS proteins: communication continues despite pulling sisters apart. *Curr Biol.* 2005;15:R843-54.
- Witsch E**, Sela M, Yarden Y. Roles for growth factors in cancer progression. *Physiology (Bethesda).* 2010;25:85-101.
- Witt KA**, Davis TP. CNS drug delivery: opioid peptides and the blood-brain barrier. *AAPS J.* 2006;8:E76-88.
- Woehler A**, Ponimaskin EG. G protein-mediated signaling: same receptor, multiple effectors. *Curr Mol Pharmacol.* 2009;2:237-48.
- Wojcik M**, Zieleniak A, Wozniak LA. New insight into A₁ adenosine receptors in diabetes treatment. *Curr Pharm Des.* 2010;16:4237-42.
- Won KA**, Reed SI. Activation of cyclin E/CDK2 is coupled to site-specific autophosphorylation and ubiquitin-dependent degradation of cyclin E. *EMBO J.* 1996;15:4182-93.
- Wright CS**. Structural comparison of the two distinct sugar binding sites in wheat germ agglutinin isolectin II. *J Mol Biol.* 1984;178:91-104.
- Wu X**, Lee VC, Chevalier E, Hwang ST. Chemokine receptors as targets for cancer therapy. *Curr Pharm Des.* 2009;15:742-57.
- Xu X**, Bieda M, Jin VX, Rabinovich A, Oberley MJ, Green R, Farnham PJ. A comprehensive ChIP-chip analysis of E2F1, E2F4, and E2F6 in normal and tumor cells reveals interchangeable roles of E2F family members. *Genome Res.* 2007;17:1550-61.
- Yang L**, Pang Y, Moses HL. TGF-beta and immune cells: an important regulatory axis in the tumor microenvironment and progression. *Trends Immunol.* 2010;31:220-7.
- Yarbro JW**. Mechanism of action of hydroxyurea. *Semin Oncol.* 1992;19:1-10.
- Yilmaz M**, Christofori G. EMT, the cytoskeleton, and cancer cell invasion. *Cancer Metastasis Rev.* 2009;28:15-33.

Yona S, Lin HH, Siu WO, Gordon S, Stacey M. Adhesion-GPCRs: emerging roles for novel receptors. *Trends Biochem Sci.* 2008;33:491-500.

Yoshida T, Zhang G, Haura EB. Targeting epidermal growth factor receptor: central signaling kinase in lung cancer. *Biochem Pharmacol.* 2010;80:613-23.

Yoshie O, Imai T, Nomiyama H. Chemokines in immunity. *Adv Immunol.* 2001;78:57-110.

Zabarovsky ER, Lerman MI, Minna JD. Tumor suppressor genes on chromosome 3p involved in the pathogenesis of lung and other cancers. *Oncogene.* 2002;21:6915-35.

Zeitlin PL, Lu L, Rhim J, Cutting G, Stetten G, Kieffer KA, Craig R, Guggino WB. A cystic fibrosis bronchial epithelial cell line: immortalization by adeno-12-SV40 infection. *Am J Respir Cell Mol Biol.* 1991;4:313-9.

Ziche M, Morbidelli L. Molecular regulation of tumour angiogenesis by nitric oxide. *Eur Cytokine Netw.* 2009;20:164-70.

Zieve GW, Turnbull D, Mullins JM, McIntosh JR. Production of large numbers of mitotic mammalian cells by use of the reversible microtubule inhibitor nocodazole. Nocodazole accumulated mitotic cells. *Exp Cell Res.* 1980;126:397-405.

Note: To the best of knowledge, I have obtained permission for the reprint of figures from the copyright owner. Please contact me in case of any copyright infringement.

Curriculum Vitae

Personal data

Name Stefan Kastner MSc
Date of birth April 14th, 1983 (Freudenstadt, Germany)
Address Rotenmühlgasse 58/12, 1120 Vienna, Austria
kastner.stefan@googlemail.com

Education

- Vienna, Austria** *The University of Vienna*
2009 - present Graduate program in Molecular Biology (Dr. rer. nat.), Boehringer Ingelheim RCV GmbH & Co KG
- Focus on molecular and cellular biology in cancer research
- Heidelberg, Germany** *The University of Heidelberg*
2006 - 2008 International graduate program in Molecular and Cellular Biology (MSc), Center of Molecular Biology Heidelberg (ZMBH)
- Focus on cancer research, (tumor) immunology, signal transduction
 - Graduation *summa cum laude* (grade 1.0)
- Heidelberg, Germany** *The University of Heidelberg*
2003 - 2006 Undergraduate program in Molecular Biotechnology (BSc)
- Focus on bioinformatics, drug development research, pharmacology
 - Graduation *summa cum laude* (grade 1.2)
- Rottenburg, Germany** *Eugen-Bolz-Gymnasium Rottenburg (high school)*
2002 Abitur (A-Levels), specialized courses: chemistry, mathematics
- Awarded to the top students in the German state Baden-Württemberg (*summa cum laude*; grade 1.0)
 - Eugen-Bolz award for outstanding social commitment and exceptional achievements at school

Experience

- Basel, Switzerland** *Novartis International Biotechnology Leadership Camp*
08/2011 Invited to represent Austria
- Business plan development for pharmaceutical product launch
- Austria, Vienna** *GlaxoSmithKline Austria*
11/2010 - 04/2011 Talents Community, University of Vienna, high potentials program
- The responsibility of pharmaceutical companies in Austria's health care
- Austria, Vienna** *Boehringer Ingelheim RCV GmbH & Co KG*
01/2009 - present Doctoral thesis, Department of Lead Discovery (Wolfgang Sommergruber)
- The role of poorly described G protein-coupled receptors in oncogenesis
- Heidelberg, Germany** *German Cancer Research Center (DKFZ)*
02/2008 - 11/2008 Master's thesis, Division of Molecular Immunology
- Characterization of the chemokine lymphotactin
- Hamilton (ON), Canada** *McMaster University at Hamilton, Centre for Gene Therapeutics*
09/2007 - 02/2008 Internship, Department of Pathology and Molecular Medicine
- V β spectratyping of human T cells following West Nile virus infection
- Heidelberg, Germany** *European Molecular Biology Laboratory (EMBL)*
04/2007 - 05/2007 Internship, Structural and Computational Biology Unit
- Electron microscopy and single particle reconstruction (yeast RNase P)
- Heidelberg, Germany** *The University of Heidelberg, University Hospital*
02/2006 - 04/2006 Internship, Department of Molecular Virology
- Subcellular localization of Dengue virus type II non-structural protein 4A

Houston (TX), USA *The University of Texas at Houston, Health Science Center*
09/2005 - 10/2005 Internship, Department of Neurology, Stroke Research
▪ Adenoviral gene transfer with primary neurons

Heidelberg, Germany *Sygnis Pharma AG*
12/2004 - 08/2007 Scientist and Bachelor's thesis, *In vivo* Pharmacology
▪ Planning, execution and analysis of animal (behavioral) experiments
▪ Cell type-specific gene expression profiling from murine α -motoneurons

Heidelberg, Germany *Private tutor*
2003 - 2008 English, mathematics, biology, chemistry

Freudenstadt, Germany *German Red Cross (DRK)*
08/2002 - 05/2003 Civilian service as an ambulance employee, rescue service

Certifications

Berlin/Hannover, Germany *International Academy of Life Sciences (IALS)*
09/2007 - 02/2008 Participant in the 2007/2008 Biomedical Exchange Program (scholarship)

Toronto (ON), Canada *Eurocentres Toronto*
09/2004 - 10/2004 Language course (English), graduated with grade 9 of 10

Publications

- 2012 Kastner S, Voss T, Keuerleber S, Glöckel C, Freissmuth M, Sommergruber W. Expression of G protein-coupled receptor 19 in human lung cancer cells is triggered by entry into S phase and supports G2/M cell cycle progression. *Mol Cancer Res.* (submitted)
- 2011 Guest speaker at the conference 'Advancing in the life science and uniting universities, corporate and government partners', Boston (MA), USA.
- 2011 Kastner S, Wernitznig A, Sommergruber W. GPR6 and GPR19 are associated with small cell lung cancer and show differential mRNA expression during the cell cycle. Poster at Gordon Research Conference 'Molecular Pharmacology', Ventura (CA), USA.
- 2008 Pitzer C, Krüger C, Plaas C, Kirsch F, Dittgen T, Müller R, Laage R, Kastner S, Suess S, Ehrenreich H, Schäbitz WR, Bach A, Schneider A. Granulocyte-colony stimulating factor (G-CSF) improves motor function and prolongs survival in a murine model of amyotrophic lateral sclerosis (ALS). *Brain.* 131:3335-47.
- 2007 Miller S, Kastner S, Krijnse-Locker J, Bühler S, Bartenschlager R. The non-structural protein 4A of Dengue virus is an integral membrane protein inducing membrane alterations in a 2K-regulated manner. *J Biol Chem.* 282:8873-82.

Vienna, 2012

(Stefan Kastner)